The University Of Sheffield.

Multi-Beam Multiplexing Design Based on Hybrid Beamforming Structures

By

Junwei Zhang

Supervisors:

Dr. Wei Liu

and

Mr. Eddie Ball

A doctoral thesis submitted in fulfilment of the requirements for the award of

Doctor of Philosophy

May 2022

Multi-Beam Multiplexing Design Based on Hybrid Beamforming Structures

Junwei Zhang

PhD Thesis

Communications Research Group

Department of Electronic and Electrical Engineering

The University of Sheffield

May 2022

Abstract

Hybrid beamforming is a combination of digital and analogue beamforming techniques to achieve a trade off between performance and cost, and it plays an important role for millimetre wave and massive MIMO based communication systems.

In this thesis, two novel designs based on hybrid beamforming structures are first proposed, which together with the corresponding inter-subarray coding schemes, can achieve multi-beam multiplexing for arbitrary directions to serve corresponding users. In the first design, based on the relationship of directions between the two required beams, the adjacent antenna spacing is regarded as a variable to be determined, while in the second design, the adjacent antenna spacing is fixed and an iterative optimisation procedure is proposed to solve the problem based on a least-square formulation.

As extended versions of the above design with a fixed antenna spacing, three novel designs considering practical application constraints are proposed to achieve multi-beam multiplexing for corresponding users. In the first scheme, to reduce the implementation complexity, one nearly equal magnitude constraint is imposed on the analogue coefficients so that beamforming can be achieved by pure phase shifters after the normalisation of magnitudes. In the second scheme, a robust design against steering vector errors is considered to guarantee limited variation of resultant beam responses due to various steering vector errors. In the third scheme, by considering both the equal magnitude constraint and steering vector errors simultaneously, a robust design with equal magnitude constraint is proposed.

Furthermore, when a large number of antennas are available, for a required level of beamforming performance, we may not need to employ all of them for each scenario. As a result, further complexity reduction can be achieved by only employing a subset of the available antennas based on the sub-aperture and overlapped subarray architectures. Moreover, by considering the polarisation states of the signals in the crossed-dipole based array, the best set of crossed-dipole antennas and dipoles can be selected to achieve the same multi-beam multiplexing effect.

Contents

List of Publications

Journal Papers

1. **J. Zhang**, W. Liu, C. Gu, S. S. Gao and Q. Luo, "Multi-Beam Multiplexing Design for Arbitrary Directions Based on the Interleaved Subarray Architecture". *IEEE Transactions on Vehicular Technology*, 69(10), 11220 − 11232, Oct. 2020 (Chapter 3).

2. **J. Zhang**, W. Liu, C. Gu, S. S. Gao and Q. Luo, "Robust Multi-Beam Multiplexing Design Based on a Hybrid Beamforming Structure with Nearly Equal Magnitude Analogue Coefficients", *IEEE Transactions on Vehicular Technology*, 71(5), 5564 − 5569, May. 2022 (Chapter 4).

3. B. Zhang, W. Liu, J. Ma, Z. Qi, **J. Zhang**, L. Han, Y. Li, X. Zhao, C. Zhang and C. Wang. "Sparse Antenna Array Based Positional Modulation Design with a Low-Complexity Metasurface", *IEEE Access*, 8, 177640 − 177646, Sep. 2020.

Conference Papers

1. **J. Zhang** and W. Liu, "Antenna Selection Design of Crossed-Dipole Arrays for Multi-Beam Multiplexing Based on a Hybrid Beamforming Structure", in *Proc. IEEE International Symposium on Circuits and Systems (ISCAS)*, Austin Texas, USA, May 2022 (Chapter 5, Section 5.3).

2. **J. Zhang** and W. Liu, "Antenna Selection for Multi-Beam Multiplexing Design Based on the Hybrid Beamforming Architecture", in *Proc. IEEE Statistical Signal Processing Workshop (SSP)*, Rio de Janeiro, Brazil, Jul. 2021, pp. 261-265 (Chapter 5, Sections 5.2.1 and 5.2.2).

3. **J. Zhang**, W. Liu, C. Gu, S. S. Gao and Q. Luo, "Dual-Beam Multiplexing Under an Equal Magnitude Constraint Based on a Hybrid Beamforming Structure", in *Proc. IEEE 31st Annual Symposium on Personal, Indoor and Mobile Radio Communications*, London, UK, Sep. 2020, pp. 1-5 (Chapter 4, Sections 4.2.1 and 4.3.1).

4. **J. Zhang**, W. Liu, C. Gu, S. S. Gao and Q. Luo, "Two-Beam Multiplexing with Inter-Subarray Coding for Arbitrary Directions Based on Interleaved Subarray Architectures", in *Proc. IEEE 30th Annual International Symposium on Personal, Indoor and Mobile Radio Communications (PIMRC)*, Istanbul, Turkey, Sep. 2019, pp. 1-5 (Chapter 3, Section 3.3).

Under Review

1. **J. Zhang** and W. Liu, "Antenna Number Minimisation for Low-Complexity Multi-Beam Multiplexing Based on Hybrid Beamforming Architectures", *IEEE Transactions on Circuits and Systems II: Express Briefs* (Chapter 5, Section 5.2).

List of Figures

List of Tables

Acknowledgements

I would like to express my sincere gratitude and appreciation to my supervisor Dr. Wei Liu for his persistent support and encouragement. Many thanks for leading me into this research area and pursuing my doctor's degree. Your conscientious attitudes towards academic works give me an excellent example and they will inspire me to work hard in the future research works.

To my parents, thank you for giving me the chance to continue my PhD study when I get my master degree in Sheffield. Your encouragement makes me become more confident in the hard PhD program.

To Songjiang Yang, Zhengyu Wan and Wenfei Yang, thank you for standing by my side when I fall into difficulties, and providing me your advice and support in my PhD studies.

To all the colleagues and friends in the communications research group, many thanks for the helps in academic studies and daily life from you in the last four years and I will keep them to be the most valuable memory in my life.

List of Abbreviations

ADC	Analogue to Digital Converter
CS	Compressive Sensing
DAC	Digital to Analogue Converter
DoA	Direction of Arrival
DoF	Degree of Freedom
FIR	Finite Impulse Response
GA	Genetic Algorithm
LS	Least Squares
MIMO	Multiple Input Multiple Output
RF	Radio Frequency
SA	Simulated Annealing
SM	Spatial Modulation
TDL	Tapped-Delay Lines
ULA	Uniform Linear Array
UPA	Uniform Planar Array
XPD	Cross-Polar Discrimination

Chapter 1

Introduction

1.1 Introduction

Array signal processing is one of the major topics of signal processing and has been widely employed in various applications, such as radar, sonar, radio astronomy and wireless communications [1–4], where multiple antennas placed at different locations are implemented for processing the received or transmitted signals.

There are three types of arrays according to geometrical dimension of the array structure, including linear arrays, where the antennas are distributed along a straight line, planar arrays, where the antennas are spread over a two-dimensional (2D) space and volumetric arrays, where the antennas are distributed in a three-dimensional (3D) volume. In this thesis, the linear array is our focus of study, but the proposed methods here can also be extended to the other two array geometries.

Specifically, array signal processing consists of three sub-areas: signal number detection, direction of arrival (DoA) estimation and beamforming. Detection theory is employed to distinguish between the signal and noises using the received signals and determine the number of signals [5]. DoA estimation is to estimate the direction of the incoming signal with an array of antennas, which is extensively used in seismology, radar detection, wireless communications and radio astronomy [6, 7]. Beamforming is a traditional technique to maintain the maximum power at a desired direction or desired directions, while minimising the power at undesired directions as much as possible.

Nowadays, beamforming is increasingly being implemented digitally; as an example, for transmit beamforming, a digital to analogue converter (DAC) is employed first to transform the received digital signal to analogue format at the baseband and then modulated to the radio frequency (RF) for each antenna; moreover, to ensure the digital beamforming technique works effectively, the large number of DACs should be synchronised. Given the higher and higher data rate and more and more antennas required for current and future wireless communication systems, especially for those employing massive MIMO techniques, it has been a significant challenge to implement such a large number of DACs working at a very high speed.

In addition to massive MIMO, another key enabling technology for the fifth-generation (5G) and beyond communication systems is the millimetre wave communication and both require the employment of a large number of antennas working at high frequencies with a wide bandwidth [8]. If the traditional beamforming process is implemented completely in the digital domain, the extremely high cost associated with the large number of high-speed DACs or analogue to digital converters (ADCs) and the high-level power consumption will render it practically infeasible. One solution to the problem is to employ the hybrid beamforming techniques [3, 8–21], where for transmit beamforming as an example, partially digital beamforming is performed first to reduce the number of digital channels [1], which are then converted into analogue via a reduced number of digital to analogue converters (DACs), and after that analogue beamforming can then be performed [22–24].

1.2 Motivation

A previous hybrid beamforming method which involves multiplexing two beams was proposed in a recent work [25, 26]. However, a limitation of the proposed method is that the directions of the two beams must satisfy a specific relationship and therefore it is not suitable for users located in arbitrary directions. The aim of the works in this thesis is to overcome this limitation by developing methods for multi-beam multiplexing designs for arbitrary user directions based on the sub-aperture subarray architectures, considering various practical factors, such as implementation complexity and robustness against

model errors.

The following is a list of three main objectives for the thesis:

1. The first objective is to simultaneously generate multiple beams serving users in arbitrary directions with the interleaved subarray architecture based on ULAs and UPAs, with the sidelobe responses suppressed to a comparatively lower level.

2. The second objective is to consider the above designs in real-world applications, taking into account two practical factors, i.e., phase-only control on analogue coefficients and robustness against steering vector errors. Three designs considering the above two constraints separately and simultaneously form a complete piece of work in Chapter 4.

3. The third objective is to reduce the overall complexity of the beamformer, where only a subset of the available antennas is selected to achieve the same multi-beam multiplexing effect based on isotropic and polarisation-sensitive crossed-dipole antennas.

1.3 Original Contributions

Corresponding to the above objectives, the main contributions in Chapters 3, 4 and 5, respectively, are shown as follows.

1. Two novel designs with varying and fixed antenna spacings, respectively, are employed to tackle the problems in [25, 26]. Beam interference due to the large antenna spacing can be mitigated and beam gain can be augmented by multiplexing multiple beams. In the first design, the adjacent antenna spacing is treated as a variable which is designed according to the specific relationship of directions between the required two beams, but a clear issue is that it may not be practical to constantly change the spacing to meet the needs of changing user directions. In the second design, to deal with the issue in the first design, the antenna spacing is fixed and independent of beam directions, and we optimise the beamformer coefficients in

multiple subarrays for best approximation between the designed and desired beam responses in a least-squares (LS) formulation. To extend the work from two beams to multiple beams and propose a general design approach, i.e., the second design, we have also considered the design based on uniform planar arrays (UPAs), which will be widely used in mmWave communications.

2. As extended versions of the first design with a fixed antenna spacing in Chapter 3, three designs considering two practical application constraints separately and simultaneously based on the sub-aperture subarray architectures are proposed to achieve multi-beam multiplexing to serve users in arbitrary directions. The novelty of this work is twofold: a MinMax constraint is imposed on the analogue coefficients of the array so that phase-only beamforming can be achieved after the normalisation of weight magnitudes; a norm constraint is introduced to enforce a robust design result against various model errors. Due to the entangled nature of the individual beams, the resultant formulation is non-convex and there is no effective solution available for such a problem, unlike the traditional equal-magnitude and robust designs for beamforming purposes. As a result, an alternate optimisation approach is provided to solve the problem, where the original problem is split into two sub-problems, and each of them becomes convex, guaranteeing the convergence of the whole alternate optimisation process.

3. Multi-beam multiplexing can be implemented by uniform linear arrays (ULAs) based on the sub-aperture subarray architectures in previous works, which leads to significant cost and complexity reduction in its implementation. However, when a large number of antennas are available, we may not need to employ all of them and a subset of the available antennas may be sufficient for a specific beamforming scenario. To further reduce the system complexity, a sparsity based l_1 norm minimisation method is imposed on the sub-aperture and overlapped subarray architectures, where each antenna is associated with one and multiple analogue coefficients, respectively. By replacing the isotropic antennas in the structure with polarisation-sensitive crossed-dipole antennas, a new steering vector is involved for

each of the sub-aperture subarray architectures and the best set of dipoles can be selected straightforwardly using the same l_1 norm minimisation method. However, one drawback of this approach is that the two complex-valued weighting coefficients associated with each crossed-dipole antenna cannot be minimised simultaneously. As a result, only the weighting coefficients of some individual dipoles may be zero-valued, rather than the complete crossed-dipoles, which may not be desired in some applications. Therefore, a design of crossed-dipole arrays based on a modified l_1 norm minimisation is proposed to guarantee a truly sparse solution.

1.4 Outline

An outline of the rest of this thesis is as follows:

In Chapter 2, basics about beamforming are first reviewed. Then, digital and analogue beamforming techniques which constitute the hybrid beamforming technique are discussed followed by two typical sub-aperture subarray architectures to achieve it. Some methods to implement multi-beam multiplexing designs such as convex optimisation and least squares (LS) minimisation are presented at the end.

In Chapter 3, a recent two-beam multiplexing design with two interleaved ULAs is first reviewed. One limitation is that the directions of two beams have to satisfy a fixed relationship and it is then derived in the context. To overcome this restriction, two novel designs are proposed where the adjacent antenna spacing in the first design is a variable and can be calculated as a function of the directions of the two required beams; in the second design, the adjacent antenna spacing is fixed and an alternate optimisation method is proposed based on a least-square formulation for both two-user and multi-user cases. Furthermore, the idea in the second design can be extended to the hybrid beamforming structure based on UPAs to achieve the same purpose with an overall satisfactory performance.

In Chapter 4, the work is focused on dealing with implementation issues of the multi-beam multiplexing hybrid beamforming architecture proposed in Chapter 3. Three novel designs considering practical application constraints based on the sub-aperture subarray

architectures are proposed to achieve multi-beam multiplexing to serve users in arbitrary directions. In the first scheme, to reduce the implementation complexity, a nearly equal magnitude constraint is imposed on the analogue coefficients so that beamforming can be achieved by merely changing the analogue phase shift of each antenna. In the second scheme, a robust design against steering vector errors is considered to guarantee limited variation of resultant beams due to various steering vector errors. In the third scheme, the constraints in the first two schemes are considered simultaneously and therefore a robust design with an equal magnitude constraint on analogue coefficients is proposed. As a benchmark, a fourth scheme without any constraints is given and the performance generated by the first three schemes can be compared with the fourth one in a quantitative way.

In Chapter 5, a review of the compressive sensing technique employed in sparse antenna array design is provided. To further reduce the overall system complexity, antenna selection designs based on the sub-aperture and overlapped subarray architectures are first introduced and design examples are provided to demonstrate the effectiveness of this method. If the polarisation state of the signal is considered, the isotropic antenna in the structure can be replaced by the crossed-dipole antenna, which consists of two orthogonally orientated dipoles, and two methods are proposed to select the best set of crossed-dipole dipoles or antennas, respectively.

Finally in Chapter 6, conclusions are drawn and an outline for potential future work is provided.

Chapter 2

Review of Hybrid Beamforming

2.1 Beamforming Based on Antenna Arrays

A narrowband linear array with adjacent antenna spacing d for transmit beamforming is shown in Figure 2.1. Ideally, all the antennas are assumed to be omnidirectional and have identical responses. There are N received antenna signals $x_n[t]$, for $n \in \{0, 1, \ldots, N-1\}$. The steering vector of the array is a function of angular frequency ω and θ, given by (for transmission model)

$$\boldsymbol{s}(\omega, \theta) = [1, e^{j\omega \frac{d}{c} \sin\theta}, \ldots, e^{j\omega(N-1)\frac{d}{c}\sin\theta}]^T, \tag{2.1}$$

where $\theta \in [-\frac{\pi}{2}, \frac{\pi}{2}]$ is measured with respect to the broadside of the linear array, c denotes the speed of propagation wave and $\{\cdot\}^T$ denotes the transpose operation. In addition, spatial aliasing needs to be taken into account because it means the signals transmitted to different directions share the same steering vector, i.e., $\boldsymbol{s}(\omega, \theta_a) = \boldsymbol{s}(\omega, \theta_b)$, where θ_a and θ_b denote two different transmission directions. Thus, the condition given below

$$e^{j\omega \frac{d}{c} \sin\theta_a} = e^{j\omega \frac{d}{c} \sin\theta_b}, \tag{2.2}$$

or equivalently

$$e^{j2\pi \frac{d}{\lambda} \sin\theta_a} = e^{j2\pi \frac{d}{\lambda} \sin\theta_b}, \tag{2.3}$$

should be satisfied. To avoid spatial aliasing, $|2\pi\frac{d}{\lambda}\sin\theta| \leq \pi$. Since $|\sin\theta| \leq 1$, $d \leq \frac{\lambda}{2}$ can be derived. Hence, for a ULA with $d = \frac{\lambda}{2}$, the steering vector in (2.1) changes to

$$\boldsymbol{s}(\theta) = [1, e^{j\pi\sin\theta}, ..., e^{j\pi(N-1)\sin\theta}]^T. \tag{2.4}$$

The beam response generated by the array is given by

$$P(\theta) = \boldsymbol{w}^H \boldsymbol{s}(\theta), \tag{2.5}$$

where $[.]^H$ denotes the Hermitian transpose and $\boldsymbol{w}$ is the weighting coefficient vector, given by

$$\boldsymbol{w} = [w_0, w_1, ..., w_{N-1}]^T. \tag{2.6}$$

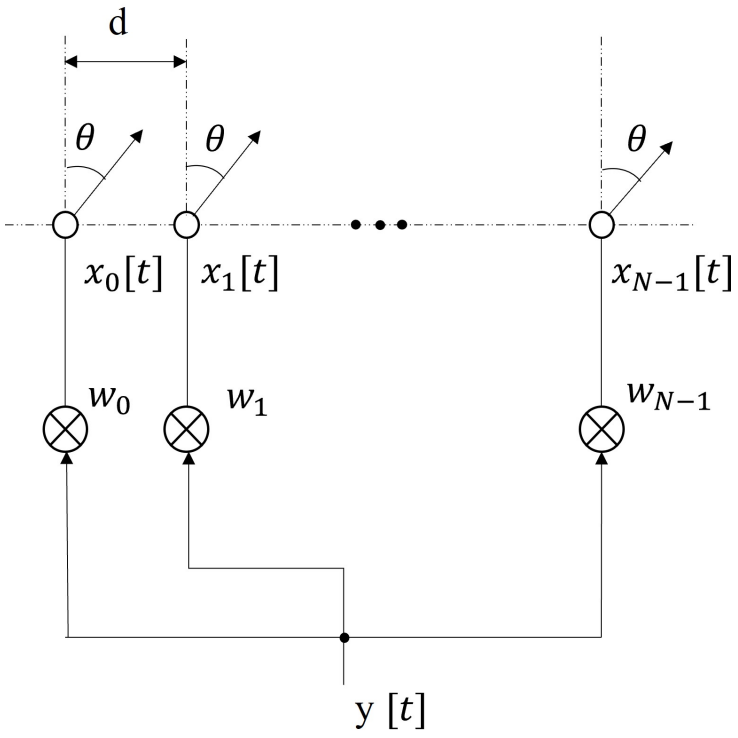

Figure 2.1: A general narrowband beamforming structure.

To describe the sensitivity of the beamformer with respect to signals transmitted to different directions, the beam pattern $|P(\theta)|$ in decibel (dB) of the array is given by

$$BP(\theta) = 20\log_{10}\frac{|P(\theta)|}{\max|P(\theta)|}. \tag{2.7}$$

As an representative example, the weighting coefficients of an array with $N = 10$ antennas are given by

$$\boldsymbol{w} = [1, 1, ..., 1]^T, \tag{2.8}$$

and the resultant beam response is displayed in Figure 2.2.

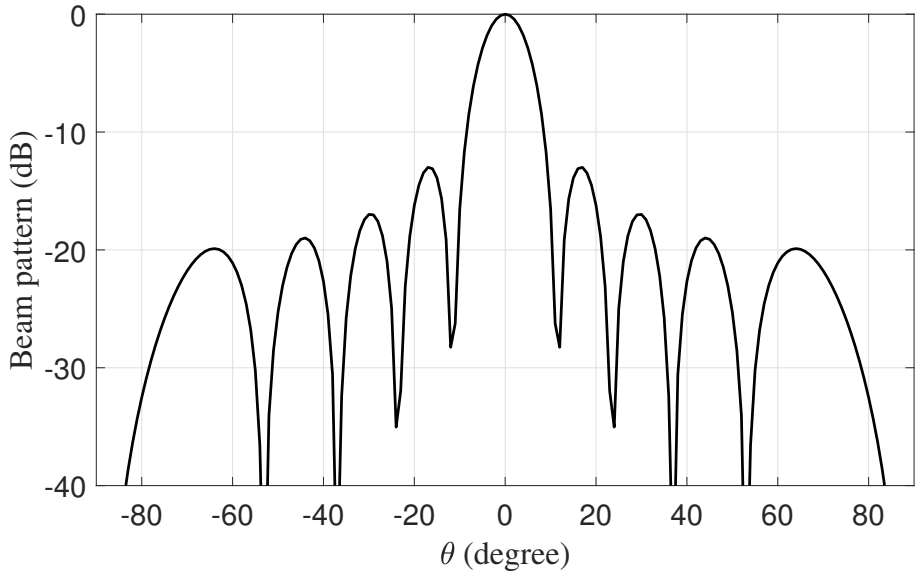

Figure 2.2: The narrowband beam response generated by an ULA with $N = 10$ antennas.

2.2 Introduction to Hybrid Beamforming

In recent years, technologies for the 5-G communication systems have been developing very quickly and two key enabling technologies are massive MIMO and mmWave communication [3, 8–11, 27–33]. In an ideal mmWave massive MIMO system, the number of RF chains which consist of hardware components such as ADCs (DACs), power amplifier, etc. should be equal to the number of antennas. To reduce hardware complexity and cost, the hybrid beamforming technique was introduced [34–36], and it is implemented by combining digital and analogue beamforming techniques together.

2.2.1 Digital Beamforming

Nowadays many array signal processing techniques such as beamforming are being achieved digitally. In digital beamforming, as shown in Figure 2.3, a digital to analogue converter

(DAC) is employed to convert the digital signal into the analogue format. This is performed at either the baseband followed by modulation to the radio frequency (RF) or directly at the radio frequency in some cases. To avoid signal aliasing, the minimum sampling frequency should be equal or higher than twice the highest frequency of the signal according to the Nyquist Sampling Theorem. However, since each antenna requires a RF chain in digital beamforming, the extremely high cost due to the large number of DACs and the high-level power consumption will make it practically infeasible if the beamforming process is implemented completely in the digital domain.

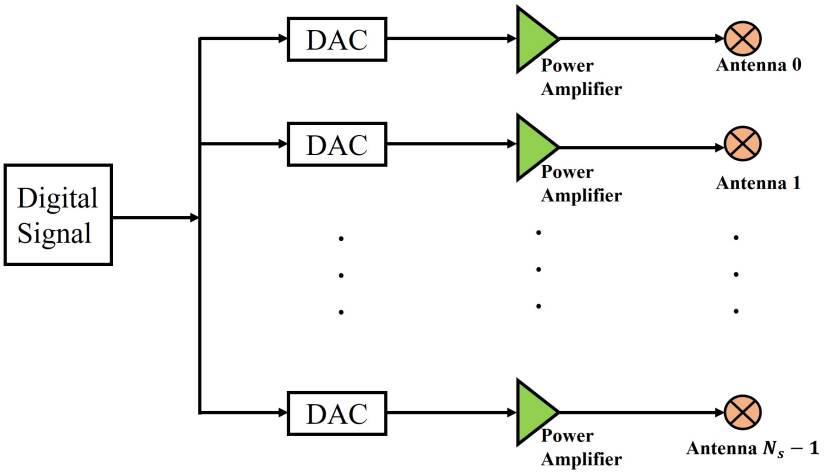

Figure 2.3: A digital beamforming structure.

2.2.2 Analogue Beamforming

To reduce the high cost associated with a fully digital implementation, two methods are exploited to tackle this issue. The first one is to implement it by employing the analogue beamforming technique [22], as shown in Figure 2.4, or some judicially designed transformations [23, 24]. As a result, some phase shifting techniques are utilised to provide an alternative solution even though the overall performance may not be satisfactory in some cases due to low phase resolution [37, 38].

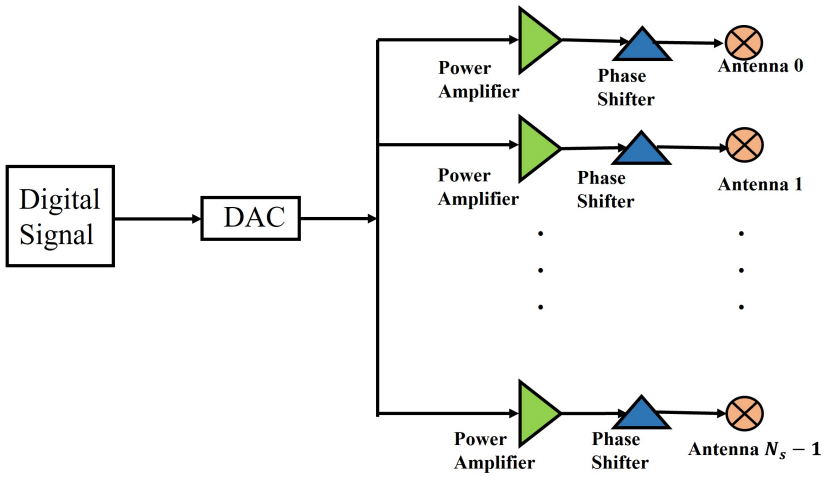

Figure 2.4: An analogue beamforming structure.

2.2.3 Typical Architectures for Hybrid Beamforming

The other one to reduce the power consumption and implementation cost is the hybrid beamforming technique [3, 8–11, 27–33], where partially digital beamforming is performed first to reduce the number of separate digital channels in the following, and then this smaller number of digital signals are converted into analogue via a reduced number of digital to analogue converters (DACs), and after that analogue beamforming can then be performed.

Various hybrid beamforming structures have been proposed in the past and one of them is the sub-aperture based hybrid beamformer [10, 27, 39–42]. There are mainly two types of implementations for the subarray scheme: one is the side-by-side type or localised subarray architecture and the other one is the interleaved subarray architecture [43, 44]. In the localised subarray architecture, all the antennas belonging to the same subarray are located within a local region next to each other, as shown in Figure 2.5; as a result, the beam width generated by this architecture is comparatively wide. For the interleaved subarray architecture shown in Figure 2.6, the antennas of each subarray are distributed over a much larger aperture and the spacing between adjacent subarray antennas is much larger than the standard array spacing. Thus, a much narrower beam can be formed by the interleaved subarray architecture, which makes it a good candidate for beam multiplexing; however, this narrow beamwidth is achieved at the cost of generating high sidelobes or

even grating lobes or spatial aliasing, although this effect can be suppressed at the digital beamforming stage to some extent with improved desired beam gain [45–47].

Clearly, the two sets of coefficients (analogue and digital) are multiplied in different ways to generate multiple beams. In particular, for the multiplexing case, the common set of analogue coefficients will be responsible for generating different beams, together with each beam's digital coefficients, which impose further constraints to the problem.

However, how to obtain a combined set of digital and analogue coefficients is a difficult problem and some solutions can be found from [48–51], where the resultant joint optimisation problem can be decomposed into subproblems of individual vectors.

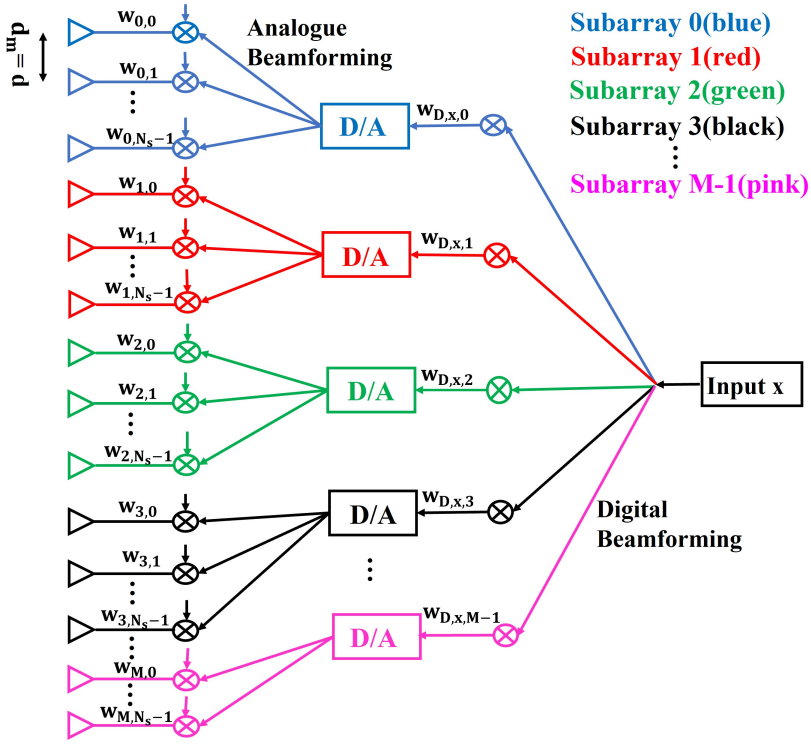

Figure 2.5: A localised ULA subarray based hybrid beamforming architecture.

2.3 Convex Optimisation

Recently, convex optimisation has become a useful tool to solve the beamforming design problem based on antenna arrays [52, 53]. If both the objective function and the constraint

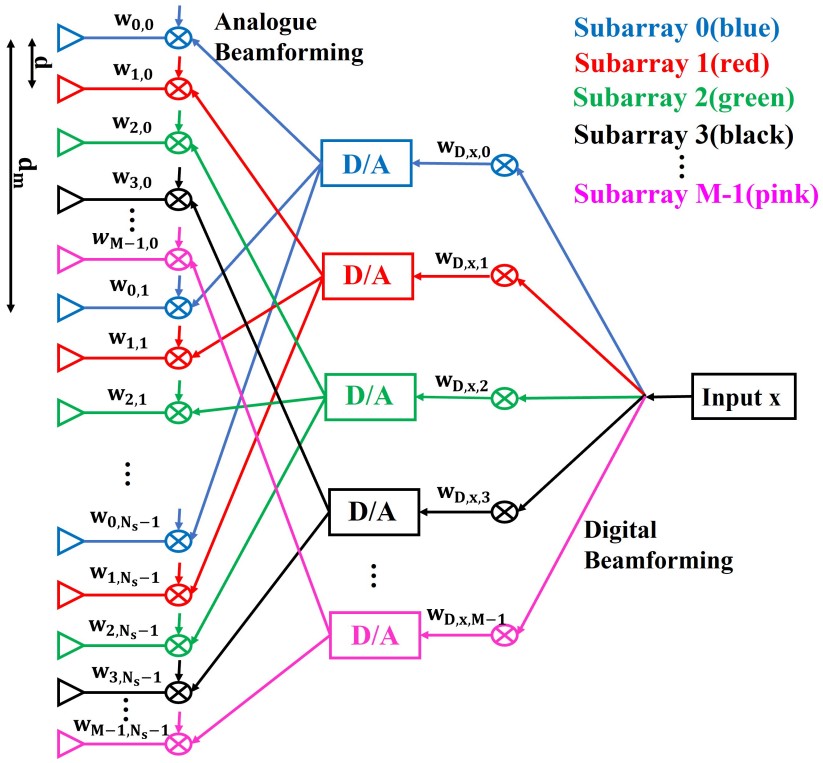

Figure 2.6: An interleaved ULA subarray based hybrid beamforming architecture.

are convex, a convex optimisation problem is formulated as

$$\begin{aligned} \min_{\boldsymbol{w}} \quad & g_0(\boldsymbol{w}) \\ \text{subject} \quad \text{to} \quad & g_k(\boldsymbol{w}) \leq a_k, \quad k \in \{1, 2, ..., K\}, \end{aligned} \tag{2.9}$$

where $\boldsymbol{w}$ denotes a set of complex-valued variables and a_k denotes the upper bound for the k-th convex constraint. For a function to be convex, the following criterion

$$g_k((1-\alpha_c)\boldsymbol{w}_a + \alpha_c \boldsymbol{w}_b) \leq (1-\alpha_c) g_k(\boldsymbol{w}_a) + \alpha_c g_k(\boldsymbol{w}_b), \tag{2.10}$$

should be satisfied for all real-valued α_c and all complex-valued weighting vectors $\boldsymbol{w}_a$ and $\boldsymbol{w}_b$ lie in the same space as $\boldsymbol{w}$, i.e., $\boldsymbol{w}_a$ and $\boldsymbol{w}_b$ are all possible values of $\boldsymbol{w}$. Some representative convex functions are usually employed in antenna array beamforming, such as the l_1 and l_2 norms of the vector $\boldsymbol{w}$.

Note that most of the array pattern synthesis problems can be formulated into a convex form and some convex optimisation algorithms such as the interior point method can be used to solve them.

For example, an antenna array with $N = 10$ antennas is employed for transmit beamforming. The mainlobe direction, fixed direction with magnitude constraint and the sidelobe regions are $\Theta_{main} = 0°$, $\Theta_0 = 30°$ and $\Theta_{side} \in [-90°, -5°] \cup [5°, 90°]$, sampled every $1°$. With the steering vector given by (2.4) and $d = \frac{\lambda}{2}$, the optimisation problem for this example is formulated as

$$\begin{aligned} \min_{\boldsymbol{w}} \quad & \| \boldsymbol{w}^H \boldsymbol{z}_s \|_2 \\ \text{subject} \quad \text{to} \quad & \boldsymbol{w}^H \boldsymbol{z}_m = 1, \\ & |\boldsymbol{w}^H \boldsymbol{z}_0| \leq 0.01, \end{aligned} \tag{2.11}$$

with

$$\boldsymbol{z}_s = \sum_{\theta \in \Theta_{side}} \boldsymbol{s}(\theta), \quad \boldsymbol{z}_m = \sum_{\theta \in \Theta_{main}} \boldsymbol{s}(\theta), \quad \boldsymbol{z}_0 = \sum_{\theta \in \Theta_0} \boldsymbol{s}(\theta). \tag{2.12}$$

The beam response generated by this array is given by Figure 2.7 and the corresponding weighting coefficients are $[0.0750 + 0.0057i, 0.0970 - 0.0071i, 0.1110 - 0.0088i, 0.1165 + 0.0086i, 0.1005 + 0.0076i, 0.1005 - 0.0076i, 0.1165 - 0.0086i, 0.1110 + 0.0088i, 0.0970 + 0.0071i, 0.0750 - 0.0057i]^T$.

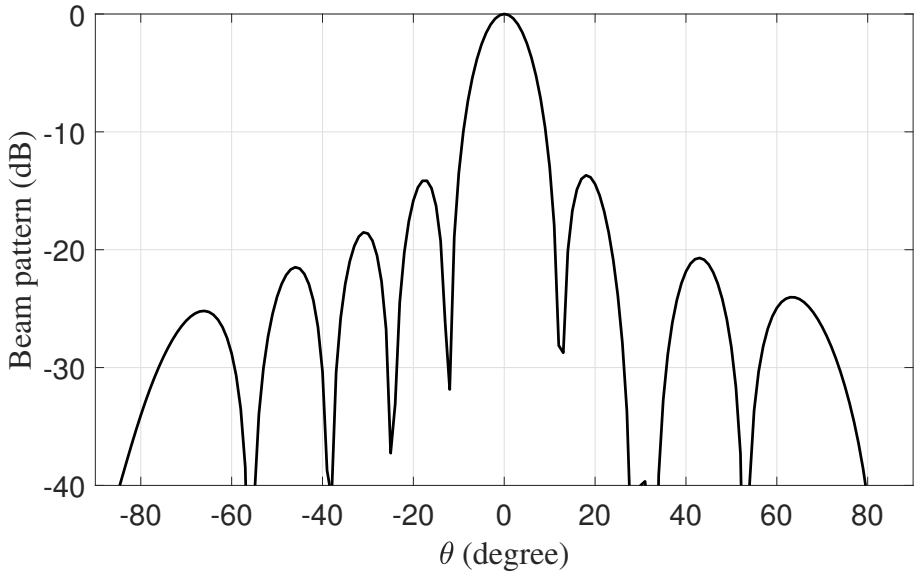

Figure 2.7: Beam response generated by (2.11) using the ULA with $N = 10$ antennas.

2.4 Least Squares Method

The least squares method is traditionally employed for designing both finite impulse response (FIR) filters and wideband beamformers [54–56]. Compared to other optimisation methods, the least squares method is more widely used because it gives a closed-form solution to the problem. In this section, we will review the standard least squares and constrained least squares methods which will be employed in the remaining chapters of this thesis.

2.4.1 Standard Formulation

The following cost function based on the LS formulation is used in the design [1, 57, 58]

$$J_{LS} = \int_{\Theta} F(\theta) \left| \boldsymbol{w}^H \boldsymbol{s}(\theta) - D(\theta) \right|^2 d\theta, \tag{2.13}$$

where Θ denotes the overall angle range of interest, $F(\theta)$ is a positive real weighting function and $D(\theta)$ is the desired beam response. In our designs, without loss of generality, we use $F(\theta) = 1 - \alpha_{LS}$ and $D(\theta) = 1$ over the mainlobe region and $F(\theta) = \alpha_{LS}$ and $D(\theta) = 0$ over the sidelobe region, where $\alpha_{LS} \in (0, 1)$ is the trade-off parameter between the mainlobe and sidelobe regions. Then, (2.13) can be expanded to a quadratic form which is given by

$$\begin{aligned} J_{LS} =& \int_{\Theta} F(\theta)(\boldsymbol{w}^H \boldsymbol{s}(\theta) - D(\theta))(\boldsymbol{w}^H \boldsymbol{s}(\theta) - D(\theta))^H d\theta \\ =& \boldsymbol{w}^H \boldsymbol{Q}_{LS} \boldsymbol{w} - \boldsymbol{w}^H \boldsymbol{z}_{LS} - \boldsymbol{z}_{LS}^H \boldsymbol{w} + d_{LS}, \end{aligned} \tag{2.14}$$

with

$$\boldsymbol{Q}_{LS} = \int_{\Theta} F(\theta) \boldsymbol{S}(\theta) d\theta, \tag{2.15}$$

$$\boldsymbol{z}_{LS} = \int_{\Theta} F(\theta)(\boldsymbol{s}(\theta) D^H(\theta)) d\theta, \tag{2.16}$$

$$d_{LS} = \int_{\Theta} F(\theta) |D(\theta)|^2 d\theta, \tag{2.17}$$

$$\boldsymbol{S}(\theta) = \boldsymbol{s}(\theta) \boldsymbol{s}(\theta)^H. \tag{2.18}$$

To solve the problem numerically, as an approximation, the cost formulation in (2.14) can be converted into a discrete version, given by

$$J_{LS_D} = \boldsymbol{w}^H \boldsymbol{Q}_{LS_D} \boldsymbol{w} - \boldsymbol{w}^H \boldsymbol{z}_{LS_D} - \boldsymbol{z}_{LS_D}^H \boldsymbol{w} + d_{LS_D}, \tag{2.19}$$

with

$$\boldsymbol{Q}_{LS_D} = (1 - \alpha_{LS}) \sum_{\theta \in \Theta_{main}} \boldsymbol{S}(\theta) + \alpha_{LS} \sum_{\theta \in \Theta_{side}} \boldsymbol{S}(\theta), \tag{2.20}$$

$$\boldsymbol{z}_{LS_D} = (1 - \alpha_{LS}) \sum_{\theta \in \Theta_{main}} \boldsymbol{s}(\theta), \tag{2.21}$$

$$d_{LS_D} = (1 - \alpha_{LS}) \sum_{\theta \in \Theta_{main}} 1. \tag{2.22}$$

Weighting coefficients $\boldsymbol{w}$ can be obtained by taking the gradient of the cost function in (2.19) with respect to $\boldsymbol{w}^H$ and then setting it to zero, given by

$$\boldsymbol{w} = \boldsymbol{Q}_{LS_D}^{-1} \boldsymbol{z}_{LS_D}. \tag{2.23}$$

In this section, an example is provided to demonstrate the effectiveness of the LS based design using an ULA with $N = 10$ antennas. The mainlobe direction and the sidelobe regions are the same as the design example in Section 2.3 and the adjacent antenna spacing $d = \frac{\lambda}{2}$. With $\alpha_{LS} = 0.7$, the resultant beam response is shown in Figure 2.8 and the weighting coefficients are $[0.0080 + 0.0000i, 0.0101 + 0.0000i, 0.0099 - 0.0000i, 0.0104 - 0.0000i, 0.0104 + 0.0000i, 0.1014 + 0.0000i, 0.1014 + 0.0000i, 0.0099 + 0.0000i, 0.0101 - 0.0000i, 0.0080 - 0.0000i]^T$.

2.4.2 Constrained Least Squares

To restrict the response of the beamformer at some particular directions or frequencies, some constraints can be added to the least squares formulation and these can be either equality or inequality constraints. A closed-form solution can be obtained by reducing the least squares problem into an unconstrained one.

Now the new objective function in a quadratic form is given by $\boldsymbol{w}^H \boldsymbol{Q}_D \boldsymbol{w}$, where $\boldsymbol{Q}_D$ denotes the correlation matrix of the array data. For a linear equality constraint, a closed-form solution can be obtained via reducing it to a low-dimensional unconstrained least squares problem [53, 59, 60].

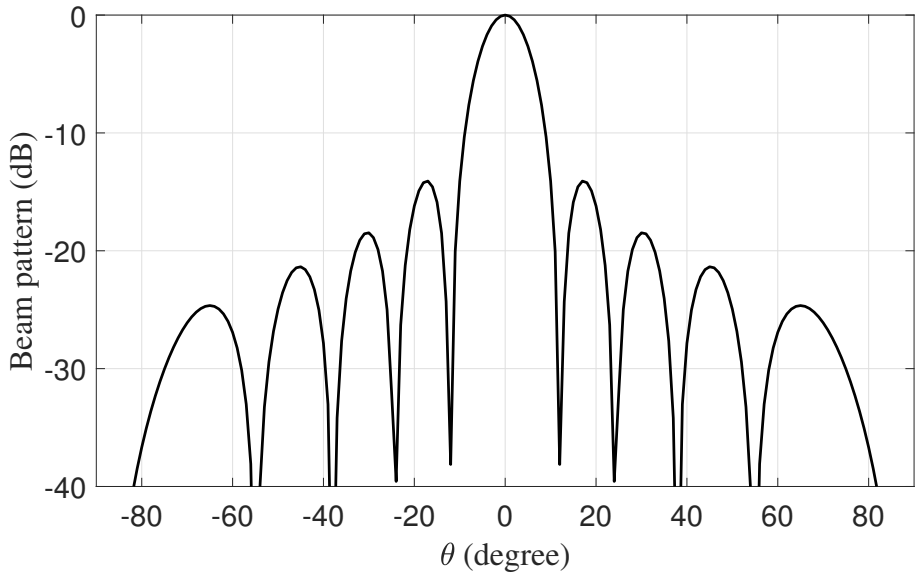

Figure 2.8: Beam response generated by (2.23) using the ULA with $N = 10$ antennas.

Now, by introducing the constraint, given by

$$\boldsymbol{C}^H \boldsymbol{w} = \boldsymbol{f}, \tag{2.24}$$

where $\boldsymbol{C}$ denotes the $N \times r$ dimensional constraint matrix and $\boldsymbol{f}$ denotes the $r \times 1$ response vector, the formulation of the constrained least squares problem is

$$\begin{aligned} \min_{\boldsymbol{w}} \quad & \boldsymbol{w}^H \boldsymbol{Q}_D \boldsymbol{w} \\ \text{subject} \quad \text{to} \quad & \boldsymbol{C}^H \boldsymbol{w} = \boldsymbol{f}. \end{aligned} \tag{2.25}$$

The solution of the problem in (2.25) is found by the Lagrange multiplier method [61–63]. First, a new Lagrangian formulation is formed by adding the real part of the constraint function $\boldsymbol{C}^H \boldsymbol{w} - \boldsymbol{f}$ to the cost formulation $\boldsymbol{w}^H \boldsymbol{Q}_D \boldsymbol{w}$ in (2.25), given by

$$G_{LS_D} = \boldsymbol{w}^H \boldsymbol{Q}_D \boldsymbol{w} + \boldsymbol{K}^H (\boldsymbol{C}^H \boldsymbol{w} - \boldsymbol{f}) + \boldsymbol{K}^T (\boldsymbol{C}^T \boldsymbol{w}^* - \boldsymbol{f}^*), \tag{2.26}$$

where $\boldsymbol{K}$ denotes the Lagrange multiplier. Note that the gradient of the constraint function formed by the second and third terms in (2.26) must be linearly independent between each other for the Lagrange multiplier to hold. This means the columns of $\boldsymbol{C}$ should be full-rank. Thus, weighting coefficients $\boldsymbol{w}$ can be obtained by taking the gradient of (2.26) with respect to $\boldsymbol{w}^*$ and then setting it to zero, given by

$$\boldsymbol{w} = -\boldsymbol{Q}_D^{-1} \boldsymbol{C} \boldsymbol{K}. \tag{2.27}$$

Because $\boldsymbol{w}$ should meet the constraint in (2.24), we have

$$-\boldsymbol{C}^H \boldsymbol{Q}_D^{-1} \boldsymbol{C}\boldsymbol{K} = \boldsymbol{f}. \tag{2.28}$$

Hence, the solution of $\boldsymbol{K}$ is given by

$$\boldsymbol{K} = -\left(\boldsymbol{C}^H \boldsymbol{Q}_D^{-1} \boldsymbol{C}\right)^{-1} \boldsymbol{f}. \tag{2.29}$$

By substituting (2.29) into (2.27), the closed-form solution of $\boldsymbol{w}$ is found as following

$$\boldsymbol{w} = \boldsymbol{Q}_D^{-1} \boldsymbol{C} \left(\boldsymbol{C}^H \boldsymbol{Q}_D^{-1} \boldsymbol{C}\right)^{-1} \boldsymbol{f}. \tag{2.30}$$

2.5 Summary

The basics about beamforming and the corresponding design methods, such as the convex optimisation and least squares design methods are reviewed in this chapter. To solve the problem associated with high cost and high power consumption, the hybrid beamforming technique which consists of a combination of analogue and digital beamforming stages is introduced followed by typical architectures of the sub-aperture based beamformer, including the localised and interleaved subarray architectures. The multi-beam multiplexing designs based on the hybrid beamforming structures in different scenarios will be presented in the following chapters.

Chapter 3

Multi-Beam Multiplexing Design Based on Least Squares

3.1 Sub-Aperture Subarray Architectures

The localised and interleaved subarray architectures based on an N-element uniform linear array have been shown in Figures 2.5 and 2.6, respectively, in Chapter 2, where the adjacent antenna spacing for the whole array is d. Suppose the N elements of the ULA are divided into M subarrays. Then, each subarray consists of $N_s = N/M$ antennas with an adjacent antenna spacing $d_m = d$ and $d_m = Md$ for the localised and interleaved subarray architectures, respectively. The corresponding phase shifts between adjacent subarrays are $e^{j2\pi N_s \frac{d}{\lambda} \sin\theta}$ and $e^{j2\pi \frac{d}{\lambda} \sin\theta}$, respectively, where the direction of angle θ is measured from the broadside of the array [64].

3.2 Multi-Beam Multiplexing Design with Direction Constraint

For $m \in \{0, 1, \cdots, M-1\}$, the beam pattern $P_m(\theta, \varphi_m)$ generated by the m-th subarray pointing to the direction φ_m is given by

$$P_m(\theta, \varphi_m) = e^{j2\pi l_m \sin\theta} \sum_{n=0}^{N_s-1} w_{A,m,n}(\varphi_m) e^{j2\pi \frac{d_m}{\lambda} n \sin\theta}, \tag{3.1}$$

where $l_m = m\frac{d}{\lambda}$ denotes the initial location of the m-th subarray in terms of the signal wavelength λ, and $w_{A,m,n}(\varphi_m)$ denotes the analogue weighting coefficient of the n-th antenna of the m-th subarray for the main beam direction pointing to φ_m. Through inter-subarray coding, the M beams are generated by the M-subarray based hybrid beamforming scheme configured by the interleaved subarray architecture. The overall beam pattern using the M subarrays with a main beam in the direction φ_j is

$$\begin{aligned} P(\theta, \varphi_j) &= \sum_{m=0}^{M-1} w_{D,j,m} P_m(\theta, \varphi_m) \\ &= \sum_{m=0}^{M-1} w_{D,j,m} e^{j2\pi l_m \sin\theta} \sum_{n=0}^{N_s-1} w_{A,m,n}(\varphi_m) e^{j2\pi \frac{d_m}{\lambda} n \sin\theta}, \end{aligned} \tag{3.2}$$

where $w_{D,j,m}$ is the digital weighting factor for the m-th subarray.

In [25, 26], the two-user scenario was considered, where there are two subarrays in total ($M = 2$) and two beams are generated by an inter-subarray coding scheme with a linear combination of analogue weighting coefficients for two subarrays. With $d = \frac{\lambda}{2}$, the analogue weighting factors of the zeroth and first subarrays are given by

$$\begin{aligned} w_{A,0,n}(\varphi_0) &= e^{-j2\pi n \sin\varphi_0}, \\ w_{A,1,n}(\varphi_1) &= e^{-j2\pi(n+\frac{1}{2})\sin\varphi_1}, \end{aligned} \tag{3.3}$$

where φ_0 and φ_1 are the desired directions for the zeroth and first users, respectively. This interleaved-subarray beamforming system generates the zeroth user's own beam naturally and the first user's beam in the direction of the zeroth user's grating lobe and vice versa, and as a result, data for the zeroth user is divided in opposite phase and data for the first user is divided in the same phase. Specifically, as proposed in [25, 45], the digital beamformer coefficient vector $\boldsymbol{w}_{D,j} (j \in \{0, 1\})$ can be characterised as follows

$$\begin{aligned} \boldsymbol{w}_{D,0} &= [w_{D,0,0}, w_{D,0,1}] = [1 \quad -1], \\ \boldsymbol{w}_{D,1} &= [w_{D,1,0}, w_{D,1,1}] = [1 \qquad 1]. \end{aligned} \tag{3.4}$$

Finally, the patterns of the zeroth and first beams are given by

$$\begin{aligned} P(\theta, \varphi_0) = &\sum_{n=0}^{N_s-1} e^{j2\pi n(\sin\theta - \sin\varphi_0)} - \\ &\sum_{n=0}^{N_s-1} e^{j2\pi(n+\frac{1}{2})(\sin\theta - \sin\varphi_1)}, \end{aligned} \tag{3.5}$$

$$P(\theta, \varphi_1) = \sum_{n=0}^{N_s-1} e^{j2\pi n(\sin\theta - \sin\varphi_0)} + \sum_{n=0}^{N_s-1} e^{j2\pi(n+\frac{1}{2})(\sin\theta - \sin\varphi_1)}, \tag{3.6}$$

respectively. Ideally (3.5) should form a beam pointing to direction φ_0 while (3.6) forms a beam pointing to direction φ_1. Generally, for a ULA of $2N_s$ antennas with adjacent antenna spacing $d = \frac{\lambda}{2}$, to have a beam pattern with its main beam direction in φ_j, one way is to steer the broadside main beam with uniform weighting as follows,

$$P(\theta, \varphi_j) = \sum_{n=0}^{2N_s-1} e^{j\pi n(\sin\theta - \sin\varphi_j)}. \tag{3.7}$$

The key is to find some appropriate parameters so that (3.5) and (3.6) will be transformed into the form of (3.7) with $j = 0$ and $j = 1$, respectively. To realise this, (3.5) is expanded into the following form

$$P(\theta, \varphi_0) = \sum_{n=0}^{N_s-1} e^{j2\pi n(\sin\theta - \sin\varphi_0)} - \sum_{n=0}^{N_s-1} e^{j\pi(2n+1)(\sin\theta - \sin\varphi_0)} e^{j\pi(2n+1)(\sin\varphi_0 - \sin\varphi_1)}. \tag{3.8}$$

It can be observed that as long as

$$e^{j\pi(\sin\varphi_0 - \sin\varphi_1)} = -1, \tag{3.9}$$

or equivalently

$$|\sin\varphi_0 - \sin\varphi_1| = 1, \tag{3.10}$$

(3.5) and (3.6) will be converted into the form of (3.7) with $j = 0$ and $j = 1$, respectively. Hence, in [26, 45], there is an important limitation to this scheme: the two user directions cannot be arbitrary and have to follow this specific relationship. Although in practice, it is hard to find two user directions meeting exactly this relationship, it theoretically verifies for the first time that it is possible to use a simple hybrid analogue and digital beamforming technique to produce two beams without spatial aliasing.

3.3 Multi-Beam Multiplexing Design with Varying Antenna Spacing

In the following, we try to overcome the restriction of the scheme in [26, 45] and design a new scheme with two interleaved subarrays which can form beams in two arbitrary directions. First, given the simple form of the digital beamformer coefficients $\boldsymbol{w}_{D,0}$ and $\boldsymbol{w}_{D,1}$ in (3.4), they are still adopted in the new scheme. Consider a general ULA with adjacent spacing $d = \alpha\frac{\lambda}{2}$, where α is an coefficient whose value will be determined later. Hence, the adjacent antenna spacing for the m-th subarray is supposed as

$$d_m = Md = M\alpha\frac{\lambda}{2} = \alpha\lambda, \tag{3.11}$$

where $M = 2$ has been used for two subarrays and the initial position l_m of the m-th subarray is

$$l_m = m\frac{d}{\lambda} = m\frac{\alpha}{2}. \tag{3.12}$$

To form a beam to direction φ_j using a ULA of $2N_s$ antennas with adjacent antenna spacing $d = \alpha\frac{\lambda}{2}$, similar to (3.7), the desired beam pattern of the j-th beam can be achieved by beam steering in combination with uniform weighting as follows

$$P(\theta, \varphi_j) = \sum_{n=0}^{2N_s-1} e^{j\alpha\pi n(\sin\theta - \sin\varphi_j)}. \tag{3.13}$$

Moreover, based on (3.2), the new antenna analogue weighting factors for the zeroth and first subarrays can be chosen to compensate for the phase difference corresponding to look directions only with uniform magnitudes as follows

$$\begin{aligned} w_{A,0,n}(\varphi_0) &= e^{-j2\alpha\pi n\sin\varphi_0}, \\ w_{A,1,n}(\varphi_1) &= e^{-j2\alpha\pi(n+\frac{1}{2})\sin\varphi_1}. \end{aligned} \tag{3.14}$$

Then, the designed beam patterns for the zeroth and first beams are given by

$$\begin{aligned} P(\theta, \varphi_0) = &\sum_{n=0}^{N_s-1} e^{j2\alpha\pi n(\sin\theta - \sin\varphi_0)} - \\ &\sum_{n=0}^{N_s-1} e^{j2\alpha\pi(n+\frac{1}{2})(\sin\theta - \sin\varphi_1)}, \end{aligned} \tag{3.15}$$

$$P(\theta,\varphi_1)=\sum_{n=0}^{N_s-1}e^{j2\alpha\pi n(\sin\theta-\sin\varphi_0)}+\sum_{n=0}^{N_s-1}e^{j2\alpha\pi(n+\frac{1}{2})(\sin\theta-\sin\varphi_1)}, \tag{3.16}$$

respectively. To find α, similar to (3.8), we modify (3.15) into

$$P(\theta,\varphi_0)=\sum_{n=0}^{N_s-1}e^{j2\alpha\pi n(\sin\theta-\sin\varphi_0)}-\sum_{n=0}^{N_s-1}e^{j\alpha\pi(2n+1)(\sin\theta-\sin\varphi_0)}e^{j\alpha\pi(2n+1)(\sin\varphi_0-\sin\varphi_1)}. \tag{3.17}$$

For (3.17) to match (3.13) when $j=0$, similar to (3.9), one solution can be obtained by satisfying

$$e^{j\alpha\pi(\sin\varphi_0-\sin\varphi_1)}=-1. \tag{3.18}$$

For arbitrary φ_0 and φ_1, the value of α can then be calculated by

$$\alpha=\frac{1}{|\sin\varphi_0-\sin\varphi_1|}. \tag{3.19}$$

Note that the minimum value of α is $\alpha_{min}=1/2=0.5$ because the angle range of the two required beam directions in $\{\varphi_0,\varphi_1\}\in[-90^\circ,90^\circ]$ results in that the maximum value of $|\sin\varphi_0-\sin\varphi_1|$ is $|\sin\varphi_0-\sin\varphi_1|_{max}=2$.

3.4 Multi-Beam Multiplexing Design with Fixed Antenna Spacing

In many applications, it may not be practical to constantly change the spacing to meet the needs of changing user directions, although this could be solved by performing antenna switching through preparing more antennas at pre-defined candidate locations than necessary for a required beam width. In this section, the beamformer coefficients will be redesigned, while maintaining the adjacent antenna spacing d as a fixed value. Although the approach introduced in this section in general can be applied to arbitrary number of beams with arbitrary directions, it is difficult to have a single general formulation to cover all the cases. As a result, we will only consider the two-beam and three-beam cases

as representative examples and following the same approach, it can be extended to more than three beams without difficulty.

Moreover, as UPAs will be widely used for mmWave communications, we will also consider a design based on UPAs to show that the approach can also be applied to two-dimensional arrays.

3.4.1 Uniform Linear Array for Two Beams

The steering vectors of the m-th interleaved and localised subarrays are given by

$$\boldsymbol{s}_m^I(\theta) = [e^{j2\pi m \frac{d}{\lambda}\sin\theta}, e^{j2\pi(m+M)\frac{d}{\lambda}\sin\theta}, ..., e^{j2\pi(m+M(N_s-1))\frac{d}{\lambda}\sin\theta}]^T, \tag{3.20}$$

and

$$\boldsymbol{s}_m^L(\theta) = [e^{j2\pi m N_s \frac{d}{\lambda}\sin\theta}, e^{j2\pi(mN_s+1)\frac{d}{\lambda}\sin\theta}, ..., e^{j2\pi((m+1)N_s-1)\frac{d}{\lambda}\sin\theta}]^T, \tag{3.21}$$

respectively, with $m \in \{0, 1, ..., M-1\}$. Then, the beam pattern generated by the m-th subarray is

$$P_m(\theta) = \boldsymbol{w}_{A,m}^H \boldsymbol{s}_m(\theta), \tag{3.22}$$

where $\boldsymbol{w}_{A,m}$ denotes the analogue coefficients for the m-th subarray containing corresponding coefficients

$$\boldsymbol{w}_{A,m} = [w_{A,m,0}, w_{A,m,1}, ..., w_{A,m,N_s-1}]^T. \tag{3.23}$$

We employ a general digital coding scheme in the interleaved subarray architecture, whose coefficients for the beam in direction φ_j are given by

$$\boldsymbol{w}_{D,j} = [w_{D,j,0}, w_{D,j,1}, ..., w_{D,j,M-1}], \tag{3.24}$$

where $w_{D,j,0}, w_{D,j,1}, ..., w_{D,j,M-1} (j \in \{0, 1, ..., J-1\})$ are MJ digital coefficients to be determined later. So the designed beam pattern for the beam pointing to direction φ_j in vector form is

$$P_{\varphi_j}(\theta) = \sum_{m=0}^{M-1} w_{D,j,m}^* P_m(\theta) = \sum_{m=0}^{M-1} w_{D,j,m}^* \boldsymbol{w}_{A,m}^H \boldsymbol{s}_m(\theta), \tag{3.25}$$

where $*$ denotes the conjugate operation. The following cost function based on least squares formulation is used in the design [1, 57, 58]

$$J_{LS} = \int_{\theta\in\Theta} F(\theta) \left|H(\theta) - D(\theta)\right|^2 d\theta, \tag{3.26}$$

where Θ denotes the overall angle range of interest, $F(\theta)$ is a positive real weighting function, and $H(\theta)$ and $D(\theta)$ are the designed and desired beam patterns, respectively. In our designs, without loss of generality, we use $F(\theta) = 1 - \beta$ and $D(\theta) = 1$ over the mainlobe region (one single direction) and $F(\theta) = \beta$ and $D(\theta) = 0$ over the sidelobe region for each beam, where $\beta \in (0, 1)$ is the trade-off parameter between the mainlobe and sidelobe regions. To balance the minimisation in the mainlobe and sidelobe regions for J beams, N_g is introduced to represent the number of sample points in the sidelobe region for each beam. A specific cost formulation combining J beams is given by

$$J_{LS} = \sum_{j=0}^{J-1} \left((1-\beta) \sum_{\theta \in \Theta_{main_j}} \left| P_{\varphi_j}(\theta) - 1 \right|^2 + \frac{\beta}{N_g} \sum_{\theta \in \Theta_{side_j}} \left| P_{\varphi_j}(\theta) \right|^2 \right), \tag{3.27}$$

where Θ_{side_j} and Θ_{main_j} denote the sidelobe and mainlobe regions, respectively, for the j-th beam. Substituting (3.25) into (3.27) with $J = 2$, the cost function J_{LS} can be rewritten as

$$\begin{aligned} J_{LS} = \sum_{J=0}^{1} \Bigg(& (1-\beta) \sum_{\theta \in \Theta_{main_j}} \left| w_{D,j,0}^* \boldsymbol{w}_{A,0}^H \boldsymbol{s}_0(\theta) + w_{D,j,1}^* \boldsymbol{w}_{A,1}^H \boldsymbol{s}_1(\theta) - 1 \right|^2 \\ & + \frac{\beta}{N_g} \sum_{\theta \in \Theta_{side_j}} \left| w_{D,j,0}^* \boldsymbol{w}_{A,0}^H \boldsymbol{s}_0(\theta) + w_{D,j,1}^* \boldsymbol{w}_{A,1}^H \boldsymbol{s}_1(\theta) \right|^2 \Bigg), \end{aligned} \tag{3.28}$$

which can be expanded as

$$\begin{aligned} J_{LS} = \sum_{j=0}^{1} \Big(& w_{D,j,0}^* \boldsymbol{w}_{A,0}^H \boldsymbol{Q}_{LS_{j0}} \boldsymbol{w}_{A,0} w_{D,j,0} + w_{D,j,1}^* \boldsymbol{w}_{A,1}^H \boldsymbol{Q}_{LS_{j1}} \boldsymbol{w}_{A,1} w_{D,j,1} \\ & + w_{D,j,0}^* \boldsymbol{w}_{A,0}^H \boldsymbol{P}_{LS_{j0}} \boldsymbol{w}_{A,1} w_{D,j,1} + w_{D,j,1}^* \boldsymbol{w}_{A,1}^H \boldsymbol{P}_{LS_{j1}} \boldsymbol{w}_{A,0} w_{D,j,0} \\ & - (w_{D,j,0}^* \boldsymbol{w}_{A,0}^H \boldsymbol{z}_{LS_{j0}} + \boldsymbol{z}_{LS_{j0}}^H \boldsymbol{w}_{A,0} w_{D,j,0}) \\ & - (w_{D,j,1}^* \boldsymbol{w}_{A,1}^H \boldsymbol{z}_{LS_{j1}} + \boldsymbol{z}_{LS_{j1}}^H \boldsymbol{w}_{A,1} w_{D,j,1}) \\ & + d_{LS_j} \Big), \end{aligned} \tag{3.29}$$

with

$$\boldsymbol{Q}_{LS_{jm}} = (1-\beta) \sum_{\theta \in \Theta_{main_j}} \boldsymbol{S}_m(\theta) + \frac{\beta}{N_g} \sum_{\theta \in \Theta_{side_j}} \boldsymbol{S}_m(\theta), \tag{3.30}$$

$$\boldsymbol{P}_{LS_{j0}} = (1-\beta) \sum_{\theta \in \Theta_{main_j}} \boldsymbol{s}_0(\theta) \boldsymbol{s}_1(\theta)^H + \frac{\beta}{N_g} \sum_{\theta \in \Theta_{side_j}} \boldsymbol{s}_0(\theta) \boldsymbol{s}_1(\theta)^H, \tag{3.31}$$

$$\boldsymbol{P}_{LS_{j1}} = (1-\beta) \sum_{\theta \in \Theta_{main_j}} \boldsymbol{s}_1(\theta)\boldsymbol{s}_0(\theta)^H + \frac{\beta}{N_g} \sum_{\theta \in \Theta_{side_j}} \boldsymbol{s}_1(\theta)\boldsymbol{s}_0(\theta)^H, \tag{3.32}$$

$$\boldsymbol{z}_{LS_{jm}} = (1-\beta) \sum_{\theta \in \Theta_{main_j}} \boldsymbol{s}_m(\theta), \tag{3.33}$$

$$d_{LS_j} = (1-\beta) \sum_{\theta \in \Theta_{main_j}} 1, \tag{3.34}$$

$$\boldsymbol{S}_m(\theta) = \boldsymbol{s}_m(\theta)\boldsymbol{s}_m(\theta)^H, \tag{3.35}$$

where $\{j, m\} \in \{0, 1\}$. Combining the analogue coefficients $\boldsymbol{w}_{A,0}$ and $\boldsymbol{w}_{A,1}$ into one vector, given by

$$\boldsymbol{w}_A = \left[\boldsymbol{w}_{A,0}^T, \boldsymbol{w}_{A,1}^T\right]^T, \tag{3.36}$$

equation (3.29) can be rewritten as

$$J_{LS} = \boldsymbol{w}_A^H \left(\boldsymbol{Q}_{LS} + \boldsymbol{P}_{LS}\tilde{\boldsymbol{I}}_0\right) \boldsymbol{w}_A - \boldsymbol{w}_A^H \boldsymbol{z}_{LS} - \boldsymbol{z}_{LS}^H \boldsymbol{w}_A + d_{LS0} + d_{LS1}, \tag{3.37}$$

with

$$\boldsymbol{Q}_{LS} = \begin{bmatrix} \boldsymbol{G}_{LS_0} & \boldsymbol{0}_{N_s} \\ \boldsymbol{0}_{N_s} & \boldsymbol{G}_{LS_1} \end{bmatrix}, \boldsymbol{P}_{LS} = \begin{bmatrix} \boldsymbol{H}_{LS_0} & \boldsymbol{0}_{N_s} \\ \boldsymbol{0}_{N_s} & \boldsymbol{H}_{LS_1} \end{bmatrix}, \tag{3.38}$$

$$\tilde{\boldsymbol{I}}_0 = \begin{bmatrix} \boldsymbol{0}_{N_s} & \boldsymbol{I}_{N_s} \\ \boldsymbol{I}_{N_s} & \boldsymbol{0}_{N_s} \end{bmatrix}, \tag{3.39}$$

$$\boldsymbol{z}_{LS} = \begin{bmatrix} \boldsymbol{w}_{D,0,0}^H \boldsymbol{z}_{LS_{00}} + \boldsymbol{w}_{D,1,0}^H \boldsymbol{z}_{LS_{10}} \\ \boldsymbol{w}_{D,0,1}^H \boldsymbol{z}_{LS_{01}} + \boldsymbol{w}_{D,1,1}^H \boldsymbol{z}_{LS_{11}} \end{bmatrix}, \tag{3.40}$$

$$\boldsymbol{G}_{LS_m} = \boldsymbol{w}_{D,0,m}^H \boldsymbol{Q}_{LS_{0m}} \boldsymbol{w}_{D,0,m} + \boldsymbol{w}_{D,1,m}^H \boldsymbol{Q}_{LS_{1m}} \boldsymbol{w}_{D,1,m}, \tag{3.41}$$

$$\begin{aligned} \boldsymbol{H}_{LS_0} &= \boldsymbol{w}_{D,0,0}^H \boldsymbol{P}_{LS_{00}} \boldsymbol{w}_{D,0,1} + \boldsymbol{w}_{D,1,0}^H \boldsymbol{P}_{LS_{10}} \boldsymbol{w}_{D,1,1}, \\ \boldsymbol{H}_{LS_1} &= \boldsymbol{w}_{D,0,1}^H \boldsymbol{P}_{LS_{01}} \boldsymbol{w}_{D,0,0} + \boldsymbol{w}_{D,1,1}^H \boldsymbol{P}_{LS_{11}} \boldsymbol{w}_{D,1,0}, \end{aligned} \tag{3.42}$$

$$\boldsymbol{w}_{D,j,m} = w_{D,j,m} \boldsymbol{I}_{N_s}, \tag{3.43}$$

where $\boldsymbol{0}_{N_s}$ and $\boldsymbol{I}_{N_s}$ are $N_s \times N_s$ all-zero and identity matrices, respectively. For a given set of $w_{D,j,m}(\{j, m\} \in \{0, 1\})$, $\boldsymbol{w}_A$ can be obtained by taking the gradient of the cost function in (3.37) with respect to $\boldsymbol{w}_A^H$ and then setting it to zero, given by

$$\boldsymbol{w}_A = \left(\boldsymbol{Q}_{LS} + \boldsymbol{P}_{LS}\tilde{\boldsymbol{I}}_0\right)^{-1} \boldsymbol{z}_{LS}. \tag{3.44}$$

On the other hand, if we know the analogue coefficients $\boldsymbol{w}_A$ already, we can obtain the optimum digital coding coefficients as follows.

Similar to (3.36), combining the digital coefficients for the two beams into one vector

$$\boldsymbol{w}_D = \left[\boldsymbol{w}_{D,0}, \boldsymbol{w}_{D,1}\right]^T = \left[w_{D,0,0}, w_{D,0,1}, w_{D,1,0}, w_{D,1,1}\right]^T, \tag{3.45}$$

equation (3.29) can be rewritten as

$$J_{LS} = \boldsymbol{w}_D^H \left(\tilde{\boldsymbol{Q}}_{LS} + \tilde{\boldsymbol{P}}_{LS}\tilde{\boldsymbol{I}}_1\right)\boldsymbol{w}_D - \boldsymbol{w}_D^H \tilde{\boldsymbol{z}}_{LS} - \tilde{\boldsymbol{z}}_{LS}^H \boldsymbol{w}_D + d_{LS0} + d_{LS1}, \tag{3.46}$$

with

$$\tilde{\boldsymbol{Q}}_{LS} = \begin{bmatrix} \tilde{\boldsymbol{G}}_{LS_{00}} & 0 & 0 & 0 \\ 0 & \tilde{\boldsymbol{G}}_{LS_{01}} & 0 & 0 \\ 0 & 0 & \tilde{\boldsymbol{G}}_{LS_{10}} & 0 \\ 0 & 0 & 0 & \tilde{\boldsymbol{G}}_{LS_{11}} \end{bmatrix}, \tilde{\boldsymbol{P}}_{LS} = \begin{bmatrix} \tilde{\boldsymbol{H}}_{LS_0} & \boldsymbol{0}_2 \\ \boldsymbol{0}_2 & \tilde{\boldsymbol{H}}_{LS_1} \end{bmatrix}, \tag{3.47}$$

$$\tilde{\boldsymbol{I}}_1 = \begin{bmatrix} 0 & 1 & 0 & 0 \\ 1 & 0 & 0 & 0 \\ 0 & 0 & 0 & 1 \\ 0 & 0 & 1 & 0 \end{bmatrix}, \tag{3.48}$$

$$\tilde{\boldsymbol{z}}_{LS} = \left[\boldsymbol{w}_A^H \ddot{\boldsymbol{z}}_{LS_{00}}, \boldsymbol{w}_A^H \ddot{\boldsymbol{z}}_{LS_{01}}, \boldsymbol{w}_A^H \ddot{\boldsymbol{z}}_{LS_{10}}, \boldsymbol{w}_A^H \ddot{\boldsymbol{z}}_{LS_{11}}\right]^T, \tag{3.49}$$

$$\tilde{\boldsymbol{G}}_{LS_{jm}} = \boldsymbol{w}_A^H \ddot{\boldsymbol{Q}}_{LS_{jm}} \boldsymbol{w}_A, \tilde{\boldsymbol{H}}_{LS_j} = \begin{bmatrix} \tilde{\boldsymbol{B}}_{LS_{j0}} & 0 \\ 0 & \tilde{\boldsymbol{B}}_{LS_{j1}} \end{bmatrix}, \tag{3.50}$$

$$\ddot{\boldsymbol{Q}}_{LS_{j0}} = \begin{bmatrix} \boldsymbol{Q}_{LS_{j0}} & \boldsymbol{0}_{N_s} \\ \boldsymbol{0}_{N_s} & \boldsymbol{0}_{N_s} \end{bmatrix}, \ddot{\boldsymbol{Q}}_{LS_{j1}} = \begin{bmatrix} \boldsymbol{0}_{N_s} & \boldsymbol{0}_{N_s} \\ \boldsymbol{0}_{N_s} & \boldsymbol{Q}_{LS_{j1}} \end{bmatrix}, \tag{3.51}$$

$$\tilde{\boldsymbol{B}}_{LS_{jm}} = \boldsymbol{w}_A^H \ddot{\boldsymbol{P}}_{LS_{jm}} \tilde{\boldsymbol{I}}_0 \boldsymbol{w}_A, \tag{3.52}$$

$$\ddot{\boldsymbol{P}}_{LS_{j0}} = \begin{bmatrix} \boldsymbol{P}_{LS_{j0}} & \boldsymbol{0}_{N_s} \\ \boldsymbol{0}_{N_s} & \boldsymbol{0}_{N_s} \end{bmatrix}, \ddot{\boldsymbol{P}}_{LS_{j1}} = \begin{bmatrix} \boldsymbol{0}_{N_s} & \boldsymbol{0}_{N_s} \\ \boldsymbol{0}_{N_s} & \boldsymbol{P}_{LS_{j1}} \end{bmatrix}, \tag{3.53}$$

$$\ddot{\boldsymbol{z}}_{LS_{j0}} = \begin{bmatrix} \boldsymbol{z}_{LS_{j0}} \\ \boldsymbol{0}_{N_s \times 1} \end{bmatrix}, \ddot{\boldsymbol{z}}_{LS_{j1}} = \begin{bmatrix} \boldsymbol{0}_{N_s \times 1} \\ \boldsymbol{z}_{LS_{j1}} \end{bmatrix}, \tag{3.54}$$

where $\boldsymbol{0}_2$ in (3.47) is a 2×2 all-zero matrix and $\boldsymbol{0}_{N_s \times 1}$ in (3.54) is an $N_s \times 1$ all-zero matrix. Given the obtained values of $\boldsymbol{w}_A$ in (3.44), $\boldsymbol{w}_D$ can be obtained by taking the gradient of the cost function in (3.46) with respect to $\boldsymbol{w}_D^H$ and then setting it to zero, given by

$$\boldsymbol{w}_D = \left(\tilde{\boldsymbol{Q}}_{LS} + \tilde{\boldsymbol{P}}_{LS} \tilde{\boldsymbol{I}}_1 \right)^{-1} \tilde{\boldsymbol{z}}_{LS}. \tag{3.55}$$

Alternate optimisation of the digital coefficients $\boldsymbol{w}_D$ and the corresponding analogue coefficients $\boldsymbol{w}_A$ can be achieved by the following iterative process:

(1) First, via initialising the digital coefficients $w_{D,0,0} = 1$, $w_{D,0,1} = -1$, $w_{D,1,0} = 1$, and $w_{D,1,1} = 1$, as in [25], the values of $\boldsymbol{w}_A$ are obtained by substituting $w_{D,0,0}$, $w_{D,0,1}$, $w_{D,1,0}$, and $w_{D,1,1}$ into (3.44).

(2) Given the obtained values of $\boldsymbol{w}_A$ in step (1), the closed-form solution of digital coefficients $\boldsymbol{w}_D$ is obtained by (3.55).

(3) Given the obtained values of $\boldsymbol{w}_D$ in step (2), the new set of values of $\boldsymbol{w}_A$ can be obtained by (3.44) again.

(4) Repeat the steps (2) and (3) until the cost function (3.44) converges. The final digital coefficients $\boldsymbol{w}_D$ and the corresponding analogue coefficients $\boldsymbol{w}_A$ are then obtained.

The convergence of the above iterative process is guaranteed. To see this, we use $J_{LS}(\boldsymbol{w}_A, \boldsymbol{w}_D)$ to represent the whole cost function. An important property of the cost function is that when $\boldsymbol{w}_A$ is fixed, $J_{LS}(\boldsymbol{w}_A, \boldsymbol{w}_D)$ is a convex function, while when $\boldsymbol{w}_D$ is fixed, $J_{LS}(\boldsymbol{w}_A, \boldsymbol{w}_D)$ is a convex function. As a result, at each iteration, given an optimised $\boldsymbol{w}_D$ in the last round, the newly optimised $\boldsymbol{w}_A$ will at least not increase the value of the cost function, while given an optimised $\boldsymbol{w}_A$ in the last round, the newly optimised $\boldsymbol{w}_D$ will at least not increase the value of the cost function, i.e., the cost function will not increase during the alternate optimisation process.

3.4.2 Uniform Linear Array for Three Beams

In this section, consider the case of $M = J = 3$. The steering vectors of the m-th interleaved and localised subarrays are given by (3.20) and (3.21), respectively, with $m \in$

$\{0,1,2\}$. Then, the digital coefficients (3.24) for the beam in direction φ_j change to

$$\boldsymbol{w}_{D,j} = [w_{D,j,0}, w_{D,j,1}, w_{D,j,2}], \tag{3.56}$$

with $j \in \{0,1,2\}$. Thus, the designed beam pattern for the beam pointing to direction φ_j changes to

$$\begin{aligned} P_{\varphi_j}(\theta) &= w^*_{D,j,0} P_0(\theta) + w^*_{D,j,1} P_1(\theta) + w^*_{D,j,2} P_2(\theta) \\ &= w^*_{D,j,0} \boldsymbol{w}^H_{A,0} \boldsymbol{s}_0(\theta) + w^*_{D,j,1} \boldsymbol{w}^H_{A,1} \boldsymbol{s}_1(\theta) + w^*_{D,j,2} \boldsymbol{w}^H_{A,2} \boldsymbol{s}_2(\theta). \end{aligned} \tag{3.57}$$

Similar to (3.29), the cost function J_{LS} combining the above three beams is given by

$$\begin{aligned} J_{LS} = \sum_{j=0}^{2} \Big(& w^*_{D,j,0} \boldsymbol{w}^H_{A,0} \boldsymbol{Q}_{LS_{j0}} \boldsymbol{w}_{A,0} w_{D,j,0} + w^*_{D,j,1} \boldsymbol{w}^H_{A,1} \boldsymbol{Q}_{LS_{j1}} \boldsymbol{w}_{A,1} w_{D,j,1} \\ & + w^*_{D,j,2} \boldsymbol{w}^H_{A,2} \boldsymbol{Q}_{LS_{j2}} \boldsymbol{w}_{A,2} w_{D,j,2} \\ & + w^*_{D,j,0} \boldsymbol{w}^H_{A,0} \boldsymbol{P}_{LS_{01j}} \boldsymbol{w}_{A,1} w_{D,j,1} + w^*_{D,j,1} \boldsymbol{w}^H_{A,1} \boldsymbol{P}_{LS_{10j}} \boldsymbol{w}_{A,0} w_{D,j,0} \\ & + w^*_{D,j,0} \boldsymbol{w}^H_{A,0} \boldsymbol{P}_{LS_{02j}} \boldsymbol{w}_{A,2} w_{D,j,2} + w^*_{D,j,2} \boldsymbol{w}^H_{A,2} \boldsymbol{P}_{LS_{20j}} \boldsymbol{w}_{A,0} w_{D,j,0} \\ & + w^*_{D,j,1} \boldsymbol{w}^H_{A,1} \boldsymbol{P}_{LS_{12j}} \boldsymbol{w}_{A,2} w_{D,j,2} + w^*_{D,j,2} \boldsymbol{w}^H_{A,2} \boldsymbol{P}_{LS_{21j}} \boldsymbol{w}_{A,1} w_{D,j,1} \\ & - (w^*_{D,j,0} \boldsymbol{w}^H_{A,0} \boldsymbol{z}_{LS_{j0}} + \boldsymbol{z}^H_{LS_{j0}} \boldsymbol{w}_{A,0} w_{D,j,0}) \\ & - (w^*_{D,j,1} \boldsymbol{w}^H_{A,1} \boldsymbol{z}_{LS_{j1}} + \boldsymbol{z}^H_{LS_{j1}} \boldsymbol{w}_{A,1} w_{D,j,1}) \\ & - (w^*_{D,j,2} \boldsymbol{w}^H_{A,2} \boldsymbol{z}_{LS_{j2}} + \boldsymbol{z}^H_{LS_{j2}} \boldsymbol{w}_{A,2} w_{D,j,2}) + d_{LS_j} \Big), \end{aligned} \tag{3.58}$$

with

$$\boldsymbol{P}_{LS_{ikj}} = (1-\beta) \sum_{\theta \in \Theta_{main_j}} \boldsymbol{s}_i(\theta) \boldsymbol{s}_k(\theta)^H + \frac{\beta}{N_g} \sum_{\theta \in \Theta_{side_j}} \boldsymbol{s}_i(\theta) \boldsymbol{s}_k(\theta)^H, \tag{3.59}$$

$\boldsymbol{Q}_{LS_{jm}}$, $\boldsymbol{z}_{LS_{jm}}$, d_{LS_j} and $\boldsymbol{S}_m(\theta)$ are the same as (3.30), (3.33), (3.34) and (3.35) with $\{m,i,k\} \in \{0,1,2\}$ but $i \neq k$. Similar to (3.36), via combining the analogue coefficients $\boldsymbol{w}_{A,0}$, $\boldsymbol{w}_{A,1}$ and $\boldsymbol{w}_{A,2}$ into one vector, given by

$$\boldsymbol{w}_A = \left[\boldsymbol{w}^T_{A,0}, \boldsymbol{w}^T_{A,1}, \boldsymbol{w}^T_{A,2} \right]^T, \tag{3.60}$$

equation (3.58) can be rewritten as

$$\begin{aligned} J_{LS} = & \boldsymbol{w}^H_A \left(\boldsymbol{Q}_{LS} + \boldsymbol{P}_{LS} \tilde{\boldsymbol{I}}_2 + \boldsymbol{R}_{LS} \tilde{\boldsymbol{I}}_3 \right) \boldsymbol{w}_A - \boldsymbol{w}^H_A \boldsymbol{z}_{LS} \\ & - \boldsymbol{z}^H_{LS} \boldsymbol{w}_A + d_{LS0} + d_{LS1} + d_{LS2}, \end{aligned} \tag{3.61}$$

with

$$\boldsymbol{Q}_{LS} = \begin{bmatrix} \boldsymbol{G}_{LS_0} & \boldsymbol{0}_{N_s} & \boldsymbol{0}_{N_s} \\ \boldsymbol{0}_{N_s} & \boldsymbol{G}_{LS_1} & \boldsymbol{0}_{N_s} \\ \boldsymbol{0}_{N_s} & \boldsymbol{0}_{N_s} & \boldsymbol{G}_{LS_2} \end{bmatrix}, \boldsymbol{P}_{LS} = \begin{bmatrix} \boldsymbol{H}_{LS_0} & \boldsymbol{0}_{N_s} & \boldsymbol{0}_{N_s} \\ \boldsymbol{0}_{N_s} & \boldsymbol{H}_{LS_1} & \boldsymbol{0}_{N_s} \\ \boldsymbol{0}_{N_s} & \boldsymbol{0}_{N_s} & \boldsymbol{H}_{LS_2} \end{bmatrix}, \boldsymbol{R}_{LS} = \begin{bmatrix} \boldsymbol{Y}_{LS_0} & \boldsymbol{0}_{N_s} & \boldsymbol{0}_{N_s} \\ \boldsymbol{0}_{N_s} & \boldsymbol{Y}_{LS_1} & \boldsymbol{0}_{N_s} \\ \boldsymbol{0}_{N_s} & \boldsymbol{0}_{N_s} & \boldsymbol{Y}_{LS_2} \end{bmatrix}, \tag{3.62}$$

$$\tilde{\boldsymbol{I}}_2 = \tilde{\boldsymbol{I}}_3^T = \begin{bmatrix} \boldsymbol{0}_{N_s} & \boldsymbol{I}_{N_s} & \boldsymbol{0}_{N_s} \\ \boldsymbol{0}_{N_s} & \boldsymbol{0}_{N_s} & \boldsymbol{I}_{N_s} \\ \boldsymbol{I}_{N_s} & \boldsymbol{0}_{N_s} & \boldsymbol{0}_{N_s} \end{bmatrix}, \tag{3.63}$$

$$\boldsymbol{z}_{LS} = \begin{bmatrix} \boldsymbol{w}_{D,0,0}^H \boldsymbol{z}_{LS_{00}} + \boldsymbol{w}_{D,1,0}^H \boldsymbol{z}_{LS_{10}} + \boldsymbol{w}_{D,2,0}^H \boldsymbol{z}_{LS_{20}} \\ \boldsymbol{w}_{D,0,1}^H \boldsymbol{z}_{LS_{01}} + \boldsymbol{w}_{D,1,1}^H \boldsymbol{z}_{LS_{11}} + \boldsymbol{w}_{D,2,1}^H \boldsymbol{z}_{LS_{21}} \\ \boldsymbol{w}_{D,0,2}^H \boldsymbol{z}_{LS_{02}} + \boldsymbol{w}_{D,1,2}^H \boldsymbol{z}_{LS_{12}} + \boldsymbol{w}_{D,2,2}^H \boldsymbol{z}_{LS_{22}} \end{bmatrix}, \tag{3.64}$$

$$\boldsymbol{G}_{LS_m} = \boldsymbol{w}_{D,0,m}^H \boldsymbol{Q}_{LS_{0m}} \boldsymbol{w}_{D,0,m} + \boldsymbol{w}_{D,1,m}^H \boldsymbol{Q}_{LS_{1m}} \boldsymbol{w}_{D,1,m} + \boldsymbol{w}_{D,2,m}^H \boldsymbol{Q}_{LS_{2m}} \boldsymbol{w}_{D,2,m}, \tag{3.65}$$

$$\begin{aligned} \boldsymbol{H}_{LS_0} &= \boldsymbol{w}_{D,0,0}^H \boldsymbol{P}_{LS_{010}} \boldsymbol{w}_{D,0,1} + \boldsymbol{w}_{D,1,0}^H \boldsymbol{P}_{LS_{011}} \boldsymbol{w}_{D,1,1} + \boldsymbol{w}_{D,2,0}^H \boldsymbol{P}_{LS_{012}} \boldsymbol{w}_{D,2,1}, \\ \boldsymbol{H}_{LS_1} &= \boldsymbol{w}_{D,0,1}^H \boldsymbol{P}_{LS_{120}} \boldsymbol{w}_{D,0,2} + \boldsymbol{w}_{D,1,1}^H \boldsymbol{P}_{LS_{121}} \boldsymbol{w}_{D,1,2} + \boldsymbol{w}_{D,2,1}^H \boldsymbol{P}_{LS_{122}} \boldsymbol{w}_{D,2,2}, \\ \boldsymbol{H}_{LS_2} &= \boldsymbol{w}_{D,0,2}^H \boldsymbol{P}_{LS_{200}} \boldsymbol{w}_{D,0,0} + \boldsymbol{w}_{D,1,2}^H \boldsymbol{P}_{LS_{201}} \boldsymbol{w}_{D,1,0} + \boldsymbol{w}_{D,2,2}^H \boldsymbol{P}_{LS_{202}} \boldsymbol{w}_{D,2,0}, \end{aligned} \tag{3.66}$$

$$\begin{aligned} \boldsymbol{Y}_{LS_0} &= \boldsymbol{w}_{D,0,0}^H \boldsymbol{P}_{LS_{020}} \boldsymbol{w}_{D,0,2} + \boldsymbol{w}_{D,1,0}^H \boldsymbol{P}_{LS_{021}} \boldsymbol{w}_{D,1,2} + \boldsymbol{w}_{D,2,0}^H \boldsymbol{P}_{LS_{022}} \boldsymbol{w}_{D,2,2}, \\ \boldsymbol{Y}_{LS_1} &= \boldsymbol{w}_{D,0,1}^H \boldsymbol{P}_{LS_{100}} \boldsymbol{w}_{D,0,0} + \boldsymbol{w}_{D,1,1}^H \boldsymbol{P}_{LS_{101}} \boldsymbol{w}_{D,1,0} + \boldsymbol{w}_{D,2,1}^H \boldsymbol{P}_{LS_{102}} \boldsymbol{w}_{D,2,0}, \\ \boldsymbol{Y}_{LS_2} &= \boldsymbol{w}_{D,0,2}^H \boldsymbol{P}_{LS_{210}} \boldsymbol{w}_{D,0,1} + \boldsymbol{w}_{D,1,2}^H \boldsymbol{P}_{LS_{211}} \boldsymbol{w}_{D,1,1} + \boldsymbol{w}_{D,2,2}^H \boldsymbol{P}_{LS_{212}} \boldsymbol{w}_{D,2,1}. \end{aligned} \tag{3.67}$$

Similar to (3.44), for a given set of $w_{D,j,m}(\{j,m\} \in \{0,1,2\})$, $\boldsymbol{w}_A$ can be obtained by

$$\boldsymbol{w}_A = \left(\boldsymbol{Q}_{LS} + \boldsymbol{P}_{LS} \tilde{\boldsymbol{I}}_2 + \boldsymbol{R}_{LS} \tilde{\boldsymbol{I}}_3 \right)^{-1} \boldsymbol{z}_{LS}. \tag{3.68}$$

Combining the digital coefficients for the three beams into one vector

$$\begin{aligned} \boldsymbol{w}_D &= \left[\boldsymbol{w}_{D,0}, \boldsymbol{w}_{D,1}, \boldsymbol{w}_{D,2} \right]^T \\ &= \left[w_{D,0,0}, w_{D,0,1}, w_{D,0,2}, w_{D,1,0}, w_{D,1,1}, w_{D,1,2}, w_{D,2,0}, w_{D,2,1}, w_{D,2,2} \right]^T, \end{aligned} \tag{3.69}$$

(3.58) can be written

$$\begin{aligned} J_{LS} = \boldsymbol{w}_D^H \left(\tilde{\boldsymbol{Q}}_{LS} + \tilde{\boldsymbol{P}}_{LS} \tilde{\boldsymbol{I}}_4 + \tilde{\boldsymbol{R}}_{LS} \tilde{\boldsymbol{I}}_5 \right) \boldsymbol{w}_D - \boldsymbol{w}_D^H \tilde{\boldsymbol{z}}_{LS} \\ - \tilde{\boldsymbol{z}}_{LS}^H \boldsymbol{w}_D + d_{LS0} + d_{LS1} + d_{LS2}, \end{aligned} \tag{3.70}$$

with

$$\tilde{\boldsymbol{Q}}_{LS} = \begin{bmatrix} \tilde{\boldsymbol{G}}_{LS_{00}} & 0 & \cdots & 0 \\ 0 & \tilde{\boldsymbol{G}}_{LS_{01}} & \ddots & \vdots \\ \vdots & \ddots & \ddots & 0 \\ 0 & \cdots & 0 & \tilde{\boldsymbol{G}}_{LS_{22}} \end{bmatrix}, \tilde{\boldsymbol{P}}_{LS} = \begin{bmatrix} \tilde{\boldsymbol{H}}_{LS_0} & \boldsymbol{0}_3 & \boldsymbol{0}_3 \\ \boldsymbol{0}_3 & \tilde{\boldsymbol{H}}_{LS_1} & \boldsymbol{0}_3 \\ \boldsymbol{0}_3 & \boldsymbol{0}_3 & \tilde{\boldsymbol{H}}_{LS_2} \end{bmatrix}, \tilde{\boldsymbol{R}}_{LS} = \begin{bmatrix} \tilde{\boldsymbol{Y}}_{LS_0} & \boldsymbol{0}_3 & \boldsymbol{0}_3 \\ \boldsymbol{0}_3 & \tilde{\boldsymbol{Y}}_{LS_1} & \boldsymbol{0}_3 \\ \boldsymbol{0}_3 & \boldsymbol{0}_3 & \tilde{\boldsymbol{Y}}_{LS_2} \end{bmatrix}, \tag{3.71}$$

$$\tilde{\boldsymbol{I}}_4 = \tilde{\boldsymbol{I}}_5^T = \begin{bmatrix} 0 & 1 & 0 & 0 & 0 & 0 & 0 & 0 & 0 \\ 0 & 0 & 1 & 0 & 0 & 0 & 0 & 0 & 0 \\ 1 & 0 & 0 & 0 & 0 & 0 & 0 & 0 & 0 \\ 0 & 0 & 0 & 0 & 1 & 0 & 0 & 0 & 0 \\ 0 & 0 & 0 & 0 & 0 & 1 & 0 & 0 & 0 \\ 0 & 0 & 0 & 1 & 0 & 0 & 0 & 0 & 0 \\ 0 & 0 & 0 & 0 & 0 & 0 & 0 & 1 & 0 \\ 0 & 0 & 0 & 0 & 0 & 0 & 0 & 0 & 1 \\ 0 & 0 & 0 & 0 & 0 & 0 & 1 & 0 & 0 \end{bmatrix}, \tag{3.72}$$

$$\tilde{\boldsymbol{z}}_{LS} = \left[\boldsymbol{w}_A^H \ddot{\boldsymbol{z}}_{LS_{00}}, \boldsymbol{w}_A^H \ddot{\boldsymbol{z}}_{LS_{01}}, \boldsymbol{w}_A^H \ddot{\boldsymbol{z}}_{LS_{02}}, \boldsymbol{w}_A^H \ddot{\boldsymbol{z}}_{LS_{10}}, \boldsymbol{w}_A^H \ddot{\boldsymbol{z}}_{LS_{11}}, \boldsymbol{w}_A^H \ddot{\boldsymbol{z}}_{LS_{12}}, \boldsymbol{w}_A^H \ddot{\boldsymbol{z}}_{LS_{20}}, \boldsymbol{w}_A^H \ddot{\boldsymbol{z}}_{LS_{21}}, \boldsymbol{w}_A^H \ddot{\boldsymbol{z}}_{LS_{22}} \right]^T, \tag{3.73}$$

$$\tilde{\boldsymbol{H}}_{LS_j} = \begin{bmatrix} \tilde{\boldsymbol{B}}_{LS_{j0}} & 0 & 0 \\ 0 & \tilde{\boldsymbol{B}}_{LS_{j1}} & 0 \\ 0 & 0 & \tilde{\boldsymbol{B}}_{LS_{j2}} \end{bmatrix}, \tilde{\boldsymbol{Y}}_{LS_j} = \begin{bmatrix} \tilde{\boldsymbol{D}}_{LS_{j0}} & 0 & 0 \\ 0 & \tilde{\boldsymbol{D}}_{LS_{j1}} & 0 \\ 0 & 0 & \tilde{\boldsymbol{D}}_{LS_{j2}} \end{bmatrix}, \tag{3.74}$$

$$\ddot{\boldsymbol{z}}_{LS_{j0}} = \begin{bmatrix} \boldsymbol{z}_{LS_{j0}} \\ \boldsymbol{0}_{N_s \times 1} \\ \boldsymbol{0}_{N_s \times 1} \end{bmatrix}, \ddot{\boldsymbol{z}}_{LS_{j1}} = \begin{bmatrix} \boldsymbol{0}_{N_s \times 1} \\ \boldsymbol{z}_{LS_{j1}} \\ \boldsymbol{0}_{N_s \times 1} \end{bmatrix}, \ddot{\boldsymbol{z}}_{LS_{j2}} = \begin{bmatrix} \boldsymbol{0}_{N_s \times 1} \\ \boldsymbol{0}_{N_s \times 1} \\ \boldsymbol{z}_{LS_{j2}} \end{bmatrix}, \tag{3.75}$$

$$\ddot{\boldsymbol{Q}}_{LS_{j0}} = \begin{bmatrix} \boldsymbol{Q}_{LS_{j0}} & \boldsymbol{0}_{N_s} & \boldsymbol{0}_{N_s} \\ \boldsymbol{0}_{N_s} & \boldsymbol{0}_{N_s} & \boldsymbol{0}_{N_s} \\ \boldsymbol{0}_{N_s} & \boldsymbol{0}_{N_s} & \boldsymbol{0}_{N_s} \end{bmatrix}, \ddot{\boldsymbol{Q}}_{LS_{j1}} = \begin{bmatrix} \boldsymbol{0}_{N_s} & \boldsymbol{0}_{N_s} & \boldsymbol{0}_{N_s} \\ \boldsymbol{0}_{N_s} & \boldsymbol{Q}_{LS_{j1}} & \boldsymbol{0}_{N_s} \\ \boldsymbol{0}_{N_s} & \boldsymbol{0}_{N_s} & \boldsymbol{0}_{N_s} \end{bmatrix}, \ddot{\boldsymbol{Q}}_{LS_{j2}} = \begin{bmatrix} \boldsymbol{0}_{N_s} & \boldsymbol{0}_{N_s} & \boldsymbol{0}_{N_s} \\ \boldsymbol{0}_{N_s} & \boldsymbol{0}_{N_s} & \boldsymbol{0}_{N_s} \\ \boldsymbol{0}_{N_s} & \boldsymbol{0}_{N_s} & \boldsymbol{Q}_{LS_{j2}} \end{bmatrix}, \tag{3.76}$$

$$\begin{aligned} \tilde{\boldsymbol{B}}_{LS_{j0}} &= \boldsymbol{w}_A^H \ddot{\boldsymbol{P}}_{LS_{j0}} \tilde{\boldsymbol{I}}_6 \boldsymbol{w}_A, \quad \tilde{\boldsymbol{D}}_{LS_{j0}} = \boldsymbol{w}_A^H \ddot{\boldsymbol{R}}_{LS_{j0}} \tilde{\boldsymbol{I}}_3 \boldsymbol{w}_A, \\ \tilde{\boldsymbol{B}}_{LS_{j1}} &= \boldsymbol{w}_A^H \ddot{\boldsymbol{P}}_{LS_{j1}} \tilde{\boldsymbol{I}}_7 \boldsymbol{w}_A, \quad \tilde{\boldsymbol{D}}_{LS_{j1}} = \boldsymbol{w}_A^H \ddot{\boldsymbol{R}}_{LS_{j1}} \tilde{\boldsymbol{I}}_6 \boldsymbol{w}_A, \\ \tilde{\boldsymbol{B}}_{LS_{j2}} &= \boldsymbol{w}_A^H \ddot{\boldsymbol{P}}_{LS_{j2}} \tilde{\boldsymbol{I}}_2 \boldsymbol{w}_A, \quad \tilde{\boldsymbol{D}}_{LS_{j2}} = \boldsymbol{w}_A^H \ddot{\boldsymbol{R}}_{LS_{j2}} \tilde{\boldsymbol{I}}_7 \boldsymbol{w}_A, \end{aligned} \tag{3.77}$$

$$\ddot{\boldsymbol{P}}_{LS_{j0}} = \begin{bmatrix} \boldsymbol{P}_{LS_{01j}} & \boldsymbol{0}_{N_s} & \boldsymbol{0}_{N_s} \\ \boldsymbol{0}_{N_s} & \boldsymbol{0}_{N_s} & \boldsymbol{0}_{N_s} \\ \boldsymbol{0}_{N_s} & \boldsymbol{0}_{N_s} & \boldsymbol{0}_{N_s} \end{bmatrix}, \ddot{\boldsymbol{P}}_{LS_{j1}} = \begin{bmatrix} \boldsymbol{0}_{N_s} & \boldsymbol{0}_{N_s} & \boldsymbol{0}_{N_s} \\ \boldsymbol{0}_{N_s} & \boldsymbol{P}_{LS_{12j}} & \boldsymbol{0}_{N_s} \\ \boldsymbol{0}_{N_s} & \boldsymbol{0}_{N_s} & \boldsymbol{0}_{N_s} \end{bmatrix}, \ddot{\boldsymbol{P}}_{LS_{j2}} = \begin{bmatrix} \boldsymbol{0}_{N_s} & \boldsymbol{0}_{N_s} & \boldsymbol{0}_{N_s} \\ \boldsymbol{0}_{N_s} & \boldsymbol{0}_{N_s} & \boldsymbol{0}_{N_s} \\ \boldsymbol{0}_{N_s} & \boldsymbol{0}_{N_s} & \boldsymbol{P}_{LS_{20j}} \end{bmatrix}, \tag{3.78}$$

$$\ddot{\boldsymbol{R}}_{LS_{j0}} = \begin{bmatrix} \boldsymbol{P}_{LS_{02j}} & \boldsymbol{0}_{N_s} & \boldsymbol{0}_{N_s} \\ \boldsymbol{0}_{N_s} & \boldsymbol{0}_{N_s} & \boldsymbol{0}_{N_s} \\ \boldsymbol{0}_{N_s} & \boldsymbol{0}_{N_s} & \boldsymbol{0}_{N_s} \end{bmatrix}, \ddot{\boldsymbol{R}}_{LS_{j1}} = \begin{bmatrix} \boldsymbol{0}_{N_s} & \boldsymbol{0}_{N_s} & \boldsymbol{0}_{N_s} \\ \boldsymbol{0}_{N_s} & \boldsymbol{P}_{LS_{10j}} & \boldsymbol{0}_{N_s} \\ \boldsymbol{0}_{N_s} & \boldsymbol{0}_{N_s} & \boldsymbol{0}_{N_s} \end{bmatrix}, \ddot{\boldsymbol{R}}_{LS_{j2}} = \begin{bmatrix} \boldsymbol{0}_{N_s} & \boldsymbol{0}_{N_s} & \boldsymbol{0}_{N_s} \\ \boldsymbol{0}_{N_s} & \boldsymbol{0}_{N_s} & \boldsymbol{0}_{N_s} \\ \boldsymbol{0}_{N_s} & \boldsymbol{0}_{N_s} & \boldsymbol{P}_{LS_{21j}} \end{bmatrix}, \tag{3.79}$$

$$\tilde{\boldsymbol{I}}_6 = \begin{bmatrix} \boldsymbol{0}_{N_s} & \boldsymbol{I}_{N_s} & \boldsymbol{0}_{N_s} \\ \boldsymbol{I}_{N_s} & \boldsymbol{0}_{N_s} & \boldsymbol{0}_{N_s} \\ \boldsymbol{0}_{N_s} & \boldsymbol{0}_{N_s} & \boldsymbol{I}_{N_s} \end{bmatrix}, \tag{3.80}$$

$$\tilde{\boldsymbol{I}}_7 = \begin{bmatrix} \boldsymbol{I}_{N_s} & \boldsymbol{0}_{N_s} & \boldsymbol{0}_{N_s} \\ \boldsymbol{0}_{N_s} & \boldsymbol{0}_{N_s} & \boldsymbol{I}_{N_s} \\ \boldsymbol{0}_{N_s} & \boldsymbol{I}_{N_s} & \boldsymbol{0}_{N_s} \end{bmatrix}, \tag{3.81}$$

where $\tilde{\boldsymbol{G}}_{LS_{jm}}$ is given by (3.50) and $\boldsymbol{0}_3$ in (3.71) is a 3×3 all-zero matrix. Given the obtained values of $\boldsymbol{w}_A$ in (3.68), $\boldsymbol{w}_D$ can be obtained by taking the gradient of the cost function in (3.70) with respect to $\boldsymbol{w}_D^H$ and then setting it to zero, given by

$$\boldsymbol{w}_D = \left(\tilde{\boldsymbol{Q}}_{LS} + \tilde{\boldsymbol{P}}_{LS} \tilde{\boldsymbol{I}}_4 + \tilde{\boldsymbol{R}}_{LS} \tilde{\boldsymbol{I}}_5 \right)^{-1} \tilde{\boldsymbol{z}}_{LS}. \tag{3.82}$$

Alternate optimisation of the digital coefficients $\boldsymbol{w}_D$ and the corresponding analogue coefficients $\boldsymbol{w}_A$ can be achieved by the following iterative process:

(1) First, via initialising the digital coefficients $w_{D,0,0} = w_{D,0,1} = w_{D,1,0} = w_{D,1,2} = w_{D,2,0} = w_{D,2,1} = w_{D,2,2} = 1$ and $w_{D,0,2} = w_{D,1,1} = -1$, the values of $\boldsymbol{w}_A$ are obtained by substituting $w_{D,j,m} (\{j, m\} \in \{0, 1, 2\})$ into (3.68).

(2) Given the obtained values of $\boldsymbol{w}_A$ in step (1), the closed-form solution of digital coefficients $\boldsymbol{w}_D$ is given by (3.82).

(3) Given the obtained values of $\boldsymbol{w}_D$ in step (2), the new set of values of $\boldsymbol{w}_A$ can be obtained by (3.68) again.

(4) Repeat the steps (2) and (3) until the cost function (3.68) converges.

3.4.3 Uniform Planar Array for Two Beams

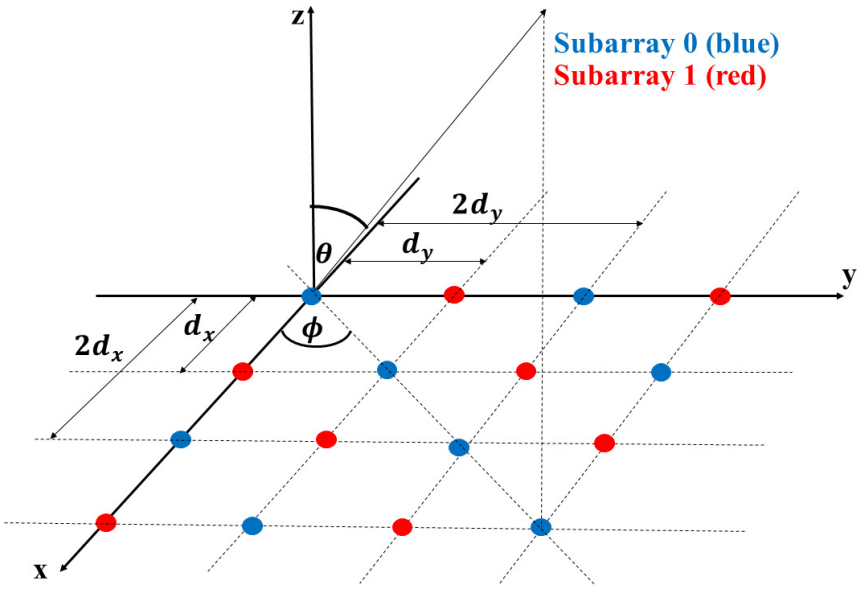

Figure 3.1: A UPA with the interleaved subarray architecture.

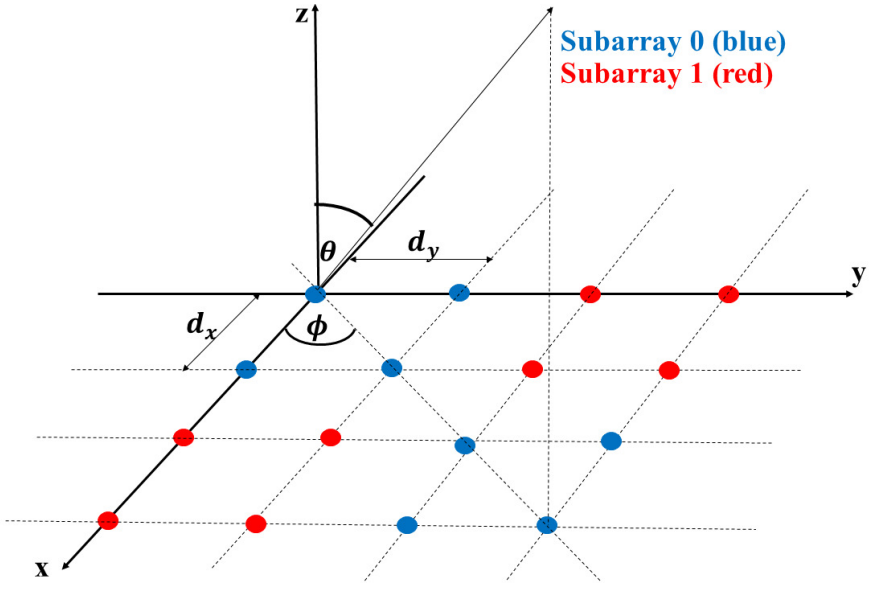

Figure 3.2: A UPA with the localised subarray architecture.

The approach introduced for designing uniform linear arrays can be extended to UPAs too and the only thing to change is the steering vector and the desired beam pattern, as for planar arrays, both elevation and azimuth angles are needed to specify a beam pattern in the three dimensional space [1, 65, 66].

Similar to the linear array case, for hybrid beamforming based on a UPA, there are also two different architectures, i.e., interleaved and localised, and an example for each case with $M = 2$ are displayed in Figures 3.1 and 3.2, which contain $2N_x$ and $2N_y$ antennas along the x-axis and y-axis, respectively. The adjacent antenna spacings along the x-axis and y-axis are d_x and d_y, respectively. Moreover, the elevation angle is $\theta \in [-90°, 90°]$ and azimuth angle is $\phi \in [-90°, 90°]$. Thus, the steering vectors of the two interleaved and localised subarrays as a function of θ and ϕ are given by

$$\begin{aligned}
&\boldsymbol{s}_0^I(\theta,\phi) = \\
&[1, e^{j2\pi\frac{2d_y}{\lambda}\sin\theta\sin\phi}, ..., e^{j2\pi\frac{2(N_y-1)d_y}{\lambda}\sin\theta\sin\phi}, e^{j2\pi(\frac{d_x}{\lambda}\sin\theta\cos\phi+\frac{d_y}{\lambda}\sin\theta\sin\phi)}, ..., \\
&e^{j2\pi(\frac{d_x}{\lambda}\sin\theta\cos\phi+\frac{(2N_y-1)d_y}{\lambda}\sin\theta\sin\phi)}, ..., e^{j2\pi(\frac{(2N_x-1)d_x}{\lambda}\sin\theta\cos\phi+\frac{(2N_y-1)d_y}{\lambda}\sin\theta\sin\phi)}]^T, \\
&\boldsymbol{s}_1^I(\theta,\phi) = \\
&[e^{j2\pi\frac{d_y}{\lambda}\sin\theta\sin\phi}, ..., e^{j2\pi\frac{(2N_y-1)d_y}{\lambda}\sin\theta\sin\phi}, e^{j2\pi\frac{d_x}{\lambda}\sin\theta\cos\phi}, ..., \\
&e^{j2\pi(\frac{d_x}{\lambda}\sin\theta\cos\phi+\frac{2(N_y-1)d_y}{\lambda}\sin\theta\sin\phi)}, ..., e^{j2\pi(\frac{(2N_x-1)d_x}{\lambda}\sin\theta\cos\phi+\frac{2(N_y-1)d_y}{\lambda}\sin\theta\sin\phi)}]^T,
\end{aligned} \tag{3.83}$$

and

$$\begin{aligned}
&\boldsymbol{s}_0^L(\theta,\phi) = \\
&[1, e^{j2\pi\frac{d_y}{\lambda}\sin\theta\sin\phi}, ..., e^{j2\pi\frac{(N_y-1)d_y}{\lambda}\sin\theta\sin\phi}, ..., e^{j2\pi\frac{(N_x-1)d_x}{\lambda}\sin\theta\cos\phi}, ..., \\
&e^{j2\pi(\frac{(N_x-1)d_x}{\lambda}\sin\theta\cos\phi+\frac{(N_y-1)d_y}{\lambda}\sin\theta\sin\phi)}, e^{j2\pi(\frac{N_xd_x}{\lambda}\sin\theta\cos\phi+\frac{N_yd_y}{\lambda}\sin\theta\sin\phi)}, \\
&..., e^{j2\pi(\frac{(2N_x-1)d_x}{\lambda}\sin\theta\cos\phi+\frac{(2N_y-1)d_y}{\lambda}\sin\theta\sin\phi)}]^T, \\
&\boldsymbol{s}_1^L(\theta,\phi) = \\
&[e^{j2\pi\frac{N_yd_y}{\lambda}\sin\theta\sin\phi}, ..., e^{j2\pi\frac{(2N_y-1)d_y}{\lambda}\sin\theta\sin\phi}, ..., e^{j2\pi(\frac{(N_x-1)d_x}{\lambda}\sin\theta\cos\phi+\frac{N_yd_y}{\lambda}\sin\theta\sin\phi)}, \\
&..., e^{j2\pi(\frac{(N_x-1)d_x}{\lambda}\sin\theta\cos\phi+\frac{(2N_y-1)d_y}{\lambda}\sin\theta\sin\phi)}, e^{j2\pi\frac{N_xd_x}{\lambda}\sin\theta\cos\phi}, ..., \\
&e^{j2\pi(\frac{N_xd_x}{\lambda}\sin\theta\cos\phi+\frac{(N_y-1)d_y}{\lambda}\sin\theta\sin\phi)}, ..., e^{j2\pi(\frac{(2N_x-1)d_x}{\lambda}\sin\theta\cos\phi+\frac{(N_y-1)d_y}{\lambda}\sin\theta\sin\phi)}]^T.
\end{aligned} \tag{3.84}$$

If all antennas are equally spaced in x and y axes, i.e., $d_x = d_y = d$, the steering

vectors of two subarrays in (3.83) and (3.84) change to

$$\begin{aligned}
&\boldsymbol{s}_0^I(\theta,\phi) = \\
&[1, e^{j2\pi\frac{2d}{\lambda}\sin\theta\sin\phi}, ..., e^{j2\pi\frac{2(N_y-1)d}{\lambda}\sin\theta\sin\phi}, e^{j2\pi\frac{d}{\lambda}(\sin\theta\cos\phi+\sin\theta\sin\phi)}, ..., \\
&e^{j2\pi\frac{d}{\lambda}(\sin\theta\cos\phi+(2N_y-1)\sin\theta\sin\phi)}, ..., e^{j2\pi\frac{d}{\lambda}((2N_x-1)\sin\theta\cos\phi+(2N_y-1)\sin\theta\sin\phi)}]^T, \\
&\boldsymbol{s}_1^I(\theta,\phi) = \\
&[e^{j2\pi\frac{d}{\lambda}\sin\theta\sin\phi}, ..., e^{j2\pi\frac{(2N_y-1)d}{\lambda}\sin\theta\sin\phi}, e^{j2\pi\frac{d}{\lambda}\sin\theta\cos\phi}, ..., \\
&e^{j2\pi\frac{d}{\lambda}(\sin\theta\cos\phi+2(N_y-1)\sin\theta\sin\phi)}, ..., e^{j2\pi\frac{d}{\lambda}((2N_x-1)\sin\theta\cos\phi+2(N_y-1)\sin\theta\sin\phi)}]^T,
\end{aligned} \tag{3.85}$$

and

$$\begin{aligned}
&\boldsymbol{s}_0^L(\theta,\phi) = \\
&[1, e^{j2\pi\frac{d}{\lambda}\sin\theta\sin\phi}, ..., e^{j2\pi\frac{(N_y-1)d}{\lambda}\sin\theta\sin\phi}, ..., e^{j2\pi\frac{(N_x-1)d}{\lambda}\sin\theta\cos\phi}, ..., \\
&e^{j2\pi\frac{d}{\lambda}((N_x-1)\sin\theta\cos\phi+(N_y-1)\sin\theta\sin\phi)}, e^{j2\pi\frac{d}{\lambda}(N_x\sin\theta\cos\phi+N_y\sin\theta\sin\phi)}, \\
&..., e^{j2\pi\frac{d}{\lambda}((2N_x-1)\sin\theta\cos\phi+(2N_y-1)\sin\theta\sin\phi)}]^T, \\
&\boldsymbol{s}_1^L(\theta,\phi) = \\
&[e^{j2\pi\frac{N_y d}{\lambda}\sin\theta\sin\phi}, ..., e^{j2\pi\frac{(2N_y-1)d}{\lambda}\sin\theta\sin\phi}, ..., e^{j2\pi\frac{d}{\lambda}((N_x-1)\sin\theta\cos\phi+N_y\sin\theta\sin\phi)}, \\
&..., e^{j2\pi\frac{d}{\lambda}((N_x-1)\sin\theta\cos\phi+(2N_y-1)\sin\theta\sin\phi)}, e^{j2\pi\frac{N_x d}{\lambda}\sin\theta\cos\phi}, ..., \\
&e^{j2\pi\frac{d}{\lambda}(N_x\sin\theta\cos\phi+(N_y-1)\sin\theta\sin\phi)}, ..., e^{j2\pi\frac{d}{\lambda}((2N_x-1)\sin\theta\cos\phi+(N_y-1)\sin\theta\sin\phi)}]^T,
\end{aligned} \tag{3.86}$$

respectively. Again, suppose the coefficients vector for the zeroth and first subarrays are represented by $\boldsymbol{w}_{A,0}$ and $\boldsymbol{w}_{A,1}$, respectively. Then, similar to (3.36), by combining $\boldsymbol{w}_{A,0}$ and $\boldsymbol{w}_{A,1}$ into one vector $\boldsymbol{w}_A$ and using the same approach as in Section 3.4.1, the final digital and analogue coefficients can be obtained for the UPA based hybrid beamforming structure.

3.4.4 Separate Direct Designs

To show the improvement by the proposed hybrid beamforming design methods from another angle, we consider a least squares design based on another two structures: a design based on the interleaved subarray architecture only without any inter-subarray coding scheme and a design based on the localised subarray architecture only without

any inter-subarray coding scheme. That is, the m-th subarray generates a beam pointing to φ_j with $m = j$, and all subarrays operate independent of each other.

Now we use $\boldsymbol{s}(\theta)$ to represent a general steering vetor and $\boldsymbol{w}_s$ to represent the corresponding beamforming coefficients. Then the cost formulation of the beam pointing to φ_j generated by the array is given by

$$\begin{aligned} J_{LS} = (1-\beta) \sum_{\theta \in \Theta_{main_j}} |\boldsymbol{w}_s^H \boldsymbol{s}(\theta) - 1|^2 \\ + \frac{\beta}{N_g} \sum_{\theta \in \Theta_{side_j}} |\boldsymbol{w}_s^H \boldsymbol{s}(\theta)|^2. \end{aligned} \tag{3.87}$$

Equation (3.87) can be expanded into a quadratic form

$$J_{LS} = \boldsymbol{w}_s^H \boldsymbol{Q}_{LS_{jm}} \boldsymbol{w}_s - \boldsymbol{w}_s^H \boldsymbol{z}_{LS_{jm}} - \boldsymbol{z}_{LS_{jm}}^H \boldsymbol{w}_s + d_{LS_j}, \tag{3.88}$$

where $\boldsymbol{Q}_{LS_{jm}}$, $\boldsymbol{z}_{LS_{jm}}$, and d_{LS_j} have been defined by (3.30), (3.33) and (3.34) using corresponding types of steering vectors. Overall, the minimisation of (3.88) with respect to $\boldsymbol{w}_s^H$, gives the following solution

$$\boldsymbol{w}_s = \boldsymbol{Q}_{LS_{jm}}^{-1} \boldsymbol{z}_{LS_{jm}}. \tag{3.89}$$

3.5 Design Examples

In this section, some design examples are provided for the two proposed methods. Assume that each subarray consists of fifteen antennas with ULA, i.e., $N_s = 15$ for the multi-user cases. Moreover, for UPA, each subarray contains $N_x = N_y = 6$ antennas along the x and y axes, respectively. The performance of the scheme in Section 3.2 and the two proposed designs in Sections 3.3 and 3.4 are compared for multiple arbitrary directions.

3.5.1 Design Examples for the Scheme in Section 3.2

Suppose that the two desired beam directions are $\varphi_0 = -48°(\sin(-48°) = -0.74)$ and $\varphi_1 = 20°(\sin(20°) = 0.34)$. For the scheme in [25], the two-beam multiplexing performance of one desired beam pointing to $-48°$ and one pointing to $20°$ is shown in Figures 3.3 and

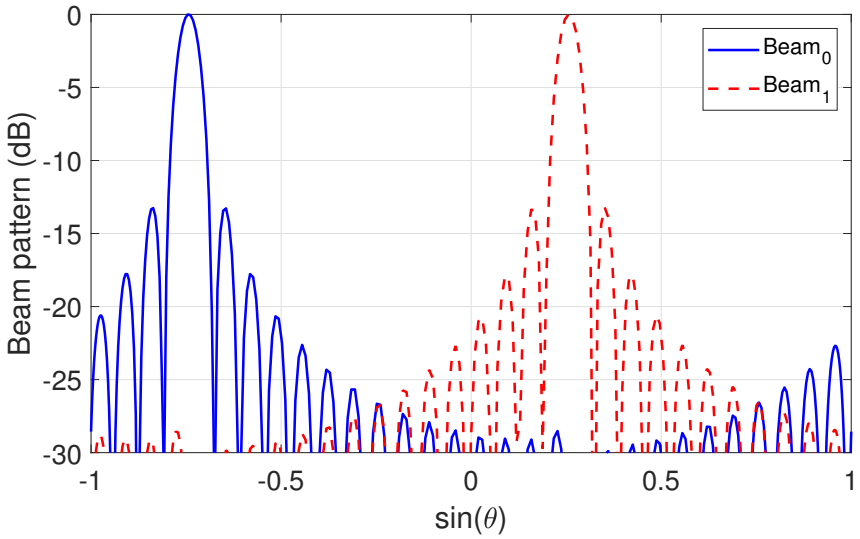

Figure 3.3: Beam patterns of two beams with $\varphi_0 = -48°$ obtained by the method in Section 3.2 with the interleaved subarray architecture.

Table 3.1: Analogue coefficients $\boldsymbol{w}_{A,0}$ and $\boldsymbol{w}_{A,1}$ with $\varphi_0 = -48°$ generated by the method in Section 3.2 with the interleaved subarray architecture.

n \ m	$\boldsymbol{w}_{A,0}$	$\boldsymbol{w}_{A,1}$	n \ m	$\boldsymbol{w}_{A,0}$	$\boldsymbol{w}_{A,1}$
0	1.0000+0.0000i	0.6911-0.7228i	8	0.9412-0.3378i	0.3935-0.9193i
1	-0.0431-0.9991i	-0.7530-0.6580i	9	-0.3780-0.9258i	-0.9360-0.3519i
2	-0.9963+0.0860i	-0.6236+0.7817i	10	-0.9087+0.4175i	-0.3096+0.9509i
3	0.1289+0.9917i	0.8089+0.5880i	11	0.4563+0.8898i	0.9638+0.2667i
4	0.9852-0.1714i	0.5511-0.8344i	12	0.8694-0.4942i	0.2233-0.9748i
5	-0.2137-0.9769i	-0.8583-0.5132i	13	-0.5311-0.8473i	-0.9838-0.1794i
6	-0.9668+0.2556i	-0.4742+0.8804i	14	-0.8236+0.5671i	-0.1351+0.9908i
7	0.2970+0.9549i	0.9008+0.4343i			

3.4, respectively. The corresponding analogue coefficients $\boldsymbol{w}_{A,0}$ and $\boldsymbol{w}_{A,1}$ are displayed in Tables 3.1 and 3.2, respectively.

We can clearly observe that in Figure 3.3, the first beam points to the direction $\sin(14.9°) = 0.26$ instead of the required $\sin(20°) = 0.34$ by the design, while in Figure 3.4, the zeroth beam points to $\sin(-41.1°) = -0.66$ instead of the required $\sin(-48°) = -0.74$,

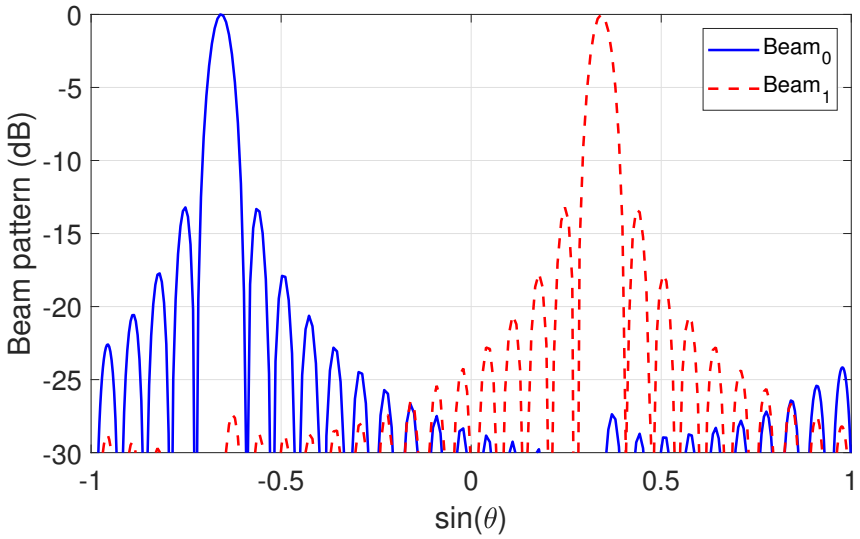

Figure 3.4: Beam patterns of two beams with $\varphi_1 = 20°$ obtained by the method in Section 3.2 with the interleaved subarray architecture.

Table 3.2: Analogue coefficients $\boldsymbol{w}_{A,0}$ and $\boldsymbol{w}_{A,1}$ with $\varphi_1 = 20°$ generated by the method in Section 3.2 with the interleaved subarray architecture.

n \ m	$\boldsymbol{w}_{A,0}$	$\boldsymbol{w}_{A,1}$	n \ m	$\boldsymbol{w}_{A,0}$	$\boldsymbol{w}_{A,1}$
0	1.0000+0.0000i	0.4762-0.8793i	8	-0.0565+0.9984i	0.8347+0.5507i
1	-0.5497-0.8354i	-0.9967+0.0818i	9	0.8651-0.5016i	0.0051-1.0000i
2	-0.3957+0.9184i	0.6132+0.7900i	10	-0.8945-0.4470i	-0.8402+0.5422i
3	0.9847-0.1742i	0.3265-0.9452i	11	0.1183+0.9930i	0.9133+0.4073i
4	-0.6868-0.7268i	-0.9700+0.2432i	12	0.7645-0.6446i	-0.1580-0.9874i
5	-0.2296+0.9733i	0.7337+0.6794	13	-0.9587-0.2843i	-0.7406+0.6720i
6	0.9393-0.3432i	0.1680-0.9858i	14	0.2895+0.9572i	0.9675+0.2530i
7	-0.8030-0.5960i	-0.9174+0.3980i			

highlighting the issue of the design in [25], where the directions of two beams have to satisfy a fixed relationship.

3.5.2 Design Examples for the Scheme in Section 3.3

For the design with varying antenna spacing, according to (3.19), α can be calculated as 0.92 for $\varphi_0 = -48^\circ$ ($\sin(-48^\circ) = -0.74$) and $\varphi_1 = 20^\circ$ ($\sin(20^\circ) = 0.34$). Thus, the adjacent antenna spacing for the two subarrays is $d_0 = d_1 = \alpha\lambda = 0.92\lambda$. The patterns of the two resultant beams generated by the design in Section 3.3 with varying antenna spacing are displayed in Figure 3.5 and the corresponding analogue coefficients $\boldsymbol{w}_{A,0}$ and $\boldsymbol{w}_{A,1}$ are listed in Table 3.3. It is clear that the two beams are in the desired directions and the design in Section 3.3 is working effectively.

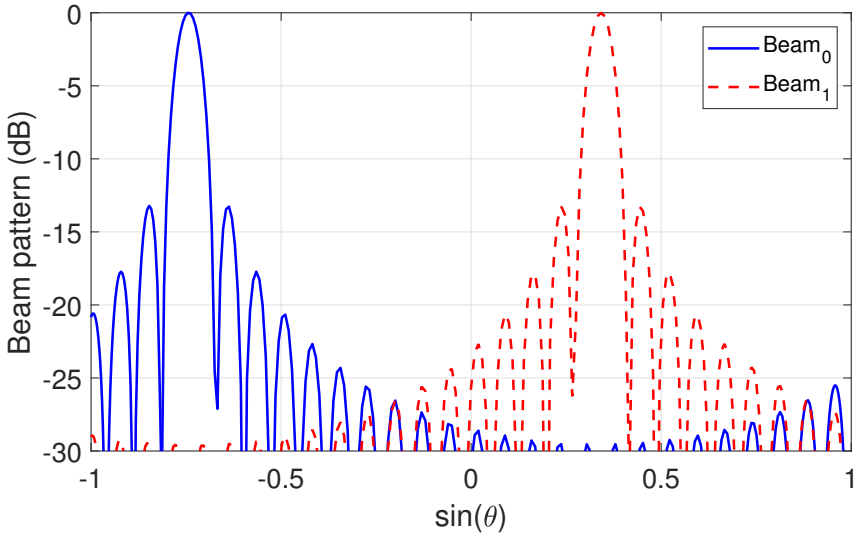

Figure 3.5: Beam patterns of two beams with $\varphi_0 = -48^\circ$ and $\varphi_1 = 20^\circ$ generated by the method in Section 3.3 with the interleaved subarray architecture.

3.5.3 Design Examples for the Scheme in Section 3.4.1

In this section, we consider one fixed antenna spacing $d = \frac{\lambda}{3}$ for the two-user case. The trade-off factor in (3.28) is chosen as $\beta = 0.65$. Because the same beam directions as the design in Sections 3.5.1 and 3.5.2 are adopted, the mainlobe directions of the zeroth and first beams are $\varphi_0 = -48^\circ$ and $\varphi_1 = 20^\circ$, respectively, and the corresponding sidelobe regions are $\sin\Theta_{side_0} \in [-1, -0.79] \cup [-0.69, 1]$ ($\sin(-48^\circ) = -0.74$) and $\sin\Theta_{side_1} \in [-1, 0.29] \cup [0.39, 1]$ ($\sin(20^\circ) = 0.34$). The number of sample points for the sidelobe

Table 3.3: Analogue coefficients $\boldsymbol{w}_{A,0}$ and $\boldsymbol{w}_{A,1}$ with $\varphi_0 = -48^\circ$ and $\varphi_1 = 20^\circ$ generated by the method in Section 3.3 with the interleaved subarray architecture.

n \ m	$\boldsymbol{w}_{A,0}$	$\boldsymbol{w}_{A,1}$	n \ m	$\boldsymbol{w}_{A,0}$	$\boldsymbol{w}_{A,1}$
0	1.0000+0.0000i	0.5486-0.8361i	8	-0.9910+0.1342i	-0.4314+0.9022
1	-0.3982-0.9173i	-0.9854-0.1703i	9	0.5177+0.8556i	0.9993+0.0365i
2	-0.6829+0.7305i	0.2362+0.9717i	10	0.5787-0.8155i	-0.3644-0.9312i
3	0.9420+0.3356i	0.7963-0.6035i	11	-0.9785-0.2061i	0.7091+0.7051i
4	-0.0673-0.9977i	-0.8711-0.4911i	12	0.2005+0.9797i	0.9291+0.3697i
5	-0.8885-0.4590i	-0.1036+0.9946i	13	0.8188-0.5740i	-0.0308-0.9995i
6	0.7748+0.6322i	0.9536-0.3010i	14	-0.8526-0.5225i	-0.9046+0.4262i
7	0.2715-0.9624i	-0.6558-0.7549			

region for each designed beam is $N_g = 191$.

With $d = \frac{\lambda}{3}$, the patterns of the zeroth and first beams obtained using the method in Section 3.4.1 ('Method in Sec. 3.4.1') are shown in Figures 3.6 and 3.7, respectively. The corresponding digital and analogue coefficients are listed in Tables 3.4 and 3.5 and the change of the cost function J_{LS} with respect to the iteration number using the interleaved subarray architecture is shown in Figure 3.8. Furthermore, the design results obtained using the method in Section 3.4.4 are also shown, where the zeroth subarray in the interleaved subarray architecture is directly used to design a beam pointing to -48° and the first subarray for the beam pointing to 20°; there are no digital schemes combining these two subarrays and each subarray operates independent of the other. They are indicated in Figures 3.6 and 3.7 as 'Separate direct design$_0$'. Moreover, the separate design results using the method in Section 3.4.4 based on the localised subarray architecture are also presented, i.e., for the whole ULA with $2N_s$ antennas, the first N_s of them are used to design the bream pointing to -48° and the last N_s of them are used to design the beam pointing to 20°; there is no digital inter-subarray coding scheme to combine these two together. This result is represented by 'Separate direct design$_1$' in Figures 3.6 and 3.7.

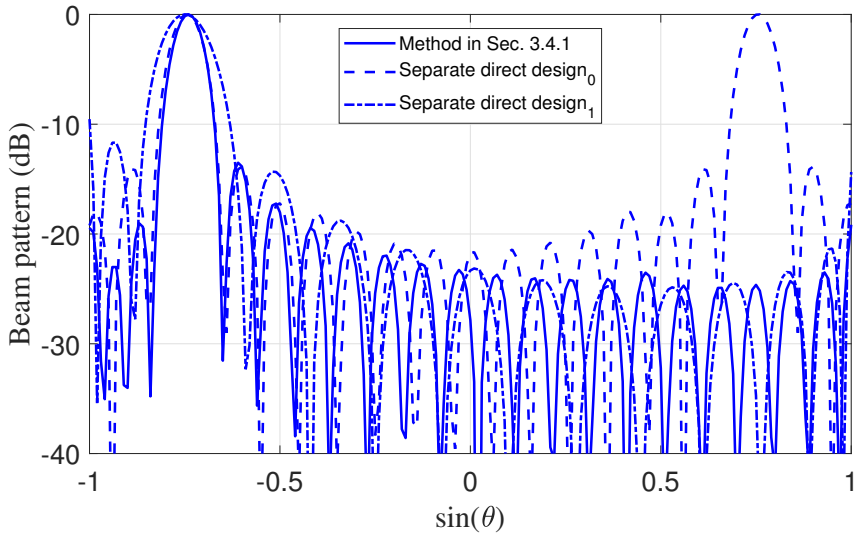

Figure 3.6: Beam patterns of the zeroth beam with $\varphi_0 = -48°$ generated by the method in Section 3.4.1 with the interleaved subarray architecture and the separate direct designs in Section 3.4.4 with the interleaved and localised subarray architectures ($d = \frac{\lambda}{3}$).

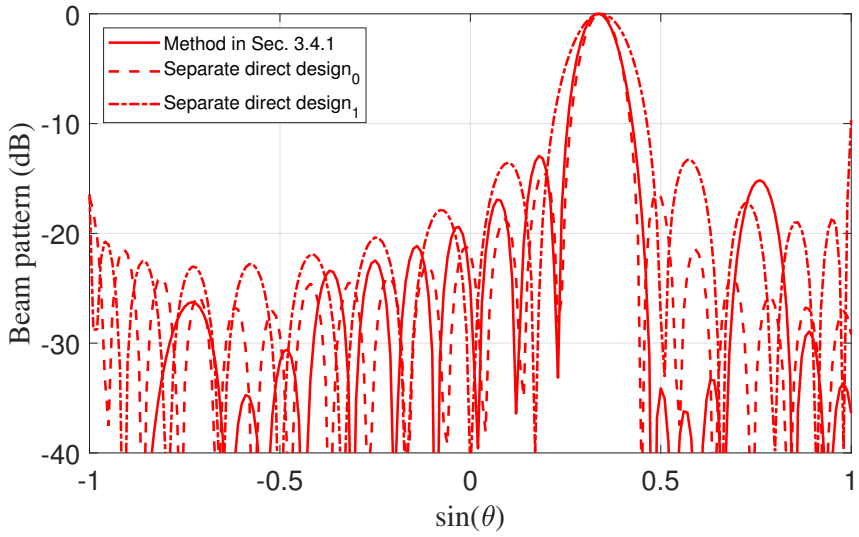

Figure 3.7: Beam patterns of the first beam with $\varphi_1 = 20°$ generated by the method in Section 3.4.1 with the interleaved subarray architecture and the separate direct designs in Section 3.4.4 with the interleaved and localised subarray architectures ($d = \frac{\lambda}{3}$).

3.5.4 Design Examples for the Scheme in Section 3.4.2

Now, consider the three-user case. Suppose that the three beam directions are $\varphi_0 = -45°$, $\varphi_1 = 0°$ and $\varphi_2 = 40°$, the corresponding sidelobe regions are $\sin\Theta_{side_0} \in [-1, -0.76] \cup$

Table 3.4: Digital coefficients $\boldsymbol{w}_{D,0}$ and $\boldsymbol{w}_{D,1}$ with $\varphi_0 = -48°$ and $\varphi_1 = 20°$ generated by the method in Section 3.4.1 with the interleaved subarray architecture ($d = \frac{1}{3}\lambda$).

m \ j	$\boldsymbol{w}_{D,0}$	$\boldsymbol{w}_{D,1}$
0	2.3982+0.5171i	0.4333-0.0590i
1	-2.4185+0.4629i	0.4371+0.0486i

Table 3.5: Analogue coefficients $\boldsymbol{w}_{A,0}$ and $\boldsymbol{w}_{A,1}$ with $\varphi_0 = -48°$ and $\varphi_1 = 20°$ generated by the method in Section 3.4.1 with the interleaved subarray architecture ($d = \frac{1}{3}\lambda$).

n \ m	$\boldsymbol{w}_{A,0}$	$\boldsymbol{w}_{A,1}$	n \ m	$\boldsymbol{w}_{A,0}$	$\boldsymbol{w}_{A,1}$
0	0.0324+0.0253i	-0.0026+0.0659i	8	0.0413-0.0935i	0.0897-0.0003i
1	-0.0061+0.0707i	-0.0465+0.0378i	9	0.0814+0.0190i	0.0296+0.0791i
2	-0.0465+0.0308i	-0.0602-0.0318i	10	0.0075+0.0896i	-0.0850+0.0409i
3	-0.0601-0.0634i	0.0380-0.0886i	11	-0.0968+0.0025i	-0.0365-0.0789i
4	0.0695-0.0639i	0.0800+0.0396i	12	-0.0074-0.0678i	0.0455-0.0319i
5	0.0628+0.0565i	-0.0120+0.0824i	13	0.0526-0.0295i	0.0679+0.0206i
6	-0.0333+0.0839i	-0.1019+0.0040i	14	0.0624+0.0224i	0.0113+0.0394i
7	-0.1047-0.0400i	0.0015-0.1116i			

$[-0.66, 1]$ ($\sin(-45°) = -0.71$), $\sin\Theta_{side_1} \in [-1, -0.05] \cup [0.05, 1]$ ($\sin(0°) = 0$) and $\sin\Theta_{side_2} \in [-1, 0.59] \cup [0.69, 1]$ ($\sin(40°) = 0.64$) and $N_g = 191$. The trade-off factor in (3.27) with $J = 3$ is $\beta = 0.65$.

With $d = \frac{1}{5}\lambda$, the patterns of the zeroth, first and second resultant beams generated by the method in Section 3.4.2 with the interleaved subarray architecture and the separate direct designs in Section 3.4.4 with the interleaved and localised subarray architectures are shown in Figures 3.9, 3.10 and 3.11, respectively. The corresponding digital and analogue coefficients obtained by the method in Section 3.4.2 with the interleaved subarray architecture are listed in Tables 3.6 and 3.7, respectively, and the cost function J_{LS} with respect to the iteration number is shown in Figure 3.12. A similar observation can be made as in the two-beam case.

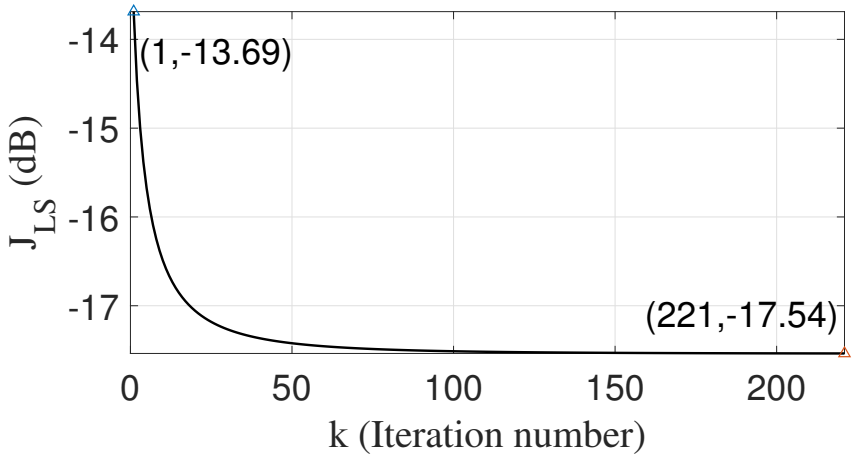

Figure 3.8: Cost function J_{LS} with respect to the iteration number k for the two-user case with $\varphi_0 = -48°$ and $\varphi_1 = 20°$ generated by the method in Section 3.4.1 with two ULAs ($d = \frac{1}{3}\lambda$).

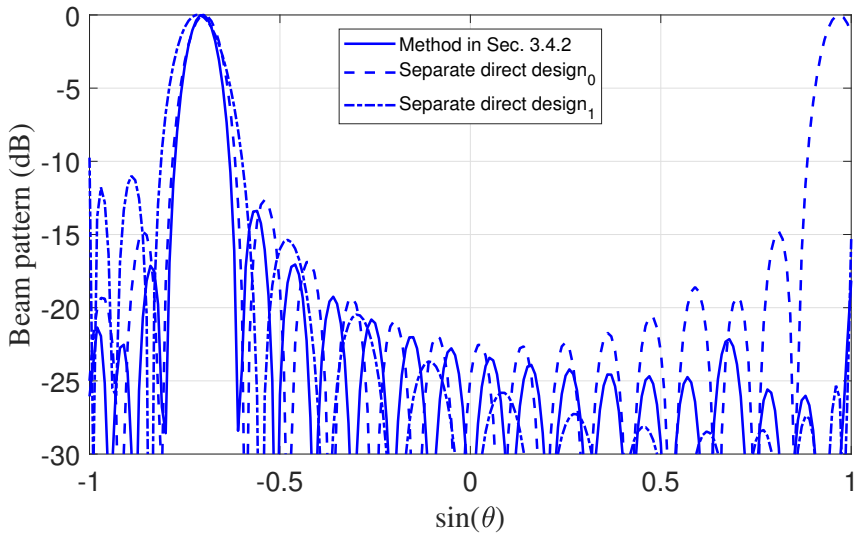

Figure 3.9: Beam patterns of the zeroth beam with $\varphi_0 = -45°$ generated by the method in Section 3.4.2 with the interleaved subarray architecture and the separate direct designs in Section 3.4.4 with the interleaved and localised subarray architectures ($d = \frac{1}{5}\lambda$).

Overall, from both sets of design examples, it can be seen that the methods in Sections 3.4.1 and 3.4.2 with a fixed antenna spacing are working effectively with the resultant beams pointing to the desired directions, while the separate direct designs based on each subarray using the method in Section 3.4.4 are not as good and in the interleaved subarray architecture, it even leads to a grating lobe as shown in Figure 3.6 for the two-user case and

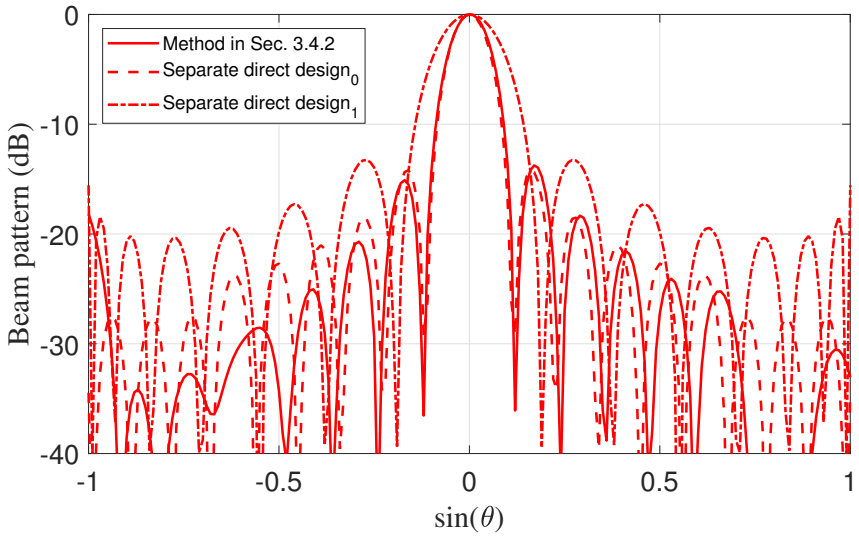

Figure 3.10: Beam patterns of the first beam with $\varphi_1 = 0°$ generated by the method in Section 3.4.2 with the interleaved subarray architecture and the separate direct designs in Section 3.4.4 with the interleaved and localised subarray architectures ($d = \frac{1}{5}\lambda$).

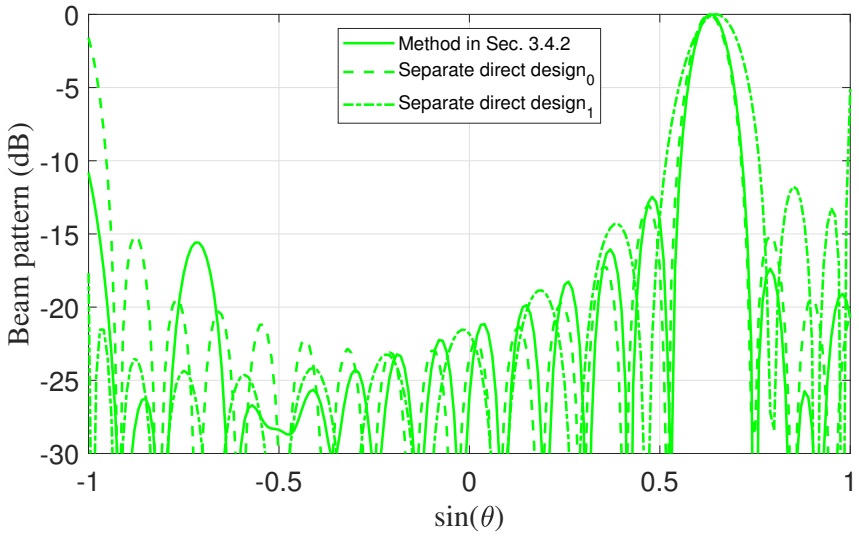

Figure 3.11: Beam patterns of the second beam with $\varphi_2 = 40°$ generated by the method in Section 3.4.2 with the interleaved subarray architecture and the separate direct designs in Section 3.4.4 with the interleaved and localised subarray architectures ($d = \frac{1}{5}\lambda$).

Figures 3.9 and 3.11 for the three-user case due to a spacing larger than half wavelength. Furthermore, based on the performances with two types of sub-array architectures in the above two cases, the interleaved subarray architecture provides a better result with a

Table 3.6: Digital coefficients $\boldsymbol{w}_{D,0}$, $\boldsymbol{w}_{D,1}$ and $\boldsymbol{w}_{D,2}$ with $\varphi_0 = -45°$, $\varphi_1 = 0°$ and $\varphi_2 = 40°$ generated by the method in Section 3.4.2 with the interleaved subarray architecture ($d = \frac{1}{5}\lambda$).

m \ j	$\boldsymbol{w}_{D,0}$	$\boldsymbol{w}_{D,1}$	$\boldsymbol{w}_{D,2}$
0	4.9278+5.7137i	-0.2379-0.1697i	-0.0174-0.0085i
1	-144.7717+286.6622i	-12.5313-2.8804i	-39.3662-72.0145i
2	-7.3737-3.0177i	0.3726-0.1392i	0.9804-2.8992i

Table 3.7: Analogue coefficients $\boldsymbol{w}_{A,0}$, $\boldsymbol{w}_{A,1}$ and $\boldsymbol{w}_{A,2}$ with $\varphi_0 = -45°$, $\varphi_1 = 0°$ and $\varphi_2 = 40°$ generated by the method in Section 3.4.2 with the interleaved subarray architecture ($d = \frac{1}{5}\lambda$).

n \ m	$\boldsymbol{w}_{A,0}$	$\boldsymbol{w}_{A,1}$	$\boldsymbol{w}_{A,2}$
0	0.0179+0.0241i	-0.0014-0.0003i	0.0333-0.0154i
1	0.0076+0.0698i	-0.0022-0.0025i	0.1090-0.0036i
2	0.0336+0.0852i	-0.0021-0.0028i	0.0905+0.0182i
3	0.0263+0.1039i	-0.0028-0.0023i	0.0865-0.0221i
4	0.0168+0.0837i	-0.0022-0.0030i	0.1151+0.0113i
5	0.0424+0.0950i	-0.0025-0.0024i	0.0836+0.0041i
6	0.0132+0.1097i	-0.0028-0.0029i	0.1067-0.0179i
7	0.0329+0.0776i	-0.0023-0.0028i	0.1066+0.0209i
8	0.0327+0.1139i	-0.0028-0.0026i	0.0850-0.0136i
9	0.0140+0.0928i	-0.0025-0.0030i	0.1147-0.0009i
10	0.0398+0.0840i	-0.0023-0.0025i	0.0900+0.0139i
11	0.0198+0.1171i	-0.0027-0.0028i	0.0915+0.0188i
12	0.0221+0.0680i	-0.0021-0.0025i	0.1056+0.0129i
13	0.0354+0.1032i	-0.0023-0.0026i	0.0741+0.0052i
14	0.0005+0.0815i	-0.0015-0.0020i	0.0458-0.0111i

narrower mainlobe beamwidth for each of the designed beams than that of the localised subarray architecture.

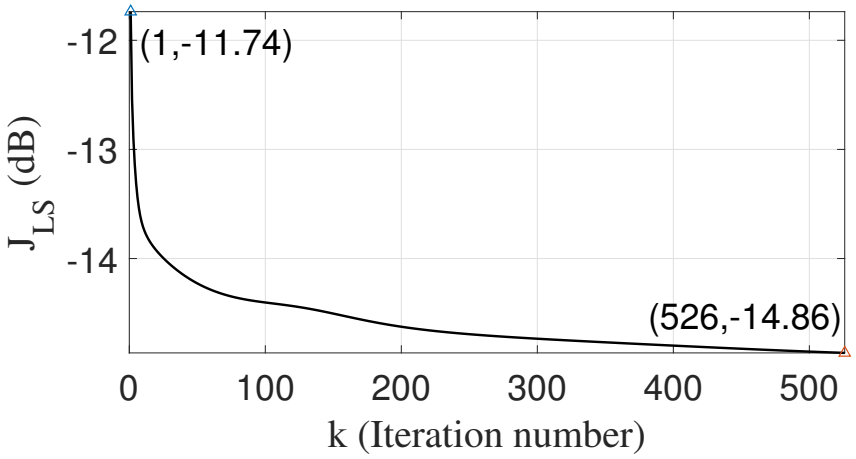

Figure 3.12: Cost function J_{LS} with respect to the iteration number k for the three-user case with $\varphi_0 = -45°$, $\varphi_1 = 0°$ and $\varphi_2 = 40°$ generated by the method in Section 3.4.2 with the interleaved subarray architecture ($d = \frac{1}{5}\lambda$).

Note that when $d = \frac{1}{3}\lambda$ and $d = \frac{1}{5}\lambda$ for the two and three users, the antenna spacing for each subarray is $\frac{2}{3}\lambda$ and $\frac{3}{5}\lambda$, respectively, and grating lobes are expected. This also highlights the positive effect of the digital scheme, which can combine the multiple subarrays together in an effective way to eliminate grating lobes.

3.5.5 Design Examples for the Scheme in Section 3.4.3

For the design based on UPA with $M = 2$, one fixed antenna spacing $d_x = d_y = \frac{1}{3}\lambda$ is employed for the two users and the number of the antennas in the whole array is $2N_x \times 2N_y = 144$. In addition, the mainlobe direction in the azimuth angle for both designed beams is selected as $\phi_{main} = 0°$ and the corresponding sidelobe region is $\phi_{side} \in [-90°, -5°] \cup [5°, 90°]$. The desired elevation angles and the corresponding sidelobe regions for the two designed beams are $\Theta_{side_0} \in [-90°, -53°] \cup [-43°, 90°]$ and $\Theta_{side_1} \in [-90°, 15°] \cup [25°, 90°]$. Moreover, the trade-off factor in the weighting function (3.28) is $\beta = 0.65$.

The patterns of the zeroth and first resultant beams generated by the method in Section 3.4.3 are shown in Figures 3.13 and 3.14, respectively, where a satisfactory design performance is achieved with both of their sidelobes being lower than -10 dB and the corresponding cost function J_{LS} with respect to the iteration number is displayed in

Figure 3.15.

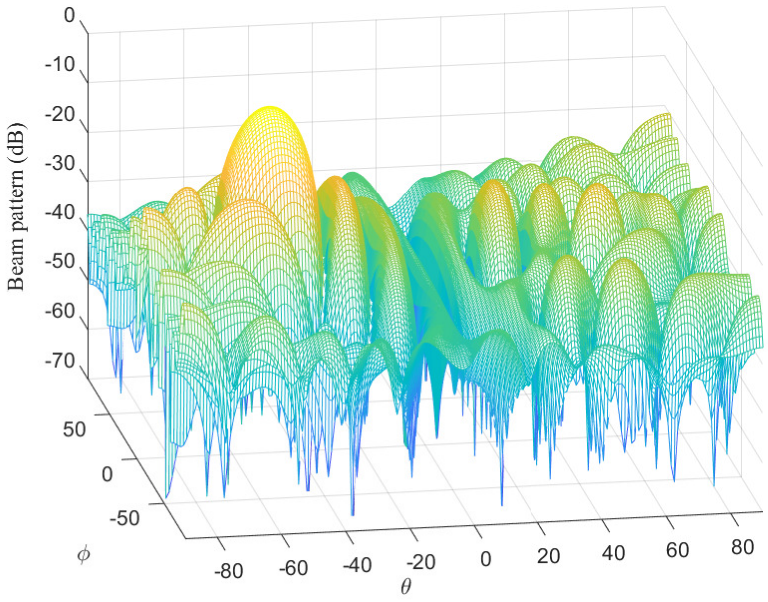

Figure 3.13: Beam pattern of the zeroth beam with $\varphi_0 = -48°$ and $\phi_{main} = 0°$ generated by the method in Section 3.4.3 with the interleaved subarray architecture ($d_x = d_y = \frac{1}{3}\lambda$).

3.6 Summary

To overcome the limitation of an existing design, two novel designs, with varying and fixed antenna spacings, respectively, have been proposed to generate multiple beams serving multiple arbitrary user directions based on the interleaved subarray architecture. As demonstrated by provided design examples based on both ULAs and UPAs, the first design with varying antenna spacing works effectively by measuring the antenna spacing in terms of the directions of the required beams but the antenna spacing is not fixed any more. By considering the antenna spacing as a fixed parameter again, the second design using the least squares approach gives a much narrower beam width for each of the designed beams compared to that generated by the separate direct design with the localised subarray architecture; and it suppresses the grating lobes more effectively compared to that generated by the separate direct design with the interleaved subarray

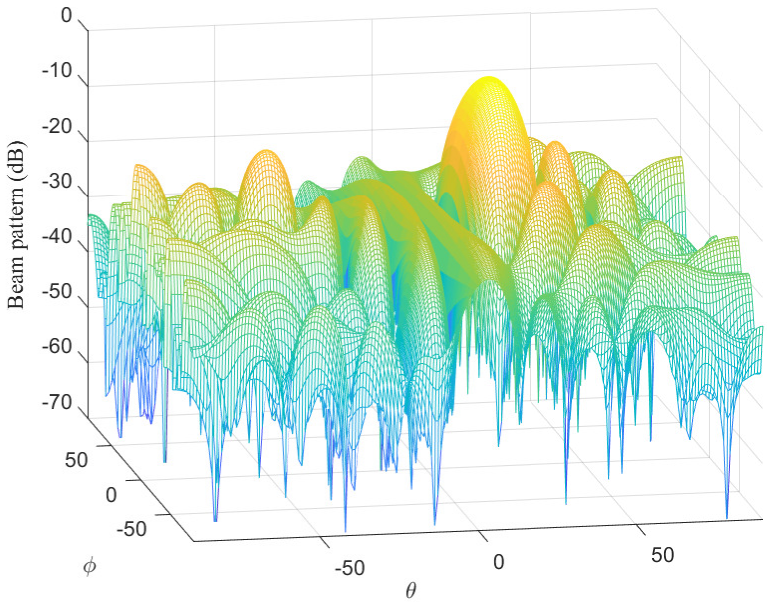

Figure 3.14: Beam pattern of the first beam with $\varphi_1 = 20°$ and $\phi_{main} = 0°$ generated by the method in Section 3.4.3 with the interleaved subarray architecture ($d_x = d_y = \frac{1}{3}\lambda$).

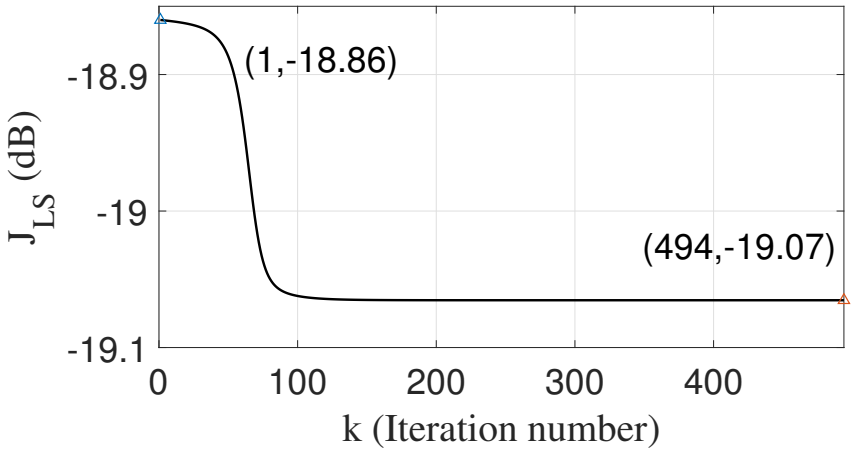

Figure 3.15: Cost function J_{LS} with respect to the iteration number k for the two-user case with $\varphi_0 = -48°$, $\varphi_1 = 20°$ and $\phi_{main} = 0°$ generated by the method in Section 3.4.3 with the interleaved subarray architecture ($d_x = d_y = \frac{1}{3}\lambda$).

architecture. In the next chapter, two practical factors are taken into consideration in the design, with three formulations studied.

Chapter 4

Robust Multi-Beam Multiplexing Design with Nearly Equal Magnitude Analogue Coefficients

4.1 Introduction

In this chapter, we extend the work in the last chapter by considering two practical application constraints. One is that the analogue coefficient of each antenna may only change its phase so that a uniform fixed-magnitude coefficient is applied to each of the analogue signals. This will reduce the implementation complexity of the analogue beamformer significantly [67–71], because only phase shifts are needed to steer the multiple user beams to different directions. The second design is related to the robustness of the system against different perturbations, such as antenna location and response errors and the mutual coupling effect [63, 72–76]. To improve the robustness of the designed beamformer, a norm-bounded error is introduced to the steering vector of the array and a corresponding constraint is placed on the overall design process. With the constraint, the difference between the desired and real beam responses obtained by this robust beamformer can be controlled below an acceptable level. Furthermore, by considering both constraints simultaneously, a third design is formulated, by which the robustness against steering vector errors is guaranteed and all analogue coefficients share the same magnitude. As

demonstrated by the provided design examples, the proposed designs can effectively generate multiple high-quality user beams with arbitrary directions to serve the corresponding users in different scenarios, which was not considered in [25, 26, 77].

Different from the traditional design for a single beam pattern with multiple main beam directions, the real challenge here is to design a common set of analogue coefficients generating independent multiple beams with each beam serving one user only, while simultaneously meeting the required constraints. Again unlike the traditional case, which is often convex, the new problem is non-convex and a novel solution will be proposed to solve it effectively following an alternate optimisation approach, as demonstrated by the provided design examples.

The remaining part of this chapter is organised as follows. The proposed design considering practical constraints for two beam users is proposed in Section 4.2, where the scheme with a nearly equal magnitude constraint on analogue coefficients is described in Section 4.2.1, the robust beamformer in the presence of steering vector errors is introduced in Section 4.2.2, the scheme considering both the nearly equal magnitude constraint and the robustness against steering vector errors is presented in Section 4.2.3, and the scheme without any constraints is shown in Section 4.2.4. Similar designs for three users are given in Section 4.3. Design examples for both the two-user and three-user cases are provided in Section 4.4 and conclusions are drawn in Section 4.5.

4.2 Two-Beam Case

A general digital coding scheme to design J beams is adopted, whose coefficients for the j-th beam ($j \in \{0, 1, ..., J-1\}$) are given by (3.24), where $w_{D,j,m} (m \in \{0, 1, ..., M-1\})$ are MJ digital coefficients to be determined later. So the designed beam response of the j-th beam in a vector form is given by (3.25) and the sum of the sidelobe responses for the J beams is given by

$$E_s = \sum_{j=0}^{J-1} \Big(\sum_{\theta \in \Theta_{side_j}} \left| P_{\varphi_j}(\theta) \right|^2 \Big) = \sum_{j=0}^{J-1} \Big(\sum_{\theta \in \Theta_{side_j}} \left| \sum_{m=0}^{M-1} w_{D,j,m}^* \boldsymbol{w}_{A,m}^H \boldsymbol{s}_m(\theta) \right|^2 \Big). \tag{4.1}$$

4.2.1 The First Scheme with Nearly Equal Magnitude Constraint on Analogue Coefficients

With $J = 2$, the sum of sidelobe patterns for the two beams is given by

$$\begin{aligned} E_s = \sum_{j=0}^{1} \Big(& w_{D,j,0}^{*} \boldsymbol{w}_{A,0}^{H} \boldsymbol{Q}_{S_{j0}} \boldsymbol{w}_{A,0} w_{D,j,0} + w_{D,j,1}^{*} \boldsymbol{w}_{A,1}^{H} \boldsymbol{Q}_{S_{j1}} \boldsymbol{w}_{A,1} w_{D,j,1} \\ & + w_{D,j,0}^{*} \boldsymbol{w}_{A,0}^{H} \boldsymbol{P}_{S_{j0}} \boldsymbol{w}_{A,1} w_{D,j,1} + w_{D,j,1}^{*} \boldsymbol{w}_{A,1}^{H} \boldsymbol{P}_{S_{j1}} \boldsymbol{w}_{A,0} w_{D,j,0} \Big), \end{aligned} \tag{4.2}$$

and (4.2) can be expanded as

$$\begin{aligned} E_s = & \boldsymbol{w}_{A,0}^{H} \left(\boldsymbol{w}_{D,0,0}^{H} \boldsymbol{Q}_{S00} \boldsymbol{w}_{D,0,0} + \boldsymbol{w}_{D,1,0}^{H} \boldsymbol{Q}_{S10} \boldsymbol{w}_{D,1,0} \right) \boldsymbol{w}_{A,0} \\ & + \boldsymbol{w}_{A,1}^{H} \left(\boldsymbol{w}_{D,0,1}^{H} \boldsymbol{Q}_{S01} \boldsymbol{w}_{D,0,1} + \boldsymbol{w}_{D,1,1}^{H} \boldsymbol{Q}_{S11} \boldsymbol{w}_{D,1,1} \right) \boldsymbol{w}_{A,1} \\ & + \boldsymbol{w}_{A,0}^{H} \left(\boldsymbol{w}_{D,0,0}^{H} \boldsymbol{P}_{S00} \boldsymbol{w}_{D,0,1} + \boldsymbol{w}_{D,1,0}^{H} \boldsymbol{P}_{S10} \boldsymbol{w}_{D,1,1} \right) \boldsymbol{w}_{A,1} \\ & + \boldsymbol{w}_{A,1}^{H} \left(\boldsymbol{w}_{D,0,1}^{H} \boldsymbol{P}_{S01} \boldsymbol{w}_{D,0,0} + \boldsymbol{w}_{D,1,1}^{H} \boldsymbol{P}_{S11} \boldsymbol{w}_{D,1,0} \right) \boldsymbol{w}_{A,0}, \end{aligned} \tag{4.3}$$

with

$$\boldsymbol{Q}_{S_{jm}} = \sum_{\theta \in \Theta_{side_j}} \boldsymbol{S}_m(\theta), \tag{4.4}$$

$$\boldsymbol{P}_{S_{j0}} = \sum_{\theta \in \Theta_{side_j}} \boldsymbol{s}_0(\theta) \boldsymbol{s}_1(\theta)^H, \boldsymbol{P}_{S_{j1}} = \sum_{\theta \in \Theta_{side_j}} \boldsymbol{s}_1(\theta) \boldsymbol{s}_0(\theta)^H, \tag{4.5}$$

where $\{j, m\} \in \{0, 1\}$, $\boldsymbol{S}_m(\theta)$ and $\boldsymbol{w}_{D,j,m}$ are given in (3.35) and (3.43), respectively. Combining the analogue coefficients $\boldsymbol{w}_{A,0}$ and $\boldsymbol{w}_{A,1}$ into one vector, given by (3.36), equation (4.3) can be rewritten as

$$E_s = \boldsymbol{w}_A^H \left(\boldsymbol{Q}_S + \boldsymbol{P}_S \tilde{\boldsymbol{I}}_0 \right) \boldsymbol{w}_A, \tag{4.6}$$

with

$$\boldsymbol{Q}_S = \begin{bmatrix} \boldsymbol{G}_{S_0} & \boldsymbol{0}_{N_s} \\ \boldsymbol{0}_{N_s} & \boldsymbol{G}_{S_1} \end{bmatrix}, \boldsymbol{P}_S = \begin{bmatrix} \boldsymbol{H}_{S_0} & \boldsymbol{0}_{N_s} \\ \boldsymbol{0}_{N_s} & \boldsymbol{H}_{S_1} \end{bmatrix}, \tag{4.7}$$

$$\boldsymbol{G}_{S_m} = \boldsymbol{w}_{D,0,m}^H \boldsymbol{Q}_{S_{0m}} \boldsymbol{w}_{D,0,m} + \boldsymbol{w}_{D,1,m}^H \boldsymbol{Q}_{S_{1m}} \boldsymbol{w}_{D,1,m}, \tag{4.8}$$

$$\begin{aligned} \boldsymbol{H}_{S_0} &= \boldsymbol{w}_{D,0,0}^H \boldsymbol{P}_{S_{00}} \boldsymbol{w}_{D,0,1} + \boldsymbol{w}_{D,1,0}^H \boldsymbol{P}_{S_{10}} \boldsymbol{w}_{D,1,1}, \\ \boldsymbol{H}_{S_1} &= \boldsymbol{w}_{D,0,1}^H \boldsymbol{P}_{S_{01}} \boldsymbol{w}_{D,0,0} + \boldsymbol{w}_{D,1,1}^H \boldsymbol{P}_{S_{11}} \boldsymbol{w}_{D,1,0}, \end{aligned} \tag{4.9}$$

where $\tilde{\boldsymbol{I}}_0$ is given by (3.39) in Chapter 3.

To minimise the sum of the sidelobe response for the two beams while guaranteeing that the mainlobes are in the corresponding desired directions, an intermediate formulation without any requirements for a given set of $w_{D,j,m}(\{j,m\} \in \{0,1\})$ can be formulated as

$$\begin{aligned} \min_{\boldsymbol{w}_A} \quad & E_s = \| \boldsymbol{L}^H \boldsymbol{w}_A \|_2, \\ \text{subject} \quad & \text{to} \\ & \boldsymbol{w}_A^H \begin{bmatrix} \boldsymbol{w}_{D,0,0}^H \boldsymbol{z}_{S_{00}} & \boldsymbol{w}_{D,1,0}^H \boldsymbol{z}_{S_{10}} \\ \boldsymbol{w}_{D,0,1}^H \boldsymbol{z}_{S_{01}} & \boldsymbol{w}_{D,1,1}^H \boldsymbol{z}_{S_{11}} \end{bmatrix} = \begin{bmatrix} 1 & 1 \end{bmatrix}, \end{aligned} \tag{4.10}$$

with

$$\boldsymbol{z}_{S_{jm}} = \sum_{\theta \in \Theta_{main_j}} \boldsymbol{s}_m(\theta), \tag{4.11}$$

where $\boldsymbol{L} = \boldsymbol{V}\boldsymbol{U}^{1/2}$, with $\boldsymbol{U}$ being the diagonal matrix including all the eigenvalues of $(\boldsymbol{Q}_S + \boldsymbol{P}_S \tilde{\boldsymbol{I}}_0)$ in (4.6) and $\boldsymbol{V}$ being the corresponding eigenvector matrix [78, 79].

To ensure the magnitudes of the analogue coefficients in the two subarrays are as close as possible to each other, we consider the MinMax approach which minimises the maximum value among the $2N_s$ coefficients for all antennas as follows

$$\min_{\boldsymbol{w}_A} \| \boldsymbol{w}_A \|_\infty, \tag{4.12}$$

where $\| \, . \, \|_\infty$ is the l_∞ norm, representing the maximum magnitude of the entries in the vector. For a given set of $w_{D,j,m}(\{j,m\} \in \{0,1\})$, using the same method as in [80] which combines the above cost function with the previous cost function in (4.10), we reach the following new formulation

$$\begin{aligned} \min_{\boldsymbol{w}_A} \quad & J_{LSE} = \frac{1-\gamma}{N_g} \| \boldsymbol{L}^H \boldsymbol{w}_A \|_2 + \gamma \| \boldsymbol{w}_A \|_\infty, \\ \text{subject} \quad & \text{to} \\ & \boldsymbol{w}_A^H \begin{bmatrix} \boldsymbol{w}_{D,0,0}^H \boldsymbol{z}_{S_{00}} & \boldsymbol{w}_{D,1,0}^H \boldsymbol{z}_{S_{10}} \\ \boldsymbol{w}_{D,0,1}^H \boldsymbol{z}_{S_{01}} & \boldsymbol{w}_{D,1,1}^H \boldsymbol{z}_{S_{11}} \end{bmatrix} = \begin{bmatrix} 1 & 1 \end{bmatrix}, \end{aligned} \tag{4.13}$$

where $\gamma \in (0,1)$ is a trade-off factor between the two parts and N_g is the number of sample points in the sidelobe region for each designed beam. The problem in (4.13) can be solved by the CVX toolbox in [78, 79].

On the other hand, if we know the analogue coefficients $\boldsymbol{w}_A$, we can obtain the optimum digital coding coefficients as follows.

Through combining the digital coefficients for two beams into one vector, given by (3.45), (4.3) can be rewritten as

$$E_s = \boldsymbol{w}_D^H \tilde{\boldsymbol{M}}_S \boldsymbol{w}_D, \tag{4.14}$$

with

$$\tilde{\boldsymbol{M}}_S = \tilde{\boldsymbol{Q}}_S + \tilde{\boldsymbol{P}}_S \tilde{\boldsymbol{I}}_1, \tag{4.15}$$

$$\tilde{\boldsymbol{Q}}_S = \begin{bmatrix} \tilde{\boldsymbol{G}}_{S_{00}} & 0 & 0 & 0 \\ 0 & \tilde{\boldsymbol{G}}_{S_{01}} & 0 & 0 \\ 0 & 0 & \tilde{\boldsymbol{G}}_{S_{10}} & 0 \\ 0 & 0 & 0 & \tilde{\boldsymbol{G}}_{S_{11}} \end{bmatrix}, \tilde{\boldsymbol{P}}_S = \begin{bmatrix} \tilde{\boldsymbol{H}}_{S_0} & \boldsymbol{0}_2 \\ \boldsymbol{0}_2 & \tilde{\boldsymbol{H}}_{S_1} \end{bmatrix}, \tag{4.16}$$

$$\tilde{\boldsymbol{G}}_{S_{jm}} = \boldsymbol{w}_A^H \ddot{\boldsymbol{Q}}_{S_{jm}} \boldsymbol{w}_A, \tilde{\boldsymbol{H}}_{S_j} = \begin{bmatrix} \tilde{\boldsymbol{B}}_{S_{j0}} & 0 \\ 0 & \tilde{\boldsymbol{B}}_{S_{j1}} \end{bmatrix}, \tag{4.17}$$

$$\ddot{\boldsymbol{Q}}_{S_{j0}} = \begin{bmatrix} \boldsymbol{Q}_{S_{j0}} & \boldsymbol{0}_{N_s} \\ \boldsymbol{0}_{N_s} & \boldsymbol{0}_{N_s} \end{bmatrix}, \ddot{\boldsymbol{Q}}_{S_{j1}} = \begin{bmatrix} \boldsymbol{0}_{N_s} & \boldsymbol{0}_{N_s} \\ \boldsymbol{0}_{N_s} & \boldsymbol{Q}_{S_{j1}} \end{bmatrix}, \tag{4.18}$$

$$\tilde{\boldsymbol{B}}_{S_{jm}} = \boldsymbol{w}_A^H \ddot{\boldsymbol{P}}_{S_{jm}} \tilde{\boldsymbol{I}}_0 \boldsymbol{w}_A, \tag{4.19}$$

$$\ddot{\boldsymbol{P}}_{S_{j0}} = \begin{bmatrix} \boldsymbol{P}_{S_{j0}} & \boldsymbol{0}_{N_s} \\ \boldsymbol{0}_{N_s} & \boldsymbol{0}_{N_s} \end{bmatrix}, \ddot{\boldsymbol{P}}_{S_{j1}} = \begin{bmatrix} \boldsymbol{0}_{N_s} & \boldsymbol{0}_{N_s} \\ \boldsymbol{0}_{N_s} & \boldsymbol{P}_{S_{j1}} \end{bmatrix}, \tag{4.20}$$

where $\tilde{\boldsymbol{I}}_1$ is given by (3.48) in Chapter 3. Given the obtained values of $\boldsymbol{w}_A$ in (4.13), the optimisation problem is formulated as

$$\begin{aligned} \min_{\boldsymbol{w}_D} \quad & \boldsymbol{w}_D^H \tilde{\boldsymbol{M}}_S \boldsymbol{w}_D, \\ \text{subject} \quad \text{to} \quad & \\ & \tilde{\boldsymbol{C}}^H \boldsymbol{w}_D = \boldsymbol{f}, \end{aligned} \tag{4.21}$$

with

$$\tilde{\boldsymbol{C}} = \begin{bmatrix} \boldsymbol{w}_A^H \ddot{\boldsymbol{z}}_{S_{00}} & 0 \\ \boldsymbol{w}_A^H \ddot{\boldsymbol{z}}_{S_{01}} & 0 \\ 0 & \boldsymbol{w}_A^H \ddot{\boldsymbol{z}}_{S_{10}} \\ 0 & \boldsymbol{w}_A^H \ddot{\boldsymbol{z}}_{S_{11}} \end{bmatrix}, \boldsymbol{f} = \begin{bmatrix} 1 \\ 1 \end{bmatrix}, \tag{4.22}$$

$$\ddot{\boldsymbol{z}}_{S_{j0}} = \begin{bmatrix} \boldsymbol{z}_{S_{j0}} \\ \boldsymbol{O}_{N_s \times 1} \end{bmatrix}, \ddot{\boldsymbol{z}}_{S_{j1}} = \begin{bmatrix} \boldsymbol{O}_{N_s \times 1} \\ \boldsymbol{z}_{S_{j1}} \end{bmatrix}. \tag{4.23}$$

The solution of problem (4.21) is given by

$$\boldsymbol{w}_D = \tilde{\boldsymbol{M}}_S^{-1} \tilde{\boldsymbol{C}} \left(\tilde{\boldsymbol{C}}^H \tilde{\boldsymbol{M}}_S^{-1} \tilde{\boldsymbol{C}} \right)^{-1} \boldsymbol{f}. \tag{4.24}$$

Alternate optimisation of digital coefficients $\boldsymbol{w}_D$ and analogue coefficients $\boldsymbol{w}_A$ can be achieved iteratively:

(1) First, to possibly increase the chance of reaching a satisfactory design result, $\boldsymbol{w}_D$ is initialised with random values and $\boldsymbol{w}_A$ are obtained by substituting $w_{D,j,m}(\{j,m\} \in \{0,1\})$ into (4.13).

(2) Given the obtained optimum values for $\boldsymbol{w}_A$ in step (1), the optimum values for $\boldsymbol{w}_D$ are obtained using (4.24).

(3) Given the obtained values of $\boldsymbol{w}_D$ in step (2), the new set of values of $\boldsymbol{w}_A$ can be obtained by (4.13) again.

(4) Repeat steps (2) and (3) until the cost function J_{LSE} in (4.13) converges.

Although the magnitudes of the coefficients in $\boldsymbol{w}_A$ cannot be exactly equal after (4.13), they have been already extremely close to each other and can be normalised to the same average value while the phase remains unchanged. As a result, the new analogue coefficients are given by

$$\boldsymbol{w}_A(n) = \frac{\boldsymbol{w}_A(n)}{|\boldsymbol{w}_A(n)|} |\bar{\boldsymbol{w}}_A|, \tag{4.25}$$

where $|\bar{\boldsymbol{w}}_A| = \frac{1}{MN_s} \sum_{n=0}^{MN_s-1} |\boldsymbol{w}_A(n)|$ denotes the average magnitude of the analogue coefficients. Thus, the analogue coefficients of $\boldsymbol{w}_A$ share the same magnitude after (4.25). Moreover, the change of the magnitude due to this normalisation operation is equivalent to an array model error considered in the following robust design, where the magnitude response of each antenna has a little deviation from the assume one. As a result, the possible negative effect of the normalisation operation is further mitigated by the robustness of the proposed design.

4.2.2 The Second Robust Scheme Against Steering Vector Errors

The above design is based on the ideal scenario that all designed steering vectors are the same as the assumed ones. In practice, to design a beamformer robust against steering vector errors, the norm-bounded error vector $\boldsymbol{e}_m$ for the m-th subarray is introduced, and the real steering vector is indicated as $\hat{\boldsymbol{s}}_m(\theta) = \boldsymbol{s}_m(\theta) + \boldsymbol{e}_m$, where $\boldsymbol{s}_m(\theta)$ denotes the assumed steering vector of the m-th subarray. Similar to the method in [81], the difference between the real and desired beam patterns generated by the m-th subarray satisfies

$$\left|\boldsymbol{w}_{A,m}^H \hat{\boldsymbol{s}}_m(\theta) - \boldsymbol{w}_{A,m}^H \boldsymbol{s}_m(\theta)\right| = \left|\boldsymbol{w}_{A,m}^H \boldsymbol{e}_m\right| \leq \epsilon_m \parallel \boldsymbol{w}_{A,m} \parallel_2, \tag{4.26}$$

where ϵ_m denotes the upper norm-bound of $\boldsymbol{e}_m$ for the m-th subarray.

By combining the norm-bounded vectors $\boldsymbol{e}_0$ and $\boldsymbol{e}_1$ into

$$\boldsymbol{e} = \left[\boldsymbol{e}_0^T, \boldsymbol{e}_1^T\right]^T, \tag{4.27}$$

the difference between the real and desired beam patterns for the j-th beam is given by

$$\begin{aligned}
&|\sum_{m=0}^{1} w_{D,j,m}^* \boldsymbol{w}_{A,m}^H (\hat{\boldsymbol{s}}_m(\theta) - \boldsymbol{s}_m(\theta))| \\
=&\left|w_{D,j,0}^* \boldsymbol{w}_{A,0}^H \boldsymbol{e}_0 + w_{D,j,1}^* \boldsymbol{w}_{A,1}^H \boldsymbol{e}_1\right| \\
=&\left|\boldsymbol{w}_A^H \begin{bmatrix} \boldsymbol{w}_{D,j,0}^H & \boldsymbol{0}_{N_s} \\ \boldsymbol{0}_{N_s} & \boldsymbol{w}_{D,j,1}^H \end{bmatrix} \boldsymbol{e}\right| \\
\leq&\sqrt{2}\epsilon_e \parallel \mathrm{diag}(\boldsymbol{w}_{D,j}) \parallel_F \parallel \boldsymbol{w}_A \parallel_2, \quad \forall j \in \{0,1\},
\end{aligned} \tag{4.28}$$

with

$$\mathrm{diag}(\boldsymbol{w}_{D,j}) = \begin{bmatrix} \boldsymbol{w}_{D,j,0}^H & \boldsymbol{0}_{N_s} \\ \boldsymbol{0}_{N_s} & \boldsymbol{w}_{D,j,1}^H \end{bmatrix}, \tag{4.29}$$

where $\parallel \cdot \parallel_F$ is the Frobenius norm, ϵ_e denotes the maximum value among ϵ_0 and ϵ_1 and diag (.) denotes the diagonalisation operation. Then, the following constraint can be incorporated into the design to make sure that the difference between the real and desired beam patterns of the j-th beam satisfies the following requirement

$$\sqrt{2}\epsilon_e \parallel \mathrm{diag}(\boldsymbol{w}_{D,j}) \parallel_F \parallel \boldsymbol{w}_A \parallel_2 \leq \zeta, \quad \forall j \in \{0,1\}, \tag{4.30}$$

where ζ denotes the change in the magnitude response at the mainlobe direction given the maximum allowable steering vector error. Hence, a new optimisation problem for the robust design can be formulated as

$$\begin{aligned} \min_{\boldsymbol{w}_A} \quad & J_{LSE} = \| \boldsymbol{L}^H \boldsymbol{w}_A \|_2, \\ \text{subject} \quad & \text{to} \\ & \boldsymbol{w}_A^H \begin{bmatrix} \boldsymbol{w}_{D,0,0}^H \boldsymbol{z}_{S_{00}} & \boldsymbol{w}_{D,1,0}^H \boldsymbol{z}_{S_{10}} \\ \boldsymbol{w}_{D,0,1}^H \boldsymbol{z}_{S_{01}} & \boldsymbol{w}_{D,1,1}^H \boldsymbol{z}_{S_{11}} \end{bmatrix} = \begin{bmatrix} 1 & 1 \end{bmatrix}, \\ & \| \operatorname{diag}(\boldsymbol{w}_{D,j}) \|_F \| \boldsymbol{w}_A \|_2 \leq \frac{\sigma}{\sqrt{2}}, \quad \forall j \in \{0,1\}, \end{aligned} \tag{4.31}$$

where $\sigma = \zeta/\epsilon_e$, $\boldsymbol{L}$ and $\boldsymbol{z}_{S_{jm}}$ are the same as in (4.10) and (4.11), respectively, in Section 4.2.1.

Alternate optimisation of the digital coefficients $\boldsymbol{w}_D$ and the corresponding analogue coefficients $\boldsymbol{w}_A$ can be obtained by the following iterative process:

(1) First, via initialising the digital coefficients $\boldsymbol{w}_D$ with random values, $\boldsymbol{w}_A$ is then obtained by substituting $w_{D,j,m}(\{j,m\} \in \{0,1\})$ into (4.31).

(2) Given the obtained value of $\boldsymbol{w}_A$ in step (1), the closed-form solution of digital coefficients $\boldsymbol{w}_D$ is obtained by (4.24).

(3) Given the obtained values of $\boldsymbol{w}_D$ in step (2), the new set of values of $\boldsymbol{w}_A$ is obtained by (4.31) again.

(4) Repeat steps (2) and (3) until the cost function J_{LSE} in (4.31) converges.

4.2.3 The Third Robust Scheme with Nearly Equal Magnitude Constraint on Analogue Coefficients

Now the two designs in Sections 4.2.1 and 4.2.2 can be combined together into a new formulation, so that the resultant beamformer is not only robust against steering vector errors, but also has all its analogue coefficients with a strictly equal magnitude.

By adding the last constraint in (4.31) into (4.13), the optimisation problem (4.13) changes to

$$\begin{aligned} \min_{\boldsymbol{w}_A} \quad & J_{LSE} = \frac{1-\gamma}{N_g} \parallel \boldsymbol{L}^H \boldsymbol{w}_A \parallel_2 + \gamma \parallel \boldsymbol{w}_A \parallel_\infty, \\ \text{subject} \quad & \text{to} \\ & \boldsymbol{w}_A^H \begin{bmatrix} \boldsymbol{w}_{D,0,0}^H \boldsymbol{z}_{S_{00}} & \boldsymbol{w}_{D,1,0}^H \boldsymbol{z}_{S_{10}} \\ \boldsymbol{w}_{D,0,1}^H \boldsymbol{z}_{S_{01}} & \boldsymbol{w}_{D,1,1}^H \boldsymbol{z}_{S_{11}} \end{bmatrix} = \begin{bmatrix} 1 & 1 \end{bmatrix}, \\ & \parallel \text{diag}(\boldsymbol{w}_{D,j}) \parallel_F \parallel \boldsymbol{w}_A \parallel_2 \leq \frac{\sigma}{\sqrt{2}}, \quad \forall j \in \{0,1\}. \end{aligned} \tag{4.32}$$

Alternate optimisation of the digital coefficients $\boldsymbol{w}_D$ and the corresponding analogue coefficients $\boldsymbol{w}_A$ can be obtained by the following iterative process:

(1) First, via initialising the digital coefficients $\boldsymbol{w}_D$ with random values, $\boldsymbol{w}_A$ is then obtained by substituting $w_{D,j,m}(\{j,m\} \in \{0,1\})$ into (4.32).

(2) Given the obtained values of $\boldsymbol{w}_A$ in step (1), the closed-form solution of digital coefficients $\boldsymbol{w}_D$ is obtained by (4.24).

(3) Given the obtained values of $\boldsymbol{w}_D$ in step (2), the new set of values of $\boldsymbol{w}_A$ is obtained by (4.32) again.

(4) Repeat steps (2) and (3) until the cost function J_{LSE} in (4.32) converges.

4.2.4 The Fourth Scheme without any Constraints

To highlight the performance of the three proposed schemes in Sections 4.2.1, 4.2.2 and 4.2.3, as a comparison, this section gives a fourth scheme without constraints for either equal magnitude on analogue coefficients or robustness against steering vector errors.

Alternate optimisation of the digital coefficients $\boldsymbol{w}_D$ and the corresponding analogue coefficients $\boldsymbol{w}_A$ can be obtained by the following iterative process:

(1) First, via initialising the digital coefficients $\boldsymbol{w}_D$ with random values, $\boldsymbol{w}_A$ is then obtained by substituting $w_{D,j,m}(\{j,m\} \in \{0,1\})$ into (4.10).

(2) Given the obtained values of $\boldsymbol{w}_A$ in step (1), the closed-form solution of digital coefficients $\boldsymbol{w}_D$ is obtained by (4.24).

(3) Given the obtained values of $\boldsymbol{w}_D$ in step (2), the new set of values of $\boldsymbol{w}_A$ is obtained by (4.10) again.

(4) Repeat steps (2) and (3) until the cost function J_{LSE} in (4.10) converges.

4.3 Three-Beam Case

4.3.1 The First Scheme with Nearly Equal Magnitude Constraint on Analogue Coefficients

The sum of sidelobe patterns in (4.1) with $J = 3$ can be expanded as

$$\begin{aligned} E_s = \sum_{j=0}^{2} \Big(& w_{D,j,0}^* \boldsymbol{w}_{A,0}^H \boldsymbol{Q}_{S_{j0}} \boldsymbol{w}_{A,0} w_{D,j,0} + w_{D,j,1}^* \boldsymbol{w}_{A,1}^H \boldsymbol{Q}_{S_{j1}} \boldsymbol{w}_{A,1} w_{D,j,1} \\ & + w_{D,j,2}^* \boldsymbol{w}_{A,2}^H \boldsymbol{Q}_{S_{j2}} \boldsymbol{w}_{A,2} w_{D,j,2} \\ & + w_{D,j,0}^* \boldsymbol{w}_{A,0}^H \boldsymbol{P}_{S_{01j}} \boldsymbol{w}_{A,1} w_{D,j,1} + w_{D,j,1}^* \boldsymbol{w}_{A,1}^H \boldsymbol{P}_{S_{10j}} \boldsymbol{w}_{A,0} w_{D,j,0} \\ & + w_{D,j,0}^* \boldsymbol{w}_{A,0}^H \boldsymbol{P}_{S_{02j}} \boldsymbol{w}_{A,2} w_{D,j,2} + w_{D,j,2}^* \boldsymbol{w}_{A,2}^H \boldsymbol{P}_{S_{20j}} \boldsymbol{w}_{A,0} w_{D,j,0} \\ & + w_{D,j,1}^* \boldsymbol{w}_{A,1}^H \boldsymbol{P}_{S_{12j}} \boldsymbol{w}_{A,2} w_{D,j,2} + w_{D,j,2}^* \boldsymbol{w}_{A,2}^H \boldsymbol{P}_{S_{21j}} \boldsymbol{w}_{A,1} w_{D,j,1} \Big), \end{aligned} \tag{4.33}$$

with

$$\boldsymbol{P}_{S_{ikj}} = \sum_{\theta \in \Theta_{side_j}} \boldsymbol{s}_i(\theta) \boldsymbol{s}_k(\theta)^H, \tag{4.34}$$

where $\{j, m, i, k\} \in \{0, 1, 2\}$ but $i \neq k$, $\boldsymbol{Q}_{S_{jm}}$ and $\boldsymbol{S}_m(\theta)$ are given in (4.4) and (3.35), respectively. By combining the analogue coefficients $\boldsymbol{w}_{A,0}$, $\boldsymbol{w}_{A,1}$ and $\boldsymbol{w}_{A,2}$ into one vector as (3.60), (4.33) can be rewritten as

$$E_s = \boldsymbol{w}_A^H \left(\boldsymbol{Q}_S + \boldsymbol{P}_S \tilde{\boldsymbol{I}}_2 + \boldsymbol{R}_S \tilde{\boldsymbol{I}}_3 \right) \boldsymbol{w}_A, \tag{4.35}$$

with

$$\boldsymbol{Q}_S = \begin{bmatrix} \boldsymbol{G}_{S_0} & \boldsymbol{0}_{N_s} & \boldsymbol{0}_{N_s} \\ \boldsymbol{0}_{N_s} & \boldsymbol{G}_{S_1} & \boldsymbol{0}_{N_s} \\ \boldsymbol{0}_{N_s} & \boldsymbol{0}_{N_s} & \boldsymbol{G}_{S_2} \end{bmatrix}, \boldsymbol{P}_S = \begin{bmatrix} \boldsymbol{H}_{S_0} & \boldsymbol{0}_{N_s} & \boldsymbol{0}_{N_s} \\ \boldsymbol{0}_{N_s} & \boldsymbol{H}_{S_1} & \boldsymbol{0}_{N_s} \\ \boldsymbol{0}_{N_s} & \boldsymbol{0}_{N_s} & \boldsymbol{H}_{S_2} \end{bmatrix}, \boldsymbol{R}_S = \begin{bmatrix} \boldsymbol{Y}_{S_0} & \boldsymbol{0}_{N_s} & \boldsymbol{0}_{N_s} \\ \boldsymbol{0}_{N_s} & \boldsymbol{Y}_{S_1} & \boldsymbol{0}_{N_s} \\ \boldsymbol{0}_{N_s} & \boldsymbol{0}_{N_s} & \boldsymbol{Y}_{S_2} \end{bmatrix}, \tag{4.36}$$

$$\boldsymbol{G}_{S_m} = \boldsymbol{w}_{D,0,m}^H \boldsymbol{Q}_{S_{0m}} \boldsymbol{w}_{D,0,m} + \boldsymbol{w}_{D,1,m}^H \boldsymbol{Q}_{S_{1m}} \boldsymbol{w}_{D,1,m} + \boldsymbol{w}_{D,2,m}^H \boldsymbol{Q}_{S_{2m}} \boldsymbol{w}_{D,2,m}, \tag{4.37}$$

$$
\begin{aligned}
\boldsymbol{H}_{S_0} &= \boldsymbol{w}_{D,0,0}^H \boldsymbol{P}_{S_{010}} \boldsymbol{w}_{D,0,1} + \boldsymbol{w}_{D,1,0}^H \boldsymbol{P}_{S_{011}} \boldsymbol{w}_{D,1,1} + \boldsymbol{w}_{D,2,0}^H \boldsymbol{P}_{S_{012}} \boldsymbol{w}_{D,2,1}, \\
\boldsymbol{H}_{S_1} &= \boldsymbol{w}_{D,0,1}^H \boldsymbol{P}_{S_{120}} \boldsymbol{w}_{D,0,2} + \boldsymbol{w}_{D,1,1}^H \boldsymbol{P}_{S_{121}} \boldsymbol{w}_{D,1,2} + \boldsymbol{w}_{D,2,1}^H \boldsymbol{P}_{S_{122}} \boldsymbol{w}_{D,2,2}, \\
\boldsymbol{H}_{S_2} &= \boldsymbol{w}_{D,0,2}^H \boldsymbol{P}_{S_{200}} \boldsymbol{w}_{D,0,0} + \boldsymbol{w}_{D,1,2}^H \boldsymbol{P}_{S_{201}} \boldsymbol{w}_{D,1,0} + \boldsymbol{w}_{D,2,2}^H \boldsymbol{P}_{S_{202}} \boldsymbol{w}_{D,2,0},
\end{aligned} \tag{4.38}
$$

$$
\begin{aligned}
\boldsymbol{Y}_{S_0} &= \boldsymbol{w}_{D,0,0}^H \boldsymbol{P}_{S_{020}} \boldsymbol{w}_{D,0,2} + \boldsymbol{w}_{D,1,0}^H \boldsymbol{P}_{S_{021}} \boldsymbol{w}_{D,1,2} + \boldsymbol{w}_{D,2,0}^H \boldsymbol{P}_{S_{022}} \boldsymbol{w}_{D,2,2}, \\
\boldsymbol{Y}_{S_1} &= \boldsymbol{w}_{D,0,1}^H \boldsymbol{P}_{S_{100}} \boldsymbol{w}_{D,0,0} + \boldsymbol{w}_{D,1,1}^H \boldsymbol{P}_{S_{101}} \boldsymbol{w}_{D,1,0} + \boldsymbol{w}_{D,2,1}^H \boldsymbol{P}_{S_{102}} \boldsymbol{w}_{D,2,0}, \\
\boldsymbol{Y}_{S_2} &= \boldsymbol{w}_{D,0,2}^H \boldsymbol{P}_{S_{210}} \boldsymbol{w}_{D,0,1} + \boldsymbol{w}_{D,1,2}^H \boldsymbol{P}_{S_{211}} \boldsymbol{w}_{D,1,1} + \boldsymbol{w}_{D,2,2}^H \boldsymbol{P}_{S_{212}} \boldsymbol{w}_{D,2,1},
\end{aligned} \tag{4.39}
$$

where $\tilde{\boldsymbol{I}}_2$ and $\tilde{\boldsymbol{I}}_3$ is given in (3.63) and $\boldsymbol{w}_{D,j,m}$ is given in (3.43).

An intermediate formulation without any requirements for the three designed beams can be expressed as

$$
\begin{aligned}
&\min_{\boldsymbol{w}_A} \quad J_{LSE} = \| \boldsymbol{L}^H \boldsymbol{w}_A \|_2, \\
&\text{subject} \quad \text{to} \\
&\boldsymbol{w}_A^H \begin{bmatrix} \boldsymbol{w}_{D,0,0}^H \boldsymbol{z}_{S_{00}} & \boldsymbol{w}_{D,1,0}^H \boldsymbol{z}_{S_{10}} & \boldsymbol{w}_{D,2,0}^H \boldsymbol{z}_{S_{20}} \\ \boldsymbol{w}_{D,0,1}^H \boldsymbol{z}_{S_{01}} & \boldsymbol{w}_{D,1,1}^H \boldsymbol{z}_{S_{11}} & \boldsymbol{w}_{D,2,1}^H \boldsymbol{z}_{S_{21}} \\ \boldsymbol{w}_{D,0,2}^H \boldsymbol{z}_{S_{02}} & \boldsymbol{w}_{D,1,2}^H \boldsymbol{z}_{S_{12}} & \boldsymbol{w}_{D,2,2}^H \boldsymbol{z}_{S_{22}} \end{bmatrix} = \begin{bmatrix} 1 & 1 & 1 \end{bmatrix},
\end{aligned} \tag{4.40}
$$

where $\boldsymbol{L} = \boldsymbol{V}\boldsymbol{U}^{1/2}$, $\boldsymbol{U}$ denotes the diagonal matrix including all eigenvalues of $(\boldsymbol{Q}_S + \boldsymbol{P}_S\tilde{\boldsymbol{I}}_2 + \boldsymbol{R}_S\tilde{\boldsymbol{I}}_3)$ in (4.35) and $\boldsymbol{V}$ the corresponding eigenvector matrix.

Similar to (4.13), the new formulation of the scheme to have a nearly equal magnitude constraint on analogue coefficients is given by

$$
\begin{aligned}
&\min_{\boldsymbol{w}_A} \quad J_{LSE} = \frac{1-\gamma}{N_g} \| \boldsymbol{L}^H \boldsymbol{w}_A \|_2 + \gamma \| \boldsymbol{w}_A \|_\infty, \\
&\text{subject} \quad \text{to} \\
&\boldsymbol{w}_A^H \begin{bmatrix} \boldsymbol{w}_{D,0,0}^H \boldsymbol{z}_{S_{00}} & \boldsymbol{w}_{D,1,0}^H \boldsymbol{z}_{S_{10}} & \boldsymbol{w}_{D,2,0}^H \boldsymbol{z}_{S_{20}} \\ \boldsymbol{w}_{D,0,1}^H \boldsymbol{z}_{S_{01}} & \boldsymbol{w}_{D,1,1}^H \boldsymbol{z}_{S_{11}} & \boldsymbol{w}_{D,2,1}^H \boldsymbol{z}_{S_{21}} \\ \boldsymbol{w}_{D,0,2}^H \boldsymbol{z}_{S_{02}} & \boldsymbol{w}_{D,1,2}^H \boldsymbol{z}_{S_{12}} & \boldsymbol{w}_{D,2,2}^H \boldsymbol{z}_{S_{22}} \end{bmatrix} = \begin{bmatrix} 1 & 1 & 1 \end{bmatrix}.
\end{aligned} \tag{4.41}
$$

On the other hand, by combining the digital coefficients for the three beams into one vector given by (3.69), (4.33) can be written as (4.14) with

$$
\tilde{\boldsymbol{M}}_S = \tilde{\boldsymbol{Q}}_S + \tilde{\boldsymbol{P}}_S\tilde{\boldsymbol{I}}_4 + \tilde{\boldsymbol{R}}_S\tilde{\boldsymbol{I}}_5, \tag{4.42}
$$

$$\tilde{\boldsymbol{Q}}_S = \begin{bmatrix} \tilde{\boldsymbol{G}}_{S_{00}} & 0 & \cdots & 0 \\ 0 & \tilde{\boldsymbol{G}}_{S_{01}} & \ddots & \vdots \\ \vdots & \ddots & \ddots & 0 \\ 0 & \cdots & 0 & \tilde{\boldsymbol{G}}_{S_{22}} \end{bmatrix}, \tilde{\boldsymbol{P}}_S = \begin{bmatrix} \tilde{\boldsymbol{H}}_{S_0} & \boldsymbol{0}_3 & \boldsymbol{0}_3 \\ \boldsymbol{0}_3 & \tilde{\boldsymbol{H}}_{S_1} & \boldsymbol{0}_3 \\ \boldsymbol{0}_3 & \boldsymbol{0}_3 & \tilde{\boldsymbol{H}}_{S_2} \end{bmatrix}, \tilde{\boldsymbol{R}}_S = \begin{bmatrix} \tilde{\boldsymbol{Y}}_{S_0} & \boldsymbol{0}_3 & \boldsymbol{0}_3 \\ \boldsymbol{0}_3 & \tilde{\boldsymbol{Y}}_{S_1} & \boldsymbol{0}_3 \\ \boldsymbol{0}_3 & \boldsymbol{0}_3 & \tilde{\boldsymbol{Y}}_{S_2} \end{bmatrix}, \tag{4.43}$$

$$\tilde{\boldsymbol{H}}_{S_j} = \begin{bmatrix} \tilde{\boldsymbol{B}}_{S_{j0}} & 0 & 0 \\ 0 & \tilde{\boldsymbol{B}}_{S_{j1}} & 0 \\ 0 & 0 & \tilde{\boldsymbol{B}}_{S_{j2}} \end{bmatrix}, \tilde{\boldsymbol{Y}}_{S_j} = \begin{bmatrix} \tilde{\boldsymbol{D}}_{S_{j0}} & 0 & 0 \\ 0 & \tilde{\boldsymbol{D}}_{S_{j1}} & 0 \\ 0 & 0 & \tilde{\boldsymbol{D}}_{S_{j2}} \end{bmatrix}, \tag{4.44}$$

$$\ddot{\boldsymbol{Q}}_{S_{j0}} = \begin{bmatrix} \boldsymbol{Q}_{S_{j0}} & \boldsymbol{0}_{N_s} & \boldsymbol{0}_{N_s} \\ \boldsymbol{0}_{N_s} & \boldsymbol{0}_{N_s} & \boldsymbol{0}_{N_s} \\ \boldsymbol{0}_{N_s} & \boldsymbol{0}_{N_s} & \boldsymbol{0}_{N_s} \end{bmatrix}, \ddot{\boldsymbol{Q}}_{S_{j1}} = \begin{bmatrix} \boldsymbol{0}_{N_s} & \boldsymbol{0}_{N_s} & \boldsymbol{0}_{N_s} \\ \boldsymbol{0}_{N_s} & \boldsymbol{Q}_{S_{j1}} & \boldsymbol{0}_{N_s} \\ \boldsymbol{0}_{N_s} & \boldsymbol{0}_{N_s} & \boldsymbol{0}_{N_s} \end{bmatrix}, \ddot{\boldsymbol{Q}}_{S_{j2}} = \begin{bmatrix} \boldsymbol{0}_{N_s} & \boldsymbol{0}_{N_s} & \boldsymbol{0}_{N_s} \\ \boldsymbol{0}_{N_s} & \boldsymbol{0}_{N_s} & \boldsymbol{0}_{N_s} \\ \boldsymbol{0}_{N_s} & \boldsymbol{0}_{N_s} & \boldsymbol{Q}_{S_{j2}} \end{bmatrix}, \tag{4.45}$$

$$\begin{aligned} \tilde{\boldsymbol{B}}_{S_{j0}} &= \boldsymbol{w}_A^H \ddot{\boldsymbol{P}}_{S_{j0}} \tilde{\boldsymbol{I}}_6 \boldsymbol{w}_A, \quad \tilde{\boldsymbol{D}}_{S_{j0}} = \boldsymbol{w}_A^H \ddot{\boldsymbol{R}}_{S_{j0}} \tilde{\boldsymbol{I}}_3 \boldsymbol{w}_A, \\ \tilde{\boldsymbol{B}}_{S_{j1}} &= \boldsymbol{w}_A^H \ddot{\boldsymbol{P}}_{S_{j1}} \tilde{\boldsymbol{I}}_7 \boldsymbol{w}_A, \quad \tilde{\boldsymbol{D}}_{S_{j1}} = \boldsymbol{w}_A^H \ddot{\boldsymbol{R}}_{S_{j1}} \tilde{\boldsymbol{I}}_6 \boldsymbol{w}_A, \\ \tilde{\boldsymbol{B}}_{S_{j2}} &= \boldsymbol{w}_A^H \ddot{\boldsymbol{P}}_{S_{j2}} \tilde{\boldsymbol{I}}_2 \boldsymbol{w}_A, \quad \tilde{\boldsymbol{D}}_{S_{j2}} = \boldsymbol{w}_A^H \ddot{\boldsymbol{R}}_{S_{j2}} \tilde{\boldsymbol{I}}_7 \boldsymbol{w}_A, \end{aligned} \tag{4.46}$$

$$\ddot{\boldsymbol{P}}_{S_{j0}} = \begin{bmatrix} \boldsymbol{P}_{S_{01j}} & \boldsymbol{0}_{N_s} & \boldsymbol{0}_{N_s} \\ \boldsymbol{0}_{N_s} & \boldsymbol{0}_{N_s} & \boldsymbol{0}_{N_s} \\ \boldsymbol{0}_{N_s} & \boldsymbol{0}_{N_s} & \boldsymbol{0}_{N_s} \end{bmatrix}, \ddot{\boldsymbol{P}}_{S_{j1}} = \begin{bmatrix} \boldsymbol{0}_{N_s} & \boldsymbol{0}_{N_s} & \boldsymbol{0}_{N_s} \\ \boldsymbol{0}_{N_s} & \boldsymbol{P}_{S_{12j}} & \boldsymbol{0}_{N_s} \\ \boldsymbol{0}_{N_s} & \boldsymbol{0}_{N_s} & \boldsymbol{0}_{N_s} \end{bmatrix}, \ddot{\boldsymbol{P}}_{S_{j2}} = \begin{bmatrix} \boldsymbol{0}_{N_s} & \boldsymbol{0}_{N_s} & \boldsymbol{0}_{N_s} \\ \boldsymbol{0}_{N_s} & \boldsymbol{0}_{N_s} & \boldsymbol{0}_{N_s} \\ \boldsymbol{0}_{N_s} & \boldsymbol{0}_{N_s} & \boldsymbol{P}_{S_{20j}} \end{bmatrix}, \tag{4.47}$$

$$\ddot{\boldsymbol{R}}_{S_{j0}} = \begin{bmatrix} \boldsymbol{P}_{S_{02j}} & \boldsymbol{0}_{N_s} & \boldsymbol{0}_{N_s} \\ \boldsymbol{0}_{N_s} & \boldsymbol{0}_{N_s} & \boldsymbol{0}_{N_s} \\ \boldsymbol{0}_{N_s} & \boldsymbol{0}_{N_s} & \boldsymbol{0}_{N_s} \end{bmatrix}, \ddot{\boldsymbol{R}}_{S_{j1}} = \begin{bmatrix} \boldsymbol{0}_{N_s} & \boldsymbol{0}_{N_s} & \boldsymbol{0}_{N_s} \\ \boldsymbol{0}_{N_s} & \boldsymbol{P}_{S_{10j}} & \boldsymbol{0}_{N_s} \\ \boldsymbol{0}_{N_s} & \boldsymbol{0}_{N_s} & \boldsymbol{0}_{N_s} \end{bmatrix}, \ddot{\boldsymbol{R}}_{S_{j2}} = \begin{bmatrix} \boldsymbol{0}_{N_s} & \boldsymbol{0}_{N_s} & \boldsymbol{0}_{N_s} \\ \boldsymbol{0}_{N_s} & \boldsymbol{0}_{N_s} & \boldsymbol{0}_{N_s} \\ \boldsymbol{0}_{N_s} & \boldsymbol{0}_{N_s} & \boldsymbol{P}_{S_{21j}} \end{bmatrix}, \tag{4.48}$$

where $\tilde{\boldsymbol{G}}_{S_{jm}}$ is given by (4.17) and $\tilde{\boldsymbol{I}}_q (q \in \{4,5,6,7\})$ is given in (3.72), (3.80) and (3.81), respectively. Given the obtained values of $\boldsymbol{w}_A$ in (4.41), to find the closed-form solution

of digital coefficients $\boldsymbol{w}_D$, the optimisation problem is formulated as (4.21) with

$$\tilde{\boldsymbol{C}} = \begin{bmatrix} \boldsymbol{w}_A^H \ddot{\boldsymbol{z}}_{S_{00}} & 0 & 0 \\ \boldsymbol{w}_A^H \ddot{\boldsymbol{z}}_{S_{01}} & 0 & 0 \\ \boldsymbol{w}_A^H \ddot{\boldsymbol{z}}_{S_{02}} & 0 & 0 \\ 0 & \boldsymbol{w}_A^H \ddot{\boldsymbol{z}}_{S_{10}} & 0 \\ 0 & \boldsymbol{w}_A^H \ddot{\boldsymbol{z}}_{S_{11}} & 0 \\ 0 & \boldsymbol{w}_A^H \ddot{\boldsymbol{z}}_{S_{12}} & 0 \\ 0 & 0 & \boldsymbol{w}_A^H \ddot{\boldsymbol{z}}_{S_{20}} \\ 0 & 0 & \boldsymbol{w}_A^H \ddot{\boldsymbol{z}}_{S_{21}} \\ 0 & 0 & \boldsymbol{w}_A^H \ddot{\boldsymbol{z}}_{S_{22}} \end{bmatrix}, \boldsymbol{f} = \begin{bmatrix} 1 \\ 1 \\ 1 \end{bmatrix}, \tag{4.49}$$

$$\ddot{\boldsymbol{z}}_{S_{j0}} = \begin{bmatrix} \boldsymbol{z}_{S_{j0}} \\ \boldsymbol{0}_{N_s \times 1} \\ \boldsymbol{0}_{N_s \times 1} \end{bmatrix}, \ddot{\boldsymbol{z}}_{S_{j1}} = \begin{bmatrix} \boldsymbol{0}_{N_s \times 1} \\ \boldsymbol{z}_{S_{j1}} \\ \boldsymbol{0}_{N_s \times 1} \end{bmatrix}, \ddot{\boldsymbol{z}}_{S_{j2}} = \begin{bmatrix} \boldsymbol{0}_{N_s \times 1} \\ \boldsymbol{0}_{N_s \times 1} \\ \boldsymbol{z}_{S_{j2}} \end{bmatrix}. \tag{4.50}$$

The solution to the problem (4.21) with $M = J = 3$ in Section 4.3.1 is given by (4.24).

Now alternate optimisation of the digital coefficients $\boldsymbol{w}_D$ and the corresponding analogue coefficients $\boldsymbol{w}_A$ can be obtained by the following iterative process:

(1) First, through initialising $\boldsymbol{w}_D$ with random values, $\boldsymbol{w}_A$ is obtained by substituting $w_{D,j,m}(\{j,m\} \in \{0,1,2\})$ into (4.41).

(2) Given the obtained optimum values for $\boldsymbol{w}_A$ in step (1), the closed-form solution for digital coefficients $\boldsymbol{w}_D$ is obtained by (4.24).

(3) Given the obtained values of $\boldsymbol{w}_D$ in step (2), the new set of values of $\boldsymbol{w}_A$ is obtained by (4.41) again.

(4) Repeat steps (2) and (3) until the cost function J_{LSE} in (4.41) converges.

4.3.2 The Second Robust Scheme Against Steering Vector Errors

Similar to (4.28), the difference between the real and desired beam patterns for the j-th beam with $M = 3$ is given by

$$\begin{aligned}
&|\sum_{m=0}^{2} w_{D,j,m}^{*} \boldsymbol{w}_{A,m}^{H}(\hat{\boldsymbol{s}}_m(\theta) - \boldsymbol{s}_m(\theta))| \\
=&\left|w_{D,j,0}^{*}\boldsymbol{w}_{A,0}^{H}\boldsymbol{e}_0 + w_{D,j,1}^{*}\boldsymbol{w}_{A,1}^{H}\boldsymbol{e}_1 + w_{D,j,2}^{*}\boldsymbol{w}_{A,2}^{H}\boldsymbol{e}_2\right| \\
=&\left|\boldsymbol{w}_A^H \begin{bmatrix} \boldsymbol{w}_{D,j,0}^H & \boldsymbol{0}_{N_s} & \boldsymbol{0}_{N_s} \\ \boldsymbol{0}_{N_s} & \boldsymbol{w}_{D,j,1}^H & \boldsymbol{0}_{N_s} \\ \boldsymbol{0}_{N_s} & \boldsymbol{0}_{N_s} & \boldsymbol{w}_{D,j,2}^H \end{bmatrix} \boldsymbol{e}\right| \\
\leq&\sqrt{3}\epsilon_e \parallel \text{diag}(\boldsymbol{w}_{D,j}) \parallel_F \parallel \boldsymbol{w}_A \parallel_2, \quad \forall j \in \{0,1,2\},
\end{aligned} \tag{4.51}$$

with

$$\text{diag}(\boldsymbol{w}_{D,j}) = \begin{bmatrix} \boldsymbol{w}_{D,j,0}^H & \boldsymbol{0}_{N_s} & \boldsymbol{0}_{N_s} \\ \boldsymbol{0}_{N_s} & \boldsymbol{w}_{D,j,1}^H & \boldsymbol{0}_{N_s} \\ \boldsymbol{0}_{N_s} & \boldsymbol{0}_{N_s} & \boldsymbol{w}_{D,j,2}^H \end{bmatrix}, \tag{4.52}$$

$$\boldsymbol{e} = \left[\boldsymbol{e}_0^T, \boldsymbol{e}_1^T, \boldsymbol{e}_2^T\right]^T, \tag{4.53}$$

where ϵ_e denotes the maximum value among ϵ_0, ϵ_1 and ϵ_2. The robust constraint against steering vector errors which is similar to (4.30) is given by

$$\sqrt{3}\epsilon_e \parallel \text{diag}(\boldsymbol{w}_{D,j}) \parallel_F \parallel \boldsymbol{w}_A \parallel_2 \leq \zeta, \quad \forall j \in \{0,1,2\}, \tag{4.54}$$

and a new optimisation problem can be formulated as

$$\begin{aligned}
&\min_{\boldsymbol{w}_A} \qquad J_{LSE} = \parallel \boldsymbol{L}^H \boldsymbol{w}_A \parallel_2, \\
&\text{subject} \quad \text{to} \\
&\boldsymbol{w}_A^H \begin{bmatrix} \boldsymbol{w}_{D,0,0}^H \boldsymbol{z}_{S_{00}} & \boldsymbol{w}_{D,1,0}^H \boldsymbol{z}_{S_{10}} & \boldsymbol{w}_{D,2,0}^H \boldsymbol{z}_{S_{20}} \\ \boldsymbol{w}_{D,0,1}^H \boldsymbol{z}_{S_{01}} & \boldsymbol{w}_{D,1,1}^H \boldsymbol{z}_{S_{11}} & \boldsymbol{w}_{D,2,1}^H \boldsymbol{z}_{S_{21}} \\ \boldsymbol{w}_{D,0,2}^H \boldsymbol{z}_{S_{02}} & \boldsymbol{w}_{D,1,2}^H \boldsymbol{z}_{S_{12}} & \boldsymbol{w}_{D,2,2}^H \boldsymbol{z}_{S_{22}} \end{bmatrix} = \begin{bmatrix} 1 & 1 & 1 \end{bmatrix}, \\
&\parallel \text{diag}(\boldsymbol{w}_{D,j}) \parallel_F \parallel \boldsymbol{w}_A \parallel_2 \leq \frac{\sigma}{\sqrt{3}}, \quad \forall j \in \{0,1,2\}.
\end{aligned} \tag{4.55}$$

Alternate optimisation of the digital coefficients $\boldsymbol{w}_D$ and the corresponding analogue coefficients $\boldsymbol{w}_A$ can be obtained by the following iterative process:

(1) First, via initialising the digital coefficients $\boldsymbol{w}_D$ with random values, $\boldsymbol{w}_A$ is then obtained by substituting $w_{D,j,m}(\{j,m\} \in \{0,1,2\})$ into (4.55).

(2) Given the obtained value of $\boldsymbol{w}_A$ in step (1), the closed-form solution for digital coefficients $\boldsymbol{w}_D$ is obtained by (4.24).

(3) Given the obtained values of $\boldsymbol{w}_D$ in step (2), the new set of values of $\boldsymbol{w}_A$ is obtained by (4.55) again.

(4) Repeat steps (2) and (3) until the cost function J_{LSE} in (4.55) converges.

4.3.3 The Third Robust Scheme with Nearly Equal Magnitude Constraint on Analogue Coefficients

By adding the last constraint in (4.55) into (4.41), the optimisation of the new problem is formulated as

$$\begin{aligned} \min_{\boldsymbol{w}_A} \quad & J_{LSE} = \frac{1-\gamma}{N_g} \parallel \boldsymbol{L}^H \boldsymbol{w}_A \parallel_2 + \gamma \parallel \boldsymbol{w}_A \parallel_\infty, \\ \text{subject} \quad & \text{to} \\ & \boldsymbol{w}_A^H \begin{bmatrix} \boldsymbol{w}_{D,0,0}^H \boldsymbol{z}_{S_{00}} & \boldsymbol{w}_{D,1,0}^H \boldsymbol{z}_{S_{10}} & \boldsymbol{w}_{D,2,0}^H \boldsymbol{z}_{S_{20}} \\ \boldsymbol{w}_{D,0,1}^H \boldsymbol{z}_{S_{01}} & \boldsymbol{w}_{D,1,1}^H \boldsymbol{z}_{S_{11}} & \boldsymbol{w}_{D,2,1}^H \boldsymbol{z}_{S_{21}} \\ \boldsymbol{w}_{D,0,2}^H \boldsymbol{z}_{S_{02}} & \boldsymbol{w}_{D,1,2}^H \boldsymbol{z}_{S_{12}} & \boldsymbol{w}_{D,2,2}^H \boldsymbol{z}_{S_{22}} \end{bmatrix} = \begin{bmatrix} 1 & 1 & 1 \end{bmatrix}, \\ & \parallel \text{diag}(\boldsymbol{w}_{D,j}) \parallel_F \parallel \boldsymbol{w}_A \parallel_2 \leq \frac{\sigma}{\sqrt{3}}, \quad \forall j \in \{0,1,2\}. \end{aligned} \tag{4.56}$$

Alternate optimisation of the digital coefficients $\boldsymbol{w}_D$ and the corresponding analogue coefficients $\boldsymbol{w}_A$ can be obtained by the following iterative process:

(1) First, via initialising the digital coefficients $\boldsymbol{w}_D$ with random values, $\boldsymbol{w}_A$ is then obtained by substituting $w_{D,j,m}(\{j,m\} \in \{0,1,2\})$ into (4.56).

(2) Given the obtained values of $\boldsymbol{w}_A$ in step (1), the closed-form solution for digital coefficients $\boldsymbol{w}_D$ is obtained by (4.24).

(3) Given the obtained values of $\boldsymbol{w}_D$ in step (2), the new set of values of $\boldsymbol{w}_A$ is obtained by (4.56) again.

(4) Repeat steps (2) and (3) until the cost function J_{LSE} in (4.56) converges.

4.3.4 The Fourth Scheme without any Constraints

Similar to the scheme for the two-user case in Section 4.2.4, alternate optimisation of the digital coefficients $\boldsymbol{w}_D$ and the corresponding analogue coefficients $\boldsymbol{w}_A$ can be obtained by the following iterative process:

(1) First, via initialising the digital coefficients $\boldsymbol{w}_D$ with random values, $\boldsymbol{w}_A$ is then obtained by substituting $w_{D,j,m}(\{j,m\} \in \{0,1,2\})$ into (4.40).

(2) Given the obtained values of $\boldsymbol{w}_A$ in step (1), the closed-form solution for digital coefficients $\boldsymbol{w}_D$ is obtained by (4.24).

(3) Given the obtained values of $\boldsymbol{w}_D$ in step (2), the new set of values of $\boldsymbol{w}_A$ is obtained by (4.40) again.

(4) Repeat steps (2) and (3) until the cost function J_{LSE} in (4.40) converges.

4.4 Design Examples

In this section, for the two-beam and three-beam cases, by assuming each subarray consists of twenty and thirty antennas, i.e., $N_s = 20$ and $N_s = 30$, design examples are provided for the four proposed schemes in Sections 4.2 and 4.3, respectively, with the interleaved and localised subarray architectures, where a fixed antenna spacing of $d = \frac{1}{3}\lambda$ and $d = \frac{1}{5}\lambda$ is employed, respectively.

For the two-beam case, the two beam directions are $\varphi_0 = -25^\circ$ and $\varphi_1 = 15^\circ$ and the corresponding sidelobe regions are $\sin\Theta_{side_0} \in [-1, -0.49] \cup [-0.35, 1]$ $(\sin(-25^\circ) = -0.42)$ and $\sin\Theta_{side_1} \in [-1, 0.19] \cup [0.33, 1]$ $(\sin(15^\circ) = 0.26)$. Moreover, for the three-user case, the three beam directions are $\varphi_0 = -30^\circ$, $\varphi_1 = 0^\circ$ and $\varphi_2 = 35^\circ$ and the corresponding sidelobe regions are $\sin\Theta_{side_0} \in [-1, -0.6] \cup [-0.4, 1]$ $(\sin(-30^\circ) = -0.5)$, $\sin\Theta_{side_1} \in$

$[-1, -0.1] \cup [0.1, 1]$ ($\sin(0^\circ) = 0$) and $\sin\Theta_{side_2} \in [-1, 0.47] \cup [0.67, 1]$ ($\sin(35^\circ) = 0.57$). For both the two-beam and three-beam cases, the numbers of sample points in the sidelobe and whole regions for each of the designed beams are $N_g = 160$ and $N_w = 201$, respectively.

4.4.1 Design Examples for the First Scheme in Section 4.2.1

The design results without and with the normalised operation (4.25) on $\boldsymbol{w}_A$ are represented by 'Interleaved' and 'Interleaved (normalisation)', respectively, for the interleaved subarray architecture; and they are represented by 'Localised' and 'Localised (normalisation)', respectively, for the localised subarray architecture.

The trade-off factor in (4.13) is chosen as $\gamma = 0.97$. The resultant patterns of the zeroth and first beams generated by the first scheme in Section 4.2.1 without and with the normalised operation (4.25) on $\boldsymbol{w}_A$ using the interleaved and localised subarray architectures are shown in Figures 4.1 and 4.2, respectively. The magnitudes of analogue coefficients $\boldsymbol{w}_A$ before the normalisation operation (4.25) with the interleaved and localised subarray architectures are shown in Figures 4.3 and 4.4, respectively. As can be seen, the variation in both beam response and analogue coefficient magnitude is minimal and can be ignored.

The change of the cost function J_{LSE} in (4.13) using the interleaved and localised subarray architectures with respect to the iteration number is shown in Figures 4.5 and 4.6, respectively. Furthermore, the digital and analogue coefficients with the interleaved subarray architecture are listed in Tables 4.1 and 4.2, and the digital and analogue coefficients with the localised subarray architecture are listed in Tables 4.3 and 4.4, respectively.

Table 4.1: Digital coefficients $\boldsymbol{w}_{D,0}$ and $\boldsymbol{w}_{D,1}$ with $\varphi_0 = -25^\circ$ and $\varphi_1 = 15^\circ$ generated by the first scheme in Section 4.2.1 with the interleaved subarray architecture.

m \ j	$\boldsymbol{w}_{D,0}$	$\boldsymbol{w}_{D,1}$
0	0.0357-0.0462i	-3.4899+1.4078i
1	2.1846+3.0735i	0.0718+0.0495i

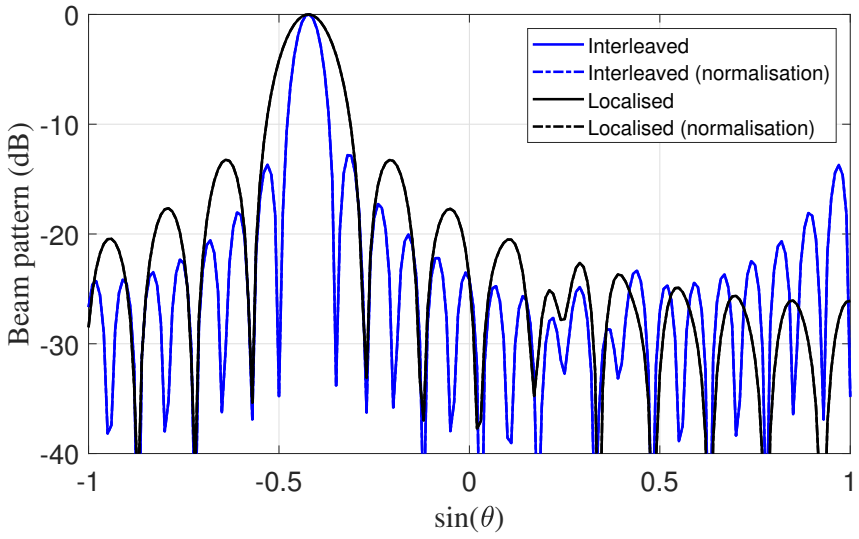

Figure 4.1: Beam patterns of the zeroth beam with $\varphi_0 = -25°$ generated by the first scheme in Section 4.2.1 with the interleaved and localised subarray architectures, respectively.

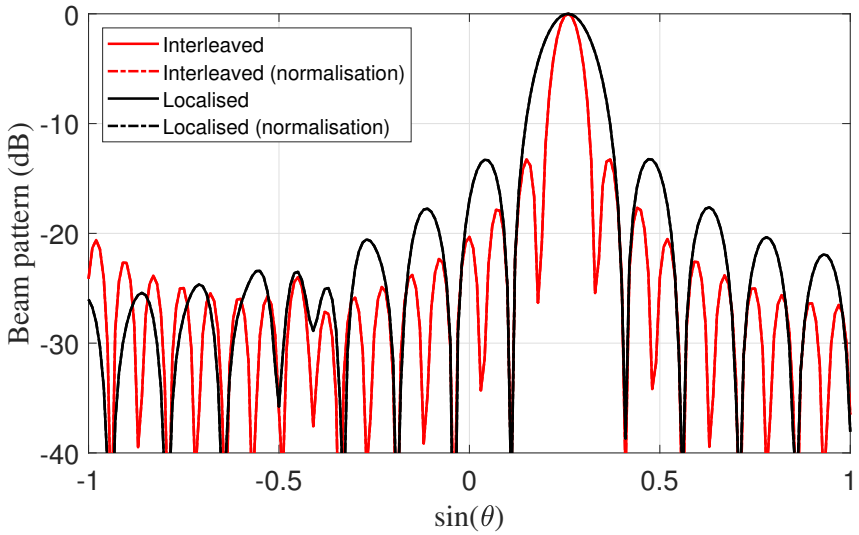

Figure 4.2: Beam patterns of the first beam with $\varphi_1 = 15°$ generated by the first scheme in Section 4.2.1 with the interleaved and localised subarray architectures, respectively.

4.4.2 Design Examples for the Second Scheme in Section 4.2.2

With $N_s = 20$, $\epsilon_e = 0.1$ is set as the upper bound on the norm of the steering vector error and given the design result, this accounts for $\sqrt{\frac{\epsilon_e^2}{N_s}} = 0.0224$ of the real steering vector norm for each subarray if digital coefficients $\boldsymbol{w}_D$ are not considered. To give more degrees

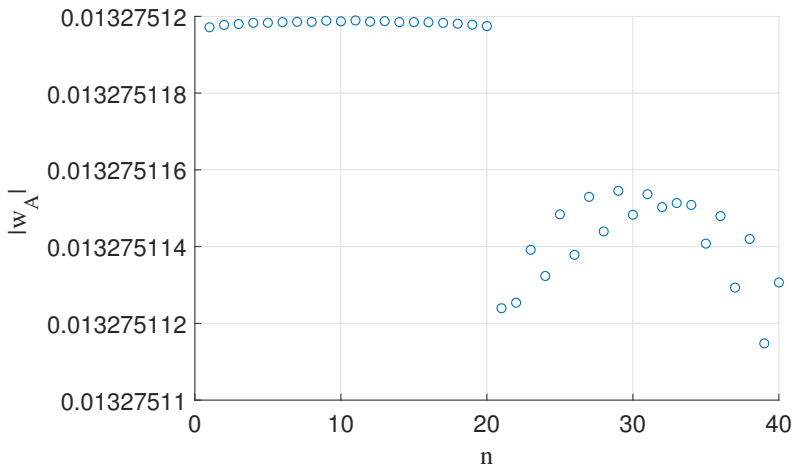

Figure 4.3: Magnitudes of the analogue coefficients $\boldsymbol{w}_A$ generated by the first scheme in Section 4.2.1 with the interleaved subarray architecture.

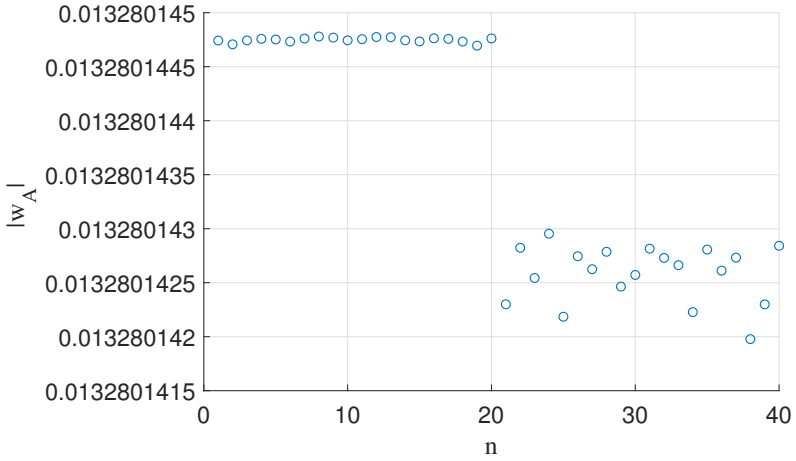

Figure 4.4: Magnitudes of the analogue coefficients $\boldsymbol{w}_A$ generated by the first scheme in Section 4.2.1 with the localised subarray architecture.

of freedom, $\zeta = 0.08$ is selected to allow 8% change in the magnitude of the pattern at the mainlobe direction given the maximum allowable steering vector error because the digital coefficients $\boldsymbol{w}_D$ will expand the error between the designed and desired patterns generated by each subarray to some extent. Hence, σ is calculated by $\sigma = \zeta/\epsilon_e = 0.8$.

By employing the same method in [82–84], to demonstrate the robustness of this scheme, the normalised variance of beam pattern for the j-th designed beam is measured

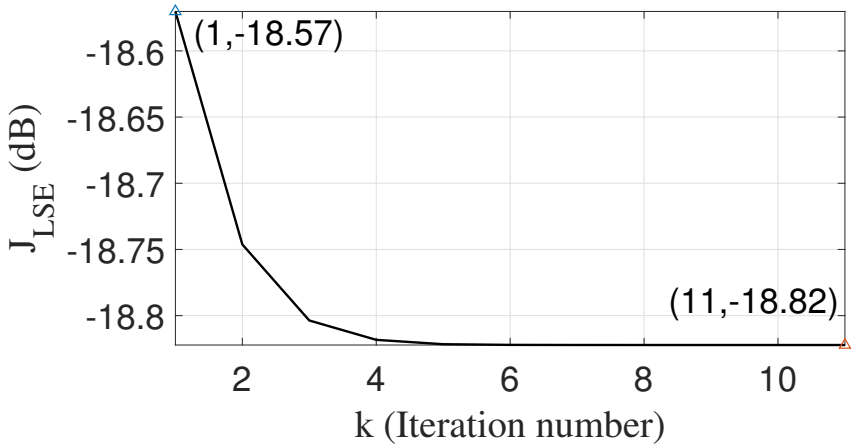

Figure 4.5: Cost function J_{LSE} in (4.13) with respect to the iteration number k generated by the first scheme in Section 4.2.1 with the interleaved subarray architecture.

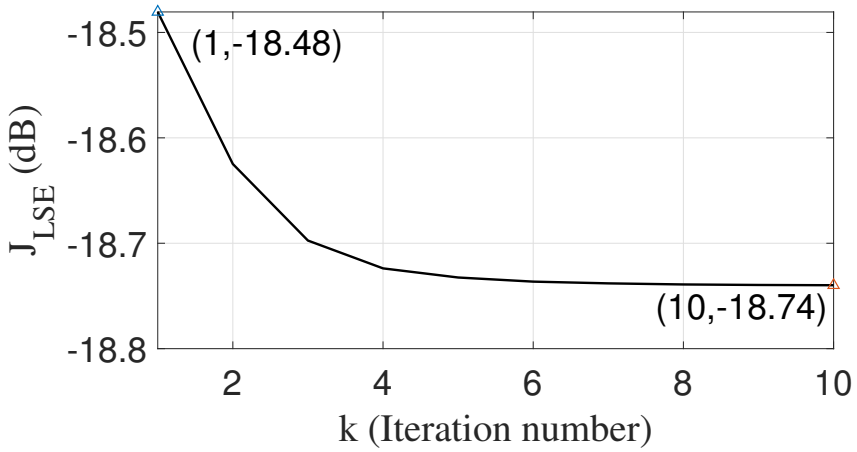

Figure 4.6: Cost function J_{LSE} in (4.13) with respect to the iteration number k generated by the first scheme in Section 4.2.1 with the localised subarray architecture.

as follows

$$var_j(\theta) = \frac{1}{K}\sum_{k=0}^{K-1} \frac{\left|P_{\varphi_j}^k(\theta) - \bar{P}_{\varphi_j}(\theta)\right|^2}{\left|\bar{P}_{\varphi_j}(\theta)\right|^2}, \tag{4.57}$$

where $\bar{P}_{\varphi_j}(\theta) = \frac{1}{K}\sum_{k=0}^{K-1} P_{\varphi_j}^k(\theta)$ denotes the average achieved beam pattern, and $P_{\varphi_j}^k(\theta)$ is the beam pattern resultant from adding the k-th randomly generated steering vector error satisfying the norm-constraint.

The mean patterns of the zeroth and first beams obtained by averaging $K = 2000$ different beam patterns are shown in Figures 4.7 and 4.8, respectively. In addition, the

Table 4.2: Analogue coefficients $\boldsymbol{w}_{A,0}$ and $\boldsymbol{w}_{A,1}$ with $\varphi_0 = -25°$ and $\varphi_1 = 15°$ generated by the first scheme in Section 4.2.1 with the interleaved subarray architecture.

n \ m	$\boldsymbol{w}_{A,0}$	$\boldsymbol{w}_{A,1}$	n \ m	$\boldsymbol{w}_{A,0}$	$\boldsymbol{w}_{A,1}$
0	-0.0123-0.0051i	-0.0035-0.0128i	10	-0.0030+0.0129i	0.0097-0.0091i
1	-0.0015-0.0132i	-0.0114+0.0067i	11	-0.0128+0.0034i	-0.0098-0.0089i
2	0.0110-0.0074i	0.0073+0.0111i	12	-0.0089-0.0098i	-0.0051+0.0122i
3	0.0117+0.0063i	0.0083-0.0104i	13	0.0043-0.0125i	0.0126+0.0041i
4	-0.0001+0.0133i	-0.0111-0.0072i	14	0.0131-0.0019i	0.0001-0.0133i
5	-0.0118+0.0060i	-0.0040+0.0126i	15	0.0080+0.0106i	-0.0132+0.0015i
6	-0.0109-0.0075i	0.0132+0.0018i	16	-0.0059+0.0119i	0.0047+0.0124i
7	0.0016-0.0132i	-0.0007-0.0133i	17	-0.0133+0.0005i	0.0114-0.0068i
8	0.0124-0.0048i	-0.0126+0.0041i	18	-0.0065-0.0116i	-0.0086-0.0101i
9	0.0100+0.0087i	0.0056+0.0120i	19	0.0069-0.0113i	-0.0084+0.0102i

Table 4.3: Digital coefficients $\boldsymbol{w}_{D,0}$ and $\boldsymbol{w}_{D,1}$ with $\varphi_0 = -25°$ and $\varphi_1 = 15°$ generated by the first scheme in Section 4.2.1 with the localised subarray architecture.

m \ j	$\boldsymbol{w}_{D,0}$	$\boldsymbol{w}_{D,1}$
0	-0.0291+0.1381i	-3.4838+1.3985i
1	2.1781+3.0603i	0.1119-0.0898i

digital and analogue coefficients generated by the interleaved subarray architecture are listed in Tables 4.5 and 4.6, respectively, and the digital and analogue coefficients generated by the localised subarray architecture are listed in Tables 4.7 and 4.8, respectively. The change of the cost function J_{LSE} in (4.31) with respect to the iteration number using the interleaved and localised subarray architectures are shown in Figures 4.9 and 4.10, respectively.

Furthermore, the normalised variances of beam patterns for the two designed beams generated by the interleaved and localised subarray architectures are shown in Figures 4.11 and 4.12, respectively. We can see for most directions, the normalised variance is

Table 4.4: Analogue coefficients $\boldsymbol{w}_{A,0}$ and $\boldsymbol{w}_{A,1}$ with $\varphi_0 = -25°$ and $\varphi_1 = 15°$ generated by the first scheme in Section 4.2.1 with the localised subarray architecture.

n \ m	$\boldsymbol{w}_{A,0}$	$\boldsymbol{w}_{A,1}$	n \ m	$\boldsymbol{w}_{A,0}$	$\boldsymbol{w}_{A,1}$
0	-0.0124-0.0049i	0.0130+0.0025i	10	-0.0118+0.0061i	-0.0098-0.0089i
1	-0.0078-0.0107i	0.0098-0.0090i	11	-0.0133-0.0008i	-0.0132+0.0013i
2	-0.0013-0.0132i	0.0003-0.0133i	12	-0.0110-0.0075i	-0.0076+0.0109i
3	0.0056-0.0121i	-0.0099-0.0089i	13	-0.0055-0.0121i	0.0042+0.0126i
4	0.0110-0.0074i	-0.0130+0.0026i	14	0.0016-0.0132i	0.0125+0.0043i
5	0.0133-0.0006i	-0.0057+0.0120i	15	0.0081-0.0105i	0.0115-0.0066i
6	0.0117+0.0064i	0.0053+0.0122i	16	0.0124-0.0048i	0.0027-0.0130i
7	0.0068+0.0114i	0.0126+0.0042i	17	0.0131+0.0022i	-0.0086-0.0101i
8	-0.0000+0.0133i	0.0112-0.0072i	18	0.0101+0.0086i	-0.0133+0.0006i
9	-0.0069+0.0113i	0.0007-0.0133i	19	0.0040+0.0127i	-0.0077+0.0108i

smaller than one; although it is about 2.62 at around -0.27 for the first beam with the interleaved subarray architecture, given that the pattern is below -60 dB for that direction, a variance of three still indicates a very low sidelobe level and overall it is a rather robust design result.

Table 4.5: Digital coefficients $\boldsymbol{w}_{D,0}$ and $\boldsymbol{w}_{D,1}$ with $\varphi_0 = -25°$, and $\varphi_1 = 15°$ generated by the second scheme in Section 4.2.2 with the interleaved subarray architecture.

m \ j	$\boldsymbol{w}_{D,0}$	$\boldsymbol{w}_{D,1}$
0	3.4291-0.9852i	-1.0681-3.5096i
1	3.2878-3.3878i	1.2416+0.3263i

4.4.3 Design Examples for the Third Scheme in Section 4.2.3

In this section, $\epsilon_e = 0.1$ and $\zeta = 0.08$ lead to $\sigma = \zeta/\epsilon_e = 0.8$ and the trade-off factor in (4.32) is $\gamma = 0.97$. With $K = 2000$, the mean patterns of the zeroth and first beams

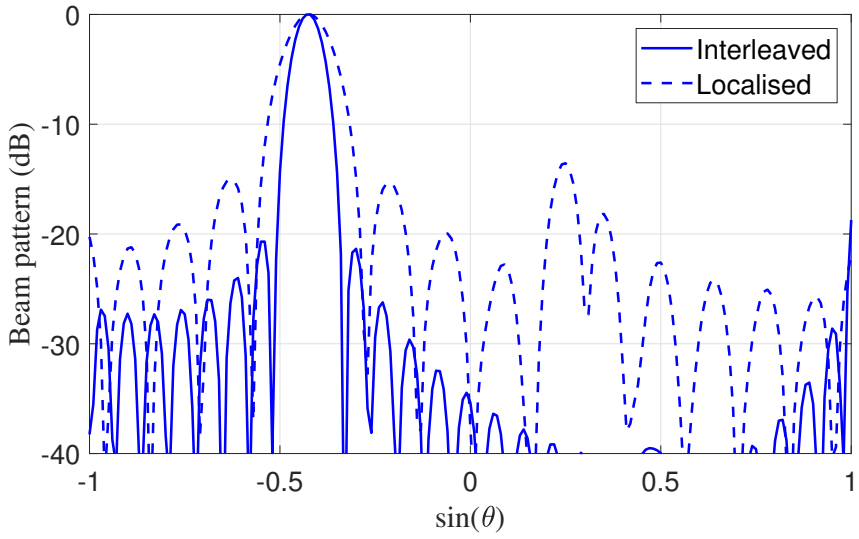

Figure 4.7: The mean patterns of the zeroth beam with $\varphi_0 = -25°$ generated by the second scheme in Section 4.2.2 with the interleaved and localised subarray architectures, respectively.

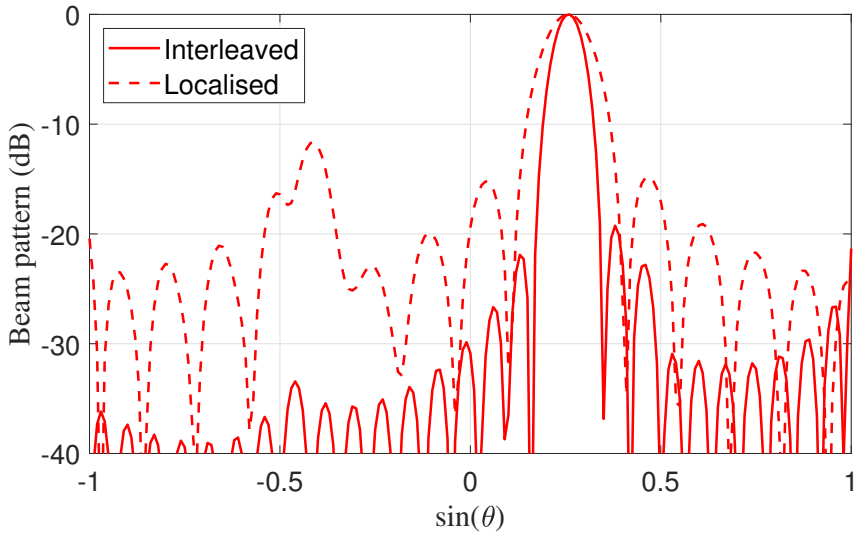

Figure 4.8: The mean patterns of the first beam with $\varphi_1 = 15°$ generated by the second scheme in Section 4.2.2 with the interleaved and localised subarray architectures, respectively.

with the interleaved and localised subarray architectures are shown in Figures 4.13 and 4.14, respectively. The magnitudes of analogue coefficients $\boldsymbol{w}_A$ before the normalisation operation (4.25) with the interleaved and localised subarray architectures are shown in

Table 4.6: Analogue coefficients $\boldsymbol{w}_{A,0}$ and $\boldsymbol{w}_{A,1}$ with $\varphi_0 = -25°$ and $\varphi_1 = 15°$ generated by the second scheme in Section 4.2.2 with the interleaved subarray architecture.

n \ m	$\boldsymbol{w}_{A,0}$	$\boldsymbol{w}_{A,1}$	n \ m	$\boldsymbol{w}_{A,0}$	$\boldsymbol{w}_{A,1}$
0	-0.0006+0.0042i	0.0084-0.0005i	10	0.0167+0.0072i	0.0017-0.0006i
1	-0.0067-0.0009i	0.0025-0.0010i	11	0.0065+0.0116i	0.0169-0.0140i
2	-0.0064-0.0063i	-0.0097+0.0083i	12	-0.0135+0.0072i	0.0018-0.0040i
3	0.0066-0.0064i	-0.0042+0.0062i	13	-0.0139-0.0007i	-0.0031+0.0181i
4	0.0131-0.0011i	0.0029+0.0139i	14	0.0011-0.0114i	0.0020+0.0086i
5	0.0020+0.0095i	-0.0019-0.0132i	15	0.0087-0.0102i	-0.0067-0.0113i
6	-0.0091+0.0137i	0.0058+0.0108i	16	0.0064+0.0048i	-0.0077-0.0064i
7	-0.0100-0.0017i	0.0145+0.0123i	17	0.0014+0.0107i	0.0068+0.0031i
8	-0.0055-0.0176i	-0.0073-0.0027i	18	-0.0042+0.0019i	0.0080-0.0001i
9	0.0063-0.0100i	-0.0224-0.0002i	19	-0.0054+0.0033i	-0.0021-0.0011i

Table 4.7: Digital coefficients $\boldsymbol{w}_{D,0}$ and $\boldsymbol{w}_{D,1}$ with $\varphi_0 = -25°$, and $\varphi_1 = 15°$ generated by the second scheme in Section 4.2.2 with the localised subarray architecture.

m \ j	$\boldsymbol{w}_{D,0}$	$\boldsymbol{w}_{D,1}$
0	0.3653-0.2511i	0.1908-4.5648i
1	4.0464-3.8462i	0.2084-0.3468i

Figures 4.15 and 4.16, respectively. Moreover, the digital and analogue coefficients with the interleaved subarray architecture are listed in Tables 4.9 and 4.10, respectively, and the digital and analogue coefficients with the localised subarray architecture in Tables 4.11 and 4.12, respectively. The change of the cost function J_{LSE} in (4.32) using the interleaved and localised subarray architectures with respect to the iteration number is shown in Figures 4.17 and 4.18, respectively.

The normalised variances of beam patterns for the two designed beams with the interleaved and localised subarray architectures are displayed in Figures 4.19 and 4.20, respectively. With the interleaved subarray architecture, again although the variances

Table 4.8: Analogue coefficients $\boldsymbol{w}_{A,0}$ and $\boldsymbol{w}_{A,1}$ with $\varphi_0 = -25°$ and $\varphi_1 = 15°$ generated by the second scheme in Section 4.2.2 with the localised subarray architecture.

n \ m	$\boldsymbol{w}_{A,0}$	$\boldsymbol{w}_{A,1}$	n \ m	$\boldsymbol{w}_{A,0}$	$\boldsymbol{w}_{A,1}$
0	0.0071+0.0233i	-0.0127+0.0096i	10	0.0080+0.0109i	0.0040-0.0038i
1	-0.0114-0.0126i	0.0210+0.0012i	11	-0.0037+0.0064i	0.0085-0.0119i
2	0.0007+0.0232i	-0.0097+0.0058i	12	0.0035+0.0134i	-0.0156-0.0064i
3	-0.0209-0.0183i	0.0248-0.0074i	13	-0.0126+0.0140i	-0.0017+0.0029i
4	-0.0044+0.0008i	-0.0116-0.0072i	14	-0.0087+0.0002i	-0.0010+0.0048i
5	-0.0085-0.0054i	-0.0035-0.0017i	15	-0.0007-0.0003i	-0.0075+0.0113i
6	0.0004-0.0168i	-0.0048+0.0000i	16	-0.0220-0.0101i	0.0265+0.0014i
7	0.0136-0.0007i	-0.0137+0.0107i	17	0.0146-0.0139i	-0.0144-0.0027i
8	0.0071-0.0078i	0.0113+0.0078i	18	-0.0170-0.0070i	0.0179-0.0065i
9	0.0154-0.0036i	0.0038-0.0005i	19	0.0168-0.0068i	-0.0177-0.0057i

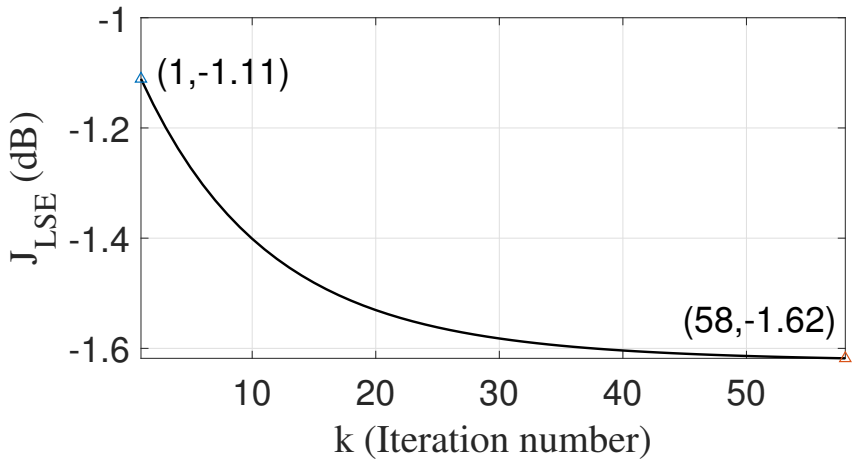

Figure 4.9: Cost function J_{LSE} in (4.31) with respect to the iteration number k generated by the second scheme in Section 4.2.2 with the interleaved subarray architecture.

of the first beam at around -0.34 and -0.19 are as high as 2.84 and 1.05, respectively, because all the beam patterns are about below -50 dB for those directions, the variation of beam patterns is still at an acceptable level.

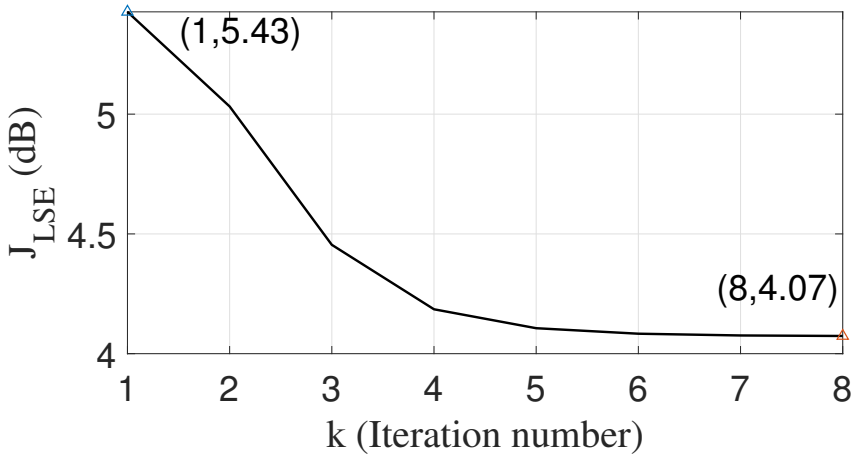

Figure 4.10: Cost function J_{LSE} in (4.31) with respect to the iteration number k generated by the second scheme in Section 4.2.2 with the localised subarray architecture.

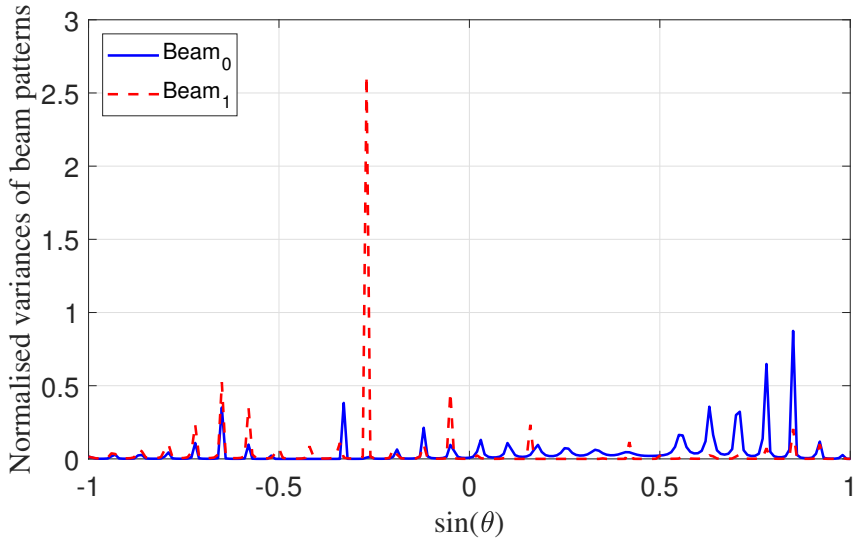

Figure 4.11: Normalised variances of beam patterns with $\varphi_0 = -25°$ and $\varphi_1 = 15°$ generated by the second scheme in Section 4.2.2 with the interleaved subarray architecture.

4.4.4 Design Examples for the Fourth Scheme in Section 4.2.4

With $K = 2000$, the mean patterns of the zeroth and first beams with the interleaved and localised subarray architectures are shown in Figures 4.21 and 4.22, respectively. Moreover, the digital and analogue coefficients with the interleaved subarray architecture are listed in Tables 4.13 and 4.14, respectively, and the digital and analogue coefficients

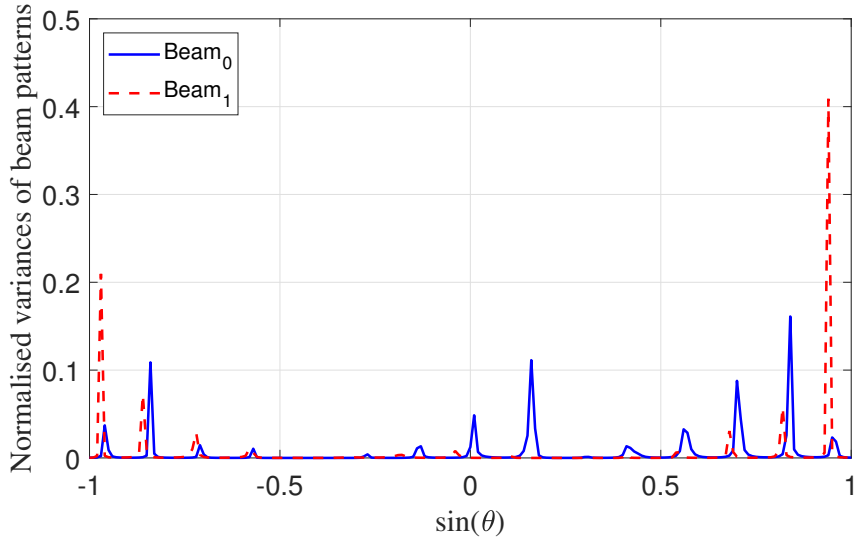

Figure 4.12: Normalised variances of beam patterns with $\varphi_0 = -25°$ and $\varphi_1 = 15°$ generated by the second scheme in Section 4.2.2 with the localised subarray architecture.

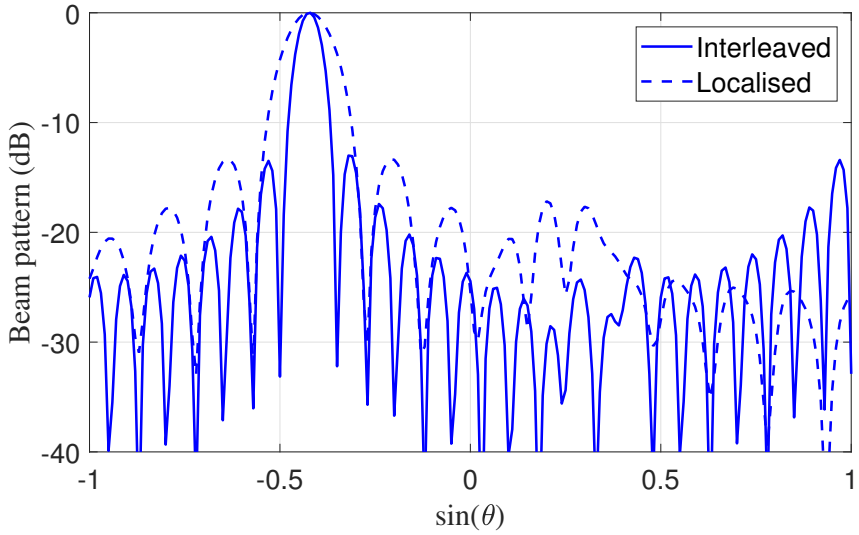

Figure 4.13: The mean patterns of the zeroth beam with $\varphi_0 = -25°$ generated by the third scheme in Section 4.2.3 with the interleaved and localised subarray architectures, respectively.

with the localised subarray architecture are listed in Tables 4.15 and 4.16, respectively. Furthermore, the change of the cost function J_{LSE} in (4.10) using the interleaved and localised subarray architectures with respect to the iteration number is shown in Figures 4.23 and 4.24, respectively.

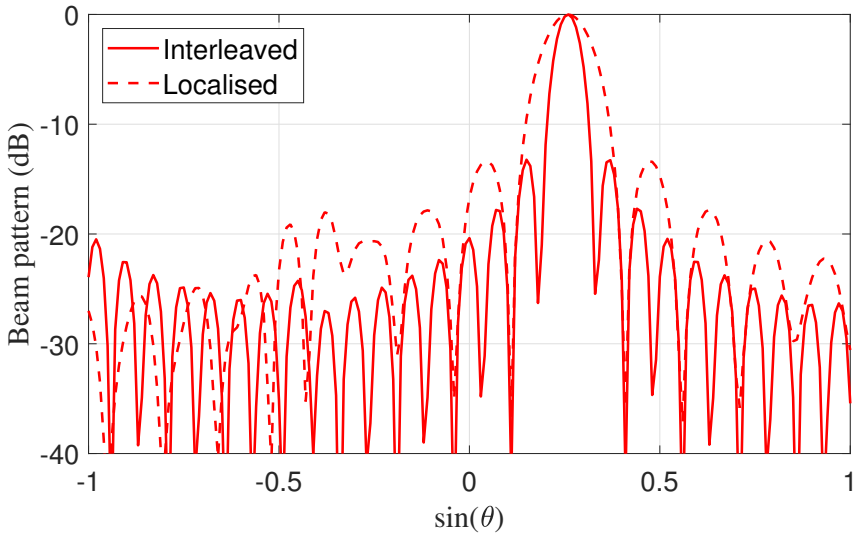

Figure 4.14: The mean patterns of the first beam with $\varphi_1 = 15°$ generated by the third scheme in Section 4.2.3 with the interleaved and localised subarray architectures, respectively.

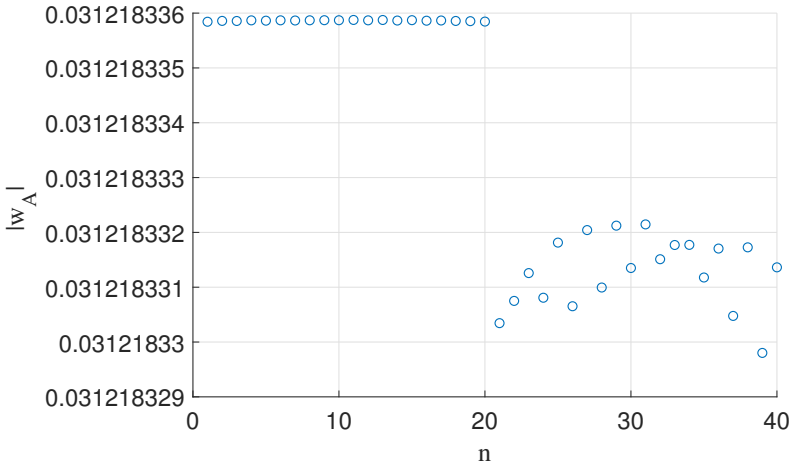

Figure 4.15: Magnitudes of the analogue coefficients $\boldsymbol{w}_A$ generated by the third scheme in Section 4.2.3 with the interleaved subarray architecture.

4.4.5 Design Examples for the First Scheme in Section 4.3.1

With $J = M = 3$, the trade-off factor in (4.41) is chosen as $\gamma = 0.99$ and the patterns of the zeroth, first and second beams generated by the scheme in Section 4.3.1 with the interleaved and localised subarray architectures are shown in Figures 4.25, 4.26 and 4.27, respectively, all with a satisfactory beam pattern. The corresponding magnitudes

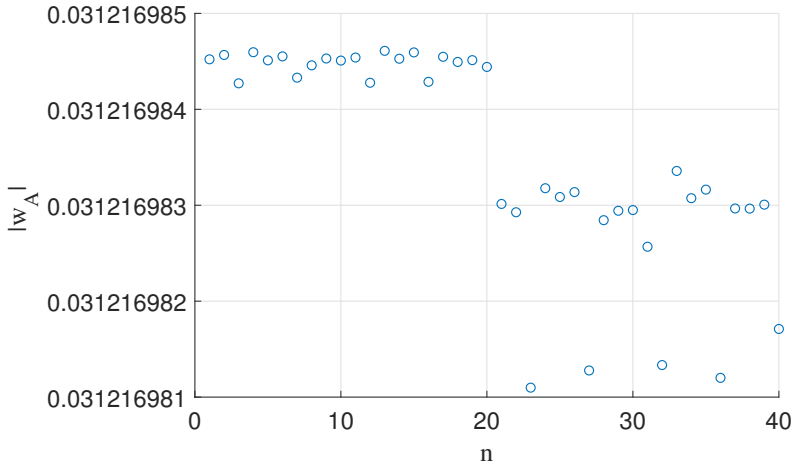

Figure 4.16: Magnitudes of the analogue coefficients $\boldsymbol{w}_A$ generated by the third scheme in Section 4.2.3 with the localised subarray architecture.

Table 4.9: Digital coefficients $\boldsymbol{w}_{D,0}$ and $\boldsymbol{w}_{D,1}$ with $\varphi_0 = -25°$ and $\varphi_1 = 15°$ generated by the third scheme in Section 4.2.3 with the interleaved subarray architecture.

m \ j	$\boldsymbol{w}_{D,0}$	$\boldsymbol{w}_{D,1}$
0	0.0395-0.0101i	-1.0430+1.2131i
1	0.9119-1.3219i	0.0034-0.0312i

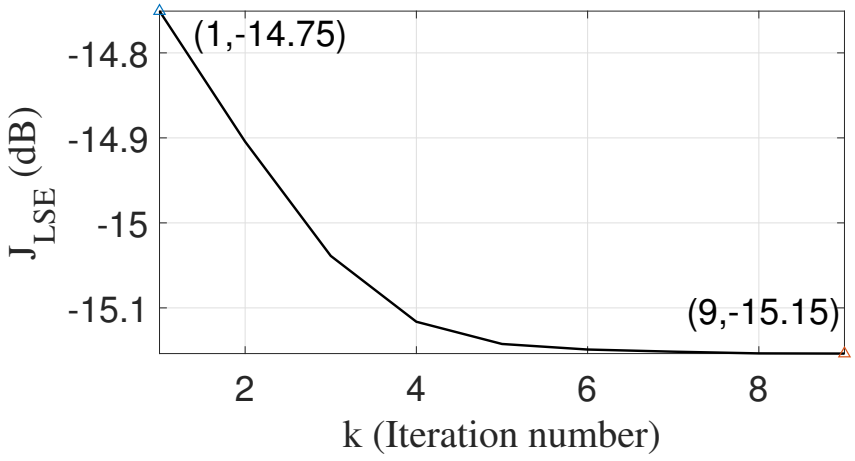

Figure 4.17: Cost function J_{LSE} in (4.32) with respect to the iteration number k generated by the third scheme in Section 4.2.3 with the interleaved subarray architecture.

Table 4.10: Analogue coefficients $\boldsymbol{w}_{A,0}$ and $\boldsymbol{w}_{A,1}$ with $\varphi_0 = -25°$ and $\varphi_1 = 15°$ generated by the third scheme in Section 4.2.3 with the interleaved subarray architecture.

n \ m	$\boldsymbol{w}_{A,0}$	$\boldsymbol{w}_{A,1}$	n \ m	$\boldsymbol{w}_{A,0}$	$\boldsymbol{w}_{A,1}$
0	-0.0202-0.0238i	0.0309+0.0042i	10	-0.0202+0.0238i	0.0128+0.0285i
1	0.0112-0.0291i	-0.0068-0.0305i	11	-0.0304-0.0069i	0.0280-0.0137i
2	0.0310-0.0035i	-0.0306+0.0063i	12	-0.0082-0.0301i	-0.0235-0.0206i
3	0.0176+0.0258i	0.0176+0.0258i	13	0.0227-0.0214i	-0.0202+0.0238i
4	-0.0145+0.0276	0.0253-0.0183i	14	0.0295+0.0101i	0.0296+0.0099i
5	-0.0312-0.0001i	-0.0254-0.0182i	15	0.0050+0.0308i	0.0084-0.0301i
6	-0.0147-0.0275i	-0.0147+0.0275i	16	-0.0251+0.0186i	-0.0312+0.0012i
7	0.0176-0.0258i	0.0300+0.0086i	17	-0.0283-0.0132i	0.0050+0.0308i
8	0.0311+0.0032i	0.0009-0.0312i	18	-0.0011-0.0312i	0.0292-0.0111i
9	0.0114+0.0291i	-0.0311+0.0023i	19	0.0268-0.0161i	-0.0165-0.0265i

Table 4.11: Digital coefficients $\boldsymbol{w}_{D,0}$ and $\boldsymbol{w}_{D,1}$ with $\varphi_0 = -25°$ and $\varphi_1 = 15°$ generated by the third scheme in Section 4.2.3 with the localised subarray architecture.

m \ j	$\boldsymbol{w}_{D,0}$	$\boldsymbol{w}_{D,1}$
0	-0.0689+0.1052i	-1.0137+1.2343i
1	0.9457-1.3114i	-0.1166+0.0792i

of analogue coefficients $\boldsymbol{w}_A$ before the normalisation operation (4.25) with the interleaved and localised subarray architectures are displayed in Figures 4.28 and 4.29, respectively.

The corresponding digital and analogue coefficients generated by the interleaved subarray architecture are listed in Tables 4.17 and 4.18, respectively, and the digital and analogue coefficients generated by the localised subarray architecture are shown in Tables 4.19 and 4.20, respectively. The change of the cost function J_{LSE} in (4.41) using the interleaved and localised subarray architectures with respect to the iteration number is shown in Figures 4.30 and 4.31, respectively.

Table 4.12: Analogue coefficients $\boldsymbol{w}_{A,0}$ and $\boldsymbol{w}_{A,1}$ with $\varphi_0 = -25°$ and $\varphi_1 = 15°$ generated by the third scheme in Section 4.2.3 with the localised subarray architecture.

n \ m	$\boldsymbol{w}_{A,0}$	$\boldsymbol{w}_{A,1}$	n \ m	$\boldsymbol{w}_{A,0}$	$\boldsymbol{w}_{A,1}$
0	-0.0206-0.0234i	-0.0174+0.0259i	10	-0.0311+0.0024i	0.0297-0.0095i
1	-0.0075-0.0303i	0.0057+0.0307i	11	-0.0261-0.0172i	0.0030-0.0311i
2	0.0119-0.0289i	0.0300+0.0085i	12	-0.0116-0.0290i	-0.0235-0.0205i
3	0.0267-0.0162i	0.0226-0.0215i	13	0.0021-0.0311i	-0.0312-0.0010i
4	0.0311-0.0023i	0.0031-0.0311i	14	0.0154-0.0272i	-0.0241+0.0199i
5	0.0292+0.0111i	-0.0175-0.0259i	15	0.0281-0.0136i	0.0054+0.0307i
6	0.0186+0.0251i	-0.0312-0.0001i	16	0.0305+0.0066i	0.0299+0.0090i
7	-0.0010+0.0312i	-0.0127+0.0285i	17	0.0236+0.0204i	0.0280-0.0139i
8	-0.0167+0.0264i	0.0118+0.0289i	18	0.0132+0.0283i	0.0135-0.0282i
9	-0.0262+0.0170i	0.0271+0.0154i	19	-0.0032+0.0311i	-0.0141-0.0279i

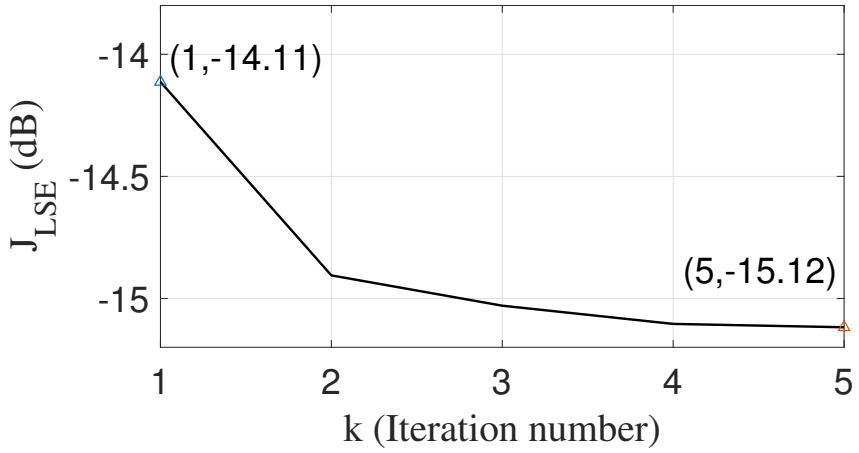

Figure 4.18: Cost function J_{LSE} in (4.32) with respect to the iteration number k generated by the third scheme in Section 4.2.3 with the localised subarray architecture.

4.4.6 Design Examples for the Second Scheme in Section 4.3.2

With $N_s = 30$, $\epsilon_e = 0.1$ is set as the upper bound on the norm of the steering vector error and given the design result, this accounts for $\sqrt{\frac{\epsilon_e^2}{N_s}} = 0.018$ of the real steering vector norm for each subarray. Similar to Section 4.4.2, $\zeta = 0.08$ and σ is then calculated by

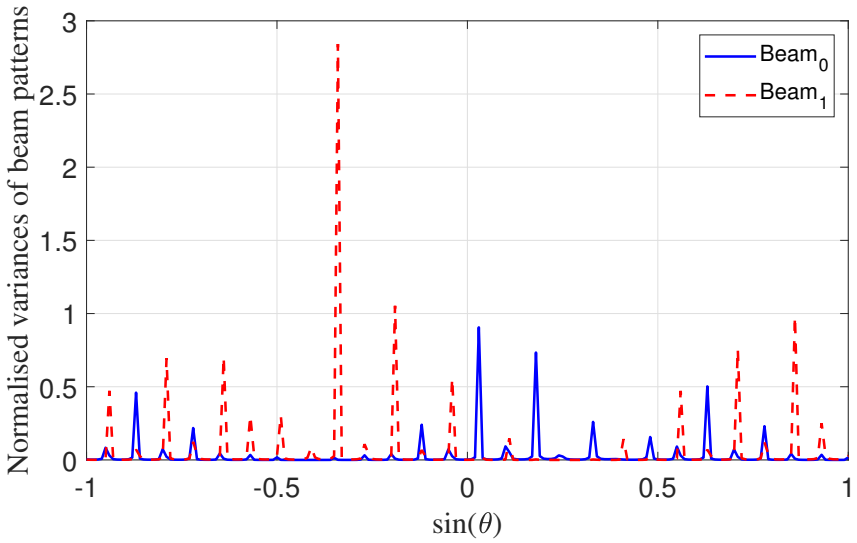

Figure 4.19: Normalised variances of beam patterns with $\varphi_0 = -25°$ and $\varphi_1 = 15°$ generated by the third scheme in Section 4.2.3 with the interleaved subarray architecture.

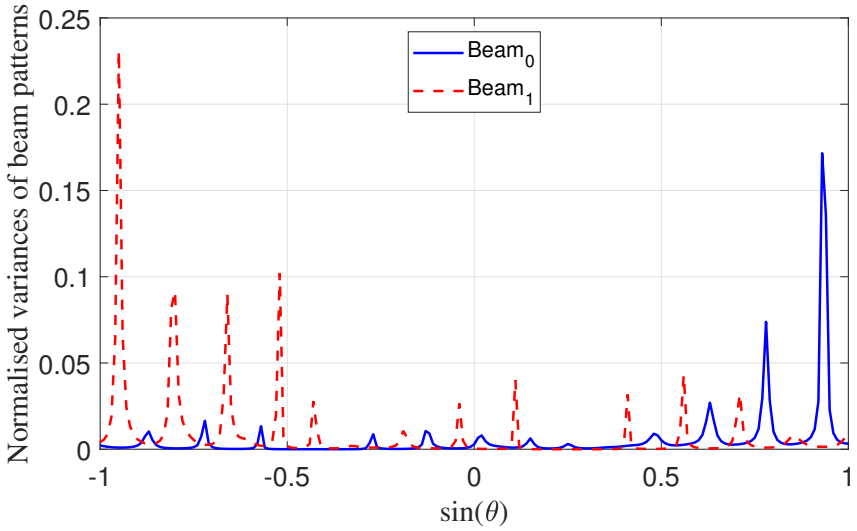

Figure 4.20: Normalised variances of beam patterns with $\varphi_0 = -25°$ and $\varphi_1 = 15°$ generated by the third scheme in Section 4.2.3 with the localised subarray architecture.

$\sigma = \zeta/\epsilon_e = 0.8$.

The mean patterns of the zeroth, first and second beams obtained by averaging $K = 2000$ different beam patterns are shown in Figures 4.32, 4.33 and 4.34, respectively. In addition, the digital and analogue coefficients with the interleaved architecture are listed

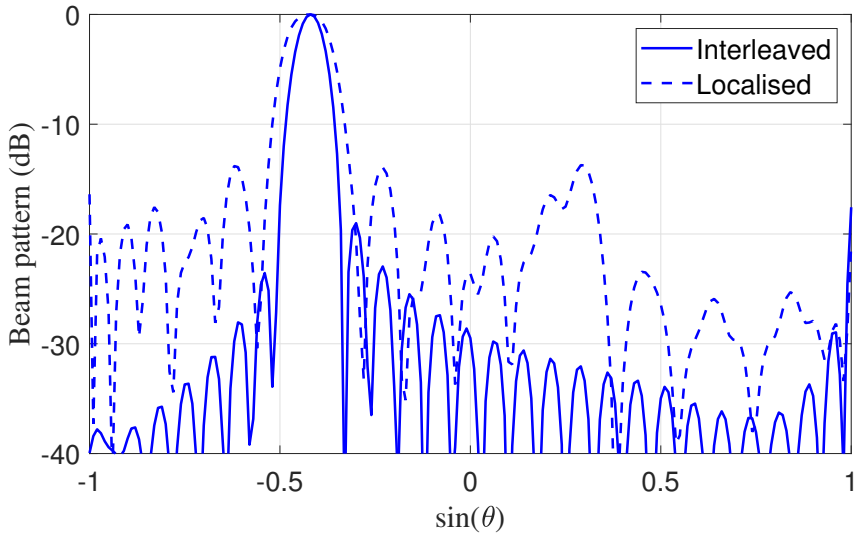

Figure 4.21: The mean patterns of the zeroth beam with $\varphi_0 = -25°$ generated by the fourth scheme in Section 4.2.4 with the interleaved and localised subarray architectures, respectively.

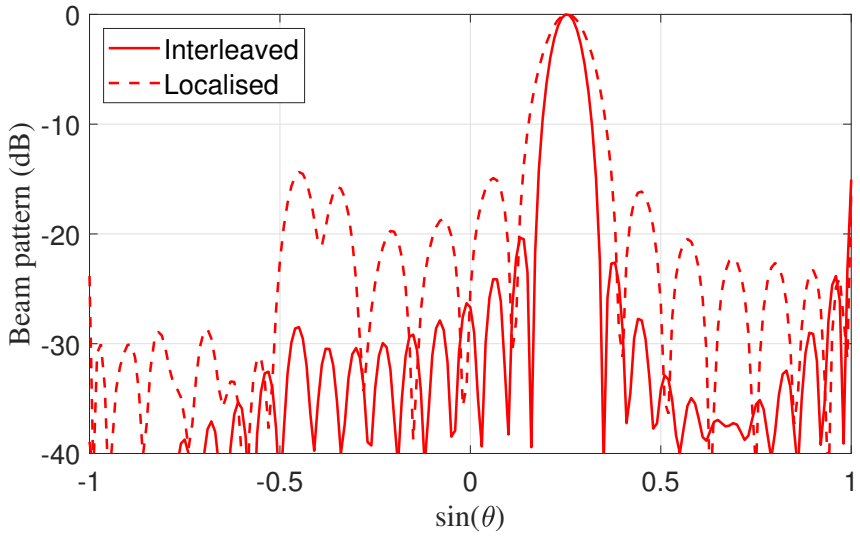

Figure 4.22: The mean patterns of the first beam with $\varphi_1 = 15°$ generated by the fourth scheme in Section 4.2.4 with the interleaved and localised subarray architectures, respectively.

in Tables 4.21 and 4.22, respectively, and the digital and analogue coefficients with the localised subarray architecture are listed in Tables 4.23 and 4.24, respectively. The change of the cost function J_{LSE} in (4.55) with respect to the iteration number for the interleaved

Table 4.13: Digital coefficients $\boldsymbol{w}_{D,0}$ and $\boldsymbol{w}_{D,1}$ with $\varphi_0 = -25°$ and $\varphi_1 = 15°$ generated by the fourth scheme in Section 4.2.4 with the interleaved subarray architecture.

m \ j	$\boldsymbol{w}_{D,0}$	$\boldsymbol{w}_{D,1}$
0	-1.9157-3.2664i	1.9681-3.9929i
1	2.1604-4.4277i	-0.7641-3.9430i

Table 4.14: Analogue coefficients $\boldsymbol{w}_{A,0}$ and $\boldsymbol{w}_{A,1}$ with $\varphi_0 = -25°$ and $\varphi_1 = 15°$ generated by the fourth scheme in Section 4.2.4 with the interleaved subarray architecture.

n \ m	$\boldsymbol{w}_{A,0}$	$\boldsymbol{w}_{A,1}$	n \ m	$\boldsymbol{w}_{A,0}$	$\boldsymbol{w}_{A,1}$
0	-0.0012+0.0059i	0.0002-0.0039i	10	-0.0007-0.0196i	0.0082+0.0169i
1	0.0010+0.0091i	-0.0042-0.0080i	11	0.0048+0.0047i	-0.0015-0.0035i
2	-0.0016-0.0015i	-0.0003+0.0009i	12	0.0144+0.0147i	-0.0169-0.0080i
3	-0.0098-0.0094i	0.0118+0.0057i	13	-0.0007+0.0021i	-0.0024+0.0011i
4	-0.0018-0.0025i	0.0044-0.0005i	14	-0.0181-0.0011i	0.0152-0.0037i
5	0.0163+0.0007i	-0.0145+0.0031i	15	-0.0057-0.0003i	0.0047-0.0044i
6	0.0091+0.0005i	-0.0079+0.0066i	16	0.0103-0.0083i	-0.0067+0.0084i
7	-0.0123+0.0102i	0.0087-0.0104i	17	0.0056-0.0057i	-0.0016+0.0076i
8	-0.0100+0.0115i	0.0034-0.0153i	18	-0.0012+0.0074i	0.0005-0.0055i
9	0.0012-0.0123i	-0.0005+0.0095i	19	-0.0002+0.0075i	-0.0031-0.0066i

Table 4.15: Digital coefficients $\boldsymbol{w}_{D,0}$ and $\boldsymbol{w}_{D,1}$ with $\varphi_0 = -25°$ and $\varphi_1 = 15°$ generated by the fourth scheme in Section 4.2.4 with the localised subarray architecture.

m \ j	$\boldsymbol{w}_{D,0}$	$\boldsymbol{w}_{D,1}$
0	-0.1277-0.2170i	2.1283-4.3912i
1	2.4273-4.9592i	-0.1494-0.5159i

and localised subarray architectures are shown in Figures 4.35 and 4.36, respectively.

Furthermore, the normalised variances of beam responses for the three designed beams

Table 4.16: Analogue coefficients $\boldsymbol{w}_{A,0}$ and $\boldsymbol{w}_{A,1}$ with $\varphi_0 = -25°$ and $\varphi_1 = 15°$ generated by the fourth scheme in Section 4.2.4 with the localised subarray architecture.

n \ m	$\boldsymbol{w}_{A,0}$	$\boldsymbol{w}_{A,1}$	n \ m	$\boldsymbol{w}_{A,0}$	$\boldsymbol{w}_{A,1}$
0	0.0665+0.0289i	-0.0463-0.0811i	10	0.7643-0.7333i	4.2803-22.5125i
1	-0.2426-0.0339i	0.1324+0.4314i	11	0.3867+0.5363i	-4.7563+20.2102i
2	0.6005+0.0661i	-0.2567-1.2669i	12	-1.2212-0.2628i	4.6983-16.5125i
3	-1.1849-0.0397i	0.4042+2.9279i	13	1.6257+0.0379i	-4.1429+12.1759i
4	1.8967-0.0385i	-0.4341-5.6075i	14	-1.6184+0.1467i	3.2315-8.0314i
5	-2.6429+0.1789i	0.2485+9.2560i	15	1.2855-0.2066i	-2.2366+4.6833i
6	3.1442-0.4031i	0.2396-13.55507i	16	-0.8694+0.1967i	1.3466-2.3259i
7	-3.2412+0.6041i	-1.1051+17.7903i	17	0.4651-0.1492i	-0.6720+0.9545i
8	2.8197-0.7805i	2.1983-21.1249i	18	-0.1979+0.0682i	0.2733+0.2992i
9	-1.9026+0.8217i	-3.3350+22.8439i	19	0.0575-0.0390i	-0.0777+0.0433i

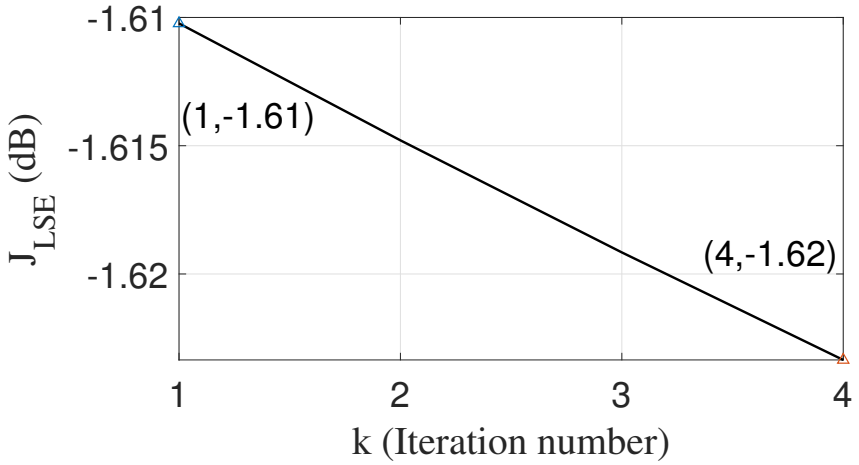

Figure 4.23: Cost function J_{LSE} in (4.10) with respect to the iteration number k generated by the fourth scheme in Section 4.2.4 with the interleaved subarray architecture.

generated by the interleaved and localised subarray architectures are shown in Figures 4.37 and 4.38, respectively. As shown in Figure 4.37, it is close to 6.07 and 1.84 at about -0.61 and 0.01, respectively, for the second beam with the interleaved subarray architecture; in Figure 4.38, it is close to 1.08 at around 0.9 for the first beam with the localised subarray architecture; given that the responses are both close to -60 dB, a variance of six still

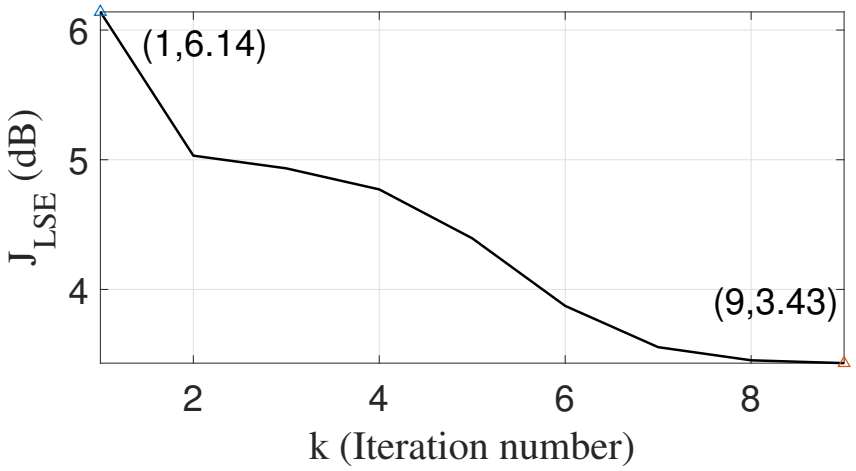

Figure 4.24: Cost function J_{LSE} in (4.10) with respect to the iteration number k generated by the fourth scheme in Section 4.2.4 with the localised subarray architecture.

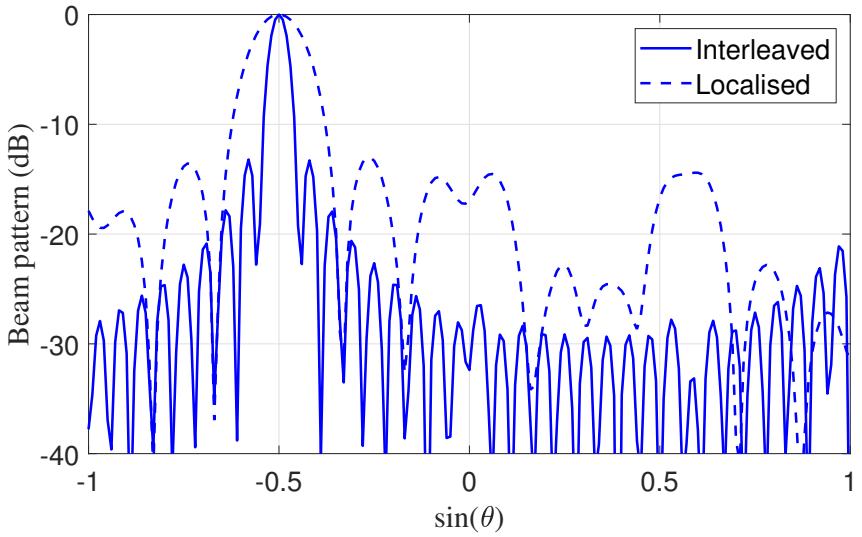

Figure 4.25: Beam patterns of the zeroth beam with $\varphi_0 = -30°$ generated by the first scheme in Section 4.3.1 with the interleaved and localised subarray architectures, respectively.

indicates a very low sidelobe level.

4.4.7 Design Examples for the Third Scheme in Section 4.3.3

In this section, $\epsilon_e = 0.1$ and $\zeta = 0.08$ lead to $\sigma = \zeta/\epsilon_e = 0.8$ and the trade-off factor in (4.56) is $\gamma = 0.99$. With $K = 2000$, the mean patterns of the zeroth, first and second

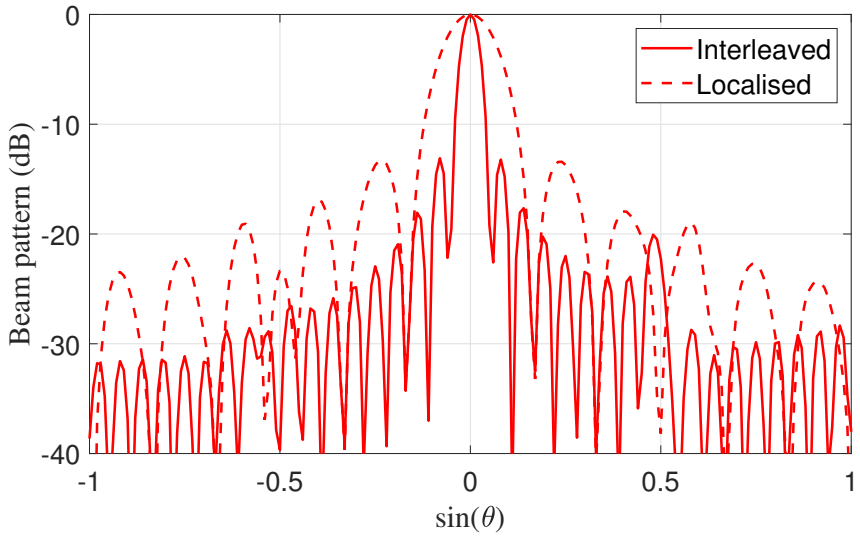

Figure 4.26: Beam patterns of the first beam with $\varphi_1 = 0°$ generated by the first scheme in Section 4.3.1 with the interleaved and localised subarray architectures, respectively.

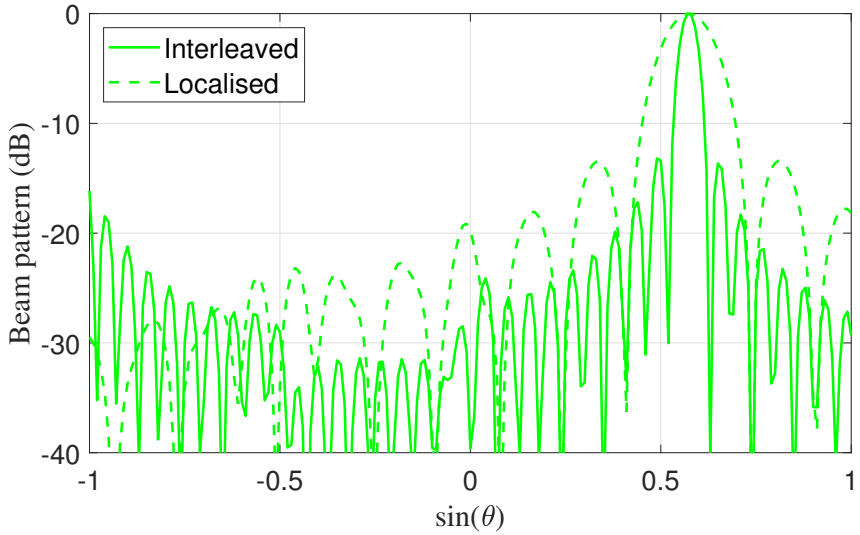

Figure 4.27: Beam patterns of the second beam with $\varphi_2 = 35°$ generated by the first scheme in Section 4.3.1 with the interleaved and localised subarray architectures, respectively.

beams with the interleaved and localised architectures are shown in Figures 4.39, 4.40 and 4.41, respectively. The corresponding magnitudes of analogue coefficients $\boldsymbol{w}_A$ before the normalisation operation (4.25) with the interleaved and localised subarray architectures can be found in Figures 4.42 and 4.43, respectively.

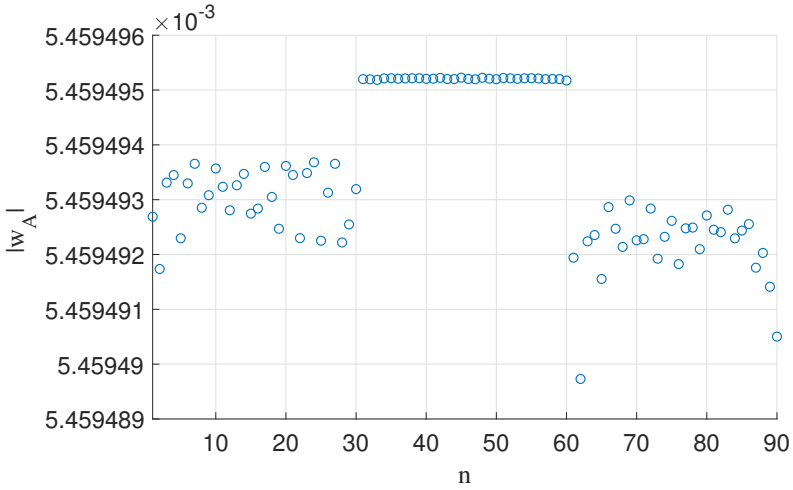

Figure 4.28: Magnitudes of the analogue coefficients $\boldsymbol{w}_A$ generated by the first scheme in Section 4.3.1 with the interleaved subarray architecture.

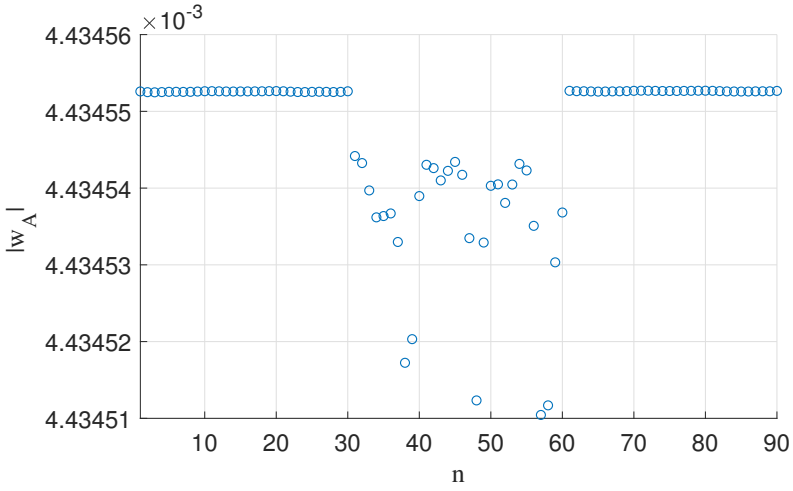

Figure 4.29: Magnitudes of the analogue coefficients $\boldsymbol{w}_A$ generated by the first scheme in Section 4.3.1 with the localised subarray architecture.

In addition, the digital and analogue coefficients with the interleaved subarray architecture are listed in Tables 4.25 and 4.26, respectively, and the digital and analogue coefficients with the localised subarray architecture are listed in Tables 4.27 and 4.28, respectively. Furthermore, the change of the cost function J_{LSE} in (4.56) using the interleaved and localised subarray architectures with respect to the iteration number is shown in Figures 4.44 and 4.45, respectively.

The normalised variances of beam patterns for the three designed beams with the

Table 4.17: Digital coefficients $\boldsymbol{w}_{D,0}$, $\boldsymbol{w}_{D,1}$ and $\boldsymbol{w}_{D,2}$ with $\varphi_0 = -30°$, $\varphi_1 = 0°$ and $\varphi_2 = 35°$ generated by the first scheme in Section 4.3.1 with the interleaved subarray architecture.

m \ j	$\boldsymbol{w}_{D,0}$	$\boldsymbol{w}_{D,1}$	$\boldsymbol{w}_{D,2}$
0	-0.2071-0.7083i	-2.9789+5.3483i	0.4279+0.36797i
1	6.0008-0.9842i	-0.0774+0.5126i	0.2600+0.04497i
2	0.1335-0.0072i	-0.1868+0.1358i	-4.6730-3.9552i

Table 4.18: Analogue coefficients $\boldsymbol{w}_{A,0}$, $\boldsymbol{w}_{A,1}$ and $\boldsymbol{w}_{A,2}$ with $\varphi_0 = -30°$, $\varphi_1 = 0°$ and $\varphi_2 = 35°$ generated by the first scheme in Section 4.3.1 with the interleaved subarray architecture.

n \ m	$\boldsymbol{w}_{A,0}$	$\boldsymbol{w}_{A,1}$	$\boldsymbol{w}_{A,2}$	n \ m	$\boldsymbol{w}_{A,0}$	$\boldsymbol{w}_{A,1}$	$\boldsymbol{w}_{A,2}$
0	-0.0031-0.0045i	0.0048-0.0026i	-0.0032-0.0044i	15	-0.0016-0.0052i	-0.0049+0.0024i	0.0005-0.0054i
1	-0.0027-0.0047i	-0.0038-0.0039i	0.0051-0.0018i	16	-0.0030-0.0046i	0.0038+0.0039i	0.0042+0.0035i
2	-0.0021-0.0050i	-0.0027+0.0048i	-0.0018+0.0052i	17	-0.0032-0.0044i	0.0024-0.0049i	-0.0055+0.0002i
3	-0.0029-0.0046i	0.0054+0.0008i	-0.0028-0.0047i	18	-0.0018-0.0051i	-0.0054-0.0009i	0.0014-0.0053i
4	-0.0033-0.0043i	-0.0009-0.0054i	0.0053-0.0011i	19	-0.0026-0.0048i	0.0008+0.0054i	0.0031+0.0045i
5	-0.0020-0.0051i	-0.0050+0.0023i	-0.0030+0.0045i	20	-0.0031-0.0045i	0.0048-0.0026i	-0.0054-0.0009i
6	-0.0025-0.0048i	0.0039+0.0038i	-0.0019-0.0051i	21	-0.0024-0.0049i	-0.0038-0.0039i	0.0023-0.0050i
7	-0.0036-0.0041i	0.0024-0.0049i	0.0055-0.0001i	22	-0.0023-0.0050i	-0.0026+0.0048i	0.0017+0.0052i
8	-0.0022-0.0050i	-0.0054-0.0010i	-0.0041+0.0036i	23	-0.0029-0.0046i	0.0054+0.0007i	-0.0051-0.0019i
9	-0.0021-0.0050i	0.0009+0.0054i	-0.0011-0.0054i	24	-0.0031-0.0045i	-0.0008-0.0054i	0.0032-0.0044i
10	-0.0036-0.0041i	0.0048-0.0025i	0.0053+0.0011i	25	-0.0022-0.0050i	-0.0049+0.0023i	0.0003+0.0054i
11	-0.0025-0.0048i	-0.0038-0.0040i	-0.0048+0.0025i	26	-0.0026-0.0048i	0.0039+0.0038i	-0.0048-0.0026i
12	-0.0017-0.0052i	-0.0025+0.0049i	-0.0002-0.0055i	27	-0.0035-0.0042i	0.0024-0.0049i	0.0041-0.0036i
13	-0.0034-0.0043i	0.0054+0.0008i	0.0049+0.0024i	28	-0.0023-0.0049i	-0.0054-0.0010i	-0.0009+0.0054i
14	-0.0030-0.0046i	-0.0008-0.0054i	-0.0053+0.0013i	29	-0.0021-0.0050i	0.0008+0.0054i	-0.0048-0.0026i

interleaved and localised subarray architectures are displayed in Figures 4.46 and 4.47, respectively. As shown in Figure 4.46, although the variances of the zeroth beam at around 0.39, 0.5 and 1.0 are about 4.94, 4.23 and 2.15, respectively, and the variances of the first beam at around -0.49 and -0.33 are as high as 2.97 and 2.77, respectively, with the interleaved subarray architecture; as shown in Figure 4.47, although the variance of

Table 4.19: Digital coefficients $\boldsymbol{w}_{D,0}$, $\boldsymbol{w}_{D,1}$ and $\boldsymbol{w}_{D,2}$ with $\varphi_0 = -30°$, $\varphi_1 = 0°$ and $\varphi_2 = 35°$ generated by the first scheme in Section 4.3.1 with the localised subarray architecture.

m \ j	$\boldsymbol{w}_{D,0}$	$\boldsymbol{w}_{D,1}$	$\boldsymbol{w}_{D,2}$
0	-0.2135+0.2427i	7.1599+1.9195i	0.0170+0.0905i
1	-5.7163+5.4685i	-0.4167-0.3700i	0.4219-0.1899i
2	-0.0177-0.1752i	0.0223+-0.0891i	3.0110-6.7764i

Table 4.20: Analogue coefficients $\boldsymbol{w}_{A,0}$, $\boldsymbol{w}_{A,1}$ and $\boldsymbol{w}_{A,2}$ with $\varphi_0 = -30°$, $\varphi_1 = 0°$ and $\varphi_2 = 35°$ generated by the first scheme in Section 4.3.1 with the localised subarray architecture.

n \ m	$\boldsymbol{w}_{A,0}$	$\boldsymbol{w}_{A,1}$	$\boldsymbol{w}_{A,2}$	n \ m	$\boldsymbol{w}_{A,0}$	$\boldsymbol{w}_{A,1}$	$\boldsymbol{w}_{A,2}$
0	0.0043-0.0012i	-0.0040-0.0020i	0.0041+0.0018i	15	0.0043-0.0011i	0.0019+0.0040i	0.0011-0.0043i
1	0.0043-0.0012i	-0.0044-0.0003i	0.0018+0.0040i	16	0.0043-0.0012i	0.0032+0.0030i	0.0036-0.0025i
2	0.0043-0.0011i	-0.0040+0.0019i	-0.0013+0.0042i	17	0.0043-0.0012i	0.0040-0.0019i	0.0044+0.0005i
3	0.0043-0.0011i	-0.0018+0.0040i	-0.0037+0.0024i	18	0.0043-0.0012i	-0.0002-0.0044i	0.0030+0.0033i
4	0.0043-0.0011i	0.0009+0.0043i	-0.0044-0.0007i	19	0.0043-0.0012i	-0.0018-0.0040i	0.0001+0.0044i
5	0.0043-0.0011i	0.0025+0.0036i	-0.0028-0.0034i	20	0.0043-0.0011i	-0.0032+0.0031i	-0.0028+0.0034i
6	0.0043-0.0011i	0.0035+0.0027i	0.0001-0.0044i	21	0.0043-0.0011i	-0.0044-0.0003i	-0.0044+0.0007i
7	0.0043-0.0012i	0.0044+0.0004i	0.0030-0.0032i	22	0.0043-0.0011i	-0.0032+0.0031i	-0.0038-0.0024i
8	0.0043-0.0012i	0.0000-0.0044i	0.0044-0.0004i	23	0.0043-0.0011i	-0.0014+0.0042i	-0.0012-0.0043i
9	0.0043-0.0012i	-0.0026-0.0036i	0.0036+0.0026i	24	0.0043-0.0011i	-0.0002+0.0044i	0.0019-0.0040i
10	0.0043-0.0012i	-0.0037-0.0025i	0.0010+0.0043i	25	0.0043-0.0012i	0.0009+0.0043i	0.0041-0.0018i
11	0.0043-0.0011i	-0.0044-0.0007i	-0.0021-0.0039i	26	0.0043-0.0012i	0.0033+0.0030i	0.0042+0.0013i
12	0.0043-0.0011i	-0.0038+0.0022i	-0.0041+0.0016i	27	0.0043-0.0012i	0.0031-0.0032i	0.0023+0.0038i
13	0.0043-0.0011i	-0.0014+0.0042i	-0.0042+0.0016i	28	0.0043-0.0012i	0.0005-0.0044i	-0.0008+0.0044i
14	0.0043-0.0011i	0.0006+0.0044i	-0.0021-0.0039i	29	0.0043-0.0012i	-0.0017-0.0041i	-0.0035+0.0027i

the first beam at around -0.83 is about 12.45 with the localised subarray architecture, because the responses are close to -60 dB, the variation of the beam patterns is still at an acceptable level.

4.4.8 Design Examples for the Fourth Scheme in Section 4.3.4

With $K = 2000$, the mean patterns of the zeroth, first and second beams with the interleaved and localised subarray architectures are shown in Figures 4.48, 4.49 and 4.50,

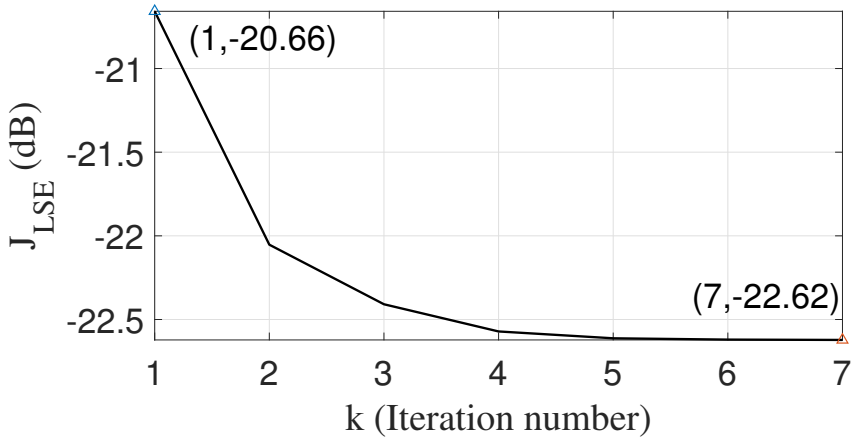

Figure 4.30: Cost function J_{LSE} in (4.41) with respect to the iteration number k generated by the first scheme in Section 4.3.1 with the interleaved subarray architecture.

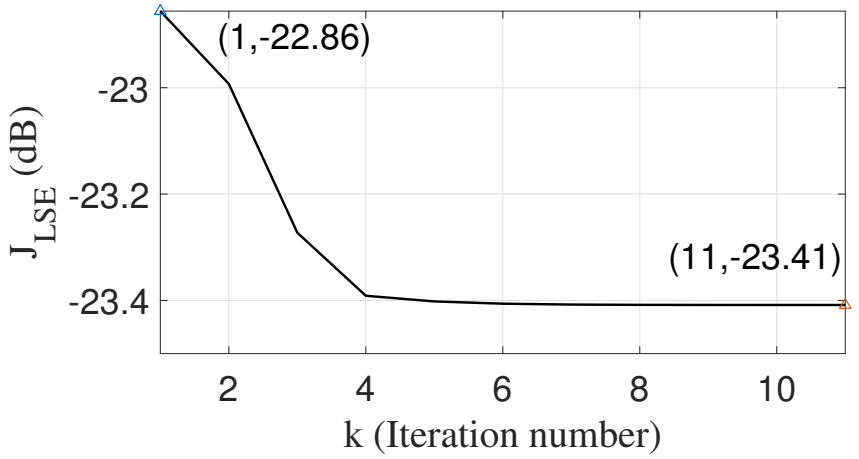

Figure 4.31: Cost function J_{LSE} in (4.41) with respect to the iteration number k generated by the first scheme in Section 4.3.1 with the localised subarray architecture.

respectively. The digital and analogue coefficients with the interleaved subarray architecture are listed in Tables 4.29 and 4.30, respectively, and the digital and analogue coefficients with the localised architecture are listed in Tables 4.31 and 4.32, respectively. Furthermore, the change of the cost function J_{LSE} in (4.40) with respect to the iteration number using the interleaved and localised subarray architectures is shown in Figures 4.51 and 4.52, respectively.

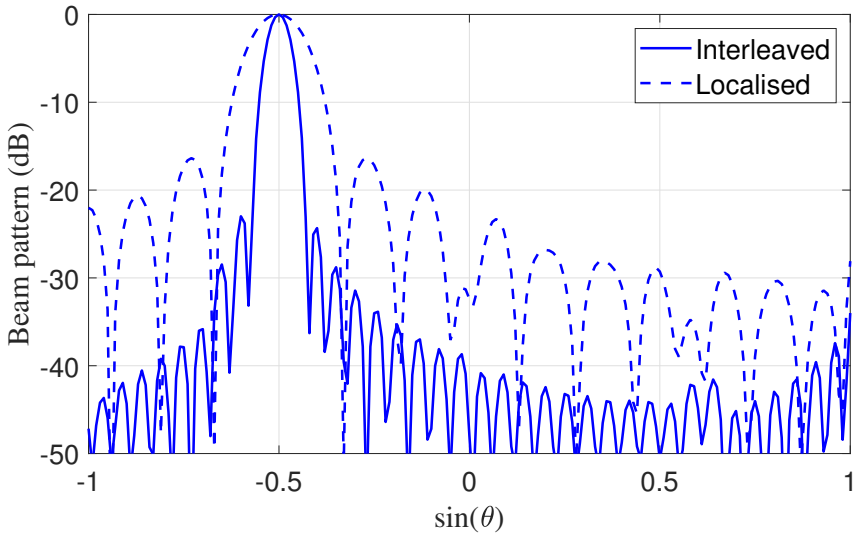

Figure 4.32: The mean patterns of the zeroth beam with $\varphi_0 = -30°$ generated by the second scheme in Section 4.3.2 with the interleaved and localised subarray architectures, respectively.

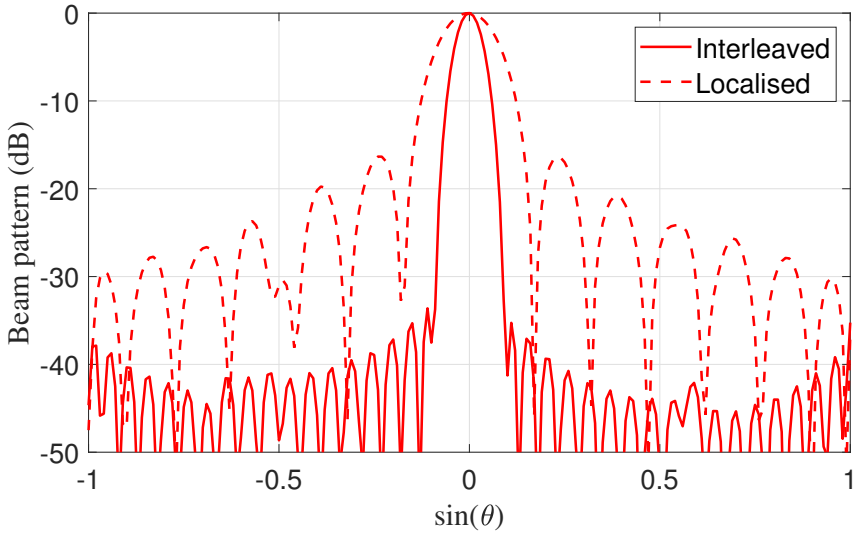

Figure 4.33: The mean patterns of the first beam with $\varphi_1 = 0°$ generated by the second scheme in Section 4.3.2 with the interleaved and localised subarray architectures, respectively.

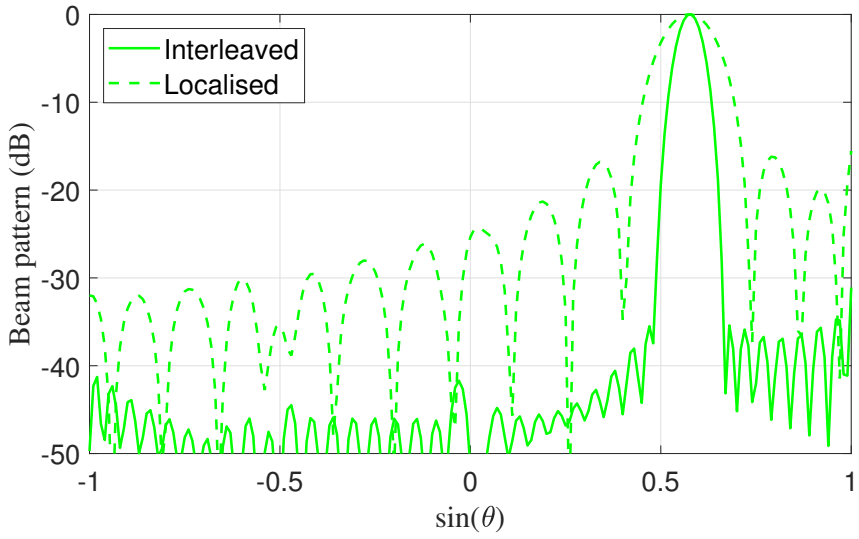

Figure 4.34: The mean patterns of the second beam with $\varphi_2 = 35°$ generated by the second scheme in Section 4.3.2 with the interleaved and localised subarray architectures, respectively.

Table 4.21: Digital coefficients $\boldsymbol{w}_{D,0}$, $\boldsymbol{w}_{D,1}$ and $\boldsymbol{w}_{D,2}$ with $\varphi_0 = -30°$, $\varphi_1 = 0°$ and $\varphi_2 = 35°$ generated by the second scheme in Section 4.3.2 with the interleaved subarray architecture.

m \ j	$\boldsymbol{w}_{D,0}$	$\boldsymbol{w}_{D,1}$	$\boldsymbol{w}_{D,2}$
0	-0.0181-0.0105i	0.0126-0.0020i	-0.0048+0.0135i
1	-0.0017+0.0018i	-0.0404+0.0160i	0.0073+0.0279i
2	0.0005+0.0073i	0.0211+0.0124i	-0.0411+0.0102i

4.4.9 Discussion on the Performances of the Four Schemes in Sections 4.2 and 4.3

To compare the average sidelobe levels for J-user cases in the four proposed schemes, the mean value of the total sidelobe patterns $\bar{P}_s$ is defined as

$$\bar{P}_s = \frac{1}{JN_g} \sum_{j=0}^{J-1} \sum_{i=0,\theta_i \in \Theta_{side_j}}^{N_g-1} \left| P_{\varphi_j}(\theta_i) \right|^2 . \tag{4.58}$$

Table 4.22: Analogue coefficients $\boldsymbol{w}_{A,0}$, $\boldsymbol{w}_{A,1}$ and $\boldsymbol{w}_{A,2}$ with $\varphi_0 = -30°$, $\varphi_1 = 0°$ and $\varphi_2 = 35°$ generated by the second scheme in Section 4.3.2 with the interleaved subarray architecture.

n \ m	$\boldsymbol{w}_{A,0}$	$\boldsymbol{w}_{A,1}$	$\boldsymbol{w}_{A,2}$	n \ m	$\boldsymbol{w}_{A,0}$	$\boldsymbol{w}_{A,1}$	$\boldsymbol{w}_{A,2}$
0	-0.2765+0.1654i	-0.0807-0.0958i	-0.1377-0.2156i	15	2.2940-1.2876i	-0.0190-0.5702i	1.8549-0.2881i
1	0.4566+0.3800i	-0.0198+0.0377i	0.1280+0.2749i	16	-1.3127-1.1359i	-1.3756-0.1782i	-0.0258-0.2909i
2	0.3080-0.5930i	-0.2358-0.1614i	0.1526-0.0505i	17	-0.7934+1.5296i	-1.1694-0.8853i	-1.0265-0.9535i
3	-0.7938-0.2298i	-0.2062-0.3080i	-0.0166-0.6932i	18	2.4332+0.0207i	-0.1069-0.2839i	1.4117+0.2625i
4	0.3391+1.0486i	-0.1960+0.1182i	-0.0122+0.4857i	19	-0.2558-1.6277i	-1.1876-0.2731i	0.2126-0.1693i
5	1.0034-0.5729i	-0.4769-0.3232i	0.1363+0.0576i	20	-1.4813+0.5800i	-0.9337-0.8345i	-0.6851-1.2494i
6	-0.8296-1.0778i	-0.2785-0.5662i	0.4565-1.1485i	21	1.6330+1.0187i	-0.1542-0.0469i	0.7260+0.4558i
7	-0.3502+1.4463i	-0.5430+0.1702i	-0.2402+0.4311i	22	0.6880-1.2602i	-0.8372-0.2544i	0.2631+0.0668i
8	1.5392+0.0911i	-0.7733-0.5073i	-0.1417+0.1339i	23	-1.3241-0.3861i	-0.5914-0.6610i	-0.2143-1.1301i
9	-0.0732-1.9232i	-0.2603-0.7555i	1.1726-1.2738i	24	0.5414+1.1906i	-0.1829+0.0586i	0.1893+0.3191i
10	-1.2754+1.0857i	-0.9674+0.1279i	-0.3768+0.1659i	25	0.9463-0.4836i	-0.4784-0.1596i	0.1417+0.2039i
11	1.3675+1.1065i	-1.0506-0.6834i	-0.1605-0.0102i	26	-0.6495-0.7577i	-0.2747-0.4126i	0.0888-0.6970i
12	1.2290-2.0836i	-0.1782-0.7615i	1.7584-0.9256i	27	-0.1391+0.7160i	-0.1484+0.0540i	-0.0206+0.8658i
13	-1.7392+0.0109i	-1.2942-0.0127i	-0.2881-0.1536i	28	0.5792+0.0799i	-0.2153-0.0626i	-0.0016+0.1716i
14	0.4072+1.7583i	-1.2085-0.8221i	-0.9939-0.4335i	29	-0.0220-0.5438i	-0.0661-0.1804i	0.1199-0.1823i

Table 4.23: Digital coefficients $\boldsymbol{w}_{D,0}$, $\boldsymbol{w}_{D,1}$ and $\boldsymbol{w}_{D,2}$ with $\varphi_0 = -30°$, $\varphi_1 = 0°$ and $\varphi_2 = 35°$ generated by the second scheme in Section 4.3.2 with the localised subarray architecture.

m \ j	$\boldsymbol{w}_{D,0}$	$\boldsymbol{w}_{D,1}$	$\boldsymbol{w}_{D,2}$
0	-0.0217+0.0491i	0.0148+0.0048i	1.7296+2.7354i
1	-2.2401+1.6286i	0.0899+0.0069i	0.0047+0.0411i
2	0.0610+0.0672i	-2.7782+0.9447i	-0.0094-0.0106i

The mean variance of beam patterns for the J beams is given by

$$\bar{v} = \frac{1}{JN_w} \sum_{j=0}^{J-1} \sum_{i=0}^{N_w-1} var_j(\theta_i). \tag{4.59}$$

To quantify the variation of the magnitudes of analogue coefficients, the normalised variance for the magnitudes of the combined analogue coefficients $\boldsymbol{w}_A$ generated by M sub-

Table 4.24: Analogue coefficients $\boldsymbol{w}_{A,0}$, $\boldsymbol{w}_{A,1}$ and $\boldsymbol{w}_{A,2}$ with $\varphi_0 = -30°$, $\varphi_1 = 0°$ and $\varphi_2 = 35°$ generated by the second scheme in Section 4.3.2 with the localised subarray architecture.

n \ m	$\boldsymbol{w}_{A,0}$	$\boldsymbol{w}_{A,1}$	$\boldsymbol{w}_{A,2}$	n \ m	$\boldsymbol{w}_{A,0}$	$\boldsymbol{w}_{A,1}$	$\boldsymbol{w}_{A,2}$
0	-0.0098-0.0258i	-0.0092-0.0302i	-0.0298-0.0126i	15	-0.0060-0.0030i	0.0142+0.0102i	-0.0076-0.0024i
1	0.0261+0.0106i	-0.0122+0.0214i	0.0116+0.0051i	16	-0.0070-0.0079i	0.0128-0.0032i	-0.0141-0.0050i
2	0.0062+0.0093i	-0.0034+0.0092i	-0.0060-0.0022i	17	-0.0025-0.0101i	0.0062-0.0112i	-0.0170-0.0057i
3	-0.0075+0.0014i	-0.0028-0.0027i	-0.0202-0.0081i	18	0.0084-0.0079i	0.0025-0.0102i	-0.0114-0.0038i
4	-0.0032+0.0037i	-0.0007+0.0065i	-0.0126-0.0048i	19	0.0158-0.0006i	0.0004-0.0076i	-0.0056-0.0017i
5	0.0001+0.0077i	0.0083+0.0147i	-0.0025-0.0005i	20	0.0099+0.0087i	-0.0066-0.0075i	-0.0088-0.0028i
6	-0.0066+0.0025i	0.0146+0.0045i	-0.0059-0.0018i	21	-0.0045+0.0132i	-0.0158-0.0043i	-0.0163-0.0053i
7	-0.0117-0.0083i	0.0104-0.0121i	-0.0152-0.0056i	22	-0.0121+0.0079i	-0.0146+0.0060i	-0.0156-0.0050i
8	-0.0039-0.0134i	0.0009-0.0165i	-0.0160-0.0060i	23	-0.0066-0.0028i	0.0000+0.0153i	-0.0059-0.0018i
9	0.0103-0.0084i	-0.0050-0.0087i	-0.0087-0.0031i	24	0.0003-0.0077i	0.0117+0.0126i	-0.0022-0.0006i
10	0.0158+0.0011i	-0.0074-0.0019i	-0.0055-0.0019i	25	-0.0030-0.0037i	0.0068+0.0014i	-0.0126-0.0039i
11	0.0081+0.0082i	-0.0105-0.0009i	-0.0113-0.0040i	26	-0.0073-0.0015i	-0.0015-0.0036i	-0.0206-0.0064i
12	-0.0030+0.0101i	-0.0125+0.0023i	-0.0169-0.0061i	27	0.0066-0.0092i	0.0099-0.0004i	-0.0061-0.0018i
13	-0.0073+0.0077i	-0.0070+0.0111i	-0.0141-0.0050i	28	0.0263-0.0097i	0.0244-0.0047i	0.0123+0.0039i
14	-0.0061+0.0027i	0.0053+0.0166i	-0.0076-0.0025i	29	-0.0105+0.0258i	-0.0257-0.0186i	-0.0305-0.0092i

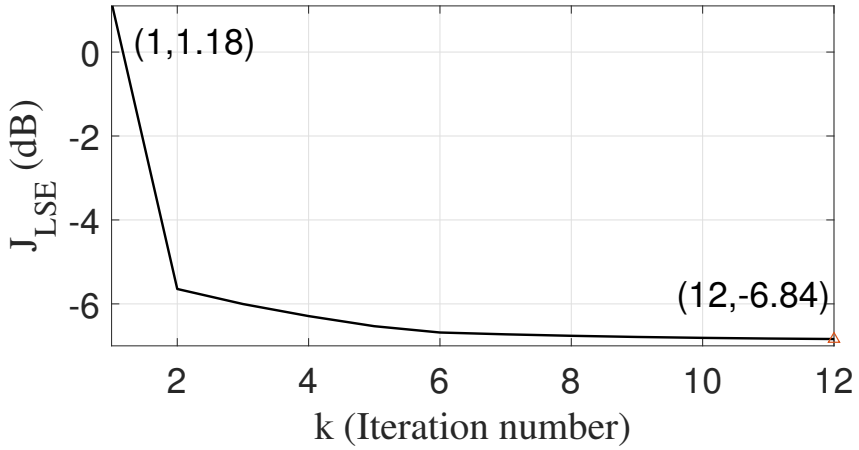

Figure 4.35: Cost function J_{LSE} in (4.55) with respect to the iteration number k generated by the second scheme in Section 4.3.2 with the interleaved subarray architecture.

arrays is given by

$$var_{|\boldsymbol{w}_A|} = \frac{1}{MN_s} \sum_{n=0}^{MN_s-1} \frac{||\boldsymbol{w}_A(n)| - |\bar{\boldsymbol{w}}_A||^2}{|\bar{\boldsymbol{w}}_A|^2}. \tag{4.60}$$

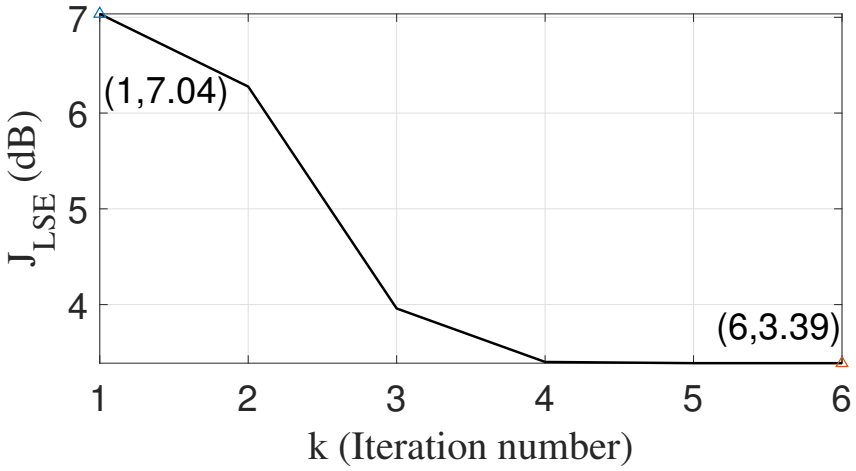

Figure 4.36: Cost function J_{LSE} in (4.55) with respect to the iteration number k generated by the second scheme in Section 4.3.2 with the localised subarray architecture.

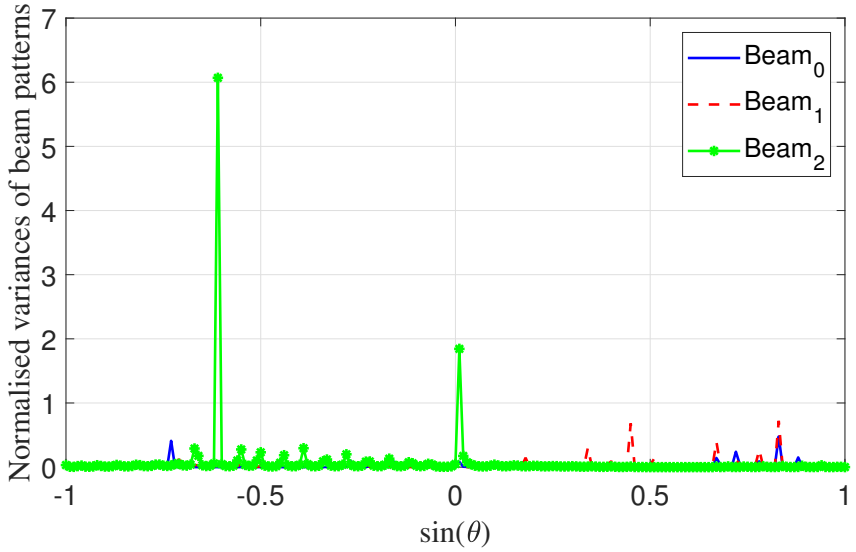

Figure 4.37: Normalised variances of beam patterns with $\varphi_0 = -30°$, $\varphi_1 = 0°$ and $\varphi_2 = 35°$ generated by the second scheme in Section 4.3.2 with the interleaved subarray architecture.

The four parameters, including (4.58), (4.59), (4.60) and computation time are compared for the above four schemes which are employed in the two-beam and three-beam cases in Tables 4.33 and 4.34, respectively.

For both the two-beam and three-beam cases, note even though the robustness is not

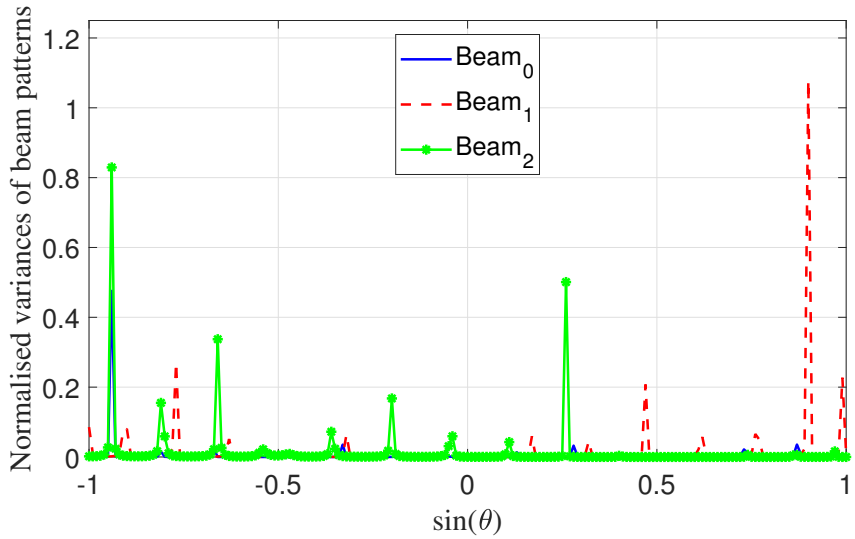

Figure 4.38: Normalised variances of beam patterns with $\varphi_0 = -30°$, $\varphi_1 = 0°$ and $\varphi_2 = 35°$ generated by the second scheme in Section 4.3.2 with the localised subarray architecture.

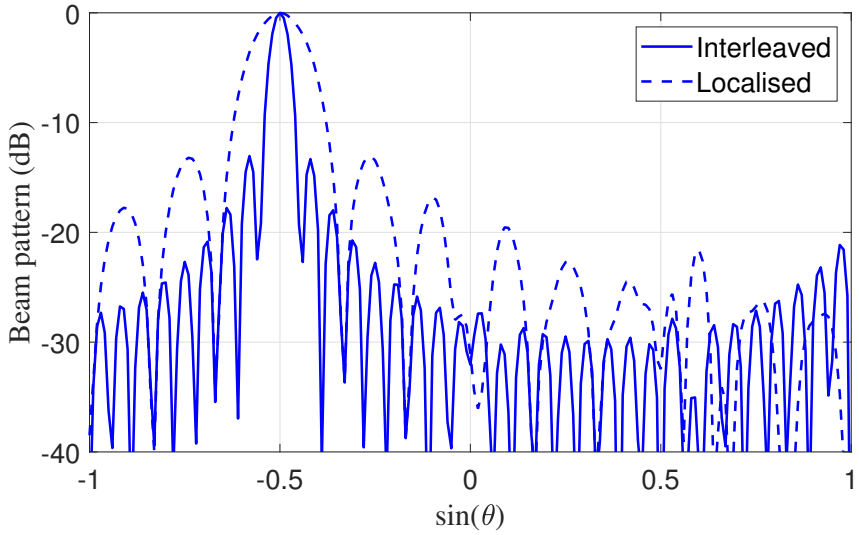

Figure 4.39: The mean patterns of the zeroth beam with $\varphi_0 = -30°$ generated by the third scheme in Section 4.3.3 with the interleaved and localised subarray architectures, respectively.

considered in the first and fourth schemes, the maximum upper norm-bound $\epsilon_e = 0.1$ is also imposed on the steering vectors for performance comparison.

For both interleaved and localised subarray architectures, the third scheme has an

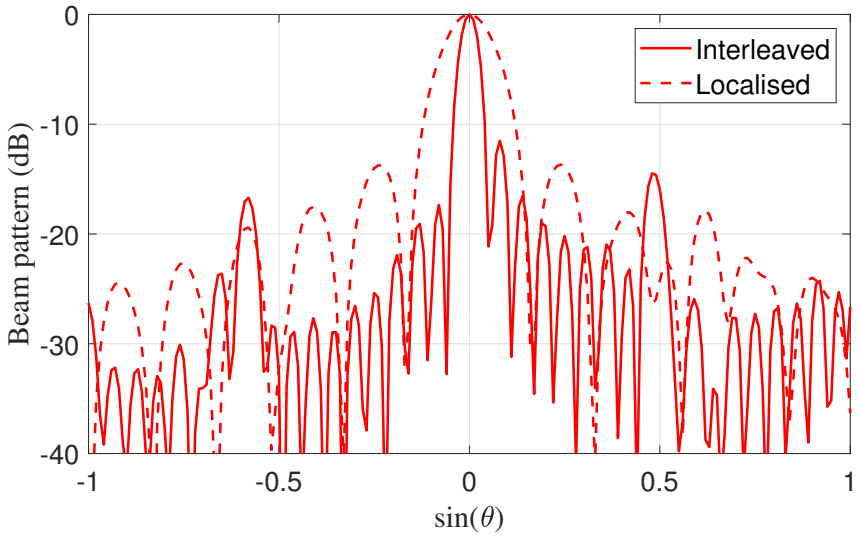

Figure 4.40: The mean patterns of the first beam with $\varphi_1 = 0°$ generated by the third scheme in Section 4.3.3 with the interleaved and localised subarray architectures, respectively.

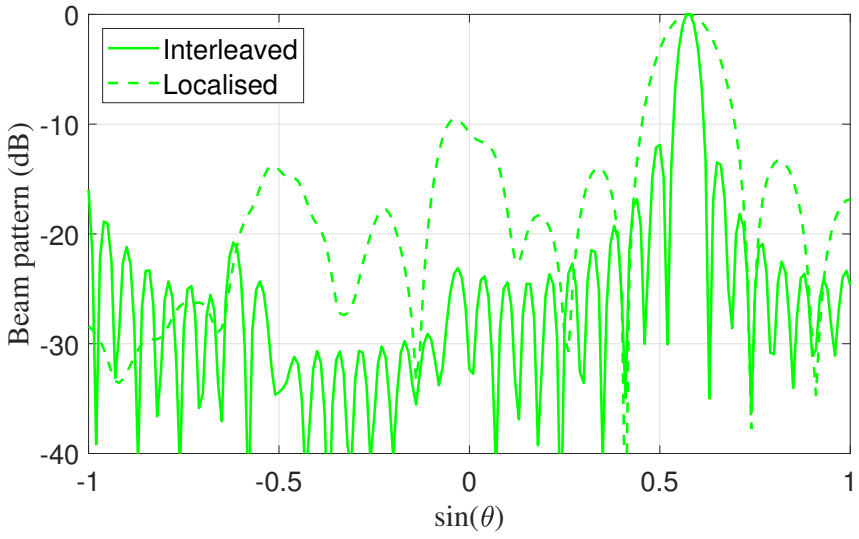

Figure 4.41: The mean patterns of the second beam with $\varphi_2 = 35°$ generated by the third scheme in Section 4.3.3 with the interleaved and localised subarray architectures, respectively.

extra robustness property against steering vector errors with much lower mean variance of beam patterns $\bar{v}$ than the first scheme at the cost of a little higher mean value of total sidelobe responses $\bar{P}_s(dB)$. On the other hand, compared to the second scheme,

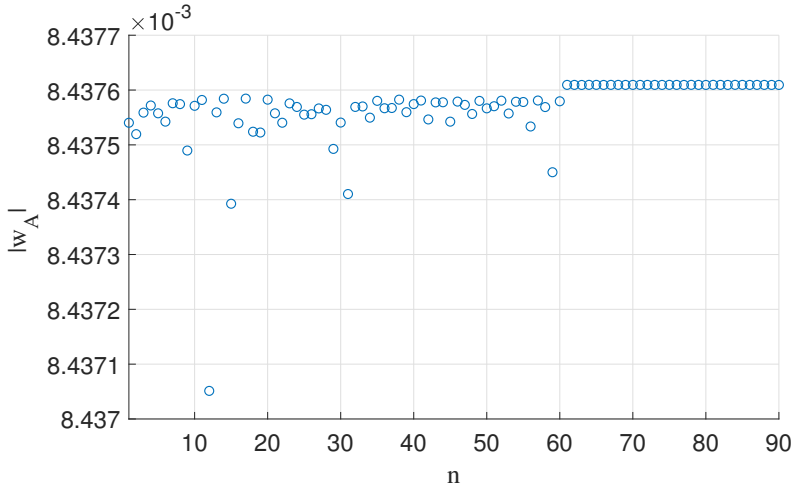

Figure 4.42: Magnitudes of the analogue coefficients $\boldsymbol{w}_A$ generated by the third scheme in Section 4.3.3 with the interleaved subarray architecture.

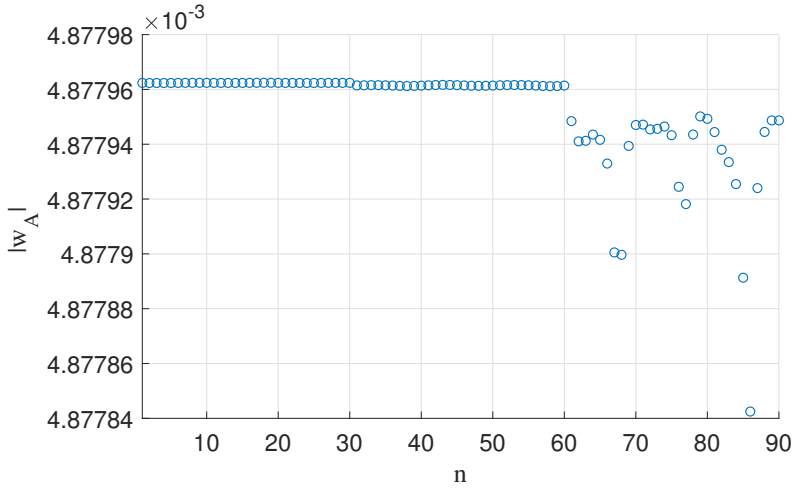

Figure 4.43: Magnitudes of the analogue coefficients $\boldsymbol{w}_A$ generated by the third scheme in Section 4.3.3 with the localised subarray architecture.

although the mean variance of beam patterns $\bar{v}$ of the third scheme is a little larger, the beamformer provides a much more uniform magnitude in its analogue coefficients due to the additional equal magnitude constraint.

As expected, $var_{|\boldsymbol{w}_A|}$ and $\bar{v}$ for the design in the fourth scheme are much higher than those of the other three schemes; however, its $\bar{P}_s$ is much lower because removal of the two additional constraints provides more degrees of freedom for the design.

Another observation is that the interleaved subarray architecture provides a much

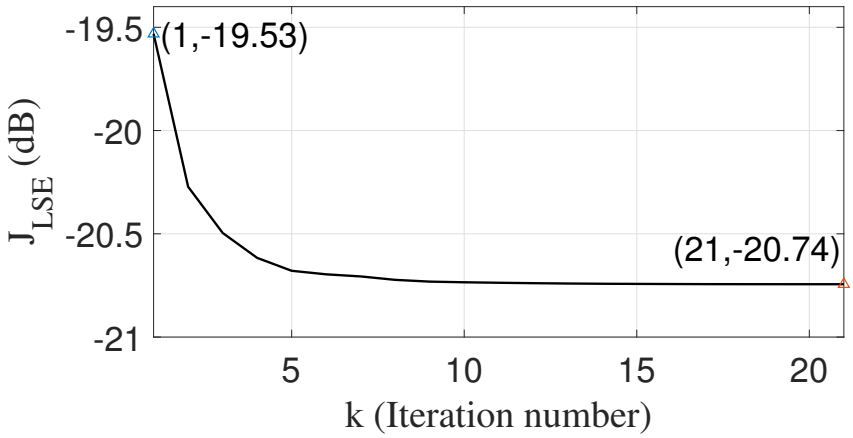

Figure 4.44: Cost function J_{LSE} in (4.55) with respect to the iteration number k generated by the third scheme in Section 4.3.3 with the interleaved subarray architecture.

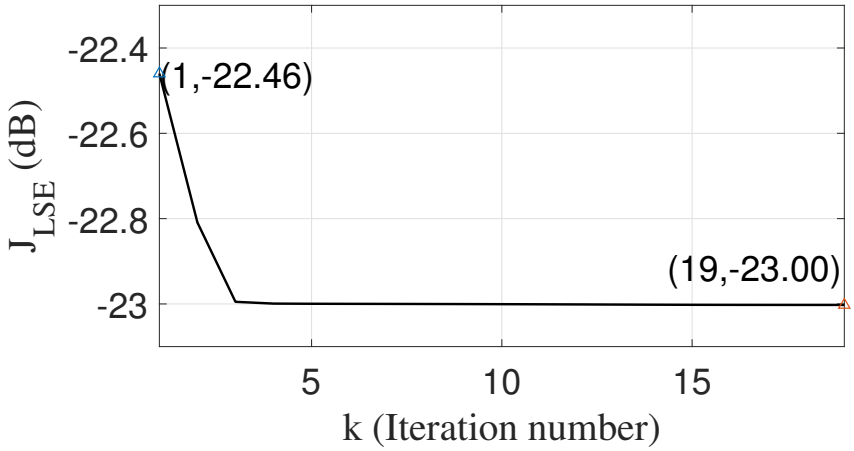

Figure 4.45: Cost function J_{LSE} in (4.55) with respect to the iteration number k generated by the third scheme in Section 4.3.3 with the localised subarray architecture.

Table 4.25: Digital coefficients $\boldsymbol{w}_{D,0}$, $\boldsymbol{w}_{D,1}$ and $\boldsymbol{w}_{D,2}$ with $\varphi_0 = -30°$, $\varphi_1 = 0°$ and $\varphi_2 = 35°$ generated by the third scheme in Section 4.3.3 with the interleaved subarray architecture.

m \ j	$\boldsymbol{w}_{D,0}$	$\boldsymbol{w}_{D,1}$	$\boldsymbol{w}_{D,2}$
0	0.0247-0.1002i	-2.9307-2.7927i	0.9742+0.0981i
1	0.0140+0.1210i	0.4613+0.3688i	4.0691+0.1210i
2	1.7121-3.5031i	0.5253+0.7462i	0.6290+0.5539i

Table 4.26: Analogue coefficients $\boldsymbol{w}_{A,0}$, $\boldsymbol{w}_{A,1}$ and $\boldsymbol{w}_{A,2}$ with $\varphi_0 = -30°$, $\varphi_1 = 0°$ and $\varphi_2 = 35°$ generated by the third scheme in Section 4.3.3 with the interleaved subarray architecture.

n \ m	$\boldsymbol{w}_{A,0}$	$\boldsymbol{w}_{A,1}$	$\boldsymbol{w}_{A,2}$	n \ m	$\boldsymbol{w}_{A,0}$	$\boldsymbol{w}_{A,1}$	$\boldsymbol{w}_{A,2}$
0	-0.0029+0.0079i	0.0079+0.0028i	0.0084-0.0012i	15	-0.0065+0.0054i	0.0011+0.0084i	-0.0084+0.0012i
1	-0.0083+0.0014i	-0.0077+0.0034i	-0.0037-0.0016i	16	-0.0068+0.0050i	-0.0024-0.0081i	0.0038+0.0076i
2	-0.0083+0.0014i	0.0056-0.0063i	-0.0062+0.0058i	17	-0.0031+0.0079i	0.0070-0.0048i	0.0061-0.0058i
3	-0.0045+0.0072i	0.0081+0.0024i	0.0075+0.0039i	18	-0.0052+0.0067i	-0.0020+0.0082i	-0.0075-0.0039i
4	-0.0043+0.0073i	-0.0084+0.0006i	0.0014-0.0083i	19	-0.0075+0.0038i	-0.0005-0.0084i	-0.0015+0.0083i
5	-0.0084+0.0008i	0.0065-0.0053i	-0.0084+0.0010i	20	-0.0037+0.0076i	0.0076-0.0037i	0.0083-0.0012i
6	-0.0056+0.0063i	0.0074+0.0041i	0.0038+0.0075i	21	-0.0035+0.0077i	-0.0048+0.0069i	-0.0037-0.0076i
7	-0.0046+0.0071i	-0.0081-0.0023i	0.0060-0.0060i	22	-0.0080+0.0027i	0.0008-0.0084i	-0.0062+0.0057i
8	-0.0083+0.0015i	0.0070-0.0047i	-0.0074-0.0041i	23	-0.0048+0.0069i	0.0082-0.0020i	0.0075+0.0038i
9	-0.0065+0.0054i	0.0060+0.0060i	-0.0013+0.0083i	24	-0.0028+0.0080i	-0.0069+0.0048i	0.0014-0.0083i
10	-0.0051+0.0067i	-0.0068-0.0050i	0.0083-0.0013i	25	-0.0083+0.0017i	0.0014-0.0083i	-0.0084+0.0010i
11	-0.0071+0.0045i	0.0070-0.0047i	-0.0035-0.0077i	26	-0.0060+0.0059i	0.0084-0.0001i	0.0039+0.0075i
12	-0.0069+0.0049i	0.0038+0.0075i	-0.0060+0.0059i	27	-0.0031+0.0079i	-0.0082+0.0021i	0.0060-0.0059i
13	-0.0059+0.0061i	-0.0047-0.0070i	0.0075+0.0039i	28	-0.0082+0.0019i	0.0007-0.0084i	-0.0074-0.0041i
14	-0.0041+0.0074i	0.0068-0.0050i	0.0016-0.0083i	29	-0.0073+0.0043i	0.0083+0.0016i	-0.0014+0.0083i

Table 4.27: Digital coefficients $\boldsymbol{w}_{D,0}$, $\boldsymbol{w}_{D,1}$ and $\boldsymbol{w}_{D,2}$ with $\varphi_0 = -30°$, $\varphi_1 = 0°$ and $\varphi_2 = 35°$ generated by the third scheme in Section 4.3.3 with the localised subarray architecture.

m \ j	$\boldsymbol{w}_{D,0}$	$\boldsymbol{w}_{D,1}$	$\boldsymbol{w}_{D,2}$
0	-6.7181-0.8825i	0.0679+0.2599i	-0.0579-0.0643i
1	0.3055+0.0959i	-1.0846+6.5454i	0.1692-0.3661i
2	0.2058+0.1459i	-0.0187-0.6561i	5.2646-5.1720i

narrower beam than that the localised subarray architecture.

Table 4.28: Analogue coefficients $\boldsymbol{w}_{A,0}$, $\boldsymbol{w}_{A,1}$ and $\boldsymbol{w}_{A,2}$ with $\varphi_0 = -30°$, $\varphi_1 = 0°$ and $\varphi_2 = 35°$ generated by the third scheme in Section 4.3.3 with the localised subarray architecture.

n \ m	$\boldsymbol{w}_{A,0}$	$\boldsymbol{w}_{A,1}$	$\boldsymbol{w}_{A,2}$	n \ m	$\boldsymbol{w}_{A,0}$	$\boldsymbol{w}_{A,1}$	$\boldsymbol{w}_{A,2}$
0	-0.0049+0.0005i	-0.0004-0.0049i	0.0048+0.0006i	15	0.0048-0.0007i	-0.0011-0.0047i	-0.0031-0.0038i
1	-0.0036+0.0033i	-0.0005-0.0049i	0.0033+0.0036i	16	0.0035-0.0034i	-0.0011-0.0048i	0.0044-0.0021i
2	-0.0008+0.0048i	-0.0007-0.0048i	-0.0099+0.0048i	17	0.0009-0.0048i	-0.0009-0.0048i	0.0045+0.0018i
3	0.0022+0.0044i	-0.0009-0.0048i	-0.0031+0.0038i	18	-0.0020-0.0044i	-0.0006-0.0048i	0.0036+0.0033i
4	0.0043+0.0022i	-0.0011-0.0048i	-0.0042+0.0024i	19	-0.0042-0.0024i	-0.0005-0.0049i	0.0021+0.0044i
5	0.0048-0.0007i	-0.0011-0.0047i	-0.0048+0.0006i	20	-0.0048+0.0005i	-0.0004-0.0049i	-0.0003+0.0049i
6	0.0035-0.0034i	-0.0011-0.0048i	-0.0043-0.0024i	21	-0.0036+0.0033i	-0.0005-0.0048i	-0.0036+0.0033i
7	0.0009-0.0048i	-0.0009-0.0048i	0.0042-0.0025i	22	-0.0008+0.0048i	-0.0007-0.0048i	-0.0049-0.0003i
8	-0.0020-0.0044i	-0.0006-0.0048i	0.0048+0.0007i	23	0.0022+0.0044i	-0.0010-0.0048i	-0.0041-0.0027i
9	-0.0042-0.0024i	-0.0005-0.0049i	0.0043+0.0023i	24	0.0043+0.0022i	-0.0011-0.0047i	-0.0025-0.0042i
10	-0.0048+0.0005i	-0.0004-0.0049i	0.0029+0.0039i	25	0.0048-0.0007i	-0.0012-0.0047i	0.0047-0.0011i
11	-0.0036+0.0033i	-0.0005-0.0048i	-0.0001+0.0049i	26	0.0035-0.0034i	-0.0011-0.0048i	0.0038+0.0030i
12	-0.0009+0.0048i	-0.0007-0.0048i	-0.0034+0.0035i	27	0.0009-0.0048i	-0.0009-0.0048i	0.0028+0.0040i
13	0.0022+0.0044i	-0.0009-0.0048i	-0.0048+0.0011i	28	-0.0020-0.0044i	-0.0006-0.0048i	0.0014+0.0047i
14	0.0043+0.0022i	-0.0011-0.0048i	-0.0047-0.0012i	29	-0.0043-0.0024i	-0.0004-0.0049i	-0.0011+0.0048i

Table 4.29: Digital coefficients $\boldsymbol{w}_{D,0}$, $\boldsymbol{w}_{D,1}$ and $\boldsymbol{w}_{D,2}$ with $\varphi_0 = -30°$, $\varphi_1 = 0°$ and $\varphi_2 = 35°$ generated by the fourth scheme in Section 4.3.4 with the interleaved subarray architecture.

m \ j	$\boldsymbol{w}_{D,0}$	$\boldsymbol{w}_{D,1}$	$\boldsymbol{w}_{D,2}$
0	3.6872+4.4921i	0.4680-1.4815i	-4.6235+9.3431i
1	6.4305+1.2107i	-2.8236+3.2178i	3.3776+5.6387i
2	6.9252-0.4310i	-7.7117+5.9106i	-4.9283-8.6278i

4.5 Summary

In this chapter, three multi-beam multiplexing designs considering practical application constraints have been proposed based on the interleaved subarray architecture. For the first design, all the analogue antenna coefficients share the same magnitude, so that only

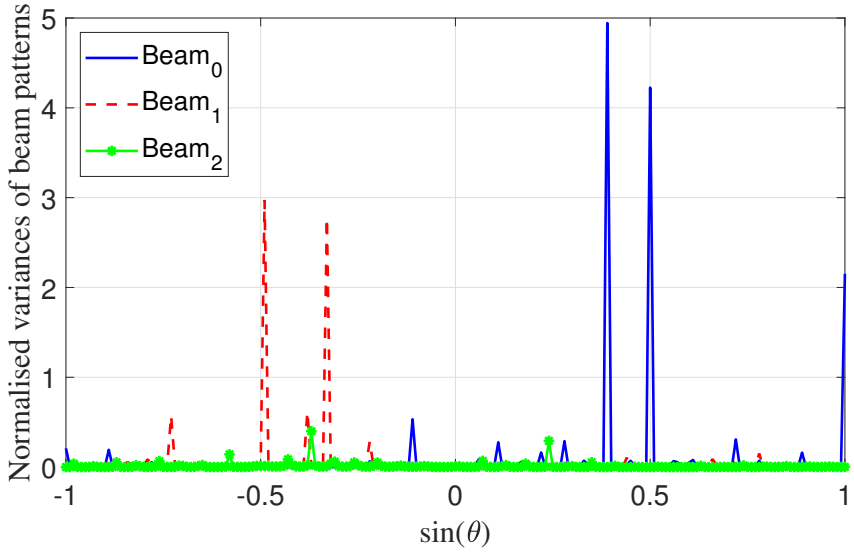

Figure 4.46: Normalised variances of beam patterns with $\varphi_0 = -30°$, $\varphi_1 = 0°$ and $\varphi_2 = 35°$ generated by the third scheme in Section 4.3.3 with the interleaved subarray architecture.

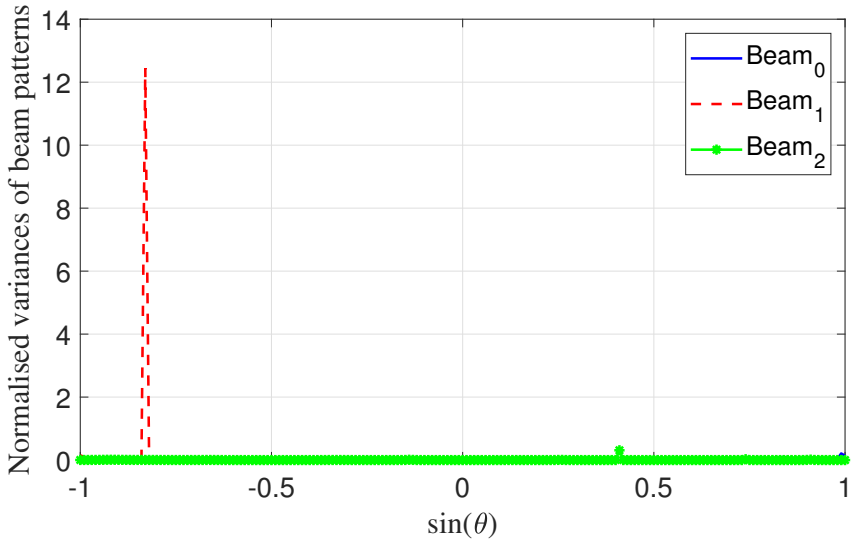

Figure 4.47: Normalised variances of beam patterns with $\varphi_0 = -30°$, $\varphi_1 = 0°$ and $\varphi_2 = 35°$ generated by the third scheme in Section 4.3.3 with the localised subarray architecture.

phase changes are needed in its implementation. In the second design, robustness of the system against various steering vector errors was considered by introducing a norm-

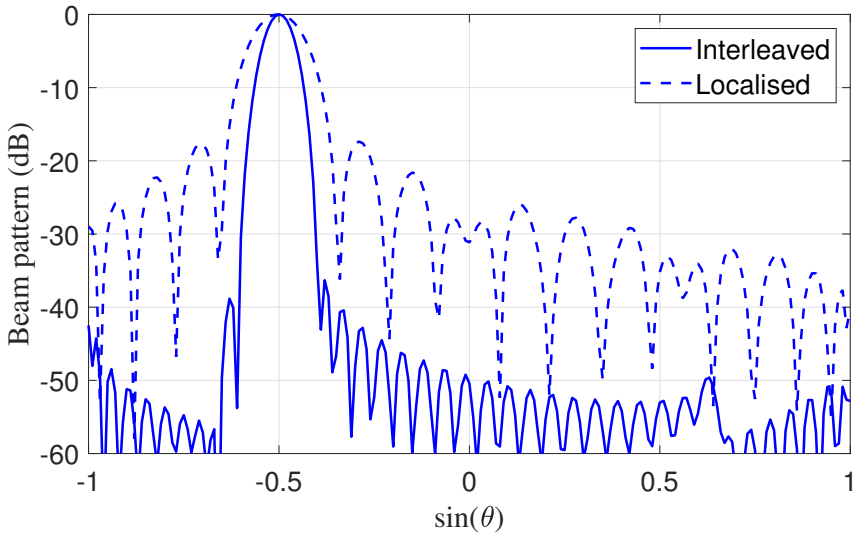

Figure 4.48: The mean patterns of the zeroth beam with $\varphi_0 = -30°$ generated by the fourth scheme in Section 4.3.4 with the interleaved and localised subarray architectures, respectively.

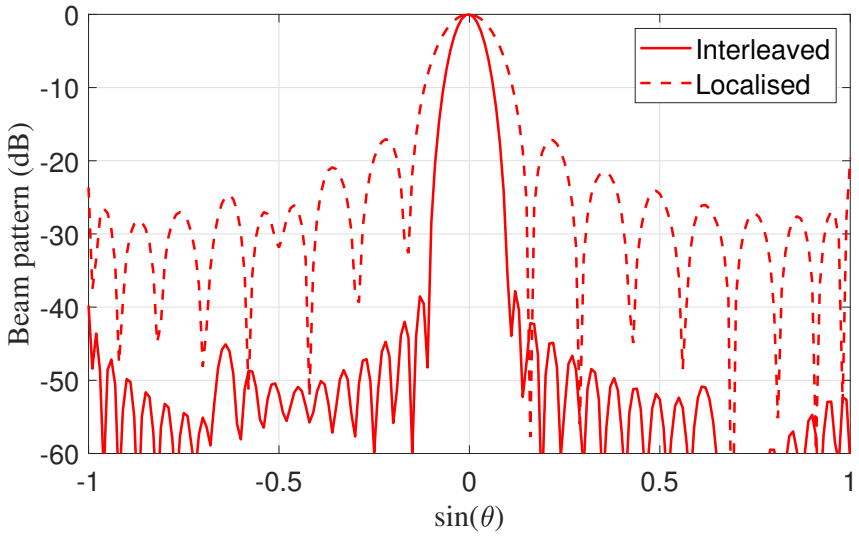

Figure 4.49: The mean patterns of the first beam with $\varphi_1 = 0°$ generated by the fourth scheme in Section 4.3.4 with the interleaved and localised subarray architectures, respectively.

bounded error in the scheme. Thirdly, both constraints are considered together, and robustness against steering vector errors and equal magnitude for all analogue coefficients are ensured simultaneously. Although the interleaved subarray architecture generates

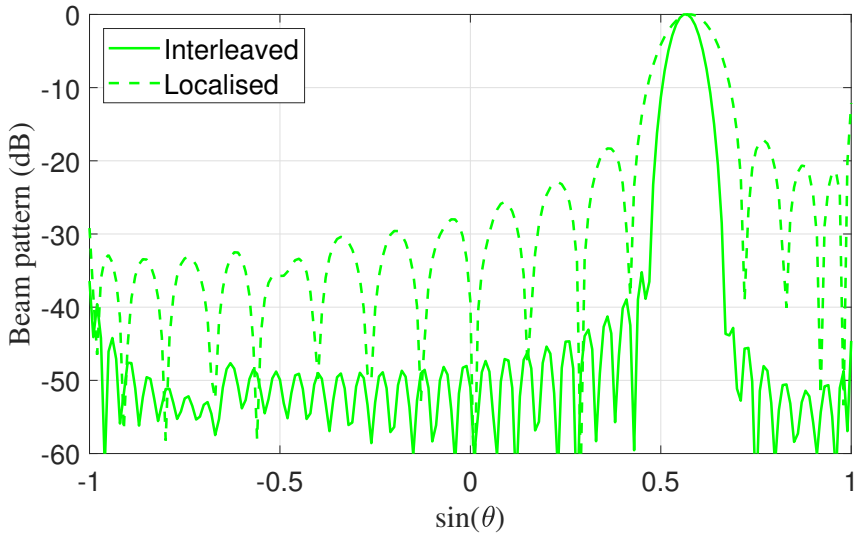

Figure 4.50: The mean patterns of the second beam with $\varphi_2 = 35^\circ$ generated by the fourth scheme in Section 4.3.4 with the interleaved and localised subarray architectures, respectively.

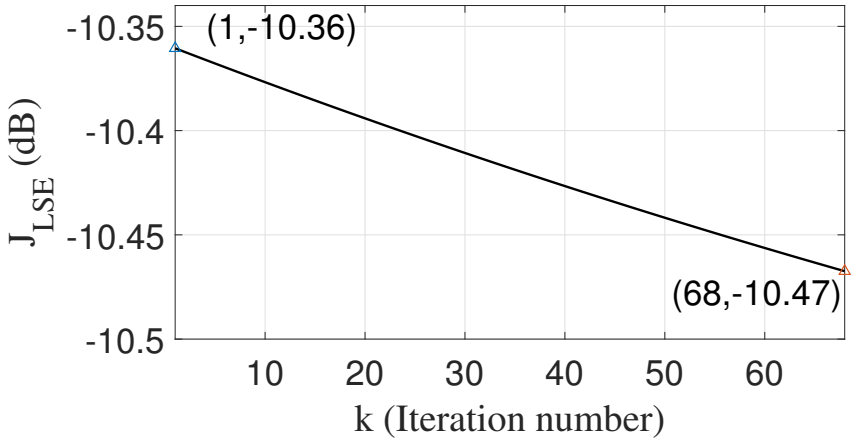

Figure 4.51: Cost function J_{LSE} in (4.40) with respect to the iteration number k generated by the fourth scheme in Section 4.3.4 with the interleaved subarray architecture.

a narrower beam width than the localised subarray architecture, its robustness against steering vector errors for the second and third designs is not as good as that of the localised one. In the next chapter, the problem of reducing the number of antennas employed in the hybrid beamforming structure will be studied.

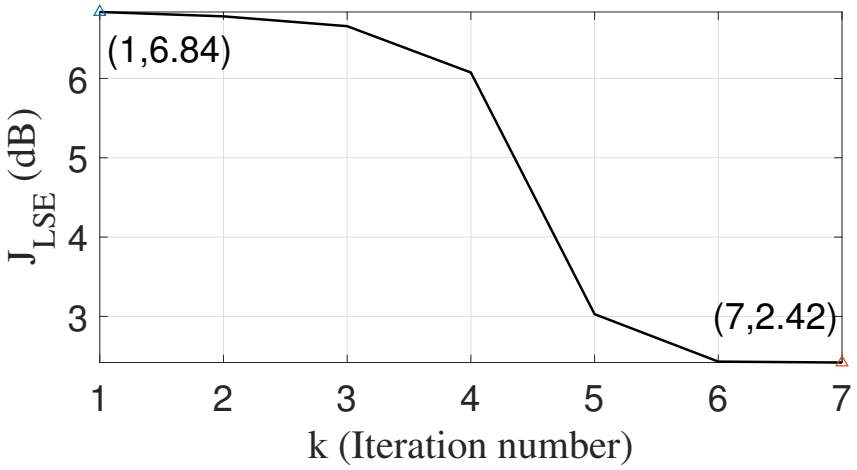

Figure 4.52: Cost function J_{LSE} in (4.40) with respect to the iteration number k generated by the fourth scheme in Section 4.3.4 with the localised subarray architecture.

Table 4.30: Analogue coefficients $\boldsymbol{w}_{A,0}$, $\boldsymbol{w}_{A,1}$ and $\boldsymbol{w}_{A,2}$ with $\varphi_0 = -30°$, $\varphi_1 = 0°$ and $\varphi_2 = 35°$ generated by the fourth scheme in Section 4.3.4 with the interleaved subarray architecture.

n \ m	$\boldsymbol{w}_{A,0}$	$\boldsymbol{w}_{A,1}$	$\boldsymbol{w}_{A,2}$	n \ m	$\boldsymbol{w}_{A,0}$	$\boldsymbol{w}_{A,1}$	$\boldsymbol{w}_{A,2}$
0	0.0000-0.0004i	-0.0004+0.0002i	0.0000-0.0005i	15	-0.0071+0.0067i	0.0114-0.0019i	-0.0059+0.0027i
1	0.0002-0.0005i	-0.0005-0.0002i	-0.0003+0.0002i	16	0.0159+0.0186i	-0.0013-0.0283i	0.0039+0.0087i
2	0.0000+0.0027i	0.0024-0.0029i	-0.0011+0.0015i	17	0.0172+0.0062i	-0.0050-0.0170i	-0.0036-0.0013i
3	0.0020+0.0024i	0.0003-0.0033i	0.0005-0.0003i	18	-0.0037-0.0009i	0.0039+0.0022i	-0.0054+0.0027i
4	0.0032-0.0014i	-0.0036-0.0018i	-0.0003-0.0003i	19	0.0077+0.0158i	0.0035-0.0207i	0.0008+0.0087i
5	-0.0011+0.0046i	0.0056-0.0046i	-0.0038+0.0029i	20	0.0150+0.0100i	-0.0023-0.0176i	-0.0010+0.0003i
6	0.0027+0.0081i	0.0036-0.0085i	0.0008+0.0011i	21	0.0016-0.0039i	-0.0024+0.0018i	-0.0028-0.0020i
7	0.0104-0.0004i	-0.0086-0.0078i	0.0013-0.0004i	22	0.0023+0.0083i	0.0033-0.0106i	-0.0012+0.0058i
8	-0.0008+0.0040i	0.0065-0.0052i	-0.0073+0.0028i	23	0.0081+0.0094i	0.0012-0.0123i	-0.0003+0.0013i
9	-0.0001+0.0135i	0.0097-0.0113i	-0.0006+0.0035i	24	0.0038-0.0024i	-0.0037-0.0004i	-0.0004-0.0016i
10	0.0184+0.0054i	-0.0114-0.0182i	0.0039+0.0015i	25	0.0009+0.0023i	0.0009-0.0037i	-0.0012+0.0058i
11	0.0041+0.0018i	0.0026-0.0069i	-0.0089+0.0007i	26	0.0023+0.0052i	0.0021-0.0052i	-0.0004+0.0010i
12	-0.0051+0.0133i	0.0138-0.0083i	-0.0036+0.0044i	27	0.0024-0.0003i	-0.0018-0.0010i	0.0003-0.0005i
13	0.0210+0.0139i	-0.0083-0.0273i	0.0053+0.0054i	28	0.0008-0.0000i	-0.0004-0.0009i	-0.0003+0.0004i
14	0.0121+0.0021i	-0.0030-0.0117i	-0.0072-0.0013i	29	-0.0001+0.0012i	0.0009-0.0006i	-0.0003+0.0001i

Table 4.31: Digital coefficients $\boldsymbol{w}_{D,0}$, $\boldsymbol{w}_{D,1}$ and $\boldsymbol{w}_{D,2}$ with $\varphi_0 = -30°$, $\varphi_1 = 0°$ and $\varphi_2 = 35°$ generated by the fourth scheme in Section 4.3.4 with the localised subarray architecture.

m \ j	$\boldsymbol{w}_{D,0}$	$\boldsymbol{w}_{D,1}$	$\boldsymbol{w}_{D,2}$
0	0.0202+0.0100i	-0.0036-0.0041i	-1.2985-0.3171i
1	1.1082-0.3723i	-0.0341+0.0282i	0.0065+0.0099i
2	0.0277+0.0270i	-1.1453-0.8884i	0.0034-0.0022i

Table 4.32: Analogue coefficients $\boldsymbol{w}_{A,0}$, $\boldsymbol{w}_{A,1}$ and $\boldsymbol{w}_{A,2}$ with $\varphi_0 = -30°$, $\varphi_1 = 0°$ and $\varphi_2 = 35°$ generated by the fourth scheme in Section 4.3.4 with the localised subarray architecture.

n \ m	$\boldsymbol{w}_{A,0}$	$\boldsymbol{w}_{A,1}$	$\boldsymbol{w}_{A,2}$	n \ m	$\boldsymbol{w}_{A,0}$	$\boldsymbol{w}_{A,1}$	$\boldsymbol{w}_{A,2}$
0	0.3528+0.2620i	-0.2691+0.5175i	-0.3995+0.2570i	15	-0.1197+0.3619i	0.5223-0.3913i	0.0596-0.0291i
1	-1.2896-0.4863i	1.1061-1.4129i	1.0863-0.6904i	16	-0.3279+0.2562i	0.2192-0.6823i	-0.1262+0.1048i
2	1.6902+0.1870i	-1.6028+1.5510i	-1.3647+0.8698i	17	0.0167-0.3322i	-0.5438+0.3630i	-0.0562+0.0300i
3	-0.6298+0.2729i	0.8206-0.3030i	0.5284-0.3348i	18	0.2731-0.3453i	-0.2838+0.7793i	0.1517-0.1252i
4	-0.7953-0.2312i	0.6439-1.0406i	0.4815-0.3056i	19	0.0305+0.3332i	0.5382-0.2998i	-0.0174+0.0260i
5	0.7203-0.2300i	-0.9004+0.5409i	-0.5247+0.3481i	20	-0.2636+0.4347i	0.3383-0.8196i	-0.2675+0.2183i
6	0.4988+0.1906i	-0.3248+0.7516i	-0.2070+0.1323i	21	-0.1013-0.3985i	-0.5220+0.3456i	0.0334-0.0373i
7	-0.5844+0.2648i	0.7647-0.5502i	0.3762-0.2385i	22	0.2560-0.5847i	-0.3074+0.9003i	0.3383-0.2761i
8	-0.3936-0.0971i	0.1823-0.6043i	0.0566-0.0305i	23	0.1969+0.5038i	0.6223-0.5259i	-0.1717+0.1490i
9	0.4335-0.2713i	-0.6788+0.5581i	-0.2985+0.1921i	24	-0.2204+0.7188i	0.2605-1.0305i	-0.4944+0.4046i
10	0.3285+0.0270i	-0.1328+0.6074i	-0.0372+0.0198i	25	-0.2431-0.7999i	-0.8113+0.9167i	0.4189-0.3521i
11	-0.3435+0.2795i	0.6571-0.4948i	0.1764+0.1083i	26	0.2649-0.6251i	-0.0592+0.8866i	0.4876-0.3998i
12	-0.3274+0.0196i	0.1912-0.6312i	-0.0380+0.0360i	27	0.2105+1.6904i	1.0346-1.9932i	-1.2237+1.0211i
13	0.2539-0.3335i	-0.5835+0.4051i	-0.1477+0.0925i	28	-0.5058-1.2925i	-1.0447+1.4677i	0.9637-0.8099i
14	0.3567-0.1221i	-0.2239+0.6192i	0.0403-0.0377i	29	0.2687+0.3549i	0.4241-0.4034i	-0.3526+0.2981i

Table 4.33: Summary of performances for the four proposed schemes in Section 4.2 with the interleaved and localised subarray architectures

Scheme	Architecture	$\bar{P}_s(dB)$	$var_{\lvert \boldsymbol{w}_A \rvert}$	$\bar{v}$	time(s)
1	Interleaved	-22.9477	0	0.1540	3.06
	Localised	-16.7977	0	0.0559	2.78
2	Interleaved	-28.2771	0.2150	0.0368	16.25
	Localised	-16.9563	0.2337	0.0052	2.24
3	Interleaved	-22.8559	0	0.0417	2.96
	Localised	-16.6738	0	0.0064	1.65
4	Interleaved	-28.3297	0.2901	0.5721	0.95
	Localised	-18.2018	1.7779	0.7755	2.15

Table 4.34: Summary of performances for the four proposed schemes in Section 4.3 with the interleaved and localised subarray architectures

Scheme	Architecture	$\bar{P}_s(dB)$	$var_{\lvert \boldsymbol{w}_A \rvert}$	$\bar{v}$	time(s)
1	Interleaved	-26.7840	0	0.2810	3.32
	Localised	-18.0340	0	0.2107	5.43
2	Interleaved	-40.4851	0.4657	0.0374	6.07
	Localised	-20.0319	0.2721	0.0104	3.04
3	Interleaved	-25.5227	0	0.0442	12.57
	Localised	-17.6199	0	0.0258	11.37
4	Interleaved	-47.7972	0.8769	15.9600	26.72
	Localised	-21.9728	0.4756	16.8101	2.75

Chapter 5

Antenna Selection for Multi-Beam Multiplexing Design

5.1 Introduction

This chapter introduces the use of compressive sensing (CS) to multi-beam multiplexing design for antenna selection and shows how it can be extended to the antenna selection design problem for hybrid beamforming with sub-aperture and overlapped subarray architectures.

Although the methods in [25, 77] can reduce the implementation complexity significantly for multi-user beamforming, further complexity reduction is possible when a large number of antennas are available in a massive MIMO system. This can be achieved by only employing a subset of the available antennas and the selected antennas for different beamforming scenarios can change accordingly. Now the new problem statement is, given a large massive MIMO array and a specific beamforming requirement, how to find the minimum number of antennas and their associated locations. This is similar to the sparse antenna array design problem, which can be solved by various methods such as genetic algorithm [85–88], simulated annealing [89, 90], Taguchi's method [91] and compressive sensing (CS) [73, 83, 92–99]. In addition to the interleaved and localised subarray architectures, the overlapped subarray architecture, where each antenna in the array is associated with two or more analogue coefficients [100–106], is also considered for antenna selection

in this chapter, and the total number of resultant analogue channels is still smaller than a traditional implementation.

Moreover, by considering the polarisation information of a signal, the design based on crossed-dipole arrays is also studied, where each antenna is associated with two complex-valued weighting coefficients. Two design methods are proposed to select the best set of crossed-dipole antennas or dipoles.

The remaining part of this chapter is organised as follows. The proposed CS-based designs with isotropic and crossed-dipole antennas are introduced in Sections 5.2 and 5.3, respectively. Design examples are provided in Section 5.4, followed by a summary in Section 5.5.

5.2 Antenna Selection Method for Arrays with Isotropic Antennas

5.2.1 Antenna Selection Based on the Sub-Aperture Subarray Architectures for Two Beams

Similar to the two-beam case in Section 4.2.1, for a given set of $w_{D,j,m}(\{j,m\} \in \{0,1\})$, to find the optimum analogue coefficients $\boldsymbol{w}_A$, an intermediate formulation without antenna selection for the two designed beams can be formulated as (4.10).

The main principle of CS based design is to select the minimum number of antennas which can still provide an exact, or almost exact beam response matching the desired one [92–94]. Ideally, this problem can be formed as the minimisation of l_0 norm (which counts the non-zero-valued coefficients) of the weighting coefficients. In practice, the l_0 norm is normally replaced by the l_1 norm for a tractable solution.

Now to find the minimum number of antennas while meeting the beamforming requirements, we can also try to minimise the l_0 norm of $\boldsymbol{w}_A$. A zero value in $\boldsymbol{w}_A$ indicates that the corresponding antenna is not needed in the design and therefore can be switched off without affecting the beamforming performance. As mentioned, in practice, the l_0 norm

is normally replaced by the l_1 norm for a tractable solution, i.e.,

$$\min_{\boldsymbol{w}_A} \parallel \boldsymbol{w}_A \parallel_1, \tag{5.1}$$

where the l_1 norm $\parallel . \parallel_1$ is used as an approximation to the l_0 norm $\parallel . \parallel_0$. By combining the above cost function in (5.1) with the cost function in (4.10), the new formulation of this problem is given by

$$\begin{aligned} \min_{\boldsymbol{w}_A} \quad & J_{LSE} = (1-\gamma) \parallel \boldsymbol{L}^H \boldsymbol{w}_A \parallel_2 + \gamma \parallel \boldsymbol{w}_A \parallel_1, \\ \text{subject} \quad & \text{to} \\ & \boldsymbol{w}_A^H \begin{bmatrix} \boldsymbol{w}_{D,0,0}^H \boldsymbol{z}_{S_{00}} & \boldsymbol{w}_{D,1,0}^H \boldsymbol{z}_{S_{10}} \\ \boldsymbol{w}_{D,0,1}^H \boldsymbol{z}_{S_{01}} & \boldsymbol{w}_{D,1,1}^H \boldsymbol{z}_{S_{11}} \end{bmatrix} = \begin{bmatrix} 1 & 1 \end{bmatrix}, \end{aligned} \tag{5.2}$$

where $\gamma \in (0,1)$ is a trade-off factor between the two parts and $\boldsymbol{z}_{S_{jm}}$ is given in (4.11).

On the other hand, if we know the analogue coefficients $\boldsymbol{w}_A$, the optimum digital coefficients $\boldsymbol{w}_D$ can be obtained by (4.24).

Alternate optimisation of digital coefficients $\boldsymbol{w}_D$ and analogue coefficients $\boldsymbol{w}_A$ can be achieved iteratively:

(1) First, via initialising the digital coefficients $\boldsymbol{w}_D$ with random values, $\boldsymbol{w}_A$ is obtained by substituting $w_{D,j,m}(\{j,m\} \in \{0,1\})$ into (5.2).

(2) Given the obtained optimum values for $\boldsymbol{w}_A$ in step (1), the optimum values for $\boldsymbol{w}_D$ are obtained using (4.24).

(3) Given the obtained values of $\boldsymbol{w}_D$ in step (2), the new set of values of $\boldsymbol{w}_A$ can be obtained by (5.2) again.

(4) Repeat steps (2) and (3) until the cost function in (5.2) converges.

5.2.2 Antenna Selection Based on the Sub-Aperture Subarray Architectures for Three Beams

Similar to (5.2), the formulation of the problem for the three-beam case is given by

$$\begin{aligned} \min_{\boldsymbol{w}_A} \quad & J_{LSE} = (1-\gamma) \parallel \boldsymbol{L}^H \boldsymbol{w}_A \parallel_2 + \gamma \parallel \boldsymbol{w}_A \parallel_1, \\ \text{subject} \quad & \text{to} \\ & \boldsymbol{w}_A^H \begin{bmatrix} \boldsymbol{w}_{D,0,0}^H \boldsymbol{z}_{S_{00}} & \boldsymbol{w}_{D,1,0}^H \boldsymbol{z}_{S_{10}} & \boldsymbol{w}_{D,2,0}^H \boldsymbol{z}_{S_{20}} \\ \boldsymbol{w}_{D,0,1}^H \boldsymbol{z}_{S_{01}} & \boldsymbol{w}_{D,1,1}^H \boldsymbol{z}_{S_{11}} & \boldsymbol{w}_{D,2,1}^H \boldsymbol{z}_{S_{21}} \\ \boldsymbol{w}_{D,0,2}^H \boldsymbol{z}_{S_{02}} & \boldsymbol{w}_{D,1,2}^H \boldsymbol{z}_{S_{12}} & \boldsymbol{w}_{D,2,2}^H \boldsymbol{z}_{S_{22}} \end{bmatrix} = \begin{bmatrix} 1 & 1 & 1 \end{bmatrix}. \end{aligned} \tag{5.3}$$

Alternate optimisation of the digital coefficients $\boldsymbol{w}_D$ and the corresponding analogue coefficients $\boldsymbol{w}_A$ can be obtained by the following iterative process:

(1) First, through initialising $\boldsymbol{w}_D$ with random values, $\boldsymbol{w}_A$ is obtained by substituting $w_{D,j,m}(\{j,m\} \in \{0,1,2\})$ into (5.3).

(2) Given the obtained optimum values for $\boldsymbol{w}_A$ in step (1), the closed-form solution for digital coefficients $\boldsymbol{w}_D$ is obtained by (4.24).

(3) Given the obtained values of $\boldsymbol{w}_D$ in step (2), the new set of values of $\boldsymbol{w}_A$ is obtained by (5.3) again.

(4) Repeat steps (2) and (3) until the cost function J_{LSE} in (5.3) converges.

5.2.3 Antenna Selection Based on the Overlapped Subarray Architecture for Two Beams

One implicit constraint imposed by both the localised and interleaved subarray architectures on the beamformer design problem is that one antenna can only be selected once at most, or there are at most one analogue channel for each antenna. However, this may not be optimum and some of the antennas could be shared by the two (or more) subarrays to provide a better beamforming result, while the total number of analogue channels can

still be kept low. In light of this, we start from the extreme case where each subarray is the same as the orignal array, whose steering vector is now given by

$$\breve{\boldsymbol{s}}_m(\theta) = [1, e^{j2\pi\frac{d}{\lambda}\sin\theta}, e^{j2\pi\frac{2d}{\lambda}\sin\theta}, ..., e^{j2\pi(2N_s-1)\frac{d}{\lambda}\sin\theta}]^T, \tag{5.4}$$

instead of (3.20) and (3.21), and for two beams, each antenna will get connected with two analogue coefficients initially. The analogue coefficient vector for the m-th 'subarray' is given by

$$\breve{\boldsymbol{w}}_{A,m} = [\breve{w}_{A,m,0}, \breve{w}_{A,m,1}, ..., \breve{w}_{A,m,2N_s-1}]^T, \tag{5.5}$$

where $m \in \{0, 1\}$. Thus, the beam pattern generated by the m-th 'subarray' is changed to

$$\breve{P}_m(\theta) = \breve{\boldsymbol{w}}_{A,m}^H \breve{\boldsymbol{s}}_m(\theta). \tag{5.6}$$

Different from (3.24) with $J = 2$, the digital coefficients imposed on the j-th beam are given by

$$\breve{\boldsymbol{w}}_{D,j} = [\breve{w}_{D,j,0}, \breve{w}_{D,j,1}], \tag{5.7}$$

and designed beam pattern for the j-th beam is

$$\begin{aligned}\breve{P}_{\varphi_j}(\theta) =& \breve{w}_{D,j,0}^* \breve{P}_0(\theta) + \breve{w}_{D,j,1}^* \breve{P}_1(\theta) \\ =& \breve{w}_{D,j,0}^* \breve{\boldsymbol{w}}_{A,0}^H \breve{\boldsymbol{s}}_0(\theta) + \breve{w}_{D,j,1}^* \breve{\boldsymbol{w}}_{A,1}^H \breve{\boldsymbol{s}}_1(\theta).\end{aligned} \tag{5.8}$$

By combining the analogue coefficients $\breve{\boldsymbol{w}}_{A,0}$ and $\breve{\boldsymbol{w}}_{A,1}$ in (5.5) into one vector, given by

$$\breve{\boldsymbol{w}}_A = \left[\breve{\boldsymbol{w}}_{A,0}^T, \breve{\boldsymbol{w}}_{A,1}^T\right]^T, \tag{5.9}$$

the optimisation problem is formulated as

$$\begin{aligned}\min_{\breve{\boldsymbol{w}}_A} \quad & J_{LSE} = (1-\gamma) \parallel \breve{\boldsymbol{L}}^H \breve{\boldsymbol{w}}_A \parallel_2 + \gamma \parallel \breve{\boldsymbol{w}}_A \parallel_1, \\ \text{subject} \quad & \text{to} \\ & \breve{\boldsymbol{w}}_A^H \begin{bmatrix} \breve{\boldsymbol{w}}_{D,0,0}^H \breve{\boldsymbol{z}}_{S_{00}} & \breve{\boldsymbol{w}}_{D,1,0}^H \breve{\boldsymbol{z}}_{S_{10}} \\ \breve{\boldsymbol{w}}_{D,0,1}^H \breve{\boldsymbol{z}}_{S_{01}} & \breve{\boldsymbol{w}}_{D,1,1}^H \breve{\boldsymbol{z}}_{S_{11}} \end{bmatrix} = \begin{bmatrix} 1 & 1 \end{bmatrix},\end{aligned} \tag{5.10}$$

with

$$\breve{\boldsymbol{z}}_{S_{jm}} = \sum_{\theta \in \Theta_{main_j}} \breve{\boldsymbol{s}}_m(\theta), \tag{5.11}$$

$$\breve{\boldsymbol{w}}_{D,j,m} = \breve{w}_{D,j,m}\boldsymbol{I}_{2N_s}, \tag{5.12}$$

where $\breve{\boldsymbol{L}}$ and $\breve{\boldsymbol{z}}_{S_{jm}}$ are similar to $\boldsymbol{L}$ and $\boldsymbol{z}_{S_{jm}}$ in (5.2), and $\boldsymbol{I}_{2N_s}$ denotes a $2N_s \times 2N_s$ identity matrix.

By combining the digital coefficients in (5.7) with $j = 0$ and $j = 1$ into

$$\breve{\boldsymbol{w}}_D = \left[\breve{\boldsymbol{w}}_{D,0}, \breve{\boldsymbol{w}}_{D,1}\right]^T = \left[\breve{w}_{D,0,0}, \breve{w}_{D,0,1}, \breve{w}_{D,1,0}, \breve{w}_{D,1,1}\right]^T, \tag{5.13}$$

the optimisation problem to obtain the digital coefficients vector $\breve{\boldsymbol{w}}_D$ is formulated as

$$\begin{aligned} \min_{\breve{\boldsymbol{w}}_D} \quad & \breve{\boldsymbol{w}}_D^H \breve{\boldsymbol{M}}_S \breve{\boldsymbol{w}}_D, \\ \text{subject} \quad & \text{to} \\ & \breve{\boldsymbol{C}}^H \breve{\boldsymbol{w}}_D = \boldsymbol{f}, \end{aligned} \tag{5.14}$$

with

$$\breve{\boldsymbol{C}} = \begin{bmatrix} \breve{\boldsymbol{w}}_A^H \dot{\boldsymbol{z}}_{S_{00}} & 0 \\ \breve{\boldsymbol{w}}_A^H \dot{\boldsymbol{z}}_{S_{01}} & 0 \\ 0 & \breve{\boldsymbol{w}}_A^H \dot{\boldsymbol{z}}_{S_{10}} \\ 0 & \breve{\boldsymbol{w}}_A^H \dot{\boldsymbol{z}}_{S_{11}} \end{bmatrix}, \boldsymbol{f} = \begin{bmatrix} 1 \\ 1 \end{bmatrix}, \tag{5.15}$$

$$\dot{\boldsymbol{z}}_{S_{j0}} = \begin{bmatrix} \breve{\boldsymbol{z}}_{S_{j0}} \\ \boldsymbol{0}_{2N_s \times 1} \end{bmatrix}, \dot{\boldsymbol{z}}_{S_{j1}} = \begin{bmatrix} \boldsymbol{0}_{2N_s \times 1} \\ \breve{\boldsymbol{z}}_{S_{j1}} \end{bmatrix}, \tag{5.16}$$

where $\breve{\boldsymbol{M}}_S$ is similar to $\tilde{\boldsymbol{M}}_S$ in (4.15) in Chapter 4 and $\boldsymbol{0}_{2N_s \times 1}$ in (5.16) is a $2N_s \times 1$ all-zero vector. The solution to the problem (5.14) is given by

$$\breve{\boldsymbol{w}}_D = \breve{\boldsymbol{M}}_S^{-1} \breve{\boldsymbol{C}} \left(\breve{\boldsymbol{C}}^H \breve{\boldsymbol{M}}_S^{-1} \breve{\boldsymbol{C}}\right)^{-1} \boldsymbol{f}. \tag{5.17}$$

Alternate optimisation of digital coefficients $\breve{\boldsymbol{w}}_D$ and analogue coefficients $\breve{\boldsymbol{w}}_A$ can be achieved iteratively:

(1) First, via initialising the digital coefficients $\breve{\boldsymbol{w}}_D$ with random values, $\breve{\boldsymbol{w}}_A$ is obtained by substituting $\breve{w}_{D,j,m}(\{j, m\} \in \{0, 1\})$ into (5.10).

(2) Given the obtained optimum values for $\breve{\boldsymbol{w}}_A$ in step (1), the optimum values for $\breve{\boldsymbol{w}}_D$ are obtained using (5.17).

(3) Given the obtained values of $\breve{\boldsymbol{w}}_D$ in step (2), the new set of values of $\breve{\boldsymbol{w}}_A$ can be obtained by (5.10) again.

(4) Repeat steps (2) and (3) until the cost function in (5.10) converges.

5.2.4 Antenna Selection Based on the Overlapped Subarray Architecture for Three Beams

Similar to (5.4), the steering vector of the m-th 'subarray' for the three-user case is

$$\breve{\boldsymbol{s}}_m(\theta) = [1, e^{j2\pi\frac{d}{\lambda}\sin\theta}, e^{j2\pi\frac{2d}{\lambda}\sin\theta}, ..., e^{j2\pi(3N_s-1)\frac{d}{\lambda}\sin\theta}]^T, \tag{5.18}$$

and the analogue coefficient vector for the m-th 'subarray' is given by

$$\breve{\boldsymbol{w}}_{A,m} = [\breve{w}_{A,m,0}, \breve{w}_{A,m,1}, ..., \breve{w}_{A,m,3N_s-1}]^T, \tag{5.19}$$

where $m \in \{0, 1, 2\}$. The digital coefficients imposed on the j-th beam are given by

$$\breve{\boldsymbol{w}}_{D,j} = [\breve{w}_{D,j,0}, \breve{w}_{D,j,1}, \breve{w}_{D,j,2}], \tag{5.20}$$

and the designed pattern for the j-th beam changes to

$$\begin{aligned}\breve{P}_{\varphi_j}(\theta) =& \breve{w}^*_{D,j,0}\breve{P}_0(\theta) + \breve{w}^*_{D,j,1}\breve{P}_1(\theta) + \breve{w}^*_{D,j,2}\breve{P}_2(\theta) \\ =& \breve{w}^*_{D,j,0}\breve{\boldsymbol{w}}^H_{A,0}\breve{\boldsymbol{s}}_0(\theta) + \breve{w}^*_{D,j,1}\breve{\boldsymbol{w}}^H_{A,1}\breve{\boldsymbol{s}}_1(\theta) + \breve{w}^*_{D,j,2}\breve{\boldsymbol{w}}^H_{A,2}\breve{\boldsymbol{s}}_2(\theta).\end{aligned} \tag{5.21}$$

By combining the analogue coefficients $\breve{\boldsymbol{w}}_{A,0}$, $\breve{\boldsymbol{w}}_{A,1}$ and $\breve{\boldsymbol{w}}_{A,2}$ into one vector, given by

$$\breve{\boldsymbol{w}}_A = \left[\breve{\boldsymbol{w}}^T_{A,0}, \breve{\boldsymbol{w}}^T_{A,1}, \breve{\boldsymbol{w}}^T_{A,2}\right]^T, \tag{5.22}$$

the formulation is given by

$$\begin{aligned}\min_{\breve{\boldsymbol{w}}_A} \quad & J_{LSE} = (1-\gamma) \parallel \breve{\boldsymbol{L}}^H \breve{\boldsymbol{w}}_A \parallel_2 + \gamma \parallel \breve{\boldsymbol{w}}_A \parallel_1, \\ \text{subject} \quad & \text{to} \\ & \breve{\boldsymbol{w}}^H_A \begin{bmatrix} \breve{\boldsymbol{w}}^H_{D,0,0}\breve{\boldsymbol{z}}_{S_{00}} & \breve{\boldsymbol{w}}^H_{D,1,0}\breve{\boldsymbol{z}}_{S_{10}} & \breve{\boldsymbol{w}}^H_{D,2,0}\breve{\boldsymbol{z}}_{S_{20}} \\ \breve{\boldsymbol{w}}^H_{D,0,1}\breve{\boldsymbol{z}}_{S_{01}} & \breve{\boldsymbol{w}}^H_{D,1,1}\breve{\boldsymbol{z}}_{S_{11}} & \breve{\boldsymbol{w}}^H_{D,2,1}\breve{\boldsymbol{z}}_{S_{21}} \\ \breve{\boldsymbol{w}}^H_{D,0,2}\breve{\boldsymbol{z}}_{S_{02}} & \breve{\boldsymbol{w}}^H_{D,1,2}\breve{\boldsymbol{z}}_{S_{12}} & \breve{\boldsymbol{w}}^H_{D,2,2}\breve{\boldsymbol{z}}_{S_{22}} \end{bmatrix} = \begin{bmatrix} 1 & 1 & 1 \end{bmatrix},\end{aligned} \tag{5.23}$$

$$\breve{\boldsymbol{w}}_{D,j,m} = \breve{w}_{D,j,m}\boldsymbol{I}_{3N_s}, \tag{5.24}$$

where $\breve{\boldsymbol{L}}$ and $\breve{\boldsymbol{z}}_{S_{jm}}$ are similar to $\breve{\boldsymbol{L}}$ and $\breve{\boldsymbol{z}}_{S_{jm}}$ in (5.10) and (5.11), respectively, and $\boldsymbol{I}_{3N_s}$ denotes a $3N_s \times 3N_s$ identity matrix.

By combining the digital coefficients in (5.20) with $j = 0$, $j = 1$ and $j = 2$ into

$$\begin{aligned}\breve{\boldsymbol{w}}_D &= \left[\breve{\boldsymbol{w}}_{D,0}, \breve{\boldsymbol{w}}_{D,1}, \breve{\boldsymbol{w}}_{D,2}\right]^T \\ &= \left[\breve{w}_{D,0,0}, \breve{w}_{D,0,1}, \breve{w}_{D,0,2}, \breve{w}_{D,1,0}, \breve{w}_{D,1,1}, \breve{w}_{D,1,2}, \breve{w}_{D,2,0}, \breve{w}_{D,2,1}, \breve{w}_{D,2,2}\right]^T,\end{aligned} \tag{5.25}$$

the optimisation is formulated as (5.14) with

$$\breve{\boldsymbol{C}} = \begin{bmatrix} \breve{\boldsymbol{w}}_A^H \dot{\boldsymbol{z}}_{S_{00}} & 0 & 0 \\ \breve{\boldsymbol{w}}_A^H \dot{\boldsymbol{z}}_{S_{01}} & 0 & 0 \\ \breve{\boldsymbol{w}}_A^H \dot{\boldsymbol{z}}_{S_{02}} & 0 & 0 \\ 0 & \breve{\boldsymbol{w}}_A^H \dot{\boldsymbol{z}}_{S_{10}} & 0 \\ 0 & \breve{\boldsymbol{w}}_A^H \dot{\boldsymbol{z}}_{S_{11}} & 0 \\ 0 & \breve{\boldsymbol{w}}_A^H \dot{\boldsymbol{z}}_{S_{12}} & 0 \\ 0 & 0 & \breve{\boldsymbol{w}}_A^H \dot{\boldsymbol{z}}_{S_{20}} \\ 0 & 0 & \breve{\boldsymbol{w}}_A^H \dot{\boldsymbol{z}}_{S_{21}} \\ 0 & 0 & \breve{\boldsymbol{w}}_A^H \dot{\boldsymbol{z}}_{S_{22}} \end{bmatrix}, \boldsymbol{f} = \begin{bmatrix} 1 \\ 1 \\ 1 \end{bmatrix}, \tag{5.26}$$

$$\dot{\boldsymbol{z}}_{S_{j0}} = \begin{bmatrix} \breve{\boldsymbol{z}}_{S_{j0}} \\ \boldsymbol{0}_{3N_s \times 1} \\ \boldsymbol{0}_{3N_s \times 1} \end{bmatrix}, \dot{\boldsymbol{z}}_{S_{j1}} = \begin{bmatrix} \boldsymbol{0}_{3N_s \times 1} \\ \breve{\boldsymbol{z}}_{S_{j1}} \\ \boldsymbol{0}_{3N_s \times 1} \end{bmatrix}, \dot{\boldsymbol{z}}_{S_{j2}} = \begin{bmatrix} \boldsymbol{0}_{3N_s \times 1} \\ \boldsymbol{0}_{3N_s \times 1} \\ \breve{\boldsymbol{z}}_{S_{j2}} \end{bmatrix}, \tag{5.27}$$

where $\breve{\boldsymbol{M}}_S$ is similar to $\breve{\boldsymbol{M}}_S$ in (5.14) and $\boldsymbol{0}_{3N_s \times 1}$ in (5.27) is a $3N_s \times 1$ all-zero vector. The solution to (5.14) for the method in Section 5.2.4 with $J = M = 3$ is given by (5.17).

Alternate optimisation of digital coefficients $\breve{\boldsymbol{w}}_D$ and analogue coefficients $\breve{\boldsymbol{w}}_A$ can be achieved iteratively:

(1) First, via initialising the digital coefficients $\breve{\boldsymbol{w}}_D$ with random values, $\breve{\boldsymbol{w}}_A$ is obtained by substituting $\breve{w}_{D,j,m}(\{j,m\} \in \{0,1,2\})$ into (5.23).

(2) Given the obtained optimum values for $\breve{\boldsymbol{w}}_A$ in step (1), the optimum values for $\breve{\boldsymbol{w}}_D$ are obtained using (5.17).

(3) Given the obtained values of $\breve{\boldsymbol{w}}_D$ in step (2), the new set of values of $\breve{\boldsymbol{w}}_A$ can be obtained by (5.23) again.

(4) Repeat steps (2) and (3) until the cost function in (5.23) converges.

5.3 Antenna Selection Method for Arrays with Crossed-Dipole Antennas

So far in all the introduced multi-beam multiplexing designs, the polarisation information of signals has not been considered yet. In this section, the polarisation information is exploited in the design by replacing the isotropic antennas in the structure with the polarisation-sensitive crossed-dipole antennas. Each antenna in the crossed-dipole array consists of two orthogonally orientated dipoles which can measure both the horizontal and vertical components of the electromagnetic field [99, 107–109]. Similar to last section, we consider the low-complexity implementation problem, i.e., when a large number of crossed-dipole antennas are available, we may not need to employ all of them and a subset of the available antennas may be sufficient for a specific beamforming scenario. Different from the isotropic antenna case [110], for crossed-dipole antennas, there are two complex-valued weighting coefficients associated with each antenna [111–117] and therefore we have two choices: either switch off the whole crossed-dipole antenna or one of the dipoles. To implement these two different schemes, two corresponding CS based design methods are proposed.

5.3.1 Polarisation-Sensitive Beamforming

For the crossed-dipole based antenna array, there are M linear crossed-dipole subarrays where each consists of N_s antennas and the overall layout is shown in Figure 5.1. Each antenna consists of two orthogonal dipoles, and the complex-valued weighting coefficients parallel to the x-axis and y-axis are $w_{n,x}$ and $w_{n,y}$, respectively, for $n \in \{0, 1, ..., N_s - 1\}$. In addition, the elevation and azimuth angles are given by $\theta \in [-\frac{\pi}{2}, \frac{\pi}{2}]$ and $\phi \in [-\pi, \pi]$, respectively [111, 118].

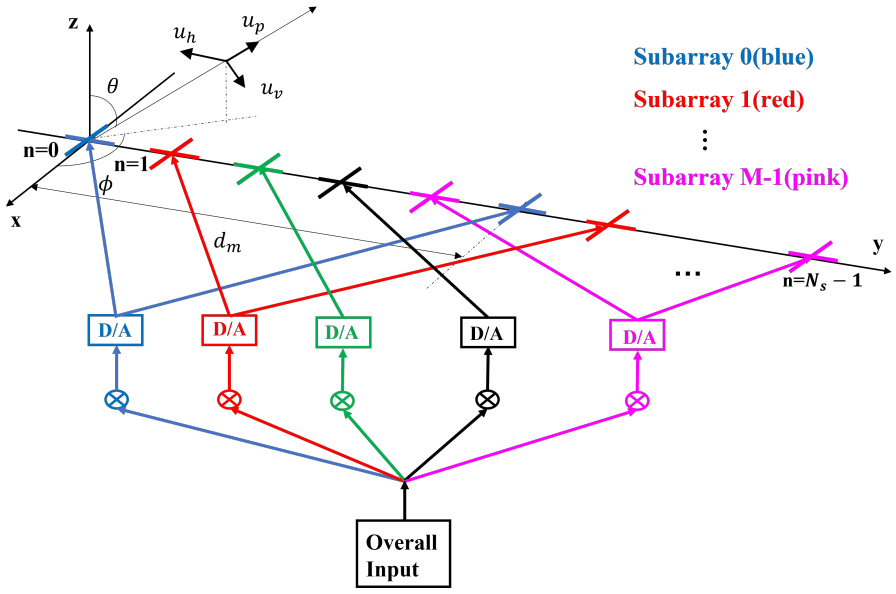

Figure 5.1: An ULA based hybrid beamforming architecture with M interleaved subarrays based on crossed-dipole antennas.

For a transverse electromagnetic (TEM) wave in the far field, the unit vector of the TEM wave is denoted by $\boldsymbol{u}_p$ and the two decomposed unit vectors which are orthogonal are $\boldsymbol{u}_h$ and $\boldsymbol{u}_v$ with $\boldsymbol{u}_h.\boldsymbol{u}_v = 0$, $\boldsymbol{u}_p.\boldsymbol{u}_h = 0$ and $\boldsymbol{u}_p.\boldsymbol{u}_v = 0$. In the transmitter coordinate system, $\boldsymbol{u}_p$ is given by

$$\boldsymbol{u}_p = [\sin\theta\cos\phi, \sin\theta\sin\phi, \cos\theta]^T. \tag{5.28}$$

However, the choice of the pair of $\boldsymbol{u}_h$ and $\boldsymbol{u}_v$ is not unique. Due to the orthogonality of these three unit vectors, they are normally defined as

$$\begin{aligned} \boldsymbol{u}_h &= [-\sin\phi, \cos\phi, 0]^T, \\ \boldsymbol{u}_v &= [\cos\theta\cos\phi, \cos\theta\sin\phi, -\sin\theta]^T. \end{aligned} \tag{5.29}$$

Note that $\boldsymbol{u}_h$ is parallel to the x-y plane due to the zero value in the z direction, and therefore $\boldsymbol{u}_h$ is defined as the unit vector of the horizontal component. Moreover, $\boldsymbol{u}_v$ is the unit vector of the vertical component since $\boldsymbol{u}_v$ is perpendicular to $\boldsymbol{u}_h$, i.e., $\boldsymbol{u}_v.\boldsymbol{u}_h = 0$.

In addition, the electric field is assumed to have transverse components [111, 119]

$$E = E_h\boldsymbol{u}_h + E_v\boldsymbol{u}_v, \tag{5.30}$$

where E_h and E_v denote the horizontal and vertical components, respectively [120], given by

$$\begin{bmatrix} E_h \\ E_v \end{bmatrix} = \begin{bmatrix} M_h e^{j\omega t} \\ M_v e^{j\omega t} \end{bmatrix} = \begin{bmatrix} m_h e^{j\psi_h} e^{j\omega t} \\ m_v e^{j\psi_v} e^{j\omega t} \end{bmatrix}, \tag{5.31}$$

where ω denotes the carrier frequency, M_h and M_v are complex numbers, m_h and m_v the magnitudes of the horizontal and vertical components, respectively, and ψ_h and ψ_v are the corresponding initial phases. Thus, the polarisation ratio is given by

$$\frac{M_v}{M_h} = \frac{m_v e^{j\psi_v}}{m_h e^{j\psi_h}} = (\tan\sigma) e^{j\eta}, \tag{5.32}$$

where $\tan\sigma$ denotes the magnitude ratio and η denotes the phase difference between the vertical and horizontal components with $\sigma \in [0, \frac{\pi}{2}]$ and $\eta \in (-\pi, \pi]$.

For the case with $m_h \neq 0$ and $\sigma \in [0, \frac{\pi}{2}]$, the magnitude of the signal can be derived by

$$\begin{aligned} M_a =& \sqrt{|M_h|^2 + |M_v|^2} \\ =& \sqrt{m_h^2 + m_v^2} = m_h \sqrt{1 + (\tan\sigma)^2} = \frac{m_h}{\cos\sigma}. \end{aligned} \tag{5.33}$$

As a result, it is easy to obtain

$$\begin{aligned} m_h &= M_a \cos\sigma, \\ m_h e^{j\psi_h} &= M_a (\cos\sigma) e^{j\psi_h}, \\ M_h &= M_a (\cos\sigma) e^{j\psi_h}. \end{aligned} \tag{5.34}$$

Similarly,

$$\begin{aligned} M_a &= \frac{m_v}{\sin\sigma}, \\ M_v &= M_a (\sin\sigma) e^{j\psi_v}. \end{aligned} \tag{5.35}$$

For $m_h = 0$ when there is no horizontal component and $\sigma = \frac{\pi}{2}$,

$$\begin{aligned}
\begin{bmatrix} M_h \\ M_v \end{bmatrix} &= \begin{bmatrix} 0 \\ m_v e^{j\psi_v} \end{bmatrix} \\
&= \frac{m_v e^{j\psi_v}}{e^{j\eta}} \begin{bmatrix} \cos\sigma \\ (\sin\sigma)e^{j\eta} \end{bmatrix} \\
&= m_v e^{j\psi_h} \begin{bmatrix} \cos\frac{\pi}{2} \\ (\sin\frac{\pi}{2})e^{j\eta} \end{bmatrix} \\
&= M_a \begin{bmatrix} (\cos\frac{\pi}{2})e^{j\psi_h} \\ (\sin\frac{\pi}{2})e^{j\psi_v} \end{bmatrix}.
\end{aligned} \tag{5.36}$$

Hence, for the case with $\sigma \in [0, \frac{\pi}{2}]$ and $\eta \in (-\pi, \pi]$, it is clear that

$$\begin{bmatrix} M_h \\ M_v \end{bmatrix} = M_a \begin{bmatrix} (\cos\sigma)e^{j\psi_h} \\ (\sin\sigma)e^{j\psi_v} \end{bmatrix}. \tag{5.37}$$

Note that the actual values of ψ_h and ψ_v do not matter and the most important thing is the relative difference between them. Hence, (5.37) is changed to

$$\begin{bmatrix} M_h \\ M_v \end{bmatrix} = M_a \begin{bmatrix} \cos\sigma \\ (\sin\sigma)e^{j\eta} \end{bmatrix}, \tag{5.38}$$

and the electric field can be given by

$$\begin{aligned}
E =& E_h \boldsymbol{u}_h + E_v \boldsymbol{u}_v \\
=& M_a((\cos\sigma)\boldsymbol{u}_h + (\sin\sigma)e^{j\eta}\boldsymbol{u}_v) \\
=& M_a(\cos\sigma[-\sin\phi, \cos\phi, 0]^T \\
&+ (\sin\sigma)e^{j\eta}[\cos\theta\cos\phi, \cos\theta\sin\phi, -\sin\theta]^T) \\
=& M_a((-\cos\sigma\sin\phi + \sin\sigma\cos\theta\cos\phi e^{j\eta})\hat{x} \\
&+ (\cos\sigma\cos\phi + \sin\sigma\cos\theta\sin\phi e^{j\eta})\hat{y} \\
&- (\sin\sigma\sin\theta e^{j\eta})\hat{z}),
\end{aligned} \tag{5.39}$$

where the carrier wave $e^{j\omega t}$ is omitted [121]. If only the x-axis and y-axis are considered, the spatial-polarisation coherent vector consisting of a signal's polarisation information is

given by [115, 122]

$$\begin{aligned} s_p(\theta,\phi,\sigma,\eta) &= \begin{bmatrix} \sin\sigma\cos\theta\cos\phi e^{j\eta} - \cos\sigma\sin\phi \\ \sin\sigma\cos\theta\sin\phi e^{j\eta} + \cos\sigma\cos\phi \end{bmatrix} \\ &= \begin{bmatrix} s_{p,x}(\theta,\phi,\sigma,\eta) \\ s_{p,y}(\theta,\phi,\sigma,\eta) \end{bmatrix}. \end{aligned} \tag{5.40}$$

5.3.2 Individual Dipole Selection for Two Beams

Consider the case of $M = 2$. The spatial steering vectors of the m-th subarray with the interleaved and localised subarray architectures are given by

$$\begin{aligned} \boldsymbol{s}_{m,s}(\theta,\phi) =& [e^{j2\pi m\frac{d}{\lambda}\sin\theta\sin\phi}, e^{j2\pi(m+M)\frac{d}{\lambda}\sin\theta\sin\phi}, \\ & ..., e^{j2\pi(m+M(N_s-1))\frac{d}{\lambda}\sin\theta\sin\phi}]^T, \end{aligned} \tag{5.41}$$

and

$$\begin{aligned} \boldsymbol{s}_{m,s}(\theta,\phi) =& [e^{j2\pi mN_s\frac{d}{\lambda}\sin\theta\sin\phi}, e^{j2\pi(mN_s+1)\frac{d}{\lambda}\sin\theta\sin\phi}, \\ & ..., e^{j2\pi((m+1)N_s-1)\frac{d}{\lambda}\sin\theta\sin\phi}]^T, \end{aligned} \tag{5.42}$$

respectively, with $m \in \{0, 1\}$. Moreover, the spatial-polarisation coherent vector consisting of a signal's polarisation information is given by (5.40).

The m-th subarray can be split into two parts and each parallel to the corresponding axis. With $f \in \{x, y\}$, the steering vector of each part for the m-th subarray is

$$\boldsymbol{s}_{m,f}(\theta,\phi,\sigma,\eta) = s_{p,f}(\theta,\phi,\sigma,\eta)\boldsymbol{s}_{m,s}(\theta,\phi). \tag{5.43}$$

The beam pattern generated by the m-th subarray is

$$\check{P}_m(\theta,\phi,\sigma,\eta) = \check{\boldsymbol{w}}_{A,m}^H \boldsymbol{s}_m(\theta,\phi,\sigma,\eta), \tag{5.44}$$

where $\check{\boldsymbol{w}}_{A,m}$ denotes the analogue coefficients for the m-th subarray, given by

$$\begin{aligned} \check{\boldsymbol{w}}_{A,m} = [& \check{w}_{A,m,x,0}, \check{w}_{A,m,y,0}, \check{w}_{A,m,x,1}, \check{w}_{A,m,y,1}, ..., \\ & \check{w}_{A,m,x,N_s-1}, \check{w}_{A,m,y,N_s-1}]^T, \end{aligned} \tag{5.45}$$

where $\check{w}_{A,m,f,n}$ is the complex-valued weighting coefficient for the n-th dipole orientated parallel to the f-axis. Similarly,

$$\begin{aligned}\boldsymbol{s}_m(\theta,\phi,\sigma,\eta) = [&s_{m,x,0}(\theta,\phi,\sigma,\eta), s_{m,y,0}(\theta,\phi,\sigma,\eta),\\ &s_{m,x,1}(\theta,\phi,\sigma,\eta), s_{m,y,1}(\theta,\phi,\sigma,\eta),\ldots,\\ &s_{m,x,N_s-1}(\theta,\phi,\sigma,\eta), s_{m,y,N_s-1}(\theta,\phi,\sigma,\eta)]^T,\end{aligned} \tag{5.46}$$

where $s_{m,f,n}(\theta,\phi,\sigma,\eta)$ is the contribution of the n-th dipole in the m-th subarray to the overall steering vector parallel to the f-axis.

The digital coding scheme for the two-beam case is employed, whose coefficients for the j-th designed beam are given by

$$\check{\boldsymbol{w}}_{D,j} = [\check{w}_{D,j,0}, \check{w}_{D,j,1}], \tag{5.47}$$

and the designed beam response for the beam in direction φ_j is

$$\begin{aligned}\check{P}_{\varphi_j}(\theta,\phi,\sigma,\eta) &= \check{w}^*_{D,j,0}\check{P}_0(\theta,\phi,\sigma,\eta) + \check{w}^*_{D,j,1}\check{P}_1(\theta,\phi,\sigma,\eta)\\ &= \check{w}^*_{D,j,0}\check{\boldsymbol{w}}^H_{A,0}\boldsymbol{s}_0(\theta,\phi,\sigma,\eta) + \check{w}^*_{D,j,1}\check{\boldsymbol{w}}^H_{A,1}\boldsymbol{s}_1(\theta,\phi,\sigma,\eta).\end{aligned} \tag{5.48}$$

Combining the analogue coefficients $\check{\boldsymbol{w}}_{A,0}$ and $\check{\boldsymbol{w}}_{A,1}$ into one vector

$$\check{\boldsymbol{w}}_A = \left[\check{\boldsymbol{w}}^T_{A,0}, \check{\boldsymbol{w}}^T_{A,1}\right]^T, \tag{5.49}$$

the formulation to find the optimum $\check{\boldsymbol{w}}_A$ with a minimum number of non-zero-valued coefficients for a given set of $\check{w}_{D,j,m}(\{j,m\} \in \{0,1\})$ is given by

$$\begin{aligned}\min_{\check{\boldsymbol{w}}_A} \quad & J_{LSE} = (1-\gamma) \parallel \check{\boldsymbol{L}}^H \check{\boldsymbol{w}}_A \parallel_2 + \gamma \parallel \check{\boldsymbol{w}}_A \parallel_1,\\ \text{subject} \quad & \text{to}\\ & \check{\boldsymbol{w}}^H_A \begin{bmatrix} \check{\boldsymbol{w}}^H_{D,0,0}\check{\boldsymbol{z}}_{S_{00}} & \check{\boldsymbol{w}}^H_{D,1,0}\check{\boldsymbol{z}}_{S_{10}} \\ \check{\boldsymbol{w}}^H_{D,0,1}\check{\boldsymbol{z}}_{S_{01}} & \check{\boldsymbol{w}}^H_{D,1,1}\check{\boldsymbol{z}}_{S_{11}} \end{bmatrix} = \begin{bmatrix} 1 & 1 \end{bmatrix},\end{aligned} \tag{5.50}$$

with

$$\check{\boldsymbol{z}}_{S_{jm}} = \sum_{\theta\in\Theta_{main_j}} \boldsymbol{s}_m(\theta,\phi,\sigma,\eta), \tag{5.51}$$

$$\check{\boldsymbol{w}}_{D,j,m} = \check{w}_{D,j,m}\boldsymbol{I}_{2N_s}, \tag{5.52}$$

where $\check{\boldsymbol{L}}$ is similar to $\boldsymbol{L}$ in (5.2) for the two-user case in Section 5.2.1.

By combining the digital coefficients for two beams into one vector

$$\check{\boldsymbol{w}}_D = \left[\check{\boldsymbol{w}}_{D,0}, \check{\boldsymbol{w}}_{D,1}\right]^T = \left[\check{w}_{D,0,0}, \check{w}_{D,0,1}, \check{w}_{D,1,0}, \check{w}_{D,1,1}\right]^T, \tag{5.53}$$

the optimisation problem is formulated as

$$\begin{aligned} \min_{\check{\boldsymbol{w}}_D} \quad & \check{\boldsymbol{w}}_D^H \grave{\boldsymbol{M}}_S \check{\boldsymbol{w}}_D, \\ \text{subject} \quad & \text{to} \\ & \grave{\boldsymbol{C}}^H \check{\boldsymbol{w}}_D = \boldsymbol{f}, \end{aligned} \tag{5.54}$$

with

$$\grave{\boldsymbol{C}} = \begin{bmatrix} \check{\boldsymbol{w}}_A^H \grave{\boldsymbol{z}}_{S_{00}} & 0 \\ \check{\boldsymbol{w}}_A^H \grave{\boldsymbol{z}}_{S_{01}} & 0 \\ 0 & \check{\boldsymbol{w}}_A^H \grave{\boldsymbol{z}}_{S_{10}} \\ 0 & \check{\boldsymbol{w}}_A^H \grave{\boldsymbol{z}}_{S_{11}} \end{bmatrix}, \boldsymbol{f} = \begin{bmatrix} 1 \\ 1 \end{bmatrix}, \tag{5.55}$$

$$\grave{\boldsymbol{z}}_{S_{j0}} = \begin{bmatrix} \check{\boldsymbol{z}}_{S_{j0}} \\ \boldsymbol{0}_{2N_s \times 1} \end{bmatrix}, \grave{\boldsymbol{z}}_{S_{j1}} = \begin{bmatrix} \boldsymbol{0}_{2N_s \times 1} \\ \check{\boldsymbol{z}}_{S_{j1}} \end{bmatrix}, \tag{5.56}$$

where $\grave{\boldsymbol{M}}_S$ is similar to $\tilde{\boldsymbol{M}}_S$ in (4.15).

The solution of the problem (5.54) is given by

$$\check{\boldsymbol{w}}_D = \grave{\boldsymbol{M}}_S^{-1} \grave{\boldsymbol{C}} \left(\grave{\boldsymbol{C}}^H \grave{\boldsymbol{M}}_S^{-1} \grave{\boldsymbol{C}} \right)^{-1} \boldsymbol{f}. \tag{5.57}$$

Alternate optimisation of the digital coefficients $\check{\boldsymbol{w}}_D$ and the corresponding analogue coefficients $\check{\boldsymbol{w}}_A$ can be achieved iteratively:

(1) First, via initialising the digital coefficients $\check{\boldsymbol{w}}_D$ with random values, $\check{\boldsymbol{w}}_A$ is obtained by substituting $\check{w}_{D,j,m}(\{j,m\} \in \{0,1\})$ into (5.50).

(2) Given the obtained optimum values for $\check{\boldsymbol{w}}_A$ in step (1), the optimum values for $\check{\boldsymbol{w}}_D$ are obtained by (5.57).

(3) Given the obtained values of $\check{\boldsymbol{w}}_D$ in step (2), the new set of values of $\check{\boldsymbol{w}}_A$ can be obtained by (5.50) again.

(4) Repeat steps (2) and (3) until the cost function in (5.50) converges.

5.3.3 Individual Dipole Selection for Three Beams

By combining the analogue coefficients $\check{\boldsymbol{w}}_{A,0}$, $\check{\boldsymbol{w}}_{A,1}$ and $\check{\boldsymbol{w}}_{A,2}$ into one vector, given by

$$\check{\boldsymbol{w}}_A = \left[\check{\boldsymbol{w}}_{A,0}^T, \check{\boldsymbol{w}}_{A,1}^T, \check{\boldsymbol{w}}_{A,2}^T\right]^T, \tag{5.58}$$

the formulation to obtain the analogue coefficients $\check{\boldsymbol{w}}_A$ for the three-user case is given by

$$\begin{aligned} \min_{\check{\boldsymbol{w}}_A} \quad & J_{LSE} = (1-\gamma) \parallel \check{\boldsymbol{L}}^H \check{\boldsymbol{w}}_A \parallel_2 + \gamma \parallel \check{\boldsymbol{w}}_A \parallel_1, \\ \text{subject} \quad & \text{to} \\ & \check{\boldsymbol{w}}_A^H \begin{bmatrix} \check{\boldsymbol{w}}_{D,0,0}^H \check{\boldsymbol{z}}_{S_{00}} & \check{\boldsymbol{w}}_{D,1,0}^H \check{\boldsymbol{z}}_{S_{10}} & \check{\boldsymbol{w}}_{D,2,0}^H \check{\boldsymbol{z}}_{S_{20}} \\ \check{\boldsymbol{w}}_{D,0,1}^H \check{\boldsymbol{z}}_{S_{01}} & \check{\boldsymbol{w}}_{D,1,1}^H \check{\boldsymbol{z}}_{S_{11}} & \check{\boldsymbol{w}}_{D,2,1}^H \check{\boldsymbol{z}}_{S_{21}} \\ \check{\boldsymbol{w}}_{D,0,2}^H \check{\boldsymbol{z}}_{S_{02}} & \check{\boldsymbol{w}}_{D,1,2}^H \check{\boldsymbol{z}}_{S_{12}} & \check{\boldsymbol{w}}_{D,2,2}^H \check{\boldsymbol{z}}_{S_{22}} \end{bmatrix} = \begin{bmatrix} 1 & 1 & 1 \end{bmatrix}, \end{aligned} \tag{5.59}$$

where $\check{\boldsymbol{L}}$ is similar to $\check{\boldsymbol{L}}$ in (5.50) in Section 5.3.2.

By combining the digital coefficients for the three beams into one vector

$$\begin{aligned} \check{\boldsymbol{w}}_D &= \left[\check{\boldsymbol{w}}_{D,0}, \check{\boldsymbol{w}}_{D,1}, \check{\boldsymbol{w}}_{D,2}\right]^T \\ &= \left[\check{w}_{D,0,0}, \check{w}_{D,0,1}, \check{w}_{D,0,2}, \check{w}_{D,1,0}, \check{w}_{D,1,1}, \check{w}_{D,1,2}, \check{w}_{D,2,0}, \check{w}_{D,2,1}, \check{w}_{D,2,2}\right]^T, \end{aligned} \tag{5.60}$$

the optimisation problem to obtain the digital coefficients $\check{\boldsymbol{w}}_D$ is given by (5.54) with

$$\grave{\boldsymbol{C}} = \begin{bmatrix} \check{\boldsymbol{w}}_A^H \grave{\boldsymbol{z}}_{S_{00}} & 0 & 0 \\ \check{\boldsymbol{w}}_A^H \grave{\boldsymbol{z}}_{S_{01}} & 0 & 0 \\ \check{\boldsymbol{w}}_A^H \grave{\boldsymbol{z}}_{S_{02}} & 0 & 0 \\ 0 & \check{\boldsymbol{w}}_A^H \grave{\boldsymbol{z}}_{S_{10}} & 0 \\ 0 & \check{\boldsymbol{w}}_A^H \grave{\boldsymbol{z}}_{S_{11}} & 0 \\ 0 & \check{\boldsymbol{w}}_A^H \grave{\boldsymbol{z}}_{S_{12}} & 0 \\ 0 & 0 & \check{\boldsymbol{w}}_A^H \grave{\boldsymbol{z}}_{S_{20}} \\ 0 & 0 & \check{\boldsymbol{w}}_A^H \grave{\boldsymbol{z}}_{S_{21}} \\ 0 & 0 & \check{\boldsymbol{w}}_A^H \grave{\boldsymbol{z}}_{S_{22}} \end{bmatrix}, \boldsymbol{f} = \begin{bmatrix} 1 \\ 1 \\ 1 \end{bmatrix}, \tag{5.61}$$

$$\grave{\boldsymbol{z}}_{S_{j0}} = \begin{bmatrix} \check{\boldsymbol{z}}_{S_{j0}} \\ \boldsymbol{0}_{2N_s \times 1} \\ \boldsymbol{0}_{2N_s \times 1} \end{bmatrix}, \grave{\boldsymbol{z}}_{S_{j1}} = \begin{bmatrix} \boldsymbol{0}_{2N_s \times 1} \\ \check{\boldsymbol{z}}_{S_{j1}} \\ \boldsymbol{0}_{2N_s \times 1} \end{bmatrix}, \grave{\boldsymbol{z}}_{S_{j2}} = \begin{bmatrix} \boldsymbol{0}_{2N_s \times 1} \\ \boldsymbol{0}_{2N_s \times 1} \\ \check{\boldsymbol{z}}_{S_{j2}} \end{bmatrix}, \tag{5.62}$$

where $\grave{\boldsymbol{M}}_S$ is similar to $\grave{\boldsymbol{M}}_S$ in (5.54) in Section 5.3.2.

The solution to (5.54) for the individual dipole selection method with $J = M = 3$ is given by (5.57).

Alternate optimisation of the digital coefficients $\check{\boldsymbol{w}}_D$ and analogue coefficients $\check{\boldsymbol{w}}_A$ is performed as follows:

(1) First, via initialising the digital coefficients $\check{\boldsymbol{w}}_D$ with random values, $\check{\boldsymbol{w}}_A$ is obtained by substituting $\check{w}_{D,j,m}(\{j,m\} \in \{0,1,2\})$ into (5.59).

(2) Given the obtained optimum values for $\check{\boldsymbol{w}}_A$ in step (1), the optimum values for $\check{\boldsymbol{w}}_D$ are obtained by (5.57).

(3) Given the obtained values of $\check{\boldsymbol{w}}_D$ in step (2), the new set of values of $\check{\boldsymbol{w}}_A$ can be obtained by (5.59) again.

(4) Repeat steps (2) and (3) until the cost function in (5.59) converges.

5.3.4 Crossed-Dipole Antenna Selection for Two Beams

One issue with the above design is that the two complex-valued weighting coefficients associated with each antenna location cannot be minimised simultaneously. For some of the crossed-dipole antennas, it will result in only one of the two dipoles being switched on while the other one switched off, which may not be convenient in practice because the crossed-dipole antenna cannot be removed completely or it is simply difficult to perform partial switch off due to the construction itself.

To switch off the whole antenna, we have to modify the formulation in (5.50) so that the complex-valued coefficients for each antenna can be minimised simultaneously.

Following the idea in [123, 124], the formulation in (5.50) can be modified to

$$\begin{aligned}
&\min_{\check{\boldsymbol{w}}_A} \quad J_{LSE} = (1-\gamma) \parallel \check{\boldsymbol{L}}^H \check{\boldsymbol{w}}_A \parallel_2 + \gamma g \quad (g \in \mathbb{R}^+), \\
&\text{subject} \quad \text{to} \\
&\qquad \check{\boldsymbol{w}}_A^H \begin{bmatrix} \check{\boldsymbol{w}}_{D,0,0}^H \check{\boldsymbol{z}}_{S_{00}} & \check{\boldsymbol{w}}_{D,1,0}^H \check{\boldsymbol{z}}_{S_{10}} \\ \check{\boldsymbol{w}}_{D,0,1}^H \check{\boldsymbol{z}}_{S_{01}} & \check{\boldsymbol{w}}_{D,1,1}^H \check{\boldsymbol{z}}_{S_{11}} \end{bmatrix} = \begin{bmatrix} 1 & 1 \end{bmatrix}, \\
&\qquad \sum_{\tilde{n}=0}^{2N_s-1} ||\check{\boldsymbol{w}}_{A_{\tilde{n}}}||_2 \leq g,
\end{aligned} \tag{5.63}$$

with

$$\check{\boldsymbol{w}}_A = [\check{w}_{A,x,0}, \check{w}_{A,y,0}, \check{w}_{A,x,1}, ..., \check{w}_{A,x,2N_s-1}, \check{w}_{A,y,2N_s-1}]^T, \tag{5.64}$$

where $\check{\boldsymbol{w}}_{A_{\tilde{n}}} = [\check{w}_{A,x,\tilde{n}}, \check{w}_{A,y,\tilde{n}}], (\tilde{n} \in \{0, 1, \ldots, 2N_s - 1\})$ and $\check{\boldsymbol{w}}_{A_{\tilde{n}}}$ consists of the weighting coefficients for all the dipoles that form the $\tilde{n}$-th antenna in $\check{\boldsymbol{w}}_A$.

To minimise the combined weighting coefficients for each crossed dipole separately, g is decomposed into

$$g = [1, \ldots, 1] \begin{bmatrix} g_0, g_1, \ldots, g_{2N_s-1} \end{bmatrix}^T = \mathbf{1}^T \boldsymbol{g}, \tag{5.65}$$

and (5.63) can be rewritten as

$$\begin{aligned}
&\min_{\check{\boldsymbol{w}}_A} \quad J_{LSE} = (1-\gamma) \parallel \check{\boldsymbol{L}}^H \check{\boldsymbol{w}}_A \parallel_2 + \gamma \mathbf{1}^T \boldsymbol{g}, \\
&\text{subject} \quad \text{to} \\
&\qquad \check{\boldsymbol{w}}_A^H \begin{bmatrix} \check{\boldsymbol{w}}_{D,0,0}^H \check{\boldsymbol{z}}_{S_{00}} & \check{\boldsymbol{w}}_{D,1,0}^H \check{\boldsymbol{z}}_{S_{10}} \\ \check{\boldsymbol{w}}_{D,0,1}^H \check{\boldsymbol{z}}_{S_{01}} & \check{\boldsymbol{w}}_{D,1,1}^H \check{\boldsymbol{z}}_{S_{11}} \end{bmatrix} = \begin{bmatrix} 1 & 1 \end{bmatrix}, \\
&\qquad ||\check{\boldsymbol{w}}_{A_{\tilde{n}}}||_2 \leq g_{\tilde{n}}, \tilde{n} \in \{0, 1, \ldots, 2N_s - 1\}.
\end{aligned} \tag{5.66}$$

Note that a value of $g_{\tilde{n}} = 0$ indicates the second constraint in (5.66) guarantees that both the real and imaginary parts of each weighting coefficient in $\check{\boldsymbol{w}}_{A_{\tilde{n}}}$ are zero and the sparse nature on antenna locations is introduced.

Now, by defining

$$\begin{aligned}
\tilde{\boldsymbol{w}}_A = &[g_0, \Re(\check{w}_{A,x,0}), \Re(\check{w}_{A,y,0}), -\Im(\check{w}_{A,x,0}), -\Im(\check{w}_{A,y,0}), \\
&g_1, \ldots, g_{2N_s-1}, \Re(\check{w}_{A,x,2N_s-1}), \ldots, -\Im(\check{w}_{A,y,2N_s-1})]^T,
\end{aligned} \tag{5.67}$$

$$\check{\boldsymbol{c}} = [\overbrace{1, 0, 0, 0, 0}^{\tilde{n}=0}, 1, 0, 0, \cdots, \overbrace{1, 0, 0, 0, 0}^{\tilde{n}=2N_s-1}]^T, \tag{5.68}$$

and

$$\tilde{\boldsymbol{s}}_m = \begin{bmatrix} \boldsymbol{0} & \boldsymbol{0} \\ \Re(\boldsymbol{s}_{m,x,0}) & \Im(\boldsymbol{s}_{m,x,0}) \\ \Re(\boldsymbol{s}_{m,y,0}) & \Im(\boldsymbol{s}_{m,y,0}) \\ -\Im(\boldsymbol{s}_{m,x,0}) & \Re(\boldsymbol{s}_{m,x,0}) \\ -\Im(\boldsymbol{s}_{m,y,0}) & \Re(\boldsymbol{s}_{m,y,0}) \\ \vdots & \vdots \\ \boldsymbol{0} & \boldsymbol{0} \\ \vdots & \vdots \\ -\Im(\boldsymbol{s}_{m,y,N_s-1}) & \Re(\boldsymbol{s}_{m,y,N_s-1}) \end{bmatrix}, \tag{5.69}$$

where $\boldsymbol{s}_{m,f,n}$ ($n \in \{0, 1, \ldots, N_s - 1\}$) denotes the contribution of the n-th dipole parallel to the f-axis to the steering vector of the m-th subarray, $\Re(.)$ and $\Im(.)$ denote the real and imaginary components, respectively.

Since the weighting coefficients in (5.67) are split into the real and imaginary parts, the digital coefficients should also be multiplied with the steering vector first and then split it into the real and imaginary parts that make up a new matrix, given by

$$\tilde{\boldsymbol{r}}_{jm} = \begin{bmatrix} \boldsymbol{0} & \boldsymbol{0} \\ \Re(\tilde{\boldsymbol{w}}_{D,j,m}^H \boldsymbol{s}_{m,x,0}) & \Im(\tilde{\boldsymbol{w}}_{D,j,m}^H \boldsymbol{s}_{m,x,0}) \\ \Re(\tilde{\boldsymbol{w}}_{D,j,m}^H \boldsymbol{s}_{m,y,0}) & \Im(\tilde{\boldsymbol{w}}_{D,j,m}^H \boldsymbol{s}_{m,y,0}) \\ -\Im(\tilde{\boldsymbol{w}}_{D,j,m}^H \boldsymbol{s}_{m,x,0}) & \Re(\tilde{\boldsymbol{w}}_{D,j,m}^H \boldsymbol{s}_{m,x,0}) \\ -\Im(\tilde{\boldsymbol{w}}_{D,j,m}^H \boldsymbol{s}_{m,y,0}) & \Re(\tilde{\boldsymbol{w}}_{D,j,m}^H \boldsymbol{s}_{m,y,0}) \\ \vdots & \vdots \\ \boldsymbol{0} & \boldsymbol{0} \\ \vdots & \vdots \\ -\Im(\tilde{\boldsymbol{w}}_{D,j,m}^H \boldsymbol{s}_{m,y,N_s-1}) & \Re(\tilde{\boldsymbol{w}}_{D,j,m}^H \boldsymbol{s}_{m,y,N_s-1}) \end{bmatrix}, \tag{5.70}$$

with

$$\tilde{\boldsymbol{w}}_{D,j,m} = \check{w}_{D,j,m} \boldsymbol{I}_{N_s}. \tag{5.71}$$

Similar to (4.7), (4.8) and (4.9), the three items which constitute the correlation matrix

of the sum of the sidelobe responses for the two beams are changed to

$$\tilde{\boldsymbol{Q}}_S = \begin{bmatrix} \tilde{\boldsymbol{G}}_{S_0} & \boldsymbol{0}_{5N_s} \\ \boldsymbol{0}_{5N_s} & \tilde{\boldsymbol{G}}_{S_1} \end{bmatrix}, \tilde{\boldsymbol{P}}_S = \begin{bmatrix} \tilde{\boldsymbol{H}}_{S_0} & \boldsymbol{0}_{5N_s} \\ \boldsymbol{0}_{5N_s} & \tilde{\boldsymbol{H}}_{S_1} \end{bmatrix}, \tag{5.72}$$

$$\tilde{\boldsymbol{G}}_{S_m} = \sum_{\theta \in \Theta_{side_0}} \tilde{\boldsymbol{r}}_{0,m} \tilde{\boldsymbol{r}}_{0,m}^T + \sum_{\theta \in \Theta_{side_1}} \tilde{\boldsymbol{r}}_{1,m} \tilde{\boldsymbol{r}}_{1,m}^T, \tag{5.73}$$

and

$$\begin{aligned} \tilde{\boldsymbol{H}}_{S_0} &= \sum_{\theta \in \Theta_{side_0}} \tilde{\boldsymbol{r}}_{0,0} \tilde{\boldsymbol{r}}_{0,1}^T + \sum_{\theta \in \Theta_{side_1}} \tilde{\boldsymbol{r}}_{1,0} \tilde{\boldsymbol{r}}_{1,1}^T, \\ \tilde{\boldsymbol{H}}_{S_1} &= \sum_{\theta \in \Theta_{side_0}} \tilde{\boldsymbol{r}}_{0,1} \tilde{\boldsymbol{r}}_{0,0}^T + \sum_{\theta \in \Theta_{side_1}} \tilde{\boldsymbol{r}}_{1,1} \tilde{\boldsymbol{r}}_{1,0}^T, \end{aligned} \tag{5.74}$$

where $\boldsymbol{0}_{5N_s}$ denotes a $5N_s \times 5N_s$ all-zero vector.

As shown in (5.67), because the values of $g_{\tilde{n}}$ for $\tilde{n} \in \{0, 1, \ldots, 2N_s - 1\}$ are included with the weighting coefficients in $\tilde{\boldsymbol{w}}_A$, it is not necessary to predefine their values and they are obtained simultaneously with the optimised weighting coefficients. Moreover, $\check{\boldsymbol{c}}$ is to select the values of $g_{\tilde{n}}$ for the optimisation and $\boldsymbol{0}$ vectors in $\tilde{\boldsymbol{s}}_m$ in (5.69) guarantee that they are not imposed to the minimise the sum of the sidelobe energy [123].

As a result, the final formulation is given as follows

$$\begin{aligned} \min_{\tilde{\boldsymbol{w}}_A} \quad & J_{LSE} = (1-\gamma) \parallel \tilde{\boldsymbol{L}}^T \tilde{\boldsymbol{w}}_A \parallel_2 + \gamma \check{\boldsymbol{c}}^T \tilde{\boldsymbol{w}}_A, \\ \text{subject} \quad & \text{to} \\ & \tilde{\boldsymbol{w}}_A^T \begin{bmatrix} \tilde{\boldsymbol{z}}_{S_{00}} & \tilde{\boldsymbol{z}}_{S_{10}} \\ \tilde{\boldsymbol{z}}_{S_{01}} & \tilde{\boldsymbol{z}}_{S_{11}} \end{bmatrix} = \begin{bmatrix} 1 & 0 & 1 & 0 \end{bmatrix}, \\ & ||\tilde{\boldsymbol{w}}_{A_{\tilde{n}}}||_2 \leq g_{\tilde{n}}, \tilde{n} \in \{0, 1, \ldots, 2N_s - 1\}, \end{aligned} \tag{5.75}$$

with

$$\tilde{\boldsymbol{z}}_{S_{jm}} = \sum_{\theta \in \Theta_{main_j}} \tilde{\boldsymbol{r}}_{jm}, \tag{5.76}$$

$$\tilde{\boldsymbol{I}}_8 = \begin{bmatrix} \boldsymbol{0}_{5N_s} & \boldsymbol{I}_{5N_s} \\ \boldsymbol{I}_{5N_s} & \boldsymbol{0}_{5N_s} \end{bmatrix}, \tag{5.77}$$

where $\tilde{\boldsymbol{L}} = \tilde{\boldsymbol{V}} \tilde{\boldsymbol{U}}^{1/2}$, with $\tilde{\boldsymbol{U}}$ being the diagonal matrix including all the eigenvalues of $(\tilde{\boldsymbol{Q}}_S + \tilde{\boldsymbol{P}}_S \tilde{\boldsymbol{I}}_8)$, $\tilde{\boldsymbol{V}}$ being the corresponding eigenvector matrix and $\boldsymbol{I}_{5N_s}$ denotes a $5N_s \times 5N_s$ identity vector.

Given the obtained values of $\tilde{\boldsymbol{w}}_A$ in (5.75), to find the closed-form solution to $\check{\boldsymbol{w}}_D$, the optimisation problem is given by (5.54) with

$$\grave{\boldsymbol{M}}_S = \grave{\boldsymbol{Q}}_S + \grave{\boldsymbol{P}}_S \tilde{\boldsymbol{I}}_1, \tag{5.78}$$

$$\grave{\boldsymbol{Q}}_S = \begin{bmatrix} \grave{\boldsymbol{G}}_{S_{00}} & 0 & 0 & 0 \\ 0 & \grave{\boldsymbol{G}}_{S_{01}} & 0 & 0 \\ 0 & 0 & \grave{\boldsymbol{G}}_{S_{10}} & 0 \\ 0 & 0 & 0 & \grave{\boldsymbol{G}}_{S_{11}} \end{bmatrix}, \grave{\boldsymbol{P}}_S = \begin{bmatrix} \grave{\boldsymbol{H}}_{S_0} & \boldsymbol{0}_2 \\ \boldsymbol{0}_2 & \grave{\boldsymbol{H}}_{S_1} \end{bmatrix}, \tag{5.79}$$

$$\tilde{\boldsymbol{c}} = [\overbrace{0,1,1,1,1}^{\tilde{n}=0}, 0, 1, 1, \cdots, \overbrace{0,1,1,1,1}^{\tilde{n}=2N_s-1}]^T, \tag{5.80}$$

$$\grave{\boldsymbol{G}}_{S_{jm}} = (\tilde{\boldsymbol{c}} \circ \tilde{\boldsymbol{w}}_A)^T \acute{\boldsymbol{Q}}_{S_{jm}} (\tilde{\boldsymbol{c}} \circ \tilde{\boldsymbol{w}}_A), \grave{\boldsymbol{H}}_{S_j} = \begin{bmatrix} \grave{\boldsymbol{B}}_{S_{j0}} & 0 \\ 0 & \grave{\boldsymbol{B}}_{S_{j1}} \end{bmatrix}, \tag{5.81}$$

$$\acute{\boldsymbol{Q}}_{S_{j0}} = \begin{bmatrix} \tilde{\boldsymbol{Q}}_{S_{j0}} & \boldsymbol{0}_{5N_s} \\ \boldsymbol{0}_{5N_s} & \boldsymbol{0}_{5N_s} \end{bmatrix}, \acute{\boldsymbol{Q}}_{S_{j1}} = \begin{bmatrix} \boldsymbol{0}_{5N_s} & \boldsymbol{0}_{5N_s} \\ \boldsymbol{0}_{5N_s} & \tilde{\boldsymbol{Q}}_{S_{j1}} \end{bmatrix}, \tag{5.82}$$

$$\grave{\boldsymbol{B}}_{S_{jm}} = (\tilde{\boldsymbol{c}} \circ \tilde{\boldsymbol{w}}_A)^T \acute{\boldsymbol{P}}_{S_{jm}} \tilde{\boldsymbol{I}}_8 (\tilde{\boldsymbol{c}} \circ \tilde{\boldsymbol{w}}_A), \tag{5.83}$$

$$\acute{\boldsymbol{P}}_{S_{j0}} = \begin{bmatrix} \tilde{\boldsymbol{P}}_{S_{j0}} & \boldsymbol{0}_{5N_s} \\ \boldsymbol{0}_{5N_s} & \boldsymbol{0}_{5N_s} \end{bmatrix}, \acute{\boldsymbol{P}}_{S_{j1}} = \begin{bmatrix} \boldsymbol{0}_{5N_s} & \boldsymbol{0}_{5N_s} \\ \boldsymbol{0}_{5N_s} & \tilde{\boldsymbol{P}}_{S_{j1}} \end{bmatrix}, \tag{5.84}$$

$$\tilde{\boldsymbol{Q}}_{S_{jm}} = \sum_{\theta \in \Theta_{side_j}} \tilde{\boldsymbol{S}}_m(\theta, \phi, \sigma, \eta), \tag{5.85}$$

$$\tilde{\boldsymbol{P}}_{S_{j0}} = \sum_{\theta \in \Theta_{side_j}} \tilde{\boldsymbol{s}}_0(\theta, \phi, \sigma, \eta) \tilde{\boldsymbol{s}}_1(\theta, \phi, \sigma, \eta)^T, \tilde{\boldsymbol{P}}_{S_{j1}} = \sum_{\theta \in \Theta_{side_j}} \tilde{\boldsymbol{s}}_1(\theta, \phi, \sigma, \eta) \tilde{\boldsymbol{s}}_0(\theta, \phi, \sigma, \eta)^T, \tag{5.86}$$

$$\tilde{\boldsymbol{S}}_m(\theta, \phi, \sigma, \eta) = \tilde{\boldsymbol{s}}_m(\theta, \phi, \sigma, \eta) \tilde{\boldsymbol{s}}_m(\theta, \phi, \sigma, \eta)^T, \tag{5.87}$$

$$\grave{\boldsymbol{C}} = \begin{bmatrix} (\tilde{\boldsymbol{c}} \circ \tilde{\boldsymbol{w}}_A)^T \grave{\boldsymbol{z}}_{S_{00}} & 0 \\ (\tilde{\boldsymbol{c}} \circ \tilde{\boldsymbol{w}}_A)^T \grave{\boldsymbol{z}}_{S_{01}} & 0 \\ 0 & (\tilde{\boldsymbol{c}} \circ \tilde{\boldsymbol{w}}_A)^T \grave{\boldsymbol{z}}_{S_{10}} \\ 0 & (\tilde{\boldsymbol{c}} \circ \tilde{\boldsymbol{w}}_A)^T \grave{\boldsymbol{z}}_{S_{11}} \end{bmatrix}, \boldsymbol{f} = \begin{bmatrix} 1 \\ 1 \end{bmatrix}, \tag{5.88}$$

$$\grave{\boldsymbol{z}}_{S_{j0}} = \begin{bmatrix} \grave{\boldsymbol{h}}_{j0} \\ \boldsymbol{0}_{5N_s \times 1} \end{bmatrix}, \grave{\boldsymbol{z}}_{S_{j1}} = \begin{bmatrix} \boldsymbol{0}_{5N_s \times 1} \\ \grave{\boldsymbol{h}}_{j1} \end{bmatrix}, \tag{5.89}$$

$$\grave{\boldsymbol{h}}_{jm} = \sum_{\theta \in \Theta_{main_j}} \begin{bmatrix} \boldsymbol{0} \\ \boldsymbol{s}_{m,x,0} \\ \boldsymbol{s}_{m,y,0} \\ -\Im(\boldsymbol{s}_{m,x,0}) + j\Re(\boldsymbol{s}_{m,x,0}) \\ -\Im(\boldsymbol{s}_{m,y,0}) + j\Re(\boldsymbol{s}_{m,y,0}) \\ \vdots \\ \boldsymbol{0} \\ \vdots \\ -\Im(\boldsymbol{s}_{m,y,N_s-1}) + j\Re(\boldsymbol{s}_{m,y,N_s-1}) \end{bmatrix}, \tag{5.90}$$

where $\circ$ denotes the Hadamard product and $\boldsymbol{0}_{5N_s \times 1}$ in (5.89) is an $5N_s \times 1$ all-zero vector.

The solution to (5.54) for the whole crossed-dipole antenna selection method with $J = M = 2$ in Section 5.3.4 is given by (5.57).

The following is the whole iterative optimisation process:

(1) First, via initialising the digital coefficients $\check{\boldsymbol{w}}_D$ with random values, $\tilde{\boldsymbol{w}}_A$ is obtained by substituting $\check{w}_{D,j,m}(\{j,m\} \in \{0,1\})$ into (5.75).

(2) Given the obtained optimum values for $\tilde{\boldsymbol{w}}_A$ in step (1), the optimum values for $\check{\boldsymbol{w}}_D$ are obtained by (5.57).

(3) Given the obtained values of $\check{\boldsymbol{w}}_D$ in step (2), the new set of values of $\tilde{\boldsymbol{w}}_A$ can be obtained by (5.75) again.

(4) Repeat steps (2) and (3) until the cost function in (5.75) converges.

5.3.5 Crossed-Dipole Antenna Selection for Three Beams

Similar to (5.75) for the two-user case in Section 5.3.4, the optimisation problem is formulated as

$$\begin{aligned} \min_{\tilde{\boldsymbol{w}}_A} \quad & J_{LSE} = (1-\gamma) \parallel \tilde{\boldsymbol{L}}^H \tilde{\boldsymbol{w}}_A \parallel_2 + \gamma \check{\boldsymbol{c}}^T \tilde{\boldsymbol{w}}_A, \\ \text{subject} \quad & \text{to} \\ & \tilde{\boldsymbol{w}}_A^H \begin{bmatrix} \tilde{\boldsymbol{z}}_{S_{00}} & \tilde{\boldsymbol{z}}_{S_{10}} & \tilde{\boldsymbol{z}}_{S_{20}} \\ \tilde{\boldsymbol{z}}_{S_{01}} & \tilde{\boldsymbol{z}}_{S_{11}} & \tilde{\boldsymbol{z}}_{S_{21}} \\ \tilde{\boldsymbol{z}}_{S_{02}} & \tilde{\boldsymbol{z}}_{S_{12}} & \tilde{\boldsymbol{z}}_{S_{22}} \end{bmatrix} = \begin{bmatrix} 1 & 0 & 1 & 0 & 1 & 0 \end{bmatrix}, \\ & ||\tilde{\boldsymbol{w}}_{A_{\tilde{n}}}||_2 \leq g_{\tilde{n}}, \tilde{n} \in \{0, 1, \ldots, 3N_s - 1\}, \end{aligned} \tag{5.91}$$

with

$$\begin{aligned} \tilde{\boldsymbol{w}}_A = & [g_0, \Re(\check{w}_{A,x,0}), \Re(\check{w}_{A,y,0}), -\Im(\check{w}_{A,x,0}), -\Im(\check{w}_{A,y,0}), \\ & g_1, \ldots, g_{3N_s-1}, \Re(\check{w}_{A,x,3N_s-1}), \ldots, -\Im(\check{w}_{A,y,3N_s-1})]^T, \end{aligned} \tag{5.92}$$

$$\check{\boldsymbol{c}} = [\overbrace{1,0,0,0,0}^{\tilde{n}=0}, 1, 0, 0, \cdots, \overbrace{1,0,0,0,0}^{\tilde{n}=3N_s-1}]^T, \tag{5.93}$$

where $\tilde{\boldsymbol{L}} = \tilde{\boldsymbol{V}} \tilde{\boldsymbol{U}}^{1/2}$ is similar to $\tilde{\boldsymbol{L}}$ in (5.75) and $\tilde{\boldsymbol{z}}_{S_{jm}}$ is given by (5.76).

With (5.60), the optimisation to obtain $\check{\boldsymbol{w}}_D$ can be formulated as (5.54) with

$$\tilde{\boldsymbol{c}} = [\overbrace{0,1,1,1,1}^{\tilde{n}=0}, 0, 1, 1, \cdots, \overbrace{0,1,1,1,1}^{\tilde{n}=3N_s-1}]^T, \tag{5.94}$$

$$\grave{\boldsymbol{C}} = \begin{bmatrix} (\tilde{\boldsymbol{c}} \circ \tilde{\boldsymbol{w}}_A)^T \grave{\boldsymbol{z}}_{S_{00}} & 0 & 0 \\ (\tilde{\boldsymbol{c}} \circ \tilde{\boldsymbol{w}}_A)^T \grave{\boldsymbol{z}}_{S_{01}} & 0 & 0 \\ (\tilde{\boldsymbol{c}} \circ \tilde{\boldsymbol{w}}_A)^T \grave{\boldsymbol{z}}_{S_{02}} & 0 & 0 \\ 0 & (\tilde{\boldsymbol{c}} \circ \tilde{\boldsymbol{w}}_A)^T \grave{\boldsymbol{z}}_{S_{10}} & 0 \\ 0 & (\tilde{\boldsymbol{c}} \circ \tilde{\boldsymbol{w}}_A)^T \grave{\boldsymbol{z}}_{S_{11}} & 0 \\ 0 & (\tilde{\boldsymbol{c}} \circ \tilde{\boldsymbol{w}}_A)^T \grave{\boldsymbol{z}}_{S_{12}} & 0 \\ 0 & 0 & (\tilde{\boldsymbol{c}} \circ \tilde{\boldsymbol{w}}_A)^T \grave{\boldsymbol{z}}_{S_{20}} \\ 0 & 0 & (\tilde{\boldsymbol{c}} \circ \tilde{\boldsymbol{w}}_A)^T \grave{\boldsymbol{z}}_{S_{21}} \\ 0 & 0 & (\tilde{\boldsymbol{c}} \circ \tilde{\boldsymbol{w}}_A)^T \grave{\boldsymbol{z}}_{S_{22}} \end{bmatrix}, \boldsymbol{f} = \begin{bmatrix} 1 \\ 1 \\ 1 \end{bmatrix}, \tag{5.95}$$

$$\grave{\boldsymbol{z}}_{S_{j0}} = \begin{bmatrix} \grave{\boldsymbol{h}}_{j0} \\ \boldsymbol{0}_{5N_s\times 1} \\ \boldsymbol{0}_{5N_s\times 1} \end{bmatrix}, \grave{\boldsymbol{z}}_{S_{j1}} = \begin{bmatrix} \boldsymbol{0}_{5N_s\times 1} \\ \grave{\boldsymbol{h}}_{j1} \\ \boldsymbol{0}_{5N_s\times 1} \end{bmatrix}, \grave{\boldsymbol{z}}_{S_{j2}} = \begin{bmatrix} \boldsymbol{0}_{5N_s\times 1} \\ \boldsymbol{0}_{5N_s\times 1} \\ \grave{\boldsymbol{h}}_{j2} \end{bmatrix}, \tag{5.96}$$

where $\grave{\boldsymbol{M}}_S$ is similar to $\grave{\boldsymbol{M}}_S$ in (5.78) in Section 5.3.4.

The solution to (5.54) for the whole crossed-dipole antenna selection method with $J = M = 3$ is given by (5.57).

Optimisation of $\check{\boldsymbol{w}}_D$ and $\tilde{\boldsymbol{w}}_A$ is achieved iteratively:

(1) First, via initialising the digital coefficients $\check{\boldsymbol{w}}_D$ with random values, $\tilde{\boldsymbol{w}}_A$ is obtained by substituting $\check{w}_{D,j,m}(\{j,m\} \in \{0,1,2\})$ into (5.91).

(2) Given the obtained optimum values for $\tilde{\boldsymbol{w}}_A$ in step (1), the optimum values for $\check{\boldsymbol{w}}_D$ are obtained by (5.57).

(3) Given the obtained values of $\check{\boldsymbol{w}}_D$ in step (2), the new set of values of $\tilde{\boldsymbol{w}}_A$ can be obtained by (5.91) again.

(4) Repeat steps (2) and (3) until the cost function in (5.91) converges.

5.4 Design Examples

5.4.1 Design Examples for Methods in Sections 5.2.1 and 5.2.3

Design examples are provided to show the effectiveness of the proposed method based on sub-aperture and overlapped subarray architectures. The two beam directions are $\varphi_0 = -25^\circ$ and $\varphi_1 = 15^\circ$ and the corresponding sidelobe regions are selected as $\Theta_{side_0} \in [-90^\circ, -35^\circ] \cup [-15^\circ, 90^\circ]$ and $\Theta_{side_1} \in [-90^\circ, 5^\circ] \cup [25^\circ, 90^\circ]$, sampled every 1°. The number of sample points in the sidelobe region for each beam is $N_g = 162$ and antennas whose amplitude of weighting coefficients falls below 2×10^{-2} will be removed.

The adjacent antenna spacing is $d = \frac{\lambda}{3}$ and $N = 2N_s = 40$ equally spaced potential antennas are prepared for both the sub-aperture and overlapped subarray architectures. To have a fair comparison, we first obtain the two resultant beams using the method in Section 5.2.1 with the interleaved subarray architecture. Then, a ULA consisting of

two interleaved subarrays is formulated using (4.10) with $N = 2N_s = 40$ and the design results are represented by 'ULA design', i.e., the result without the proposed l_1 norm minimisation.

The trade-off factor in (5.2) and (5.10) is chosen as $\gamma = 0.60$. The resultant patterns of the two beams generated by the method in Section 5.2.1 with the interleaved subarray architecture and 'ULA design' are shown in Figure 5.2. For the 'ULA design', the change of the cost function in (4.10) with respect to the iteration number, the digital and analogue coefficients are listed in Figure 5.3, Tables 5.1 and 5.2, respectively; for the method in Section 5.2.1 with the interleaved subarray architecture, the change of the cost function in (5.2) with respect to the iteration number, the digital and analogue coefficients are listed in Figure 5.4, Tables 5.3 and 5.4, respectively.

As shown in Figure 5.2, the performance for 'ULA design' is obviously better than that generated by the method in Section 5.2.1 with the interleaved subarray architecture, as it uses all the available antennas.

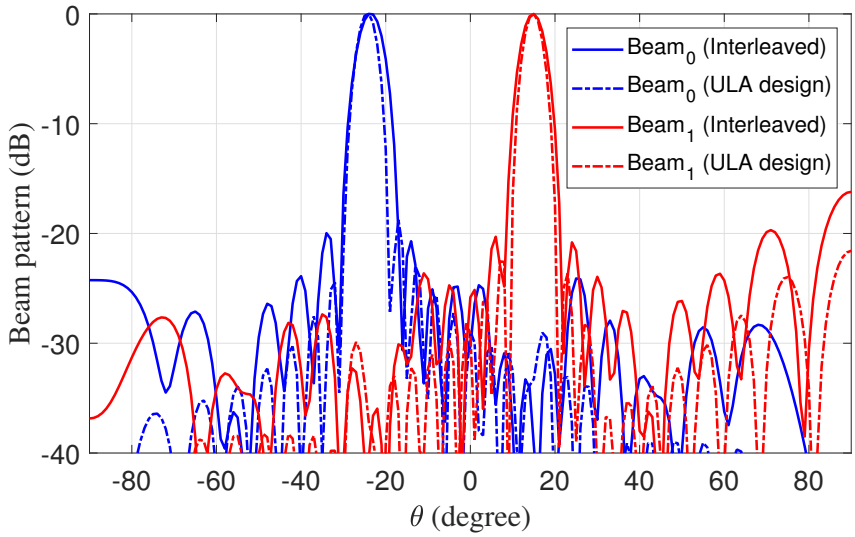

Figure 5.2: Beam patterns of the two beams with $\varphi_0 = -25°$ and $\varphi_1 = 15°$ generated by the method in Section 5.2.1 with the interleaved subarray architecture and 'ULA design', respectively.

Overall, the responses of the zeroth and first beams generated by the method in Section 5.2.1 with the interleaved and localised subarray architectures and the method in Section 5.2.3 with the overlapped subarray architecture are shown in Figures 5.5 and 5.6,

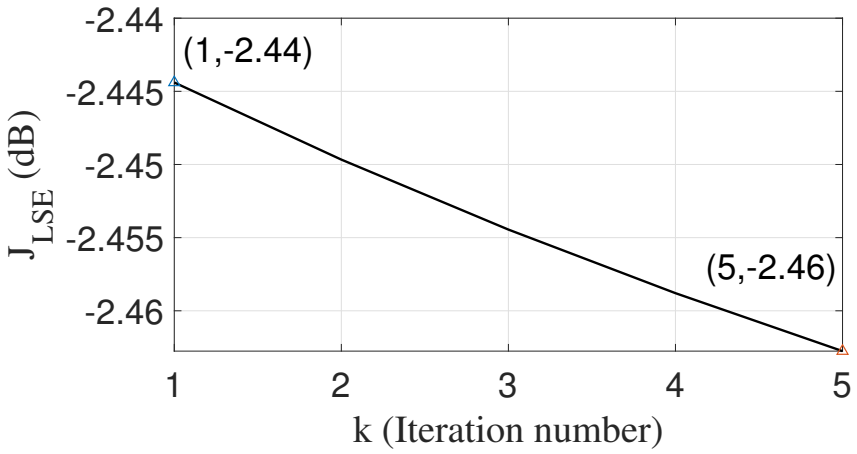

Figure 5.3: Cost function J_{LSE} in (4.10) with respect to the iteration number k generated by the 'ULA design' in Section 5.2.1.

Table 5.1: Digital coefficients $\boldsymbol{w}_{D,0}$ and $\boldsymbol{w}_{D,1}$ with $\varphi_0 = -25°$ and $\varphi_1 = 15°$ generated by the 'ULA design' in Section 5.2.1.

m \ j	$\boldsymbol{w}_{D,0}$	$\boldsymbol{w}_{D,1}$
0	0.9999+0.0250i	1.0007-0.0214i
1	-1.0005+0.0248i	0.9999+0.0210i

respectively. For the method in Section 5.2.1 with the localised architecture, the change of the cost function in (5.2), the digital and analogue coefficients are listed in Figure 5.7, Tables 5.5 and 5.6, respectively; for the method in Section 5.2.3 with the overlapped subarray architecture, the change of the cost function in (5.10), the digital and analogue coefficients are presented in Figure 5.8, Tables 5.7 and 5.8, respectively.

5.4.2 Design Examples for Methods in Sections 5.2.2 and 5.2.4

The three beam directions are $\varphi_0 = -30°$, $\varphi_1 = 0°$ and $\varphi_2 = 35°$ and the corresponding sidelobe regions are selected as $\Theta_{side_0} \in [-90°, -35°] \cup [-25°, 90°]$, $\Theta_{side_1} \in [-90°, -5°] \cup [5°, 90°]$ and $\Theta_{side_2} \in [-90°, 30°] \cup [40°, 90°]$ with $N_g = 172$. Antennas whose amplitude of weighting coefficients falls below 3×10^{-3} will be removed.

The adjacent antenna spacing is $d = \frac{\lambda}{5}$ and $N = 3N_s = 75$ equally spaced potential

Table 5.2: Analogue coefficients $\boldsymbol{w}_{A,0}$ and $\boldsymbol{w}_{A,1}$ with $\varphi_0 = -25°$ and $\varphi_1 = 15°$ generated by the 'ULA design' in Section 5.2.1.

n \ m	$\boldsymbol{w}_{A,0}$	$\boldsymbol{w}_{A,1}$	n \ m	$\boldsymbol{w}_{A,0}$	$\boldsymbol{w}_{A,1}$
0	0.0194-0.0057i	0.0071+0.0220i	10	0.0091-0.0040i	-0.0193-0.0425i
1	-0.0022-0.0006i	0.0155+0.0180i	11	0.0562-0.0392i	0.0297+0.0298i
2	-0.0251+0.0271i	-0.0189-0.0131i	12	0.0073-0.0100i	0.0498+0.0250i
3	-0.0058+0.0108i	-0.0414-0.0122i	13	-0.0165+0.0547i	-0.0194-0.0033i
4	0.0059-0.0458i	0.0139-0.0014i	14	0.0015+0.0285i	-0.0515+0.0105i
5	-0.0057-0.0317i	0.0552-0.0209i	15	-0.0131-0.0362i	0.0010+0.0016i
6	0.0225+0.0377i	0.0045-0.0021i	16	-0.0213-0.0253i	0.0264-0.0295i
7	0.0403+0.0352i	-0.0337+0.0561i	17	0.0136+0.0121i	0.0017-0.0118i
8	-0.0289-0.0100i	-0.0073+0.0267i	18	0.0267+0.0058i	-0.0037+0.0224i
9	-0.0675-0.0038i	-0.0075+0.0589i	19	0.0007-0.0053i	0.0064+0.0140i

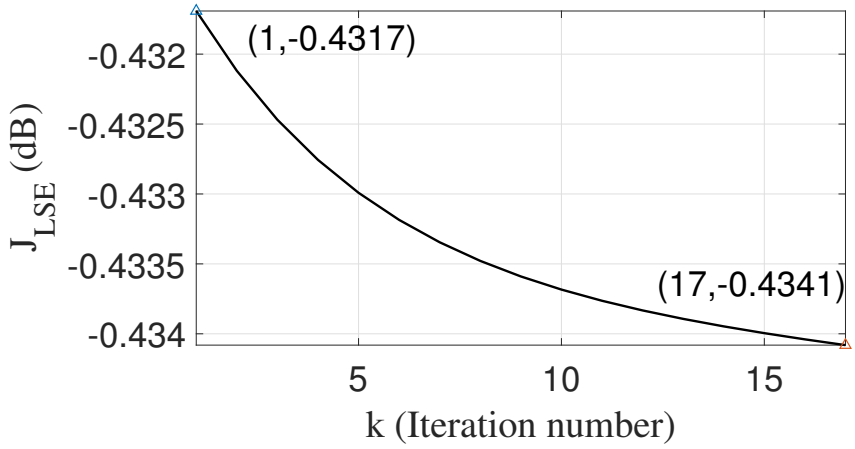

Figure 5.4: Cost function J_{LSE} in (5.2) with respect to the iteration number k generated by the method in Section 5.2.1 with the interleaved subarray architecture.

antennas are prepared for both the sub-aperture and overlapped subarray architectures and the trade-off factor in (5.3) and (5.23) is $\gamma = 0.6$. The patterns of the zeroth, first and second beams generated by the method in Section 5.2.2 with the interleaved and localised subarray architectures and the method in Section 5.2.4 with the overlapped subarray architecture are displayed in Figures 5.9, 5.10 and 5.11, respectively.

Table 5.3: Digital coefficients $\boldsymbol{w}_{D,0}$ and $\boldsymbol{w}_{D,1}$ with $\varphi_0 = -25°$ and $\varphi_1 = 15°$ generated by the method in Section 5.2.1 with the interleaved subarray architecture.

m \ j	$\boldsymbol{w}_{D,0}$	$\boldsymbol{w}_{D,1}$
0	1.0031+0.0255i	0.9977-0.0135i
1	-0.9972+0.0255i	1.0026+0.0133i

Table 5.4: Analogue coefficients $\boldsymbol{w}_{A,0}$ and $\boldsymbol{w}_{A,1}$ with $\varphi_0 = -25°$ and $\varphi_1 = 15°$ generated by the method in Section 5.2.1 with the interleaved subarray architecture.

n \ m	$\boldsymbol{w}_{A,0}$	$\boldsymbol{w}_{A,1}$	n \ m	$\boldsymbol{w}_{A,0}$	$\boldsymbol{w}_{A,1}$
0	-0.0177+0.0265i	-0.0236-0.0130i	7	0.0647-0.0418i	-0.0241-0.0511i
1	-0.0002-0.0516i	-0.0392-0.0047i	8	0.0119-0.0170i	0.0264+0.0322i
2	-0.0110-0.0283i	0.0221-0.0029i	9	-0.0242+0.0531i	0.0543+0.0333i
3	0.0308+0.0436i	0.0587-0.0301i	10	-0.0020+0.0344i	-0.0526+0.0014i
4	0.0511+0.0350i	-0.0365+0.0689i	11	-0.0041-0.0322i	0.0270-0.0191i
5	-0.0317-0.0119i	-0.0046+0.0312i	12	-0.0166-0.0277i	
6	-0.0805-0.0006i	-0.0069-0.0676i			

Table 5.5: Digital coefficients $\boldsymbol{w}_{D,0}$ and $\boldsymbol{w}_{D,1}$ with $\varphi_0 = -25°$ and $\varphi_1 = 15°$ generated by the method in Section 5.2.1 with the localised subarray architecture.

m \ j	$\boldsymbol{w}_{D,0}$	$\boldsymbol{w}_{D,1}$
0	0.6082+0.5462i	-0.0004+0.0042i
1	0.0006-0.0056i	-1.1817+0.2790i

For the method in Section 5.2.2 with the interleaved subarray architecture, the change of the cost function in (5.3) with respect to the iteration number, the digital and analogue coefficients are presented in Figure 5.12, Tables 5.9 and 5.10, respectively; with the localised subarray architecture, the change of the cost function, the digital and analogue coefficients are displayed in Figure 5.13 and Tables 5.11 and 5.12, respectively.

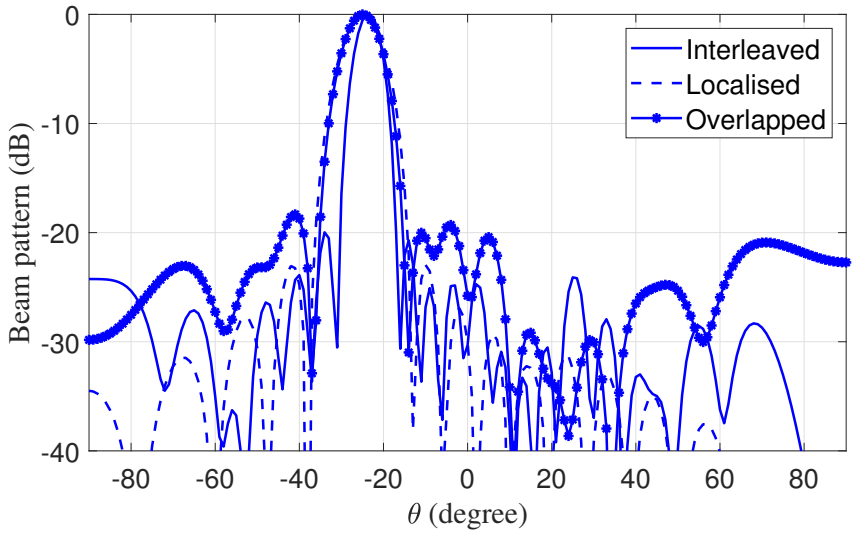

Figure 5.5: Beam patterns of the zeroth beam with $\varphi_0 = -25°$ generated by the method in Section 5.2.1 with the interleaved and localised subarray architectures and the method in Section 5.2.3 with the overlapped subarray architecture.

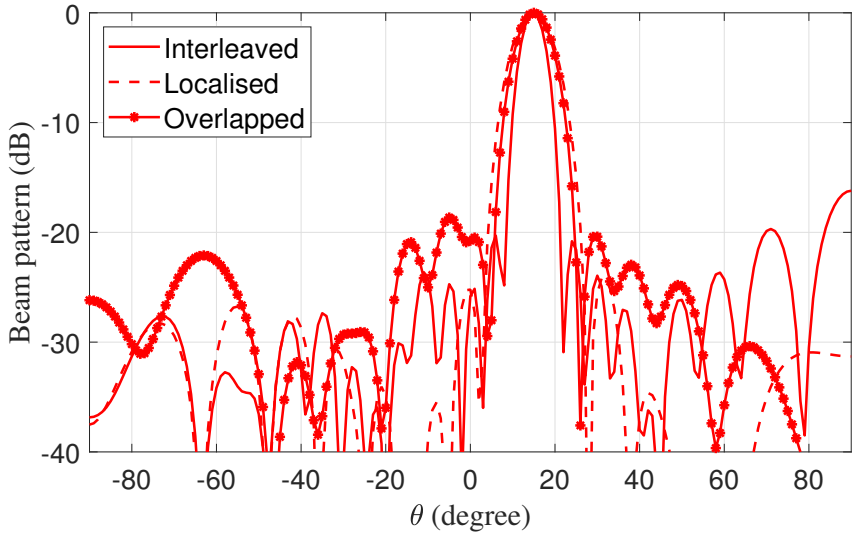

Figure 5.6: Beam patterns of the first beam with $\varphi_1 = 15°$ generated by the method in Section 5.2.1 with the interleaved and localised subarray architectures and the method in Section 5.2.3 with the overlapped subarray architecture.

As for the method in Section 5.2.4 with the overlapped subarray architecture, the change of the cost function (5.23) with respect to the iteration number, the digital and analogue coefficients are shown in Figure 5.14, Tables 5.13 and 5.14, respectively.

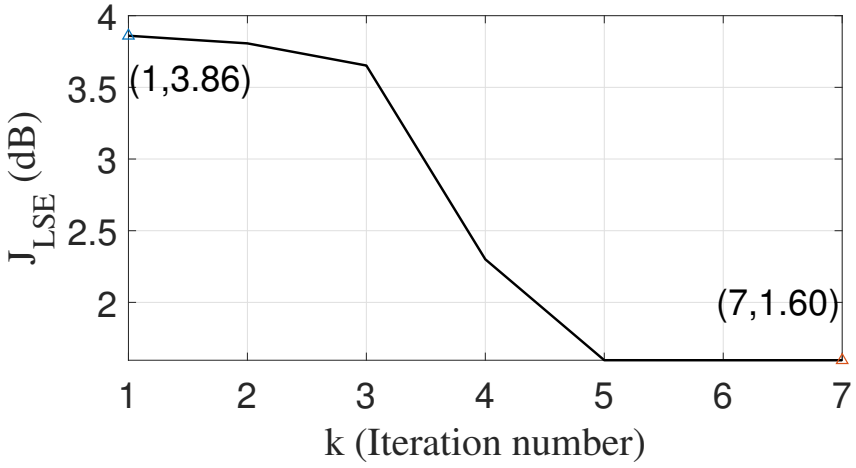

Figure 5.7: Cost function J_{LSE} in (5.2) with respect to the iteration number k generated by the method in Section 5.2.1 with the localised subarray architecture.

Table 5.6: Analogue coefficients $\boldsymbol{w}_{A,0}$ and $\boldsymbol{w}_{A,1}$ with $\varphi_0 = -25°$ and $\varphi_1 = 15°$ generated by the method in Section 5.2.1 with the localised subarray architecture.

n \ m	$\boldsymbol{w}_{A,0}$	$\boldsymbol{w}_{A,1}$	n \ m	$\boldsymbol{w}_{A,0}$	$\boldsymbol{w}_{A,1}$
0	0.0273-0.0209i	-0.0043+0.0240i	10	-0.0843+0.0112i	0.0144+0.0589i
1	-0.0144-0.0344i	-0.0341+0.0167i	11	-0.0424+0.0728i	-0.0111+0.0459i
2	-0.0271-0.0226i	-0.0248-0.0058i	12	0.0266+0.0758i	-0.0464+0.0423i
3	-0.0529+0.0140i	-0.0377-0.0340i	13	0.0676+0.0237i	-0.0333+0.0059i
4	-0.0250+0.0575i	-0.0120-0.0312i	14	0.0616-0.0304i	-0.0481-0.0146i
5	0.0355+0.0588i	0.0125-0.0622i	15	0.0099-0.0620i	-0.0179-0.0185i
6	0.0697+0.0164i	0.0332-0.0327i	16	-0.0371-0.0404i	-0.0032-0.0374i
7	0.0632-0.0495i	0.0586-0.0182i	17	-0.0350+0.0045i	0.0182-0.0159i
8	0.0035-0.0841i	0.0568+0.0129i	18	-0.0307+0.0213i	
9	-0.0651-0.0548i	0.0408+0.0425i	19	0.0117+0.0325i	

5.4.3 Design Examples for Methods in Sections 5.3.2 and 5.3.4

With $\phi = 90°$, the directions of the two beams and the corresponding sidelobe regions are the same as the case in Section 5.4.1 where the number of sample points is $N_g = 162$. In addition, the polarisation information is given by $\eta = 100°$ and $\sigma = 45°$. Antennas whose

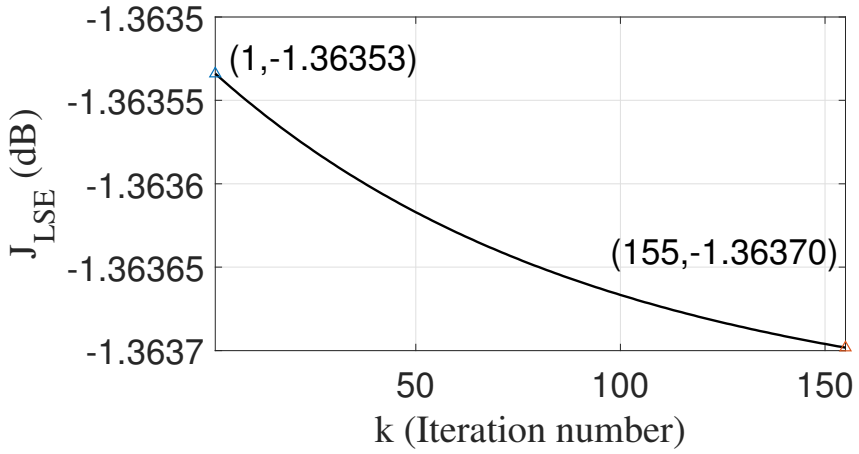

Figure 5.8: Cost function J_{LSE} in (5.10) with respect to the iteration number k generated by the method in Section 5.2.3 with the overlapped subarray architecture.

Table 5.7: Digital coefficients $\breve{\boldsymbol{w}}_{D,0}$ and $\breve{\boldsymbol{w}}_{D,1}$ with $\varphi_0 = -25^\circ$ and $\varphi_1 = 15^\circ$ generated by the method in Section 5.2.3 with the overlapped subarray architecture.

m \ j	$\breve{\boldsymbol{w}}_{D,0}$	$\breve{\boldsymbol{w}}_{D,1}$
0	0.9985+0.0034i	1.0017-0.0039i
1	-1.0016+0.0034i	0.9983+0.0039i

Table 5.8: Analogue coefficients $\breve{\boldsymbol{w}}_{A,0}$ and $\breve{\boldsymbol{w}}_{A,1}$ with $\varphi_0 = -25^\circ$ and $\varphi_1 = 15^\circ$ generated by the method in Section 5.2.3 with the overlapped subarray architecture.

n \ m	$\breve{\boldsymbol{w}}_{A,0}$	$\breve{\boldsymbol{w}}_{A,1}$	n \ m	$\breve{\boldsymbol{w}}_{A,0}$	$\breve{\boldsymbol{w}}_{A,1}$
0	0.0124+0.0218i	0.0237-0.0034i	7	0.0325-0.0237i	-0.0154-0.0344i
1	0.0179+0.0245i	0.0239-0.0078i	8	0.0305-0.0314i	0.0235+0.0224i
2	0.0334+0.0284i	0.0254-0.0150i	9	-0.0131+0.0352i	0.0297+0.0212i
3	-0.0491-0.0149i	-0.0247+0.0321i	10	0.0005+0.0335i	0.0409+0.0180i
4	-0.0457+0.0015i	-0.0144+0.0468i	11	-0.0080-0.0221i	-0.0342+0.0002i
5	-0.0247-0.0003i	-0.0049-0.0543i	12		-0.0209+0.0075i
6	0.0397-0.0196i	-0.0137-0.0385i			

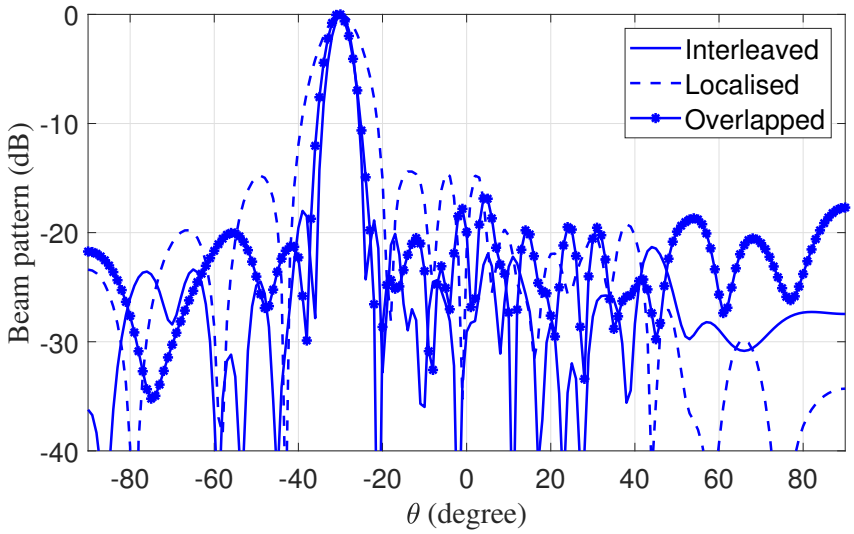

Figure 5.9: Beam patterns of the zeroth beam with $\varphi_0 = -30°$ generated by the method in Section 5.2.2 with the interleaved and localised subarray architectures and the method in Section 5.2.4 with the overlapped subarray architecture.

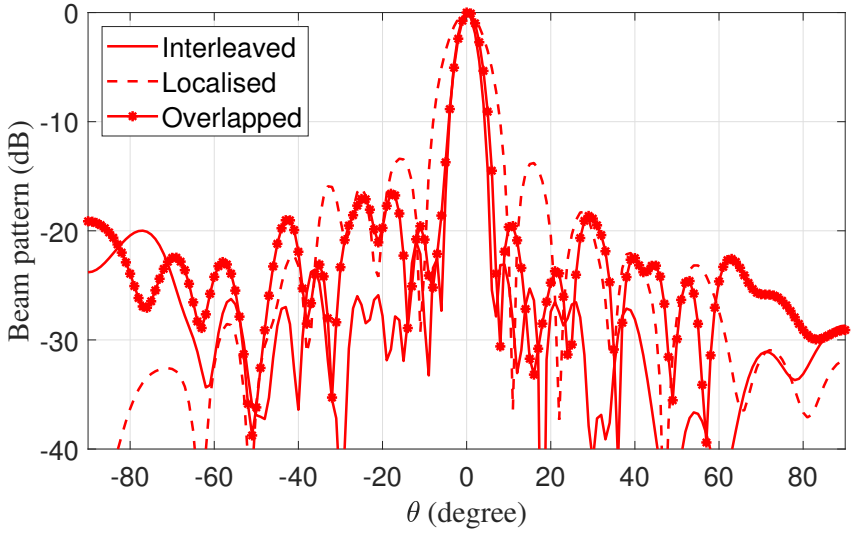

Figure 5.10: Beam patterns of the first beam with $\varphi_1 = 0°$ generated by the method in Section 5.2.2 with the interleaved and localised subarray architectures and the method in Section 5.2.4 with the overlapped subarray architecture.

amplitude of weighting coefficients falls below 1×10^{-2} will be removed.

The number of potential antennas for each subarray is $N_s = 25$ and the adjacent antenna spacing is $d = \frac{\lambda}{3}$. The trade-off factor in (5.50) and (5.75) is $\gamma = 0.5$. The design

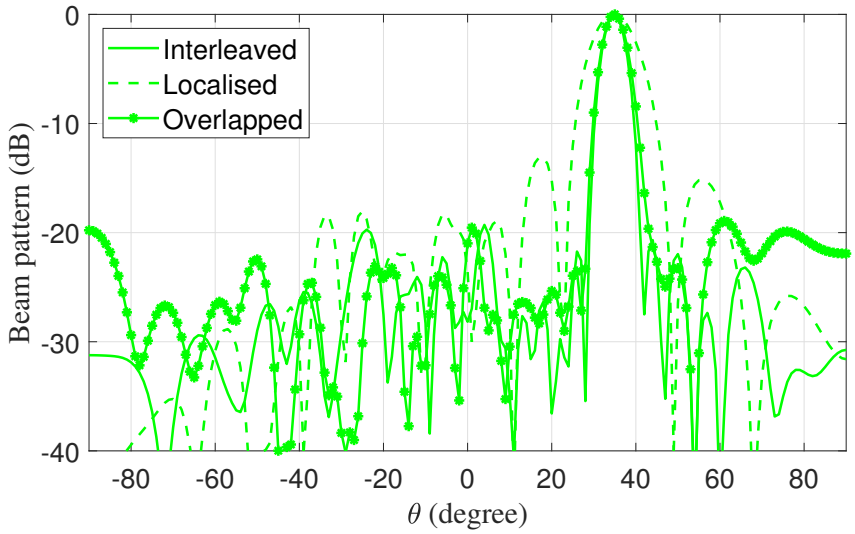

Figure 5.11: Beam patterns of the second beam with $\varphi_2 = 35°$ generated by the method in Section 5.2.2 with the interleaved and localised subarray architectures and the method in Section 5.2.4 with the overlapped subarray architecture.

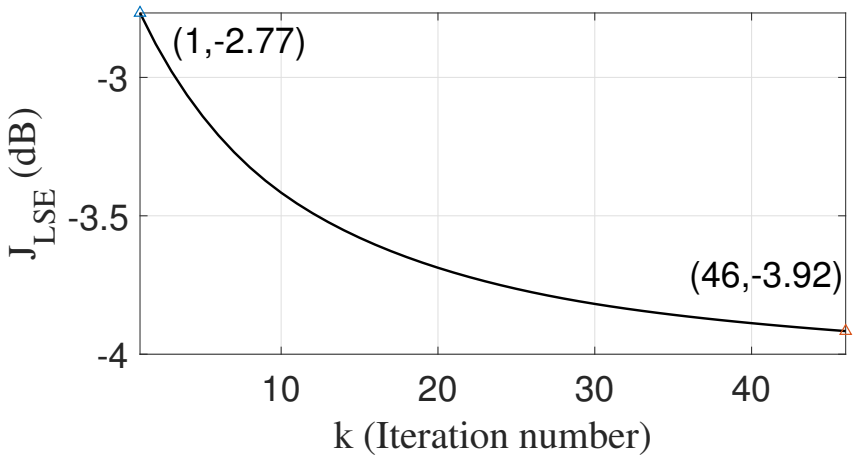

Figure 5.12: Cost function J_{LSE} in (5.3) with respect to the iteration number k generated by the method in Section 5.2.2 with the interleaved subarray architecture.

results generated by the method in Sections 5.3.2 with the interleaved and localised subarray architectures are represented by 'Interleaved (dipole selection)' and 'Localised (dipole selection)', respectively; and the design results generated by the method in Section 5.3.4 with the interleaved and localised subarray architectures are represented by 'Interleaved (antenna selection)' and 'Localised (antenna selection)', respectively.

The responses of the zeroth and first beams generated by 'Interleaved (dipole se-

Table 5.9: Digital coefficients $\boldsymbol{w}_{D,0}$, $\boldsymbol{w}_{D,1}$ and $\boldsymbol{w}_{D,2}$ with $\varphi_0 = -30°$, $\varphi_1 = 0°$ and $\varphi_2 = 35°$ generated by the method in Section 5.2.2 with the interleaved subarray architecture.

m \ j	$\boldsymbol{w}_{D,0}$	$\boldsymbol{w}_{D,1}$	$\boldsymbol{w}_{D,2}$
0	1.4139+2.1642i	3.1473-1.6133i	1.7837+4.4997i
1	2.8829+3.8112i	-2.2939-5.5635i	-4.9232-4.3008i
2	3.9811-4.5091i	4.2128-0.0159i	-0.7812-2.7842i

Table 5.10: Analogue coefficients $\boldsymbol{w}_{A,0}$, $\boldsymbol{w}_{A,1}$ and $\boldsymbol{w}_{A,2}$ with $\varphi_0 = -30°$, $\varphi_1 = 0°$ and $\varphi_2 = 35°$ generated by the method in Section 5.2.2 with the interleaved subarray architecture.

n \ m	$\boldsymbol{w}_{A,0}$	$\boldsymbol{w}_{A,1}$	$\boldsymbol{w}_{A,2}$
0	-0.0012+0.0029i	0.0009+0.0038i	0.0005+0.0030i
1	0.0047-0.0015i	-0.0004+0.0069i	0.0043-0.0011i
2	0.0033+0.0033i	-0.0030+0.0086i	0.0036-0.0035i
3	-0.0029+0.0041i	-0.0054+0.0077i	-0.0009+0.0031i
4	0.0075+0.0001i	-0.0002+0.0034i	0.0060+0.0008i
5	0.0059+0.0051i	0.0048+0.0009i	0.0079-0.0042i
6	-0.0044+0.0033i	-0.0058+0.0049i	0.0051+0.0025i
7	0.0089+0.0024i	-0.0017+0.0036i	0.0117-0.0021i
8	0.0080+0.0077i	0.0054+0.0029i	0.0023+0.0022i
9	-0.0043+0.0008i	-0.0041+0.0021i	0.0122+0.0017i
10	0.0083+0.0038i	-0.0026+0.0021i	0.0020-0.0042i
11	0.0081+0.01012i	0.0040+0.0039i	0.0090+0.0047i
12	0.0065+0.0035i	0.0018+0.0032i	0.0042-0.0033i
13	0.0057+0.0110i		0.0043+0.0047i
14	0.0048+0.0019i		0.0040-0.0011i
15	0.0024+0.0091i		0.0006-0.0032i
16	0.0035+0.0003i		
17	0.0000+0.0055i		

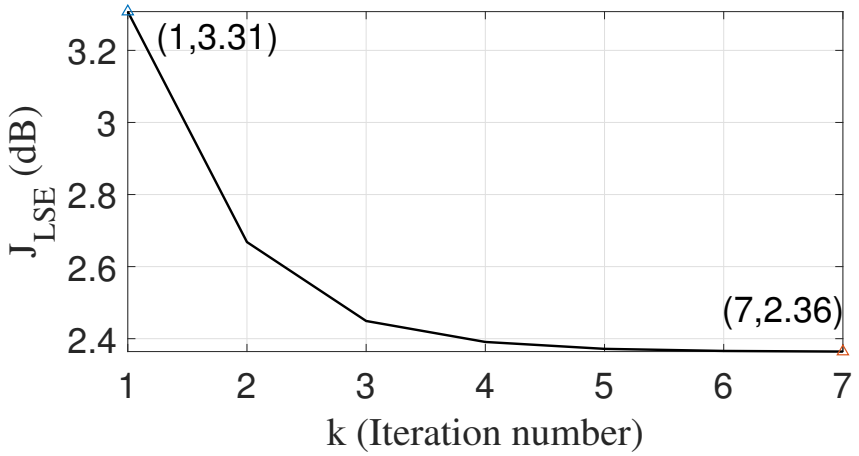

Figure 5.13: Cost function J_{LSE} in (5.3) with respect to the iteration number k generated by the method in Section 5.2.2 with the localised subarray architecture.

Table 5.11: Digital coefficients $\boldsymbol{w}_{D,0}$, $\boldsymbol{w}_{D,1}$ and $\boldsymbol{w}_{D,2}$ with $\varphi_0 = -30°$, $\varphi_1 = 0°$ and $\varphi_2 = 35°$ generated by the method in Section 5.2.2 with the localised subarray architecture.

m \ j	$\boldsymbol{w}_{D,0}$	$\boldsymbol{w}_{D,1}$	$\boldsymbol{w}_{D,2}$
0	0.7627-0.0739i	3.5621+3.4832i	0.0240-0.0647i
1	4.5649-6.2028i	-0.5104-0.5376i	0.3109+0.6342i
2	0.2046-0.2861i	-0.0136+0.0436i	2.2414-4.5061i

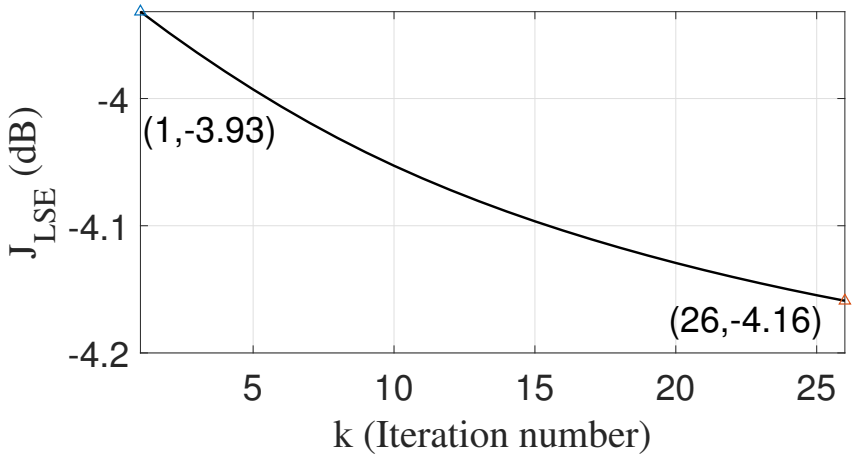

Figure 5.14: Cost function J_{LSE} in (5.23) with respect to the iteration number k generated by the method in Section 5.2.4 with the overlapped subarray architecture.

Table 5.12: Analogue coefficients $\boldsymbol{w}_{A,0}$, $\boldsymbol{w}_{A,1}$ and $\boldsymbol{w}_{A,2}$ with $\varphi_0 = -30°$, $\varphi_1 = 0°$ and $\varphi_2 = 35°$ generated by the method in Section 5.2.2 with the localised subarray architecture.

n \ m	$\boldsymbol{w}_{A,0}$	$\boldsymbol{w}_{A,1}$	$\boldsymbol{w}_{A,2}$
0	0.0148-0.0135i	-0.0055-0.0120i	0.0141-0.0158i
1	0.0079-0.0088i	-0.0025+0.0031i	0.0047+0.0177i
2	0.0127-0.0129i	-0.0072+0.0067i	0.0017+0.0091i
3	0.0025-0.0037i	0.0019+0.0103i	-0.0091+0.0064i
4	0.0202-0.0169i	0.0031+0.0020i	-0.0105-0.0028i
5	0.0218-0.0228i	0.0036-0.0011i	-0.0021-0.0065i
6	0.0149-0.0167i	0.0048-0.0091i	0.0113-0.0154i
7	0.0063-0.0032i	-0.0061-0.0047i	0.0098+0.0106i
8	0.0144-0.0116i	-0.0050-0.0007i	0.0012+0.0062i
9	0.0091-0.0103i	-0.0037+0.0041i	-0.0158+0.0058i
10	0.0137-0.0159i	-0.0021+0.0087i	-0.0026-0.0196i
11		0.0082+0.0040i	0.0064-0.0061i
12		0.0043-0.0014i	0.0065+0.0017i
13		0.0017-0.0039i	0.0063+0.0127i
14		-0.0033-0.0083i	-0.0045+0.0061i
15		-0.0079+0.0000i	-0.0109+0.0107i
16		-0.0054-0.0002i	-0.0028-0.0221i
17		0.0034+0.0122i	

Table 5.13: Digital coefficients $\breve{\boldsymbol{w}}_{D,0}$, $\breve{\boldsymbol{w}}_{D,1}$ and $\breve{\boldsymbol{w}}_{D,2}$ with $\varphi_0 = -30°$, $\varphi_1 = 0°$ and $\varphi_2 = 35°$ generated by the method in Section 5.2.4 with the overlapped subarray architecture.

m \ j	$\breve{\boldsymbol{w}}_{D,0}$	$\breve{\boldsymbol{w}}_{D,1}$	$\breve{\boldsymbol{w}}_{D,2}$
0	-3.2633-0.5000i	0.8392-4.2364i	-3.3422-2.7035i
1	-4.0600-3.4336i	-2.1647-1.7629i	2.2263+2.0223i
2	3.4947+4.3276i	2.6824-4.8840i	2.4512+0.3788i

Table 5.14: Analogue coefficients $\breve{\boldsymbol{w}}_{A,0}$, $\breve{\boldsymbol{w}}_{A,1}$ and $\breve{\boldsymbol{w}}_{A,2}$ with $\varphi_0 = -30°$, $\varphi_1 = 0°$ and $\varphi_2 = 35°$ generated by the method in Section 5.2.4 with the overlapped subarray architecture.

n \ m	$\breve{\boldsymbol{w}}_{A,0}$	$\breve{\boldsymbol{w}}_{A,1}$	$\breve{\boldsymbol{w}}_{A,2}$
0	0.0031+0.0017i	-0.0003+0.0033i	0.0028+0.0013i
1	0.0026+0.0025i	-0.0012+0.0053i	0.0048+0.0033i
2	0.0050+0.0068i	-0.0029+0.0077i	-0.0023+0.0027i
3	-0.0015+0.0030i	-0.0051+0.0082i	0.0055+0.0059i
4	0.0039+0.0081i	-0.0038+0.0031i	0.0011+0.0043i
5	0.0027+0.0028i	0.0053-0.0004i	0.0042+0.0074i
6	0.0010+0.0040i	-0.0034+0.0031i	0.0018+0.0053i
7	-0.0016+0.0082i	-0.0077+0.0047i	0.0022+0.0065i
8	0.0032-0.0008i	0.0043+0.0016i	0.0009+0.0068i
9	0.0005+0.0051i	0.0025+0.0018i	0.0010+0.0044i
10	-0.0019+0.0049i	-0.0096+0.0028i	-0.0005+0.0034i
11	0.0045+0.0000i	0.0042+0.0041i	
12	-0.0001+0.0034i	-0.0051-0.0002i	
13	-0.0016+0.0032i	0.0030+0.0057i	
14	0.0040+0.0007i		

lection)', 'Localised (dipole selection)', 'Interleaved (antenna selection)' and 'Localised (antenna selection)' are shown in Figures 5.15 and 5.16, respectively.

For the design in Section 5.3.2 with the interleaved subarray architecture, the change of the cost function in (5.50) with respect to the iteration number, the digital and analogue coefficients are shown in Figure 5.17, Tables 5.15 and 5.16, respectively; with the localised subarray architecture, the change of the cost function in (5.50) with respect to the iteration number, the digital and analogue coefficients are displayed in Figure 5.18, Tables 5.17 and 5.18, respectively.

For the design in Section 5.3.4 with the interleaved subarray architecture, the change of the cost function in (5.75), the corresponding digital and analogue coefficients are

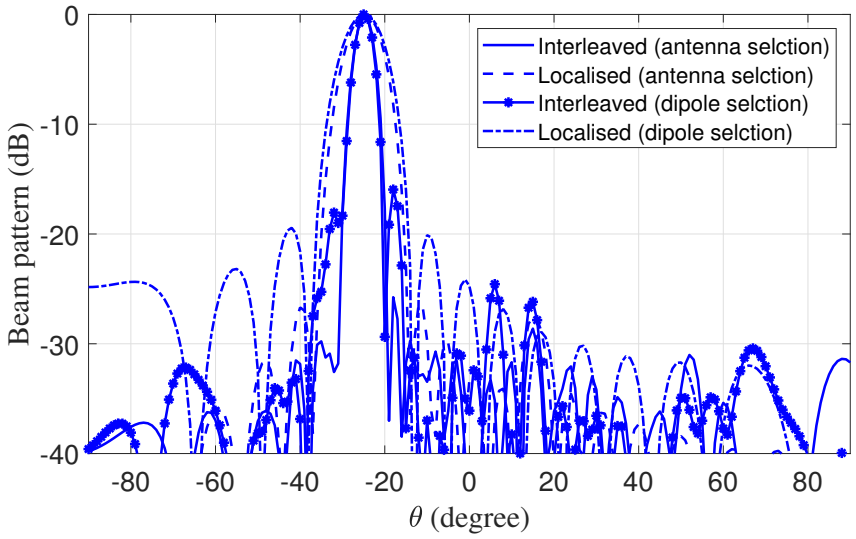

Figure 5.15: Beam patterns of the zeroth beam with $\varphi_0 = -25°$ generated by the method in Sections 5.3.2 and 5.3.4 with the interleaved and localised subarray architectures.

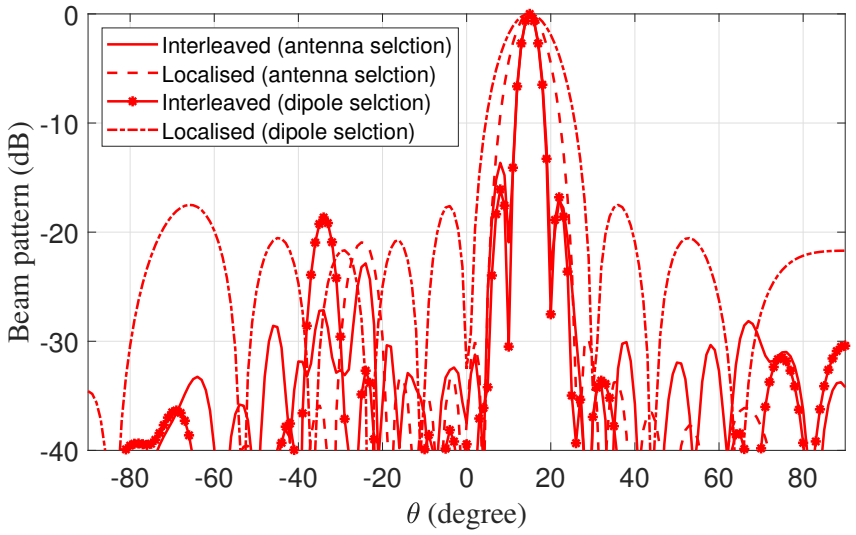

Figure 5.16: Beam patterns of the first beam with $\varphi_1 = 15°$ generated by the method in Sections 5.3.2 and 5.3.4 with the interleaved and localised subarray architectures.

shown in Figure 5.19, Tables 5.19 and 5.20, respectively; with the localised subarray architecture, the change of the cost function in (5.75), the corresponding digital and analogue coefficients are displayed in Figure 5.20, Tables 5.21 and 5.22, respectively.

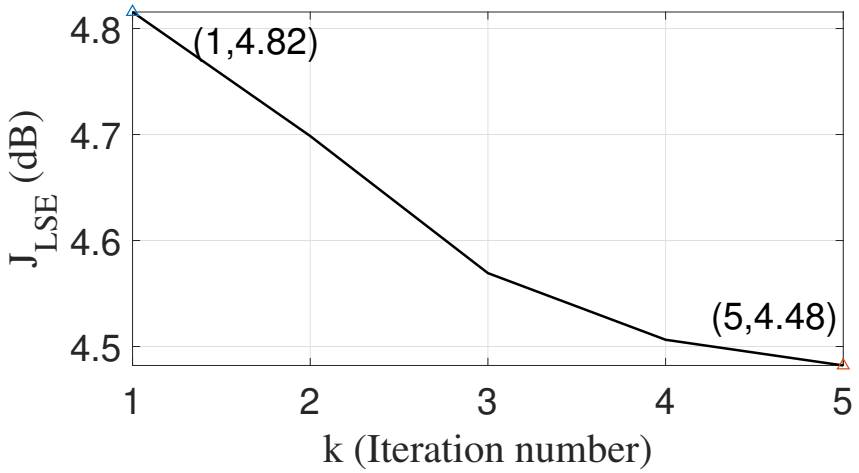

Figure 5.17: Cost function J_{LSE} in (5.50) with respect to the iteration number k generated by the method in Section 5.3.2 with the interleaved subarray architecture.

Table 5.15: Digital coefficients $\check{\boldsymbol{w}}_{D,0}$ and $\check{\boldsymbol{w}}_{D,1}$ with $\varphi_0 = -25°$ and $\varphi_1 = 15°$ generated by the method in Section 5.3.2 with the interleaved subarray architecture.

m \ j	$\check{\boldsymbol{w}}_{D,0}$	$\check{\boldsymbol{w}}_{D,1}$
0	0.9152+0.7591i	-0.4030-0.2577i
1	0.1012-0.7403i	0.1230-0.4837i

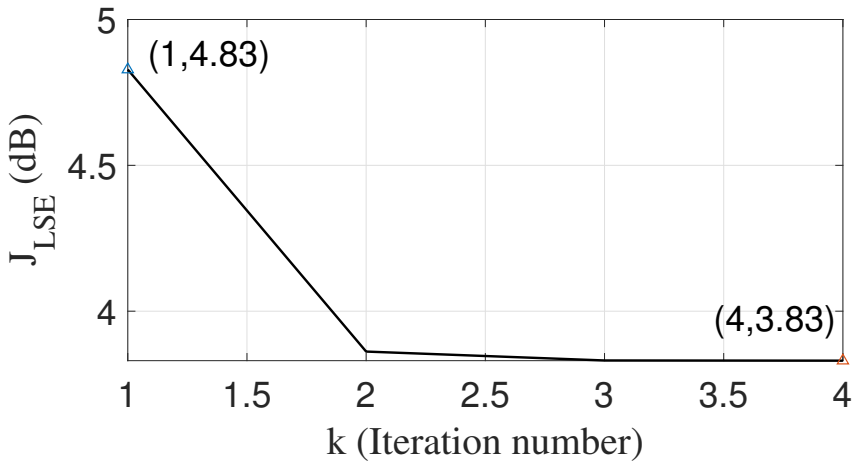

Figure 5.18: Cost function J_{LSE} in (5.50) with respect to the iteration number k generated by the method in Section 5.3.2 with the localised subarray architecture.

Table 5.16: Analogue coefficients $\check{\boldsymbol{w}}_{A,0}$ and $\check{\boldsymbol{w}}_{A,1}$ with $\varphi_0 = -25°$ and $\varphi_1 = 15°$ generated by the method in Section 5.3.2 with the interleaved subarray architecture.

n \ m	$\check{\boldsymbol{w}}_{A,0}$	$\check{\boldsymbol{w}}_{A,1}$	n \ m	$\check{\boldsymbol{w}}_{A,0}$	$\check{\boldsymbol{w}}_{A,1}$
0	0.0076-0.0109i	0.0007-0.0126i	14	-0.0536+0.0731i	-0.0570-0.0898i
1	-0.0415-0.0125i	0.0148+0.0029i	15	-0.0387+0.0331i	0.0802-0.0324i
2	-0.0336+0.0011i	0.0340+0.0315i	16	-0.0133-0.0740i	0.1161+0.0162i
3	0.0284-0.0553i	-0.0200+0.0234i	17	0.0046-0.0739i	-0.0051+0.0561i
4	0.0492-0.0596i	-0.0617+0.0067i	18	0.0327+0.0185i	-0.0501+0.0456i
5	0.0179+0.0451i	-0.0063+0.0474i	19	0.0237+0.0242i	0.0404+0.0679i
6	0.0096+0.0712i	-0.0209-0.0382i	20	0.0434-0.0249i	-0.0433-0.0227i
7	0.0413+0.0039i	0.0358-0.0479i	21	-0.0160+0.0615i	0.0014-0.0808i
8	-0.0183+0.0026i	-0.0667-0.0708i	22	0.0105-0.0064i	-0.0553-0.0080i
9	-0.0210-0.0148i	0.0583-0.0086i	23	-0.0073-0.0126i	0.0365-0.0364i
10	-0.0743+0.0673i	0.0167+0.0755i	24		0.0705+0.0628i
11	0.0255-0.0023i	0.0789-0.0057i	25		0.0173+0.0531i
12	0.0011-0.0914i	-0.0287+0.0766i	26		-0.0460+0.0056i
13	0.0141+0.0055i	-0.1045-0.0540i	27		-0.0328-0.0124i

Table 5.17: Digital coefficients $\check{\boldsymbol{w}}_{D,0}$ and $\check{\boldsymbol{w}}_{D,1}$ with $\varphi_0 = -25°$ and $\varphi_1 = 15°$ generated by the method in Section 5.3.2 with the localised subarray architecture.

m \ j	$\check{\boldsymbol{w}}_{D,0}$	$\check{\boldsymbol{w}}_{D,1}$
0	-0.0084-0.0010i	1.7973-6.8311i
1	2.1889+2.0972i	0.0039+0.0009i

5.4.4 Design Examples for Methods in Sections 5.3.3 and 5.3.5

With $\phi = 0°$, the directions of the three beams are the same as the case in Section 5.4.2 and the corresponding sidelobe regions are $\Theta_{side_0} \in [-90°, -40°] \cup [-20°, 90°]$, $\Theta_{side_1} \in [-90°, -10°] \cup [10°, 90°]$ and $\Theta_{side_2} \in [-90°, 25°] \cup [45°, 90°]$, where the number of sample points for each designed beam is $N_g = 162$. Moreover, the polarisation information is

Table 5.18: Analogue coefficients $\check{\boldsymbol{w}}_{A,0}$ and $\check{\boldsymbol{w}}_{A,1}$ with $\varphi_0 = -25°$ and $\varphi_1 = 15°$ generated by the method in Section 5.3.2 with the localised subarray architecture.

n \ m	$\check{\boldsymbol{w}}_{A,0}$	$\check{\boldsymbol{w}}_{A,1}$	n \ m	$\check{\boldsymbol{w}}_{A,1}$
0	0.0018+0.0148i	-0.0110+0.0050i	10	0.0286+0.0049i
1	-0.0166+0.0117i	-0.0038+0.0146i	11	0.0210-0.0180i
2	-0.0217-0.0107i	0.0115+0.0142i	12	-0.0006-0.0272i
3	-0.0009-0.0256i	0.0197+0.0004i	13	-0.0193-0.0150i
4	0.0208-0.0122i	0.0151-0.0170i	14	-0.0222+0.0047i
5	0.0174+0.0105i	-0.0035-0.0242i	15	-0.0093+0.0173i
6	-0.0008+0.0149i	-0.0233-0.0139i	16	0.0067+0.0170i
7		-0.0260+0.0094i	17	0.0146+0.0039i
8		-0.0099+0.0273i	18	0.0098-0.0071i
9		0.0143+0.0246i		

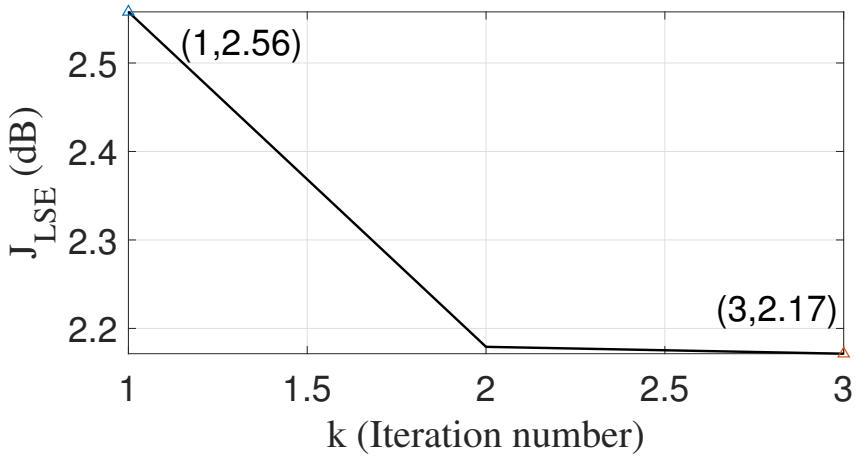

Figure 5.19: Cost function J_{LSE} in (5.75) with respect to the iteration number k generated by the method in Section 5.3.4 with the interleaved subarray architecture.

given by $\eta = 100°$ and $\sigma = 45°$ and antennas whose amplitude of weighting coefficients falls below 5×10^{-4} will be removed.

The number of potential antennas for each subarray is $N_s = 25$ and the adjacent antenna spacing is $d = \frac{\lambda}{5}$. The trade-off factor in (5.59) and (5.91) is $\gamma = 0.5$ and the responses of the zeroth, first and second beams generated by the method in Sections

Table 5.19: Digital coefficients $\check{\boldsymbol{w}}_{D,0}$ and $\check{\boldsymbol{w}}_{D,1}$ with $\varphi_0 = -25°$ and $\varphi_1 = 15°$ generated by the method in Section 5.3.4 with the interleaved subarray architecture.

m \ j	$\check{\boldsymbol{w}}_{D,0}$	$\check{\boldsymbol{w}}_{D,1}$
0	-0.0360-0.4840i	0.1973-0.2002i
1	0.0235+0.3151i	0.4480-0.4543i

Table 5.20: Analogue coefficients $\tilde{\boldsymbol{w}}_{A,0}$ and $\tilde{\boldsymbol{w}}_{A,1}$ with $\varphi_0 = -25°$ and $\varphi_1 = 15°$ generated by the method in Section 5.3.4 with the interleaved subarray architecture.

n \ m	$\tilde{\boldsymbol{w}}_{A,0}(x)$	$\tilde{\boldsymbol{w}}_{A,0}(y)$	n \ m	$\tilde{\boldsymbol{w}}_{A,1}(x)$	$\tilde{\boldsymbol{w}}_{A,1}(y)$
0	-0.0022-0.0137i	-0.0075+0.0002i	0	0.0073-0.0172i	-0.0087-0.0119i
1	-0.0131+0.0008i	-0.0034+0.0079i	1	0.0072+0.0406i	0.0407+0.0058i
2	0.0213+0.0205i	0.0171-0.0098i	2	-0.0509-0.0397i	-0.0505+0.0403i
3	0.0324-0.0110i	0.0049-0.0287i	3	-0.0243-0.0377i	-0.0416+0.0155i
4	-0.0390-0.0064i	-0.0142+0.0253i	4	0.0720-0.0104i	0.0058-0.0641i
5	-0.0474+0.0469i	0.0228+0.0621i	5	0.0690+0.0044i	0.0165-0.0680i
6	0.0314+0.0074i	0.0041-0.0274i	6	-0.0326+0.0441i	0.0338+0.0352i
7	0.0237-0.0922i	-0.0843-0.0553i	7	-0.0546+0.0569i	0.0450+0.0706i
8	-0.0267-0.0018i	-0.0098+0.0261i	8	-0.0055-0.0266i	-0.0243-0.0006i
9	0.0326+0.1020i	0.1128-0.0051i	9	0.0008-0.0769i	-0.0799-0.0214i
10	0.0492+0.0050i	0.0144-0.0496i	10	0.0382+0.0579i	0.0704-0.0410i
11	-0.0737-0.0675i	-0.0859+0.0580i	11	0.0076+0.0196i	0.0173-0.0034i
12	-0.0682+0.0218i	0.0123+0.0738i	12	-0.0627-0.0145i	-0.0226+0.0660i
13	0.0788+0.0231i	0.0422-0.0777i	13	-0.0375-0.0143i	-0.0152+0.0296i
14	0.0615-0.0557i	-0.0555-0.0676i	14	0.0410-0.0275i	-0.0269-0.0428i
15	-0.0612+0.0065i	0.0009+0.0666i	15	0.0406-0.0194i	-0.0117-0.0363i
16	-0.0328+0.0826i	0.0805+0.0330i	16	-0.0010+0.0262i	0.0299+0.0023i
17	0.0330-0.0158i	-0.0159-0.0346i	17	-0.0090+0.0326i	0.0242+0.0122i
18	-0.0107-0.0821i	-0.0765+0.0130i	18	-0.0077-0.0133i	-0.0100+0.0051i
19	0.0407+0.0457i	0.0409-0.0365i			
20	0.0198-0.0030i	-0.0019-0.0142i			
21	-0.0320-0.0122i	-0.0042+0.0246i			
22	-0.0127+0.0109i	0.0043+0.0106i			

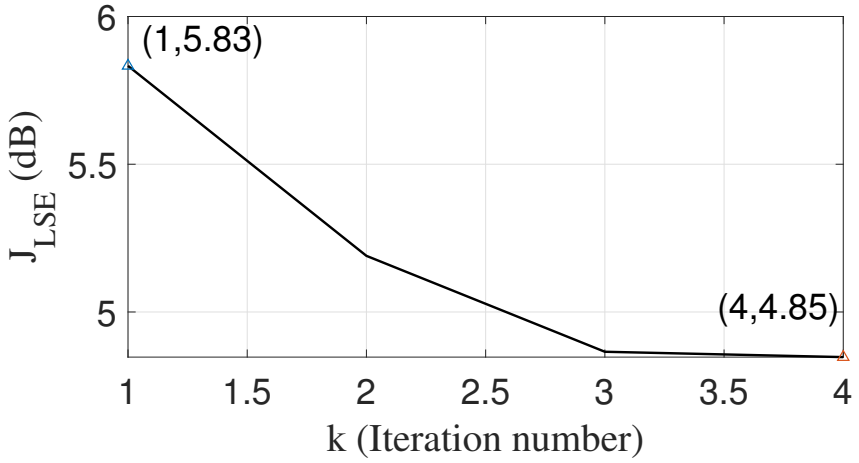

Figure 5.20: Cost function J_{LSE} in (5.75) with respect to the iteration number k generated by the method in Section 5.3.4 with the localised subarray architecture.

Table 5.21: Digital coefficients $\check{\boldsymbol{w}}_{D,0}$ and $\check{\boldsymbol{w}}_{D,1}$ with $\varphi_0 = -25°$ and $\varphi_1 = 15°$ generated by the method in Section 5.3.4 with the localised subarray architecture.

m \ j	$\check{\boldsymbol{w}}_{D,0}$	$\check{\boldsymbol{w}}_{D,1}$
0	0.0002+0.0003i	-0.2043-0.1818i
1	-0.3071-0.4159i	-0.0010-0.0007i

5.3.3 and 5.3.5 with the interleaved and localised subarray architectures are displayed in Figures 5.21, 5.22 and 5.23, respectively.

For the method in Section 5.3.3 with the interleaved subarray architecture, the change of the cost function in (5.59) with respect to the iteration number, the digital and analogue coefficients are shown in Figure 5.24, Tables 5.23 and 5.24, respectively; with the localised subarray architecture, the change of the cost function in (5.59) with respect to the iteration number, the digital and analogue coefficients are presented in Figure 5.25, Tables 5.25 and 5.26, respectively.

For the method in Section 5.3.5 with the interleaved subarray architecture, the change of the cost function in (5.91) with respect to the iteration number, the digital and analogue coefficients are shown in Figure 5.26, Tables 5.27 and Tables 5.28, 5.29, 5.30, respectively; with the localised subarray architecture, the change of the cost function in (5.91) with

Table 5.22: Analogue coefficients $\tilde{\boldsymbol{w}}_{A,0}$ and $\tilde{\boldsymbol{w}}_{A,1}$ with $\varphi_0 = -25°$ and $\varphi_1 = 15°$ generated by the method in Section 5.3.4 with the localised subarray architecture.

n \ m	$\tilde{\boldsymbol{w}}_{A,0}(x)$	$\tilde{\boldsymbol{w}}_{A,0}(y)$	n \ m	$\tilde{\boldsymbol{w}}_{A,1}(x)$	$\tilde{\boldsymbol{w}}_{A,1}(y)$
0	0.0361+0.0018i	0.0064+0.0360i	0	-0.0108+0.0189i	0.0157+0.0167i
1	0.0489+0.0154i	0.0264-0.0437i	1	0.0152+0.0230i	0.0228-0.0102i
2	0.0420+0.0429i	0.0467-0.0306i	2	0.0261+0.0084i	0.0111-0.0225i
3	0.0072+0.0703i	0.0667+0.0033i	3	0.0312-0.0214i	-0.0139-0.0310i
4	-0.0349+0.0617i	0.0549+0.0428i	4	0.0034-0.0502i	-0.0441-0.0114i
5	-0.1207+0.0802i	0.0549+0.0428i	5	-0.0458-0.0409i	-0.0438+0.0354i
6	-0.0893+0.0102i	-0.0060+0.0865i	6	-0.0654+0.0093i	-0.0020+0.0590i
7	-0.1651-0.0782i	-0.1011+0.1430i	7	-0.0377+0.0596i	0.0474+0.0429i
8	-0.0365-0.0613i	-0.0647+0.0244i	8	0.0253+0.0754i	0.0715-0.0089i
9	0.0068-0.2616i	-0.2461-0.0480i	9	0.0827+0.0327i	0.0419-0.0708i
10	0.0324-0.0564i	-0.0488-0.0402i	10	0.0814-0.0463i	-0.0286-0.0798i
11	0.2433-0.1514i	-0.1035-0.2613i	11	0.0168-0.0898i	-0.0772-0.0272i
12	0.0324+0.0001i	0.0062-0.0304i	12	-0.0596-0.0692i	-0.0719+0.0399i
13	0.2541+0.1822i	0.2093-0.2091i	13	-0.0926-0.0003i	-0.0148+0.0837i
14	0.0080+0.0183i	0.0187-0.0051i	14	-0.0595+0.0727i	0.0562+0.0664i
15	-0.0070+0.2923i	0.2861+0.0615i	15	0.0158+0.0849i	0.0775-0.0034i
16	-0.2248+0.0841i	0.0404+0.2182i	16	0.0693+0.0357i	0.0431-0.0550i
17	-0.1534-0.1114i	-0.1391+0.1337i	17	0.0650-0.0263i	-0.0128-0.0615i
18	0.0233-0.0990i	-0.0836-0.0371i	18	0.0208-0.0641i	-0.0550-0.0309i
19	0.0669-0.0184i	-0.0098-0.0744i	19	-0.0305-0.0502i	-0.0490+0.0208i
20			20	-0.0475-0.0044i	-0.0110+0.0417i
21			21	-0.0245+0.0257i	0.0183+0.0250i
22			22	0.0028+0.0299i	0.0280+0.0035i
23			23	0.0197+0.0171i	0.0186-0.0155i

respect to the iteration number, the digital and analogue coefficients are shown in Figure 5.27, Tables 5.31 and 5.32, 5.33, 5.34, respectively.

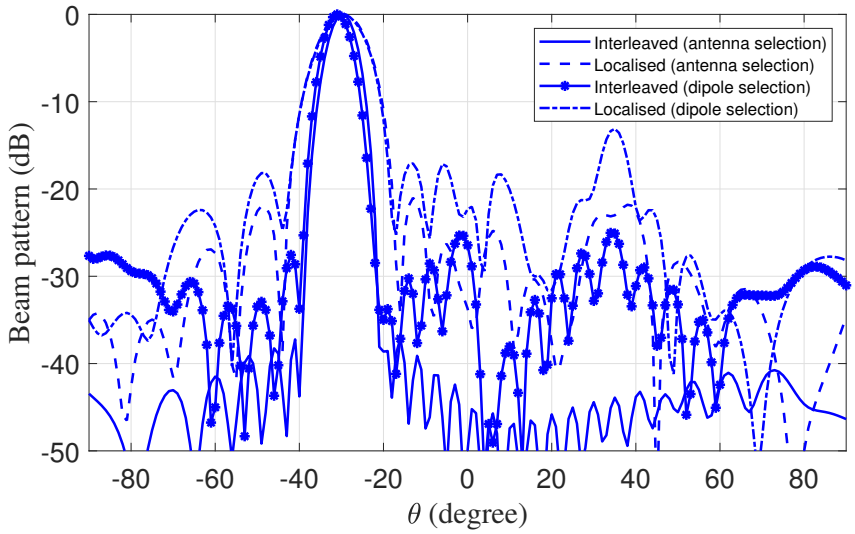

Figure 5.21: Beam patterns of the zeroth beam with $\varphi_0 = -30°$ generated by the method in Sections 5.3.3 and 5.3.5 with the interleaved and localised subarray architectures.

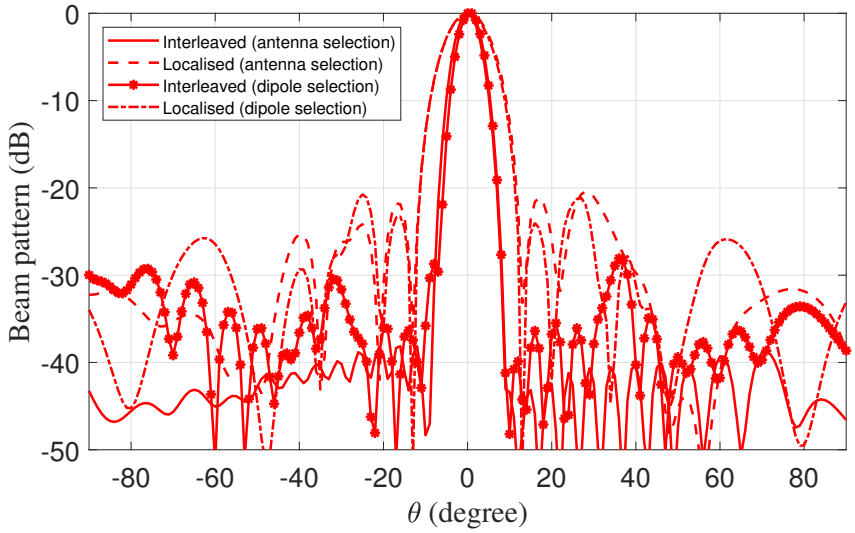

Figure 5.22: Beam patterns of the first beam with $\varphi_1 = 0°$ generated by the method in Sections 5.3.3 and 5.3.5 with the interleaved and localised subarray architectures.

5.4.5 Performance Discussion on Methods in Sections 5.2 and 5.3

Overall, the mean value of the total sidelobe responses $\bar{P}_s$, the number of antennas, i.e., $||\boldsymbol{w}||_0$ for the sub-aperture subarray architectures ($||\breve{\boldsymbol{w}}_A||_0$ for the overlapped subarray architecture), and the indexes of the antennas are compared for the two-beam and three-

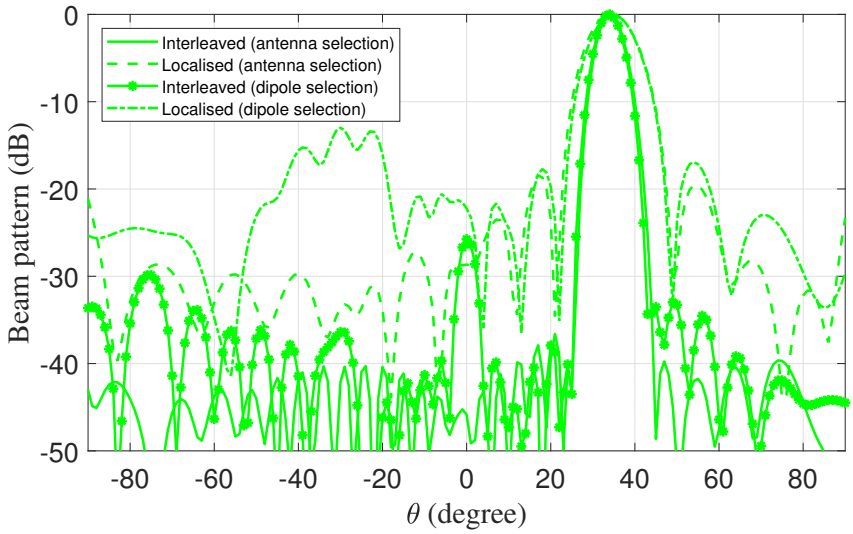

Figure 5.23: Beam patterns of the second beam with $\varphi_2 = 35^\circ$ generated by the method in Sections 5.3.3 and 5.3.5 with the interleaved and localised subarray architectures.

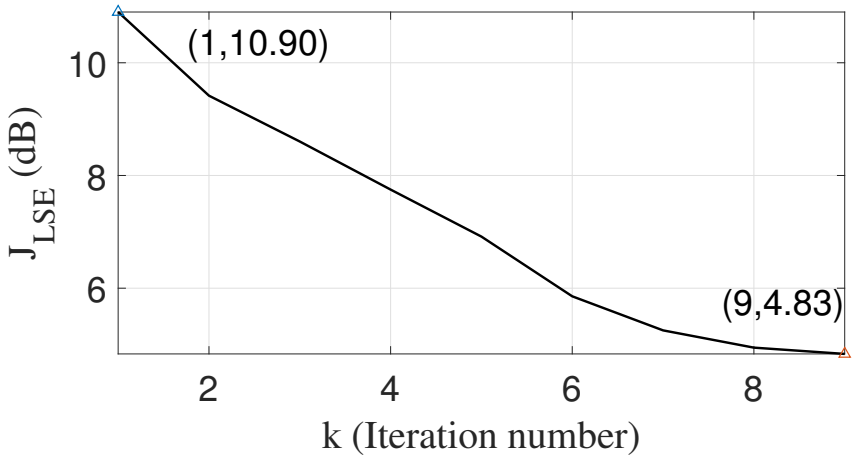

Figure 5.24: Cost function J_{LSE} in (5.59) with respect to the iteration number k generated by the method in Section 5.3.3 with the interleaved subarray architecture.

beam cases generated by the methods in Sections 5.2.1 (Section 5.2.3) and Section 5.2.2 (Section 5.2.4) in Tables 5.35 and 5.36, respectively. Since the antennas indexed by 12, 19, 21 and 23 are overlapped for the two-beam case and 45 and 54 are overlapped for the three-beam case. Since the number of employed antenna channels is $||\breve{\boldsymbol{w}}_A||_0 = 25$ and $||\breve{\boldsymbol{w}}_A||_0 = 40$ for the two-user and three-user cases, the total number of antennas for the overlapped subarray architecture is 21 and 38, respectively.

Moreover, $\bar{P}_s$ and the number of dipoles (or antennas), i.e., $||\breve{\boldsymbol{w}}||_0$ (or $\frac{||\tilde{\mathbf{w}}||_0}{5}$) are com-

Table 5.23: Digital coefficients $\check{\boldsymbol{w}}_{D,0}$, $\check{\boldsymbol{w}}_{D,1}$ and $\check{\boldsymbol{w}}_{D,2}$ with $\varphi_0 = -30°$, $\varphi_1 = 0°$ and $\varphi_2 = 35°$ generated by the method in Section 5.3.3 with the interleaved subarray architecture.

m \ j	$\check{\boldsymbol{w}}_{D,0}$	$\check{\boldsymbol{w}}_{D,1}$	$\check{\boldsymbol{w}}_{D,2}$
0	18.0194+0.6830i	20.7692-0.9484i	-20.3796-0.6238i
1	-32.2175-0.5644i	-22.5883+1.5614i	-1.7159+0.9703i
2	42.8450+0.6540i	13.9430-1.9325i	11.4011-1.0900i

Table 5.24: Analogue coefficients $\check{\boldsymbol{w}}_{A,0}$, $\check{\boldsymbol{w}}_{A,1}$ and $\check{\boldsymbol{w}}_{A,2}$ with $\varphi_0 = -30°$, $\varphi_1 = 0°$ and $\varphi_2 = 35°$ generated by the method in Section 5.3.3 with the interleaved subarray architecture.

n \ m	$\check{\boldsymbol{w}}_{A,0}$	$\check{\boldsymbol{w}}_{A,1}$	$\check{\boldsymbol{w}}_{A,2}$	n \ m	$\check{\boldsymbol{w}}_{A,0}$	$\check{\boldsymbol{w}}_{A,1}$	$\check{\boldsymbol{w}}_{A,2}$
0	-0.0006+0.0003i	-0.0005-0.0003i	0.0011-0.0001i	15	-0.0010-0.0017i	0.0145+0.0022i	0.0109+0.0019i
1	0.0008-0.0012i	0.0026-0.0013i	0.0010-0.0006i	16	0.0075+0.0018i	0.0145+0.0015i	0.0022-0.0053i
2	0.0014+0.0006i	-0.0002-0.0007i	-0.0004-0.0011i	17	0.0017-0.0028i	0.0022-0.0080i	0.0056-0.0020i
3	-0.0020+0.0009i	0.0014+0.0005i	0.0030+0.0002i	18	-0.0057+0.0011i	0.0149+0.0035i	0.0006+0.0009i
4	0.0026-0.0029i	0.0006-0.0003i	0.0035-0.0012i	19	0.0028-0.0015i	-0.0015-0.0005i	0.0053+0.0023i
5	0.0029+0.0009i	0.0058-0.0023i	-0.0015-0.0042i	20	-0.0010-0.0023i	0.0064+0.0011i	0.0023-0.0033i
6	0.0002-0.0018i	-0.0014-0.0059i	0.0048+0.0011i	21	0.0069+0.0023i	0.0033-0.0056i	0.0046-0.0004i
7	-0.0036+0.0012i	0.0034+0.0007i	0.0065-0.0016i	22	0.0019-0.0024i	0.0093+0.0034i	0.0020+0.0016i
8	0.0006+0.0011i	0.0006-0.0019i	-0.0008-0.0083i	23	-0.0033-0.0001i	-0.0004-0.0004i	0.0020+0.0004
9	0.0041-0.0034i	0.0069-0.0016i	0.0007-0.0010i	24	0.0021-0.0015i	-0.0004-0.0008i	
10	-0.0012-0.0013i	-0.0020-0.0154i	0.0052+0.0025i	25	0.0148-0.0131i	0.0026+0.0008i	
11	0.0043+0.0010i	0.0030+0.0005i	0.0118-0.0011i	26	-0.0010+0.0000i	0.0004-0.0006i	
12	0.0017-0.0039i	0.0026-0.0067i	0.0016-0.0068i	27	0.0004-0.0010i	0.0032+0.0018i	
13	-0.0062+0.0018i	0.0187-0.0011i	0.0035-0.0023i	28	0.0016+0.0014i	0.0004-0.0003i	
14	0.0049-0.0030i	0.0002-0.0082i	0.0029+0.0029i				

pared for the two-beam and three-beam cases generated by the individual dipole selection and whole antenna selection methods in Sections 5.3.2 (Section 5.3.4) and Section 5.3.3 (Section 5.3.5) in Tables 5.37 and 5.38, respectively.

As shown in the beam responses (Figures 5.5 and 5.6 for the two-user case and Figures 5.9, 5.10 and 5.11 for the three-user case) and Tables 5.35 and 5.36, the beamwidth of each of the multiple beams generated by the localised subarray architecture is the widest

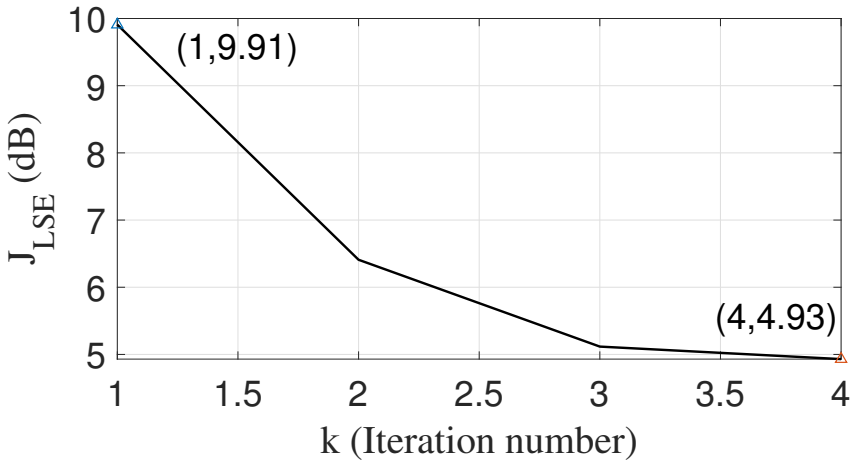

Figure 5.25: Cost function J_{LSE} in (5.59) with respect to the iteration number k generated by the method in Section 5.3.3 with the localised subarray architecture.

Table 5.25: Digital coefficients $\check{\boldsymbol{w}}_{D,0}$, $\check{\boldsymbol{w}}_{D,1}$ and $\check{\boldsymbol{w}}_{D,2}$ with $\varphi_0 = -30°$, $\varphi_1 = 0°$ and $\varphi_2 = 35°$ generated by the method in Section 5.3.3 with the localised subarray architecture.

m \ j	$\check{\boldsymbol{w}}_{D,0}$	$\check{\boldsymbol{w}}_{D,1}$	$\check{\boldsymbol{w}}_{D,2}$
0	6.2242+0.5470i	149.1934+3.5533i	1.2924+0.4855i
1	-82.2014+3.4024i	-0.6135+2.0848i	-22.6064+0.4303i
2	-18.2272+6.2611i	1.1136-0.1611i	-108.2200-3.5179i

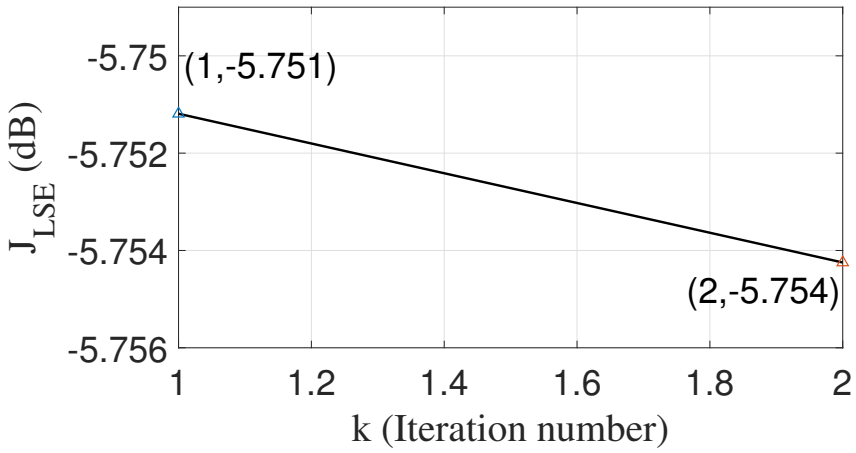

Figure 5.26: Cost function J_{LSE} in (5.91) with respect to the iteration number k generated by the method in Section 5.3.5 with the interleaved subarray architecture.

Table 5.26: Analogue coefficients $\check{\boldsymbol{w}}_{A,0}$, $\check{\boldsymbol{w}}_{A,1}$ and $\check{\boldsymbol{w}}_{A,2}$ with $\varphi_0 = -30°$, $\varphi_1 = 0°$ and $\varphi_2 = 35°$ generated by the method in Section 5.3.3 with the localised subarray architecture.

n \ m	$\check{\boldsymbol{w}}_{A,0}$	$\check{\boldsymbol{w}}_{A,1}$	$\check{\boldsymbol{w}}_{A,2}$
0	-0.0003+0.0015i	-0.0033+0.0011i	0.0018-0.0006i
1	0.0003-0.0014i	0.0046+0.0003i	-0.0019+0.0040i
2	-0.0006-0.0000i	-0.0001-0.0012i	0.0013-0.0023i
3	-0.0002+0.0010i	0.0005+0.0004i	0.0015-0.0007i
4	-0.0002+0.0014i	0.0007-0.0002i	-0.0013+0.0022i
5	-0.0008+0.0000i	-0.0023-0.0012i	0.0004-0.0006i
6	-0.0002+0.0011i	0.0000+0.0010i	-0.0001-0.0012i
7	-0.0008+0.0000i	-0.0007-0.0004i	0.0006+0.0005i
8	-0.0002+0.0014i	0.0002+0.0006i	0.0011+0.0004i
9	-0.0002+0.0011i	-0.0002+0.0009i	-0.0001+0.0012i
10	-0.0006+0.0000i	0.0018-0.0006i	-0.0016+0.0006i
11	0.0001-0.0014i	-0.0003-0.0011i	0.0009-0.0008i
12	-0.0002+0.0015i	-0.0018-0.0010i	0.0008-0.0007i
13		-0.0008-0.0006i	0.0017-0.0002i
14		0.0005+0.0008i	-0.0010+0.0017i
15		0.0019+0.0025i	-0.0031-0.0002i
16		0.0001-0.0030i	

Table 5.27: Digital coefficients $\check{\boldsymbol{w}}_{D,0}$, $\check{\boldsymbol{w}}_{D,1}$ and $\check{\boldsymbol{w}}_{D,2}$ with $\varphi_0 = -30°$, $\varphi_1 = 0°$ and $\varphi_2 = 35°$ generated by the method in Section 5.3.5 with the interleaved subarray architecture.

m \ j	$\check{\boldsymbol{w}}_{D,0}$	$\check{\boldsymbol{w}}_{D,1}$	$\check{\boldsymbol{w}}_{D,2}$
0	1.4617+0.0000i	2.0968+0.0000i	-12.5385-0.0000i
1	7.5534-0.0000i	8.5673+0.0000i	-4.7630-0.0000i
2	-2.2396-0.0000i	5.0794-0.0000i	9.7547+0.0000i

Table 5.28: Analogue coefficients $\tilde{\boldsymbol{w}}_{A,0}$ with $\varphi_0 = -30°$, $\varphi_1 = 0°$ and $\varphi_2 = 35°$ generated by the method in Section 5.3.5 with the interleaved subarray architecture.

n \ m	$\tilde{\boldsymbol{w}}_{A,0}(x)$	$\tilde{\boldsymbol{w}}_{A,0}(y)$	n \ m	$\tilde{\boldsymbol{w}}_{A,0}(x)$	$\tilde{\boldsymbol{w}}_{A,0}(y)$
0	0.0013+0.0012i	-0.0015+0.0007i	12	-0.0108+0.0094i	0.0080+0.0103i
1	-0.0011-0.0002i	0.0000+0.0001i	13	-0.0023+0.0067i	0.0057+0.0045i
2	-0.0010-0.0003i	-0.0001+0.0016i	14	-0.0009-0.0129i	-0.0130-0.0022i
3	0.0019+0.0021i	0.0012-0.0012i	15	-0.0101+0.0022i	0.0026+0.0106i
4	-0.0024-0.0021i	-0.0017+0.0011i	16	-0.0058+0.0083i	0.0045+0.0069i
5	-0.0046-0.0023i	-0.0022+0.0057i	17	0.0029-0.0064i	-0.0049-0.0039i
6	0.0015+0.0076i	0.0047-0.0009i	18	-0.0043-0.0011i	-0.0012+0.0045i
7	-0.0017-0.0031i	-0.0020+0.0010i	19	-0.0055+0.0041i	-0.0012+0.0045i
8	-0.0085-0.0072i	-0.0103+0.0086i	20	0.0017-0.0011i	-0.0004-0.0021i
9	-0.0042+0.0116i	0.0100+0.0043i	21	-0.0003-0.0007i	-0.0007+0.0007i
10	-0.0005+0.0009i	0.0008+0.0008i	22	-0.0029+0.0009i	-0.0003+0.0007i
11	-0.0070-0.0140i	-0.0151+0.0051i	23	0.0006+0.0000i	-0.0001+0.0002i

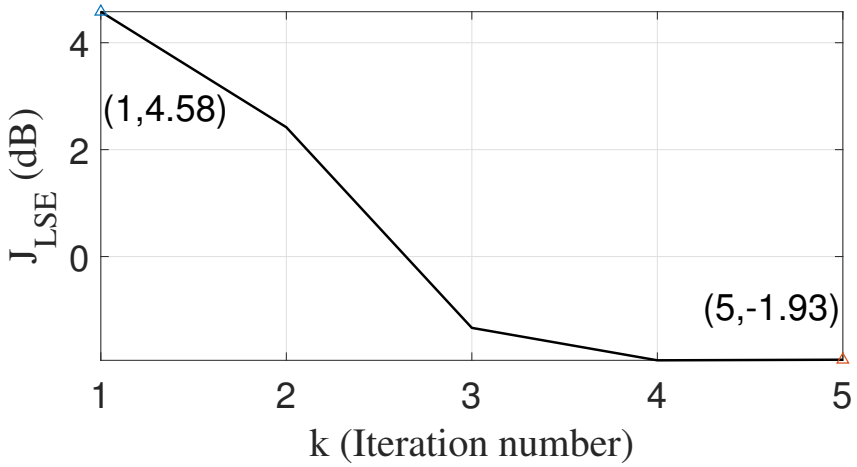

Figure 5.27: Cost function J_{LSE} in (5.91) with respect to the iteration number k generated by the method in Section 5.3.5 with the localised subarray architecture.

while the interleaved architecture gives the narrowest result for each beam. The number of active antennas for the overlapped subarray architecture is the fewest among the three subarray architectures as it has the the most degrees of freedom due to the maximum

Table 5.29: Analogue coefficients $\tilde{\boldsymbol{w}}_{A,1}$ with $\varphi_0 = -30°$, $\varphi_1 = 0°$ and $\varphi_2 = 35°$ generated by the method in Section 5.3.5 with the interleaved subarray architecture.

n \ m	$\tilde{\boldsymbol{w}}_{A,1}(x)$	$\tilde{\boldsymbol{w}}_{A,1}(y)$	n \ m	$\tilde{\boldsymbol{w}}_{A,1}(x)$	$\tilde{\boldsymbol{w}}_{A,1}(y)$
0	-0.0006+0.0004i	0.0002-0.0002i	11	0.0013-0.0087i	-0.0077-0.0021i
1	-0.0002-0.0010i	-0.0005-0.0004i	12	-0.0082+0.0002i	-0.0004+0.0069i
2	-0.0017+0.0001i	-0.0007+0.0019i	13	0.0002+0.0075i	0.0061+0.0013i
3	0.0010+0.0024i	0.0022-0.0005i	14	0.0044-0.0044i	-0.0034+0.0044i
4	0.0016-0.0019i	-0.0011-0.0019i	15	-0.0044-0.0032i	-0.0029+0.0034i
5	-0.0041-0.0027i	-0.0035+0.0037i	16	-0.0029+0.0047i	0.0029+0.0032i
6	-0.0015+0.0055i	0.0046+0.0019i	17	0.0030-0.0003i	0.0003-0.0025i
7	0.0046+0.0001i	0.0011-0.0041i	18	-0.0005-0.0023i	-0.0019+0.0002i
8	-0.0033-0.0074i	-0.0077+0.0025i	19	-0.0021+0.0011i	0.0002+0.0019i
9	-0.0066+0.0050i	0.0039+0.0060i	20	0.0006+0.0005i	0.0007-0.0005i
10	0.0045+0.0052i	0.0051-0.0028i			

Table 5.30: Analogue coefficients $\tilde{\boldsymbol{w}}_{A,2}$ with $\varphi_0 = -30°$, $\varphi_1 = 0°$ and $\varphi_2 = 35°$ generated by the method in Section 5.3.5 with the interleaved subarray architecture.

n \ m	$\tilde{\boldsymbol{w}}_{A,2}(x)$	$\tilde{\boldsymbol{w}}_{A,2}(y)$	n \ m	$\tilde{\boldsymbol{w}}_{A,2}(x)$	$\tilde{\boldsymbol{w}}_{A,2}(y)$
0	-0.0012+0.0002i	-0.0003+0.0011i	11	-0.0045+0.0085i	0.0063+0.0064i
1	-0.0004+0.0013i	0.0012+0.0008i	12	-0.0004-0.0049i	-0.0044-0.0003i
2	0.0001-0.0014i	-0.0012-0.0005i	13	-0.0134-0.0051i	-0.0063+0.0117i
3	-0.0046-0.0014i	-0.0022+0.0045i	14	-0.0081+0.0066i	0.0038+0.0087i
4	-0.0045+0.0042i	0.0030+0.0043i	15	0.0008+0.0005i	0.0007-0.0006i
5	0.0012-0.0004i	-0.0002-0.0010i	16	-0.0052-0.0045i	-0.0051+0.0041i
6	-0.0076-0.0059i	-0.0064+0.0057i	17	-0.0058+0.0015i	0.0008+0.0059i
7	-0.0123+0.0045i	0.0026+0.0122i	18	-0.0002+0.0019i	0.0015+0.0004i
8	0.0002+0.0045i	0.0037+0.0007i	19	-0.0006-0.0016i	-0.0014+0.0004i
9	-0.0048-0.0088i	-0.0079+0.0038i	20	-0.0016-0.0001i	-0.0006+0.0018i
10	-0.0177+0.0022i	-0.0029+0.0155i	21	-0.0006+0.0006i	0.0006+0.0002i

Table 5.31: Digital coefficients $\check{\boldsymbol{w}}_{D,0}$, $\check{\boldsymbol{w}}_{D,1}$ and $\check{\boldsymbol{w}}_{D,2}$ with $\varphi_0 = -30°$, $\varphi_1 = 0°$ and $\varphi_2 = 35°$ generated by the method in Section 5.3.5 with the localised subarray architecture.

m \ j	$\check{\boldsymbol{w}}_{D,0}$	$\check{\boldsymbol{w}}_{D,1}$	$\check{\boldsymbol{w}}_{D,2}$
0	1.8273-0.0535i	-0.1286-0.0769i	-83.3013-0.4824i
1	47.4426-0.0572i	-1.1127-0.0685i	0.4486+0.0114i
2	-0.8998-0.0512i	40.5920+0.9504i	0.1779-0.0146i

Table 5.32: Analogue coefficients $\tilde{\boldsymbol{w}}_{A,0}$ with $\varphi_0 = -30°$, $\varphi_1 = 0°$ and $\varphi_2 = 35°$ generated by the method in Section 5.3.5 with the localised subarray architecture.

n \ m	$\tilde{\boldsymbol{w}}_{A,0}(x)$	$\tilde{\boldsymbol{w}}_{A,0}(y)$	n \ m	$\tilde{\boldsymbol{w}}_{A,0}(x)$	$\tilde{\boldsymbol{w}}_{A,0}(y)$
0	0.0053+0.0015i	-0.0043+0.0023i	8	0.0001-0.0005i	-0.0003+0.0016i
1	-0.0018+0.0077i	0.0022+0.0012i	9	-0.0004-0.0001i	-0.0007+0.0003i
2	0.0006+0.0004i	-0.0008+0.0012i	10	-0.0006-0.0003i	-0.0008-0.0017i
3	-0.0002-0.0006i	0.0015+0.0014i	11	0.0013+0.0003i	-0.0008-0.0017i
4	-0.0007-0.0004i	-0.0010+0.0018i	12	0.0004+0.0004i	0.0005+0.0005i
5	-0.0002+0.0001i	-0.0010-0.0004i	13	-0.0009+0.0002i	-0.0004+0.0020i
6	0.0006+0.0002i	-0.0005-0.0044i	14	0.0000+0.0005i	0.0001+0.0004i
7	0.0008-0.0000i	0.0020+0.0032i	15	-0.0061-0.0008i	0.0003-0.0069i

number of analogue channels.

In Tables 5.37 and 5.38, the number of dipoles required for the dipole selection method is much fewer than that of the whole antenna selection method with both the interleaved and localised subarray architectures. Furthermore, as shown in Figures 5.15 and 5.16 for the two-user case and Figures 5.21, 5.22 and 5.23 for the three-user case, the beam width generated by each of the dipole selection and antenna selection methods with the localised subarray architecture is wider than that by the interleaved subarray architecture based on the crossed-dipole arrays.

Table 5.33: Analogue coefficients $\tilde{\boldsymbol{w}}_{A,1}$ with $\varphi_0 = -30°$, $\varphi_1 = 0°$ and $\varphi_2 = 35°$ generated by the method in Section 5.3.5 with the localised subarray architecture.

n \ m	$\tilde{\boldsymbol{w}}_{A,1}(x)$	$\tilde{\boldsymbol{w}}_{A,1}(y)$	n \ m	$\tilde{\boldsymbol{w}}_{A,1}(x)$	$\tilde{\boldsymbol{w}}_{A,1}(y)$
0	-0.0017-0.0036i	0.0096-0.0021i	7	0.0009-0.0038i	0.0008+0.0009i
1	0.0000+0.0052i	-0.0119-0.0022i	8	-0.0018+0.0006i	-0.0021+0.0001i
2	-0.0003-0.0007i	0.0010+0.0008i	9	-0.0008-0.0005i	0.0032+0.0024i
3	-0.0004-0.0004i	-0.0002+0.0001i	10	0.0007+0.0028i	-0.0015-0.0023i
4	0.0012+0.0008i	-0.0014+0.0001i	11	-0.0017+0.0058i	-0.0101-0.0074i
5	0.0005+0.0003i	0.0031+0.0017i	12	0.0026-0.0036i	0.0055+0.0085i
6	0.0014+0.0023i	-0.0015-0.0024i			

Table 5.34: Analogue coefficients $\tilde{\boldsymbol{w}}_{A,2}$ with $\varphi_0 = -30°$, $\varphi_1 = 0°$ and $\varphi_2 = 35°$ generated by the method in Section 5.3.5 with the localised subarray architecture.

n \ m	$\tilde{\boldsymbol{w}}_{A,2}(x)$	$\tilde{\boldsymbol{w}}_{A,2}(y)$	n \ m	$\tilde{\boldsymbol{w}}_{A,2}(x)$	$\tilde{\boldsymbol{w}}_{A,2}(y)$
0	0.0011+0.0006i	-0.0010+0.0039i	6	-0.0029+0.0001i	-0.0000+0.0006i
1	-0.0010+0.0003i	-0.0007+0.0026i	7	-0.0006+0.0000i	-0.0008+0.0035i
2	-0.0006-0.0001i	-0.0000+0.0001i	8	-0.0007+0.0002i	-0.0000+0.0006i
3	-0.0009+0.0002i	-0.0009+0.0042i	9	-0.0008-0.0003i	-0.0005+0.0023i
4	-0.0030+0.0001i	0.0003+0.0006i	10	0.0026-0.0008i	0.0001+0.0052i
5	-0.0004-0.0001i	-0.0009+0.0034i			

5.5 Summary

The optimum antenna selection problem for multi-beam multiplexing design based on both isotropic and polarisation-sensitive antennas has been solved through a series of proposed l_1 norm minimisation methods. First, the design based on isotropic antennas with the overlapped subarray architecture has provided a better result due to more degrees of freedom available. Second, by choosing to either select the individual dipoles of each crossed-dipole antenna or select the whole crossed-dipole antennas, two methods for

Table 5.35: Summary of performances for the two beams generated by the method in Section 5.2.1 with the interleaved and localised subarray architectures and the method in Section 5.2.3 with the overlapped subarray architecture.

Architecture	Interleaved	Localised	Overlapped
$\|\|\boldsymbol{w}_A\|\|_0(\|\|\breve{\boldsymbol{w}}_A\|\|_0)$	25	38	25(21)
$\bar{P}_s(dB)$	-27.33	-29.63	-24.73
Indexes of the antennas	4, 5, 7-12, 14-19, 21-26, 28-30, 32, 33	0-20, 22-37, 39	10-30

Table 5.36: Summary of performances for the three beams generated by the method in Section 5.2.2 with the interleaved and localised subarray architectures and the method in Section 5.2.4 with the overlapped subarray architecture.

Architecture	Interleaved	Localised	Overlapped
$\|\|\boldsymbol{w}_A\|\|_0(\|\|\breve{\boldsymbol{w}}_A\|\|_0)$	47	46	40(38)
$\bar{P}_s(dB)$	-25.72	-16.31	-21.82
Indexes of the antennas	$6-9$, 11, 12, 14-18, 20, 21, 23-25, 27, 29, 30, 32-34, 36-41, 43-46, 48-50, 52-55, 57-59, 62, 63, $65-67$	0, 3, 4, 7, 8, 12, 16, 17, 20, 21, 24-27, $30-33$, 35, 36, 38, 39, 41-44, 47-52, 55-58, 60, 61, 64, 66-69, 72-74	3, 9, 12, 14, 15, 18, 21, 23, 24, 26, 27, $29-31$, 33, 35, 36, 38-45, $47-49$, 51, 52, 54, 56-58, 60, 61, 63, 66

Table 5.37: Summary of performances for the two beams generated by the dipole selection and antenna selection methods in Sections 5.3.2 and 5.3.4, respectively, with the interleaved and localised subarray architectures.

Architecture	Interleaved (dipole selection)	Localised (dipole selection)	Interleaved (antenna selection)	Localised (antenna selection)
$\|\|\check{\boldsymbol{w}}_A\|\|_0(\frac{\|\|\tilde{\boldsymbol{w}}_A\|\|_0}{5})$	52(42)	26(26)	84(42)	88(44)
$\bar{P}_s(dB)$	-33.48	-22.66	-33.90	-33.62

Table 5.38: Summary of performances for the three beams generated by the dipole selection and antenna selection methods in Sections 5.3.3 and 5.3.5, respectively, with the interleaved and localised subarray architectures.

Architecture	Interleaved (dipole selection)	Localised (dipole selection)	Interleaved (antenna selection)	Localised (antenna selection)
$\|\|\check{\boldsymbol{w}}_A\|\|_0(\frac{\|\|\tilde{\boldsymbol{w}}_A\|\|_0}{5})$	82(58)	46(41)	134(67)	80(40)
$\bar{P}_s(dB)$	-33.69	-22.36	-43.43	-25.30

the design with polarisation-sensitive crossed-dipole antennas have been developed. The dipole selection method with the localised subarray architecture employs the fewest number of dipoles at the cost of the highest sidelobe responses, while the antenna selection method with the interleaved subarray architecture gives the lowest sidelobe responses.

Chapter 6

Conclusions and Future Works

6.1 Conclusions

In this thesis, some basic concepts of beamforming, such as the steering vector, spatial aliasing and beam pattern, were first reviewed; then, a particular area of low-cost beamforming, i.e., hybrid beamforming, was introduced, where the digital and analogue beamforming techniques are performed at different stages, followed by the related sub-aperture subarray architectures, such as the interleaved and localised ones to achieve it.

With a simple digital coding scheme and a common set of analogue coefficients, one previous technique can only multiplex two beams whose directions have to meet a specific relationship. To overcome this limitation, two multi-beam multiplexing design schemes for arbitrary directions, with varying and fixed antenna spacings, respectively, have been proposed based on the interleaved subarray architecture. This method can also be extended to design multi-dimensional antenna arrays, such as UPAs, where the antennas are distributed in a planar geometry. As demonstrated by provided design examples, the adjacent antenna spacing for the first design can be calculated as a closed-form solution according to the beam directions; in addition, the second design can generate much narrower beams with a low sidelobe response compared to other designs without inter-subarray coding.

To implement the multi-beam multiplexing idea in a real world, some practical factors have to be taken into consideration and three novel designs have been proposed based

on the interleaved and localised subarray architectures. While the first design considers the problem of significantly reducing the implementation complexity of the analogue beamformer, the second design considers another very important problem, i.e., robustness against various model errors. Although robustness has been considered in many different engineering problems, they take different forms for different specific problems, with corresponding individualised solutions. For the third design, it is a natural extension of the work in both the first and second designs and together they form a complete piece of work. Furthermore, for the second and third designs, although the localised subarray architecture gives a wider beam width than the interleaved one, it provides better robust property against steering vector errors due to lower values of the normalised beam response variance.

To further reduce the complexity, the optimum antenna (dipole) selection problem for multi-beam multiplexing design based on a hybrid beamforming structure has been solved through a series of proposed l_1 norm minimisation methods. As shown by design examples, the proposed design with both the sub-aperture and overlapped subarray architectures can effectively reduce the number of antennas (channels) while meeting the beamforming requirements, such as mainlobe control and sidelobe responses. Even though the beam width generated by the interleaved subarray architecture is the narrowest among the three types of architectures, the overlapped subarray architecture employs the fewest number of antennas due to having the most degrees of freedom (DoFs) from antenna channels.

The same idea can be applied to the array structure with crossed-dipole antennas from two different aspects: either select the individual dipoles of each crossed-dipole antenna or the whole crossed-dipole antennas. Compared to the whole antenna selection method, the individual dipole selection method employs a reduced number of dipoles because of more degrees of freedom (DoFs) from a relaxed constraint. The dipole selection method with the localised subarray architecture employs the fewest number of dipoles at the cost of the highest sidelobe responses, while the antenna selection method with the interleaved subarray architecture gives the lowest sidelobe responses.

6.2 Future Works

Multi-beam multiplexing design for arbitrary directions and corresponding antenna selection design have been achieved based on the sub-aperture subarray architectures, which are constructed in a traditional mathematical model. In future work, the quaternion model can be employed to the multi-beam multiplexing design [115, 125–127]. This means that the weighting coefficients, steering vectors and the responses are quaternion-valued and each value consists of a real part and three imaginary parts. If the quaternion model is employed into the antenna select design, the four coefficients associated with each antenna have to be minimised simultaneously to guarantee a non-uniform solution.

Another idea is that the antenna selection design for multi-beam multiplexing based on narrowband array can be extended to the wideband case. Specifically, each antenna in the array is associated with multiple weighting coefficients because the Tapped-Delay Lines (TDLs) length is larger than one. To introduce sparsity in the array, all the weighting coefficients associated with each antenna have to be zero-valued and therefore the corresponding whole antenna can be removed. Thus, the number of antennas of the wideband beamformer to generate multiple beams simultaneously can be minimised and the overall complexity of the system can be reduced to a lower level.

Similar to Chapter 5, by employing the hybrid beamforming technique for the array structure based on crossed-dipole antennas, how to design the beam response with respect to the polarisation information, i.e., the auxiliary angle and the phase difference, will be another interesting topic for future research. To describe how polarised an antenna is, cross-polar discrimination (XPD), which is the ratio between co-polarisation received power and the cross-polarisation received power over the sector or beamwidth angle [128, 129], can be introduced in the array design. Cross-polar discrimination is significant for the low level correlation between orthogonally polarised propagation channels since the correlation from antennas can degrade the receive diversity in massive MIMO and this will be another interesting topic for future research.

Since the adjacent antenna spacing the whole array is smaller than half wavelength, the mutual coupling between adjacent antennas cannot be avoided in practical imple-

mentations and its effect can be considered in multi-beam multiplexing design based on hybrid beamforming structures.

Furthermore, the operating principle of spatial modulation (SM) [130–132] is to map a set of information bits into two carrying units, where the first unit is selected from a constellation diagram and the second one is to choose the transmitted antennas. Different from the conventional amplitude and phase modulation methods, the overall efficiency of the MIMO system serving multiple users is improved by exploiting the spatial dimension of the antenna indices in the array with the interleaved subarray architecture. The proposed multi-beam multiplexing designs can be studied in the context of spatial modulation too in the future.

References

[1] W. Liu and S. Weiss, *Wideband Beamforming: Concepts and Techniques.* John Wiley & Sons, Mar. 2010.

[2] H. V. Trees, *Optimum Array Processing: Part IV of Detection, Estimation, and Modulation Theory.* New Yorks, U.S.A.: John Wiley & Sons, 2002.

[3] Q. Luo, S. Gao, W. Liu, and C. Gu, *Low-cost Smart Antennas.* Wiley Press, Mar. 2019.

[4] M. S. Brandstein and D. W. (Eds.), *Microphone Arrays: Signal Processing Techniques and Applications.* Springer, 2001.

[5] D. M. Green, J. A. Swets *et al.*, *Signal detection theory and psychophysics.* Wiley Press, 1966, vol. 1.

[6] I. Bekkerman and J. Tabrikian, "Target detection and localization using MIMO radars and sonars," *IEEE Transactions on Signal Processing*, vol. 54, no. 10, pp. 3873–3883, Oct. 2006.

[7] H. Krim and M. Viberg, "Two decades of array signal processing research: the parametric approach," *IEEE Signal Processing Magazine*, vol. 13, no. 4, pp. 67–94, Jul. 1996.

[8] F. Boccardi, R. W. Heath, A. Lozano, T. L. Marzetta, and P. Popovski, "Five disruptive technology directions for 5G," *IEEE Communications Magazine*, vol. 52, no. 2, pp. 74–80, Feb. 2014.

[9] W. Roh, J. Seol, J. Park *et al.*, "Millimeter-wave beamforming as an enabling technology for 5G cellular communications: Theoretical feasibility and prototype results," *IEEE Communications Magazine*, vol. 53, no. 2, pp. 106–113, Feb. 2014.

[10] S. Han, C. I. I, Z. Xu, and C. Rowell, "Large-scale antenna systems with hybrid analog and digital beamforming for millimeter wave 5G," *IEEE Communications Magazine*, vol. 53, no. 1, pp. 186–194, Jan. 2015.

[11] A. F. Molisch, V. V. Ratnam, S. Han *et al.*, "Hybrid beamforming for massive MIMO: A survey," *IEEE Communications Magazine*, vol. 55, no. 9, pp. 134–141, Sep. 2017.

[12] J. Li, X. Li, L. Xiao, and S. Zhou, "Joint multi-beam and channel tracking for mmWave hybrid beamforming multi-user systems," *IEEE Wireless Communications Letters*, vol. 10, no. 7, pp. 1513–1517, 2021.

[13] V. Kumar, Shreeshail, U. S. Pandey, K. S. Beenamole, and R. K. Gangwar, "Low cost hybrid beamforming network for 2-D multi-beams in active phased array antenna," in *Proc. XXXIVth General Assembly and Scientific Symposium of the International Union of Radio Science (URSI GASS)*, Rome, Italy, 2021.

[14] S. Payami, K. Nikitopoulos, M. Khalily, and R. Tafazolli, "A signal processing framework for Agile RF beamforming: From RF-Chain-Free to hybrid beamformers," *IEEE Transactions on Communications*, vol. 69, no. 6, pp. 4038–4053, 2021.

[15] L. Yan, Y. Chen, C. Han, and J. Yuan, "Joint inter-path and intra-path multiplexing for Terahertz widely-spaced multi-subarray hybrid beamforming systems," *IEEE Transactions on Communications*, vol. 70, no. 2, pp. 1391–1406, 2022.

[16] L. Pang, W. Wu, Y. Zhang, Y. Yuan, Y. Chen, A. Wang, and J. Li, "Joint power allocation and hybrid beamforming for downlink mmWave-NOMA systems," *IEEE Transactions on Vehicular Technology*, vol. 70, no. 10, pp. 10 173–10 184, 2021.

[17] R. Rajamäki, S. P. Chepuri, and V. Koivunen, "Hybrid beamforming for active

sensing using sparse arrays," *IEEE Transactions on Signal Processing*, vol. 68, pp. 6402–6417, 2020.

[18] G. Yang, T. Wei, and Y. C. Liang, "Joint hybrid and passive beamforming for millimeter wave symbiotic radio systems," *IEEE Wireless Communications Letters*, vol. 10, no. 10, pp. 2294–2298, 2021.

[19] W. Wang, W. Zhang, and J. Wu, "Optimal beam pattern design for hybrid beamforming in millimeter wave communications," *IEEE Transactions on Vehicular Technology*, vol. 69, no. 7, pp. 7987–7991, 2020.

[20] Y. Zhang, J. Du, Y. Chen, X. Li, K. M. Rabie, and R. Khkrel, "Dual-iterative hybrid beamforming design for millimeter-wave massive multi-user MIMO systems with sub-connected structure," *IEEE Transactions on Vehicular Technology*, vol. 69, no. 11, pp. 13 482–13 496, 2020.

[21] K. Izadinasab, A. W. Shaban, and O. Damen, "Detection for hybrid beamforming millimeter wave massive MIMO systems," *IEEE Communications Letters*, vol. 25, no. 4, pp. 1168–1172, 2021.

[22] V. Venkateswaran and A. van der Veen, "Analog beamforming in MIMO communications with phase shift networks and online channel estimation," *IEEE Transactions on Signal Processing*, vol. 58, no. 8, pp. 4131–4143, Aug. 2010.

[23] O. Oliaei, "A two-antenna low-IF beamforming MIMO receiver," in *Proc. IEEE Global Communications Conference*, Washington, DC, USA, Nov. 2007, pp. 3591–3595.

[24] C. Miller, W. Liu, and R. J. Langley, "Reduced complexity MIMO receiver with real-valued beamforming," in *Proc. IEEE International Conference on Computer and Information Technology*, Liverpool, UK, Oct. 2015, pp. 31–36.

[25] M. Shimizu, "Millimeter-wave beam multiplexing method using subarray type hybrid beamforming of interleaved configuration with inter-subarray coding," *Inter-*

national journal of wireless information networks, vol. 24, no. 3, pp. 217–224, Sep. 2017.

[26] M. Shimizu, A. Honda, S. Ishikawa *et al.*, "Millimeter-wave beam multiplexing method using hybrid beamforming," in *Proc. IEEE 27th Annual International Symposium on Personal, Indoor, and Mobile Radio Communications (PIMRC)*, Valencia, Spain, Sep. 2016, pp. 1–6.

[27] F. Sohrabi and W. Yu, "Hybrid analog and digital beamforming for mmWave OFDM large-scale antenna arrays," *IEEE Journal on Selected Areas in Communications*, vol. 35, no. 7, pp. 1432–1443, Jul. 2017.

[28] S. A. Busari, K. M. S. Huq, S. Mumtaz *et al.*, "Generalized hybrid beamforming for vehicular connectivity using THz massive MIMO," *IEEE Transactions on Vehicular Technology*, vol. 68, no. 9, pp. 8372–8383, Sep. 2019.

[29] K. Satyanarayana, M. El-Hajjar, P. Kuo, A. Mourad, and L. Hanzo, "Hybrid beamforming design for full-duplex millimeter wave communication," *IEEE Transactions on Vehicular Technology*, vol. 68, no. 2, pp. 1394–1404, Feb. 2019.

[30] S. Payami, M. Ghoraishi, M. Dianati, and M. Sellathurai, "Hybrid beamforming with a reduced number of phase shifters for massive MIMO systems," *IEEE Transactions on Vehicular Technology*, vol. 67, no. 6, pp. 4843–4851, Jun. 2018.

[31] Z. Zheng and H. Gharavi, "Spectral and energy efficiencies of millimeter wave MIMO with configurable hybrid precoding," *IEEE Transactions on Vehicular Technology*, vol. 68, no. 6, pp. 5732–5746, Jun. 2019.

[32] M. M. Molu, P. Xiao, M. Khalily, K. Cumanan, L. Zhang, and R. Tafazolli, "Low-complexity and robust hybrid beamforming design for multi-antenna communication systems," *IEEE Transactions on Wireless Communications*, vol. 17, no. 3, pp. 1445–1459, Mar. 2018.

[33] A. Li and C. Masouros, "Energy-efficient SWIPT: From fully digital to hybrid analog–digital beamforming," *IEEE Transactions on Vehicular Technology*, vol. 67, no. 4, pp. 3390–3405, Apr. 2018.

[34] X. Zhang, A. F. Molisch, and S. Kung, "Variable-phase-shift-based RF-baseband codesign for MIMO antenna selection," *IEEE Transactions on Signal Processing*, vol. 53, no. 11, pp. 4091–4103, Nov. 2005.

[35] P. Sudarshan, N. B. Mehta, A. F. Molisch, and J. Zhang, "Channel statistics-based RF pre-processing with antenna selection," *IEEE Transactions on Wireless Communications*, vol. 5, no. 12, pp. 3501–3511, Dec. 2006.

[36] Y. Cai, K. Xu, A. Liu, M. Zhao, B. Champagne, and L. Hanzo, "Two-timescale hybrid analog-digital beamforming for mmwave full-duplex MIMO multiple-relay aided systems," *IEEE Journal on Selected Areas in Communications*, vol. 38, no. 9, pp. 2086–2103, 2020.

[37] S. Denno and T. Ohira, "Modified constant modulus algorithm for digital signal processing adaptive antennas with microwave analog beamforming," *IEEE Transactions on Antennas and Propagation*, vol. 50, no. 6, pp. 850–857, 2002.

[38] R. Eickhoff, R. Kraemer, I. Santamaria, and L. Gonzalez, "Developing energy-efficient MIMO radios," *IEEE Vehicular Technology Magazine*, vol. 4, no. 1, pp. 34–41, 2009.

[39] X. Huang and Y. Guo, "Frequency-domain AoA estimation and beamforming with wideband hybrid arrays," *IEEE Transactions on Wireless Communications*, vol. 10, no. 8, pp. 2543–2553, Aug. 2011.

[40] T. S. Rappaport, S. Sun, R. Mayzus *et al.*, "Millimeter wave mobile communications for 5G cellular: It will work!" *IEEE Access*, vol. 1, pp. 335–349, May 2013.

[41] J. A. Zhang, X. Huang, V. Dyadyuk, and Y. J. Guo, "Massive hybrid antenna array for millimeter-wave cellular communications," *IEEE Wireless Communications*, vol. 22, no. 1, pp. 79–87, Feb. 2015.

[42] R. W. Heath, N. González-Prelcic, S. Rangan, W. Roh, and A. M. Sayeed, "An overview of signal processing techniques for millimeter wave MIMO systems," *IEEE Journal of Selected Topics in Signal Processing*, vol. 10, no. 3, pp. 436–453, Apr. 2016.

[43] Y. Guo, X. Huang, and V. Dyadyuk, "A hybrid adaptive antenna array for long-range mm-Wave communications," *IEEE Antennas and Propagation Magazine*, vol. 54, no. 2, pp. 271–282, Apr. 2012.

[44] S. Fujio, C. Kojima, T. Shimura *et al.*, "Robust beamforming method for SDMA with interleaved subarray hybrid beamforming," in *Proc. IEEE 27th Annual International Symposium on Personal, Indoor, and Mobile Radio Communications (PIMRC)*, Valencia, Spain, Sep. 2016, pp. 1–5.

[45] T. Shimura, T. Ohshima, H. Ashida *et al.*, "Millimeter-wave TX phased array with phase adjusting function between transmitters for hybrid beamforming with interleaved subarrays," in *Proc. 46th European Microwave Conference (EuMC)*, London, UK, Oct. 2016, pp. 1572–1575.

[46] P. Rocca, R. Haupt, and A. Massa, "Sidelobe reduction through element phase control in uniform subarrayed array antennas," *IEEE Antennas and Wireless Propagation Letters*, vol. 8, no. 1, pp. 437–440, Feb. 2009.

[47] Z. Li, A. Honda, T. Shimura *et al.*, "Multi-user mmWave communication by interleaved beamforming with inter-subarray coding," in *Proc. IEEE 28th Annual International Symposium on Personal, Indoor, and Mobile Radio Communications (PIMRC)*, Montreal, QC, Canada, Oct. 2017, pp. 1–6.

[48] M. Majidzadeh, A. Moilanen, N. Tervo, H. Pennanen, A. Tolli, and M. Latva-aho, "Partially connected hybrid beamforming for large antenna arrays in multi-user MISO systems," in *Proc. IEEE 28th Annual International Symposium on Personal, Indoor, and Mobile Radio Communications (PIMRC)*, Montreal, QC, Canada, 2017, pp. 1–6.

[49] X. Yu, J. Shen, J. Zhang, and K. B. Letaief, "Alternating minimization algorithms for hybrid precoding in millimeter wave MIMO systems," *IEEE Journal of Selected Topics in Signal Processing*, vol. 10, no. 3, pp. 485–500, 2016.

[50] J. Chen, "Hybrid beamforming with discrete phase shifters for millimeter-wave massive MIMO systems," *IEEE Transactions on Vehicular Technology*, vol. 66, no. 8, pp. 7604–7608, 2017.

[51] A. Beck, "On the convergence of alternating minimization for convex programming with applications to iteratively reweighted least squares and decomposition schemes," *SIAM Journal on Optimization*, vol. 25, no. 1, pp. 185–209, 1996.

[52] A. B. Gershman, N. D. Sidiropoulos, S. Shahbazpanahi, M. Bengtsson, and B. Ottersten, "Convex optimization-based beamforming," *IEEE Signal Processing Magazine*, vol. 27, no. 3, pp. 62–75, May 2010.

[53] R. G. Lorenz and S. P. Boyd, "Robust minimum variance beamforming," *IEEE Transactions on Signal Processing*, vol. 53, no. 5, pp. 1684–1696, May 2005.

[54] H. Chen and W. Ser, "Design of robust broadband beamformers with passband shaping characteristics using Tikhonov regularization," *IEEE Transactions on Audio, Speech, and Language Processing*, vol. 17, no. 4, pp. 665–681, May 2009.

[55] Y. Zhao, W. Liu, and R. J. Langley, "Subband design of fixed wideband beamformers based on the least squares approach," *Signal Processing*, vol. 91, no. 4, pp. 1060–1065, 2011.

[56] A. Tkacenko, P. P. Vaidyanathan, and T. Q. Nguyen, "On the eigenfilter design method and its applications: a tutorial," *IEEE Transactions on Circuits and Systems II: Analog and Digital Signal Processing*, vol. 50, no. 9, pp. 497–517, Sep. 2003.

[57] S. Doclo and M. Moonen, "Design of broadband beamformers robust against gain and phase errors in the microphone array characteristics," *IEEE Transactions on Signal Processing*, vol. 51, no. 10, pp. 2511–2526, Oct. 2003.

[58] Y. Zhao, W. Liu, and R. Langley, "Application of the least squares approach to fixed beamformer design with frequency-invariant constraints," *IET Signal Processing*, vol. 5, no. 3, pp. 281–291, Jun. 2011.

[59] Å. Björck, *Numerical methods for least squares problems*. Philadelphia, PA, U.S.A.: Society for Industrial and Applied Mathematics (SIAM), 1996.

[60] Z. Tian, K. L. Bell, and H. L. Van Trees, "A recursive least squares implementation for LCMP beamforming under quadratic constraint," *IEEE Transactions on Signal Processing*, vol. 49, no. 6, pp. 1138–1145, Jun. 2001.

[61] D. P. Bertsekas, *Constrained optimization and Lagrange multiplier methods*. Academic press, 2014.

[62] J. Li, P. Stoica, and Z. Wang, "On robust Capon beamforming and diagonal loading," *IEEE Transactions on Signal Processing*, vol. 51, no. 7, pp. 1702–1715, Jul. 2003.

[63] S. Shahbazpanahi, A. B. Gershman, Z. Luo, and K. M. Wong, "Robust adaptive beamforming for general-rank signal models," *IEEE Transactions on Signal Processing*, vol. 51, no. 9, pp. 2257–2269, Sep. 2003.

[64] J. Zhang, W. Liu, C. Gu, S. S. Gao, and Q. Luo, "Two-beam multiplexing with inter-subarray coding for arbitrary directions based on interleaved subarray architectures," in *Proc. IEEE 30th Annual International Symposium on Personal, Indoor and Mobile Radio Communications (PIMRC)*, Istanbul, Turkey, Sep. 2019, pp. 1–5.

[65] S. Kim and Y. E. Wang, "Two-dimensional planar array for digital beamforming and direction-of-arrival estimations," *IEEE Transactions on Vehicular Technology*, vol. 58, no. 7, pp. 3137–3144, Sep. 2009.

[66] W. Liu, "Design and implementation of a rectangular frequency invariant beamformer with a full azimuth angle coverage," *Journal of the Franklin Institute*, vol. 348, no. 3, pp. 2556–2569, Nov. 2011.

[67] B. Zhang, W. Liu, Y. Li, X. Zhao, and C. Wang, "Directional modulation design under a constant magnitude constraint for weight coefficients," *IEEE Access*, vol. 7, pp. 154 711–154 718, Oct. 2019.

[68] C. Lu, W. Sheng, Y. Han, and X. Ma, "A novel adaptive phase-only beamforming algorithm based on semidefinite relaxation," in *Proc. IEEE International Symposium on Phased Array Systems and Technology*, Waltham, MA, USA, Oct. 2013, pp. 617–621.

[69] P. J. Kajenski, "Phase only antenna pattern notching via a semidefinite programming relaxation," *IEEE Transactions on Antennas and Propagation*, vol. 60, no. 5, pp. 2562–2565, May 2012.

[70] R. V. Gatti, L. Marcaccioli, and R. Sorrentino, "A novel phase-only method for shaped beam synthesis and adaptive nulling," in *Proc. IEEE European Microwave Conference*, Munich, Germany, 2003, pp. 739–742.

[71] I. D. Olin, "Flat-top sector beams using only array element phase weighting: A metaheuristic optimization approach," Naval Res. Lab., Washington, DC, USA, Formal Report, Oct. 2012.

[72] S. A. Vorobyov, A. B. Gershman, Z. Luo, and N. Ma, "Adaptive beamforming with joint robustness against mismatched signal steering vector and interference nonstationarity," *IEEE Signal Processing Letters*, vol. 11, no. 2, pp. 108–111, Feb. 2004.

[73] M. B. Hawes and W. Liu, "Compressive sensing-based approach to the design of linear robust sparse antenna arrays with physical size constraint," *IET Microwaves, Antennas & Propagation*, vol. 8, no. 10, pp. 736–746, Jul. 2014.

[74] S. Kim, A. Magnani, A. Mutapcic, S. P. Boyd, and Z. Luo, "Robust beamforming via worst-case SINR maximization," *IEEE Transactions on Signal Processing*, vol. 56, no. 4, pp. 1539–1547, Apr. 2008.

[75] S. A. Vorobyov, A. B. Gershman, and Z. Luo, "Robust adaptive beamforming using worst-case performance optimization: a solution to the signal mismatch problem," *IEEE Transactions on Signal Processing*, vol. 51, no. 2, pp. 313–324, Feb. 2003.

[76] Y. Zhao and W. Liu, "Robust wideband beamforming with frequency response variation constraint subject to arbitrary norm-bounded error," *IEEE Transactions on Antennas and Propagation*, vol. 60, no. 5, pp. 2566–2571, May 2012.

[77] J. Zhang, W. Liu, C. Gu, S. S. Gao, and Q. Luo, "Multi-beam multiplexing design for arbitrary directions based on the interleaved subarray architecture," *IEEE Transactions on Vehicular Technology*, vol. 69, no. 10, pp. 11 220–11 232, Oct. 2020.

[78] Y. Zhao, W. Liu, and R. J. Langley, "Adaptive wideband beamforming with frequency invariance constraints," *IEEE Transactions on Antennas and Propagation*, vol. 59, no. 4, pp. 1175–1184, Apr. 2011.

[79] M. Grant and S. Boyd, "CVX: Matlab software for disciplined convex programming, version 2.1," http://cvxr.com/cvx, Mar. 2014.

[80] J. Zhang, W. Liu, C. Gu, S. Gao, and Q. Luo, "Dual-beam multiplexing under an equal magnitude constraint based on a hybrid beamforming structure," in *Proc. IEEE 31st Annual International Symposium on Personal, Indoor and Mobile Radio Communications (PIMRC)*, London, UK, Aug. 2020, pp. 1–5.

[81] M. Rubsamen and M. Pesavento, "Maximally robust capon beamformer," *IEEE Transactions on Signal Processing*, vol. 61, no. 8, pp. 2030–2041, Apr. 2013.

[82] B. Zhang, W. Liu, and X. Gou, "Compressive sensing based sparse antenna array design for directional modulation," *IET Microwaves, Antennas & Propagation*, vol. 11, no. 5, pp. 634–641, 2017.

[83] M. B. Hawes and W. Liu, "Sparse array design for wideband beamforming with reduced complexity in tapped delay-lines," *IEEE/ACM Transactions on Audio, Speech, and Language Processing*, vol. 22, no. 8, pp. 1236–1247, Aug. 2014.

[84] J. Zhang, W. Liu, C. Gu, S. S. Gao, and Q. Luo, "Robust multi-beam multiplexing design based on a hybrid beamforming structure with nearly equal magnitude analogue coefficients," *IEEE Transactions on Vehicular Technology*, vol. 71, no. 5, pp. 5564–5569, 2022.

[85] M. B. Hawes and W. Liu, "Location optimisation of robust sparse antenna arrays with physical size constraint," *IEEE Antennas and Wireless Propagation Letters*, vol. 11, pp. 1303–1306, Nov. 2012.

[86] R. L. Haupt, "Thinned arrays using genetic algorithms," *IEEE Transactions on Antennas and Propagation*, vol. 42, no. 7, pp. 993–999, Jul. 1994.

[87] K. K. Yan and Y. Lu, "Sidelobe reduction in array-pattern synthesis using genetic algorithm," *IEEE Transactions on Antennas and Propagation*, vol. 45, no. 7, pp. 1117–1122, Jul. 1997.

[88] L. Cen, W. Ser, Z. Yu, and S. Rahardja, "An improved genetic algorithm for aperiodic array synthesis," in *Proc. IEEE International Conference on Acoustics, Speech and Signal Processing*, Las Vegas, NV, USA, Mar. 2008, pp. 2465–2468.

[89] S. Repetto and A. Trucco, "Designing superdirective microphone arrays with a frequency-invariant beam pattern," *IEEE Sensors Journal*, vol. 6, no. 3, pp. 737–747, Jun. 2006.

[90] A. Trucco and V. Murino, "Stochastic optimization of linear sparse arrays," *IEEE Journal of Oceanic Engineering*, vol. 24, no. 3, pp. 291–299, Jul. 1999.

[91] W. Weng, F. Yang, and A. Z. Elsherbeni, "Linear antenna array synthesis using Taguchi's method: A novel optimization technique in electromagnetics," *IEEE Transactions on Antennas and Propagation*, vol. 55, no. 3, pp. 723–730, Mar. 2007.

[92] L. Cen, W. Ser, W. Cen, and Z. L. Yu, "Linear sparse array synthesis via convex optimization," in *Proc. IEEE International Symposium on Circuits and Systems*, Paris, France, May 2010, pp. 4233–4236.

[93] L. Carin, "On the relationship between compressive sensing and random sensor arrays," *IEEE Antennas and Propagation Magazine*, vol. 51, no. 5, pp. 72–81, Oct. 2009.

[94] G. Prisco and M. D'Urso, "Exploiting compressive sensing theory in the design of sparse arrays," in *Proc. IEEE RadarCon (RADAR)*, Kansas City, MO, USA, May 2011, pp. 865–867.

[95] L. Li, W. Zhang, and F. Li, "The design of sparse antenna array," *CoRR*, vol. arXiv.org/abs/0811.0705, 2008.

[96] M. B. Hawes and W. Liu, "Sparse vector sensor array design based on quaternionic formulations," in *Proc. of the European Signal Processing Conference*, Lisbon, Portugal, Sep. 2014.

[97] M. B. Hawes and W. Liu, "A quaternion-valued reweighted minimisation approach to sparse vector sensor array design," in *Proc. of the International Conference on Digital Signal Processing*, Hong Kong, China, Aug. 2014.

[98] ——, "Design of fixed beamformers based on vector-sensor arrays," *International Journal of Antennas and Propagation*, vol. 2015, 2015.

[99] M. Hawes, L. Mihaylova, and W. Liu, "Location and orientation optimization for spatially stretched tripole arrays based on compressive sensing," *IEEE Transactions on Signal Processing*, vol. 65, no. 9, pp. 2411–2420, May 2017.

[100] T. Azar, "Overlapped subarrays: Review and update [education column]," *IEEE Antennas and Propagation Magazine*, vol. 55, no. 2, pp. 228–234, Apr. 2013.

[101] N. Song, T. Yang, and H. Sun, "Overlapped subarray based hybrid beamforming for millimeter wave multiuser massive MIMO," *IEEE Signal Processing Letters*, vol. 24, no. 5, pp. 550–554, May 2017.

[102] J. Eisenbeis, P. Ramos López, T. Mahler, C. Von Vangerow, and T. Zwick, "Low complexity antenna array concept using overlapped subarray based hybrid beam-

forming," in *Proc. IEEE Asia-Pacific Microwave Conference (APMC)*, Kyoto, Japan, Nov. 2018, pp. 669–671.

[103] Z. Xiong, Z. Xu, D. Song, and S. Xiao, "On the weighting optimisation of the antenna with overlapped subarrays architecture," *IET Microwaves, Antennas & Propagation*, vol. 9, no. 10, pp. 1035–1044, 2015.

[104] S. M. Duffy, D. D. Santiago, and J. S. Herd, "Design of overlapped subarrays using an RFIC beamformer," in *Proc. IEEE Antennas and Propagation Society International Symposium*, Honolulu, HI, USA, Jun. 2007, pp. 1949–1952.

[105] A. Hassanien and S. A. Vorobyov, "Phased-MIMO radar: A tradeoff between phased-array and MIMO radars," *IEEE Transactions on Signal Processing*, vol. 58, no. 6, pp. 3137–3151, Jun. 2010.

[106] Z. Wang, J. Zhu, J. Wang, and G. Yue, "An overlapped subarray structure in hybrid millimeter-wave multi-user MIMO system," in *Proc. IEEE Global Communications Conference (GLOBECOM)*, Abu Dhabi, AE, 2018, pp. 1–6.

[107] X. Zhong, A. B. Premkumar, and H. Wang, "Multiple wideband acoustic source tracking in 3-D space using a distributed acoustic vector sensor array," *IEEE Sensors Journal*, vol. 14, no. 8, pp. 2502–2513, Aug. 2014.

[108] G. Zhang, "A novel spatially spread electromagnetic vector sensor for high-accuracy 2-D DOA estimation," *Multidimensional Systems and Signal Processing*, vol. 28, May 2017.

[109] W. Yang, W. Xia, Z. He, and Y. Sun, "Polarimetric detection for vector-sensor processing in quaternion proper Gaussian noises," *Multidimensional Systems and Signal Processing*, vol. 27, May 2015.

[110] J. Zhang and W. Liu, "Antenna selection for multi-beam multiplexing design based on the hybrid beamforming architecture," in *Proc. IEEE Statistical Signal Processing Workshop (SSP)*, Rio de Janeiro, Brazil, 2021, pp. 261–265.

[111] R. Compton, "The tripole antenna: An adaptive array with full polarization flexibility," *IEEE Transactions on Antennas and Propagation*, vol. 29, no. 6, pp. 944–952, Nov. 1981.

[112] B. Leprettre, N. Martin, F. Glangeaud, and J. Navarre, "Three-component signal recognition using time, time-frequency, and polarization information-application to seismic detection of avalanches," *IEEE Transactions on Signal Processing*, vol. 46, no. 1, pp. 83–102, Jan. 1998.

[113] R. Bansal, "Tripole to the rescue [antennas]," *IEEE Antennas and Propagation Magazine*, vol. 43, no. 2, pp. 106–107, Apr. 2001.

[114] K. T. Wong, "Blind beamforming/geolocation for wideband-FFHs with unknown hop-sequences," *IEEE Transactions on Aerospace and Electronic Systems*, vol. 37, no. 1, pp. 65–76, Jan. 2001.

[115] X. Lan and W. Liu, "Fully quaternion-valued adaptive beamforming based on crossed-dipole arrays," *Electronics*, vol. 6, no. 2, pp. 34(1–16), 2017.

[116] X. Lan, W. Liu, and H. Y. T. Ngan, "Joint DOA and polarization estimation with crossed-dipole and tripole sensor arrays," *IEEE Transactions on Aerospace and Electronic Systems*, vol. 56, no. 6, pp. 4965–4973, 2020.

[117] X. Lan and W. Liu, "Direction of arrival estimation based on a mixed signal transmission model employing a linear tripole array," *IEEE Access*, vol. 9, pp. 47 828–47 841, 2021.

[118] X. Zhang, Z. Liu, W. Liu, and Y. Xu, "Quasi-vector-cross-product based direction finding algorithm with a spatially stretched tripole"," in *Proc. of the IEEE TENCON Conference*, Xi'an, China, Oct. 2013.

[119] R. Compton, "On the performance of a polarization sensitive adaptive array," *IEEE Transactions on Antennas and Propagation*, vol. 29, no. 5, pp. 718–725, 1981.

[120] G. Deschamps, "Techniques for handling elliptically polarized waves with special reference to antennas: Part II - geometrical representation of the polarization of a plane electromagnetic wave," *Proc. of the IRE*, vol. 39, no. 5, pp. 540–544, 1951.

[121] B. Zhang, W. Liu, and X. Lan, "Orthogonally polarized dual-channel directional modulation based on crossed-dipole arrays," *IEEE Access*, vol. 7, pp. 34 198–34 206, 2019.

[122] X. Zhang, W. Liu, Y. Xu, and Z. Liu, "Quaternion-valued robust adaptive beamformer for electromagnetic vector-sensor arrays with worst-case constraint," *Signal Processing*, vol. 104, pp. 274–283, Nov. 2014.

[123] M. B. Hawes, W. Liu, and L. Mihaylova, "Compressive sensing based design of sparse tripole arrays," *Sensors*, vol. 15, no. 12, pp. 31 056–31 068, 2015.

[124] J. Zhang and W. Liu, "Antenna selection design of crossed-dipole arrays for multi-beam multiplexing based on a hybrid beamforming structure," in *Proc. IEEE International Symposium on Circuits and Systems (ISCAS)*, Austin Texas, USA, 2022.

[125] M. Jiang, W. Liu, Y. Li, and X. Zhang, "Frequency-domain quaternion-valued adaptive filtering and its application to wind profile prediction," in *Proc. of the IEEE TENCON Conference*, Xi'an, China, Oct. 2013.

[126] M. Jiang, W. Liu, and Y. Li, "Adaptive beamforming for vector-sensor arrays based on reweighted zero-attracting quaternion-valued LMS algorithm," *IEEE Transactions on Circuits and Systems II: Express Briefs*, vol. 63, pp. 274–278, Mar. 2016.

[127] ——, "Properties of a general quaternion-valued gradient operator and its application to signal processing," *Frontiers of Information Technology & Electronic Engineering*, vol. 17, pp. 83–95, Feb. 2016.

[128] Y. G. Lim, Y. J. Cho, T. Oh, Y. Lee, and C. B. Chae, "Relationship between cross-polarization discrimination (XPD) and spatial correlation in indoor small-cell MIMO systems," *IEEE Wireless Communications Letters*, vol. 7, no. 4, pp. 654–657, 2018.

[129] S. Yamada, D. Choudhury, C. Thakkar, A. Chakrabarti, K. Dasgupta, S. Daneshgar, and B. D. Horine, "Cross-polarization discrimination and port-to-port isolation enhancement of dual-polarized antenna structures enabling polarization MIMO," *IEEE Antennas and Wireless Propagation Letters*, vol. 18, no. 11, pp. 2409–2413, 2019.

[130] R. Y. Mesleh, H. Haas, S. Sinanovic, C. W. Ahn, and S. Yun, "Spatial modulation," *IEEE Transactions on Vehicular Technology*, vol. 57, no. 4, pp. 2228–2241, 2008.

[131] M. Wen, B. Zheng, K. J. Kim, M. Di Renzo, T. A. Tsiftsis, K. C. Chen, and N. Al-Dhahir, "A survey on spatial modulation in emerging wireless systems: Research progresses and applications," *IEEE Journal on Selected Areas in Communications*, vol. 37, no. 9, pp. 1949–1972, 2019.

[132] P. Yang, M. Di Renzo, Y. Xiao, S. Li, and L. Hanzo, "Design guidelines for spatial modulation," *IEEE Communications Surveys Tutorials*, vol. 17, no. 1, pp. 6–26, 2015.